

**ANALYSIS OF THERMALLY CONNECTED RESIDENTIAL  
APPLIANCES**

by  
**Stephen L. Caskey**

**A Dissertation**

*Submitted to the Faculty of Purdue University  
In Partial Fulfillment of the Requirements for the degree of*

**Doctor of Philosophy**



School of Mechanical Engineering

West Lafayette, Indiana

May 2019

**THE PURDUE UNIVERSITY GRADUATE SCHOOL  
STATEMENT OF COMMITTEE APPROVAL**

Dr. Eckhard A. Groll, Chair

School of Mechanical Engineering

Dr. James E. Braun

School of Mechanical Engineering

Dr. Neera Jain

School of Mechanical Engineering

Dr. William T. Horton

Lyles School of Civil Engineering

**Approved by:**

Dr. Jay P. Gore

Head of the Graduate Program

*To my wonderful family and friends*

## ACKNOWLEDGMENTS

I would like to first thank Professor Eckhard A. Groll, Dr. Ing. As my advisor throughout graduate school and mentor since my first study abroad experience, your guidance and confidence enabled me grow into the engineer I am today. Prof. William J. Hutzler, thank you for your advice and guidance during the difficult times at Camp Atterbury. Thank you to the Whirlpool corporation and specifically, Ron Voglewede, Eric Bowler, and Jason Schneeman. Your dedication to sustainable technologies is unparalleled and made this research possible. A special thank you to the entire TLK team and the TU-Braunschweig for hosting and making me feel a part of the team. To Wilhelm Tegethoff, your genuine kindness was a significant factor in the success of this work, thank you for being a wonderful host and mentor during my stays in Germany. To my patient and supportive colleagues, Abhinav Krishna, Christian Bach, Derek Kultgen, and Chris Katinas, your kind words and laughter always came when it was most needed. To the entire Herrick Laboratories family, Frank Lee, Bob Brown, Donna Cackley, Kimberly Stockment, and Cindy Cory, thank you for everything you do. Thank you to Alison Kirkham, my life teammate, and to Priscilla Caskey-Shively my thoughtful sister. Thank you to Ben Ward and Robin Kruger, the friends who were always really brothers. A final thank you to my entire family and friends, your love and laughter have been my carrot throughout this entire journey.

## TABLE OF CONTENTS

LIST OF TABLES .....	10
LIST OF FIGURES .....	11
NOMENCLATURE .....	17
ABSTRACT.....	18
1. INTRODUCTION .....	20
1.1 Motivation.....	20
1.2 Scope.....	21
1.3 Approach.....	24
1.4 Objectives .....	26
2. APPLIANCE BACKGROUND .....	28
2.1 Refrigerator-Freezers .....	28
2.1.1 Electrical Consumption.....	29
2.1.2 Efficiency Ratings.....	29
2.1.3 Cycle Characteristics .....	29
2.1.4 Controls.....	31
2.1.5 Energy Saving Methods.....	32
Refrigerant Migration .....	32
Replacement Refrigerants.....	32
Compressor .....	33
Cabinet .....	33
Fans.....	34
Defrost Control .....	34
Different Cycle Configurations.....	34
Alternative Refrigeration Technologies.....	35
2.2 Dishwasher.....	35
2.2.1 Usage Frequency.....	35
2.2.2 Electrical Consumption.....	36
2.2.3 Water Consumption .....	36
2.2.4 Cycle Characteristics .....	37

2.2.5 Controls .....	39
2.2.6 Energy Saving Methods .....	41
Sense Soil Level.....	41
Reuse Waste Water .....	41
Alternative Heating Sources .....	41
2.3 Clothes Washer .....	42
2.3.1 Usage Frequency.....	42
2.3.2 Electrical Consumption.....	43
2.3.3 Water Consumption .....	44
2.3.4 Efficiency Ratings.....	44
2.3.5 Cycle Characteristics .....	45
2.3.6 Controls.....	46
2.3.7 Energy Saving Methods.....	46
Water Temperature .....	47
Water Extraction .....	47
Microprocessor Introduction.....	47
Wash Performance .....	48
Alternative Heating Sources .....	48
Miscellaneous .....	48
2.4 Clothes Dryer .....	49
2.4.1 Usage Frequency.....	49
2.4.2 Electrical Consumption.....	50
2.4.3 Efficiency Ratings.....	50
2.4.4 Cycle Characteristics .....	50
2.4.5 Controls.....	52
2.4.6 Energy Saving Methods.....	53
Cycle Termination .....	53
Component Improvements.....	53
Heat Pump Dryers.....	53
Miscellaneous .....	54
2.5 Cooking Oven.....	54

2.5.1 Usage Frequency.....	54
2.5.2 Electrical Consumption.....	54
2.5.3 Efficiency Ratings.....	55
2.5.4 Sample Cabinet .....	55
2.5.5 Cycle Characteristics .....	55
2.5.6 Energy Saving Methods.....	55
3. THERMODYNAMIC APPLIANCE MODELICA MODELS .....	57
3.1 TLK-TIL Modelica Thermal Library .....	57
3.2 Clothes Dryer.....	58
3.2.1 Cycle Controller.....	58
3.2.2 Exhaust Heat Exchanger .....	60
3.2.3 External Model.....	60
3.2.4 Dymola Simulation Results .....	60
3.3 Refrigerator-Freezer.....	63
3.3.1 Compressor .....	63
3.3.2 Condenser .....	63
3.3.3 Expansion.....	64
3.3.4 Evaporator.....	64
3.3.5 Steady State Simulation Results .....	65
3.3.6 Compressor Capacity Controller.....	68
3.3.7 Transient Simulation Results .....	68
3.3.8 Discussion .....	72
3.4 Dishwasher.....	72
3.4.1 Cycle Controller.....	73
Timer Control.....	74
Heating Control.....	74
Fill and Drain Control.....	75
Heat Loop Control .....	75
Overall Control .....	75
3.4.2 Modelica Components .....	76
3.4.3 External Connection.....	77

3.4.4 Traditional DW Simulation Results .....	78
3.4.5 Heat Loop DW Simulation Results.....	80
3.5 Clothes Washer .....	82
3.5.1 Approach.....	82
3.6 Integrated Appliance System .....	83
3.6.1 Approach.....	83
3.6.2 Appliance Schedule .....	84
3.6.3 Simple Storage Tank.....	85
3.6.4 Simulation Results .....	85
4. EXPERIMENTAL TEST STAND .....	88
4.1 Clothes Dryer .....	88
4.1.1 Overall Approach.....	89
4.1.2 Fin-and-Tube Heat Exchanger .....	89
4.1.3 Temperature Mesh and Relative Humidity Measurements.....	90
4.1.4 Hot Wire Anemometer .....	91
4.1.5 Auxiliary Fan .....	91
4.1.6 Insulation.....	91
4.2 Refrigerator-Freezer.....	92
4.2.1 Overall Approach.....	93
4.2.2 Flat-Plate Heat Exchanger .....	94
4.3 Dishwasher.....	94
4.4 Clothes Washer .....	94
4.5 Buffer Tank and Piping Backbone.....	96
4.6 Controls and DAQ System (LabVIEW) .....	98
4.6.1 Front Panel Control.....	98
4.7 Cycle Results .....	99
4.7.1 Clothes Dryer .....	99
Duct Airflow Rate.....	100
4.7.2 Refrigerator-Freezer.....	100
4.7.3 Dishwasher.....	101
4.7.4 Clothes Washer .....	102

Normal –Warm Wash .....	102
Normal – Hot Wash .....	103
Sanitization Wash .....	104
5. VALIDATION OF MODELICA APPLIANCE MODELS .....	105
5.1 Clothes Dryer .....	105
5.2 Refrigerator-Freezer.....	107
5.3 Dishwasher.....	112
5.4 Clothes Washer .....	114
5.5 Integrated Appliance System .....	116
6. PARAMETRIC STUDY .....	119
6.1 Baseline Operation.....	119
6.2 Ideal Appliance Modifications.....	119
6.2.1 Clothes Dryer .....	120
6.2.2 Refrigerator-Freezer.....	122
6.2.3 Dishwasher.....	124
6.2.4 Clothes Washer .....	126
6.3 Storage Tank Volume .....	126
6.3.1 300 L Tank.....	127
6.3.2 150L Tank .....	130
7. CONCLUSIONS.....	133
7.1 Contribution to the Field.....	133
7.2 Overall Findings .....	134
7.3 Recommended Future Work.....	135
REFERENCES .....	137
APPENDIX A – WASTE HEAT ANALYSIS.....	140
APPENDIX B - EES CODE.....	147
APPENDIX C – CUSTOM MODELICA COMPONENTS .....	157
APPENDIX D – TIL LIBRARY MODELICA COMPONENT DESCRIPTIONS.....	164
PUBLICATIONS.....	168

## LIST OF TABLES

Table 1: Summary of household refrigerator performance with water cooling and air cooling condenser .....	142
Table 2: Summary of clothes dryer heat recovery .....	143
Table 3: Summary of bulk energy recovery from the clothes washer, dishwasher and cooking oven .....	144

## LIST OF FIGURES

Figure 1: Global Breakdown of World Energy Consumption (Buildings Energy Data Book, 2011) .....	21
Figure 2: Residential Site Energy Consumption by End Use (Buildings Energy Data Book, 2011) .....	22
Figure 3: Historic Trend of Refrigerator-Freezer Annual Consumption and Unit Size (Bansal et al., 2011) .....	23
Figure 4: Historic Trend of Clothes Washer and Dishwasher Energy Consumption per cycle (Bansal et al., 2011) .....	23
Figure 5: Schematic of Proposed Integrated Appliance Test Stand .....	26
Figure 6: Overall Basic RF Temperature Control Flow Chart (Left) and Basic Defrost Timer Control Flow Chart (Right).....	31
Figure 7: Example DW Sensing Wash Cycle with Sump Temperature and Power Consumption (Whirlpool Corp. 2017) .....	38
Figure 8: Calculated Thermal Capacity of Entire DW during Water Heating Cycles as a Function of the Starting Water Temperature .....	39
Figure 9: Overall DW Control Flow Chart.....	40
Figure 10: Profile of CW Wash and Rinse Temperature Settings from a VA and HA Study Compared to the Department of Energy Test Procedure (Tomlinson et al., 1998) .....	45
Figure 11: Overall CW Control Flow Chart .....	46
Figure 12: Temperature Readings on Several Locations of a CD during a Sample Drying Cycle (Butturini et al., 2004).....	51
Figure 13: Relative Humidity Readings on Three Locations of a CD during a Sample Drying Cycle (Butturini et al., 2004).....	52
Figure 14: Overall CD Control Flow Chart using Moisture or Timer Condition.....	53
Figure 15: Clothes Dryer Modelica Controller for High Heat-5 kg load .....	59
Figure 16: Testing the Clothes Dryer Cycle Controller with the Heat Recovery Components....	59
Figure 17: Creating External Connections for Clothes Dryer Model.....	60
Figure 18: Breakdown of Heat Transfer Rate CD Modelica Simulating 3/8" Diameter.....	61
Figure 19: HX Air and Water Temperatures of the CD Modelica Simulating Heat Recovery using 3/8" Diameter.....	61
Figure 20: Breakdown of Heat Transfer Rate CD Modelica Simulating Ideal HX Surface Area	62

Figure 21: HX Air and Water Temperatures of the CD Modelica Simulating Heat Recovery using Ideal Surface Area.....	62
Figure 22: RF Water-cooled Condenser – Modelica Flat-Plate Model Geometric Inputs .....	64
Figure 23: RF Evaporator – Modelica Fin-and-Tube HX Model Geometric Inputs .....	65
Figure 24: Basic RF Modelica Model with No Control .....	66
Figure 25: Ph Diagram of Simulated Basic RF Model.....	66
Figure 26: Ts Diagram of Simulated Basic RF Model .....	67
Figure 27: Temperature Plot of Condenser and Evaporator HX Nodes from the Basic RF Model .....	67
Figure 28: Testing Cooling Loop with Simple Storage Connected to Refrigerator-Freezer Modelica Model .....	69
Figure 29: RF Simulated Compressor Suction/Discharge Pressures (top) and Power consumption (bottom) when connected to Water Storage Tank .....	70
Figure 30: Sample of Experimental RF Power Consumption while Rejecting Heat to Fixed Volume of Water (Small, S. 2017) .....	70
Figure 31: RF Simulated Evaporator Air-side Temperatures (top) and Refrigerant Heat Transfer (bottom) when connected to single volume water tank .....	71
Figure 32: RF Simulated Cooling Water, Compressor Discharge Temperatures (top) and Superheat, Subcooling Temperatures (bottom) .....	72
Figure 33: DW Modelica Diagram and Parameter Window for the Timer Controller.....	74
Figure 34: DW Modelica Diagram and Parameter Window for the Temperature Controller .....	75
Figure 35: Parametric Inputs for DW Cycle Controller.....	76
Figure 36: DW Modelica Model Diagram for Testing the DW Cycle Controller.....	77
Figure 37: External DW Modelica Model for Integrated System.....	78
Figure 38: Traditional DW Simulated Temperatures Versus Experimental Data .....	79
Figure 39: Traditional DW Simulated Electric Element Power Versus Experimental Data .....	79
Figure 40: DW Modelica Water Sump Temperature – Simulated versus Experimental.....	80
Figure 41: Heat Loop Driven DW Simulated Temperatures Versus Experimental Data.....	81
Figure 42: Heat Loop Driven DW Simulated Electric Element Power Versus Experimental Data .....	81
Figure 43: Sample Approach to CW Modelica Model .....	82
Figure 44: Modelica components representing 4 appliances connected to a central storage tank for heat recovery .....	84

Figure 45: Plot of 1-Week Appliance Schedule for Dishwasher, Clothes Washer, and Clothes Dryer .....	85
Figure 46: Integrated Appliance Model - Impact of Tank Volume on Temperature over Time ..	86
Figure 47: Rate of Heat Transfer between each Appliance and 454 L (120 gal.) Storage Tank ..	86
Figure 48: Amount of Energy Collected by Each Appliance with 454 L (120 gal.) Storage Tank .....	87
Figure 49: Schematic of Entire Integrated Appliance Test Stand with Instrumentation .....	88
Figure 50: Clothes Dryer Exhaust Duct Layout on Heat Recovery Approach and Measurements .....	89
Figure 51: Image of Clothes Dryer Fin-and-Tube Heat Exchanger with Geometry Details .....	90
Figure 52: 4-Point Thermocouple Grid and Relative Humidity Probe on Clothes Dryer Duct Before (Left)/After (Right) Heat Exchanger .....	90
Figure 53: Flow Straightener (Left) and Hot Wire Anemometer (Right).....	91
Figure 54: Insulating Internal Duct of Vented Clothes Dryer (Before-left / After-Right) .....	92
Figure 55: Clothes Dryer Duct After Insulation .....	92
Figure 56: Schematic of Refrigerator Test Stand with Instrumentation .....	93
Figure 57: Back of Test Stand Refrigerator with Flat-Pate Heat Exchanger and Instrumentation	94
Figure 58: Back of Test Stand Refrigerator after Insulation Installed.....	94
Figure 59: Schematic of Proposed Drain Tank with Heat Recovery for the Clothes Washer .....	95
Figure 60: Test Stand Clothes Washer Cycle Setting Front Panel .....	96
Figure 61: Test Stand Layout for Appliances, Buffer Tank, and Piping Mounting (BT Wall)....	97
Figure 62: Piping Wall Layout with Pump, Valve, Flow Meter and Power Supply Locations for Each Appliance and Buffer Tank (Top-North Side / Bottom-South side).....	98
Figure 63: Main Front Panel Display with Monitored Channels and Controls for Different Modes .....	99
Figure 64: Clothes Dryer Air Flow Across 9 Drying Cycles, Before and After Cleaning .....	100
Figure 65: Sample Data Set of Refrigerator Test Stand – Total Power Consumption and Measured Pressures .....	101
Figure 66: Sample Data Set of Refrigerator Test Stand – Inlet and Outlet Water Temperatures and Volumetric Flow Rate.....	101
Figure 67: Test Stand Data of Dishwasher Cycle Operation Temperatures and Power Consumption – Cycle 3 .....	102
Figure 68: Clothes Washer Cycle 2 with Normal Warm Wash.....	103

Figure 69: Clothes Washer Cycle 5 with Normal Hot Wash.....	103
Figure 70: Clothes Washer Cycle 9 with Sanitization .....	104
Figure 71: Curve-Fit for Clothes Dryer Exhaust Dry Bulb Temperature and Relative Humidity .....	105
Figure 72: Clothes Dryer Experimental Data of Air Temperatures and Flow Rate – Cycle 6...	106
Figure 73: Clothes Dryer Experimental Data of Water Temperatures and Flow Rate – Cycle 6	106
Figure 74: Updated Refrigerator-Freezer Approach in Modelica.....	107
Figure 75: Refrigerator-Freezer Measured Total Unit Power Consumption and Calculated Compressor Power Draw and Refrigerant Mass Flow Rate using AHRI Compressor Map .....	108
Figure 76: Tuned Refrigerator-Freezer Model Simulated Compressor Refrigerant Mass Flow Rate and Power Draw.....	109
Figure 77: Measured Refrigerator-Freezer Pressure Ratio, Total Electrical Consumption and Compressor Suction Superheat .....	110
Figure 78: Simulated Refrigerator-Freezer Compressor Pressure Ratio, Electric Consumption and Suction Superheat Temperature .....	111
Figure 79: Refrigerator-Freezer Water-Cooled Condenser, Measured Water Temperatures and Calculated Heat Transfer Capacity .....	111
Figure 80: Tuned Refrigerator-Freezer Model Simulated Condenser Water Temperatures and Heat Exchanger Capacity .....	112
Figure 81: Updated Dishwasher Modeling Approach with DHW Fill Valve, Sump Volume, and Cycle Controller.....	113
Figure 82: Tuned Dishwasher Modelica Plot of Sump Temperature and Power Consumption.	114
Figure 83: Detailed Clothes Washer Modelica Approach for Waste-Water Heat Recovery .....	115
Figure 84: Clothes Washer Cycle 9 Sanitization - Heat Recovery Process.....	115
Figure 85: Simulated Heat Recovery Process of Clothes Washer Waste Water for Sanitization Cycle, Water Temperatures and Flow Rates.....	116
Figure 86: Modelica Icon View of Integrated Appliances System.....	117
Figure 87: Test Stand Storage Tank Temperatures Compared to Refrigerator Water Supply and Return Temperatures during several Compressor Cycles.....	117
Figure 88: Simulated Storage Tank Temperatures Compared to Refrigerator-Freezer Water Supply and Return Temperatures during Several Compressor Cycles .....	118
Figure 89: Measurement Versus Simulation of TIRA HX and Ideal HX – Cycle 6 .....	121

Figure 90: Simulation Comparison between Heat Exchanger Types for Clothes Dryer Heat Recovery at 1000 seconds – Cycle 6 (Left: Test Stand Cross-flow, Right: Ideal Area Counter-flow) .....	121
Figure 91: Simulated RF TIRA and Ideal Condenser Flow rate – Heat Transfer, Power Consumption, and Total Energy in 1-Day .....	123
Figure 92: Simulated Refrigerator-Freezer TIRA and Ideal Condenser Cell Temperatures of Water and Refrigerant.....	123
Figure 93: Compare TIRA, Ideal, and Baseline Dishwasher Performance during 1-week Simulation, 1 <sup>st</sup> Cycle with 49C Initial Tank Temperature .....	125
Figure 94: Compare TIRA, Ideal, and Baseline Dishwasher Performance during 1-week Simulation, Last (6 <sup>th</sup> ) Cycle with 49C Initial Tank Temperature .....	125
Figure 95: Impact on Storage Tank Temperatures from Dishwasher Operation in 3 Configurations (Left: after first cycle, Right: after the 6 <sup>th</sup> cycle) .....	126
Figure 96: 1-Week 303 L (80 gal.) Ideal Simulation of 5 Storage Tank Temperatures .....	127
Figure 97: 1-Week 303 L (80 gal.) Ideal Simulation of Refrigerator Condenser Capacity and Compressor Power Consumption .....	128
Figure 98: 1-Week 303 L (80 gal.) Ideal Simulation of Dishwasher Cycle 1 Sump Temperature, HX Heat Transfer Rate, Electric Element Power Draw, and Total Energy .....	128
Figure 99: 1-Week 303 L (80 gal.) Ideal Simulation of Dishwasher Cycle 6 Sump Temperature, Heat Loop Heat Transfer Rate, Electric Element Power Draw, and Total Energy .....	129
Figure 100: 1-Week 150 L (50 gal.) Ideal Simulation of 5 Storage Tank Temperatures .....	130
Figure 101: 1-Week 150 L (50 gal.) Ideal Simulation of Refrigerator Condenser Capacity and Compressor Power Consumption .....	131
Figure 102: 1-Week 150 L (50 gal.) Ideal Simulation of Dishwasher Cycle 1 Sump Temperature, HX Heat Transfer Rate, Electric Element Power Draw, and Total Energy .....	131
Figure 103: 1-Week 150 L (50 gal.) Ideal Simulation of Dishwasher Cycle 6 Sump Temperature, Heat Loop Heat Transfer Rate, Electric Element Power Draw, and Total Energy .....	132
Figure 104: Storage tank temperature for water cooled condenser of household refrigerator ...	143
Figure 105: Impact of the storage tank volume size on the water temperature stored in the tank .....	143
Figure 106: Cooled dryer exhaust air leaving the waste heat exchanger as a function of the storage tank volume.....	144
Figure 107: Diagram View of CD Cycle Controller.....	157
Figure 108: Modelica Code for CD Cycle Controller .....	158
Figure 109: Diagram View of RF Capacity Controller Components .....	159

Figure 110: Modelica Code for RF Capacity Controller .....	160
Figure 111: DW Modelica Diagram of Wash Step Controller .....	161
Figure 112: DW Modelica Diagram of Heat Step Controller .....	162
Figure 113: DW Modelica Diagram of Overall DW Cycle Controller .....	163
Figure 114: TIL SIM Component for Selecting the Refrigerant (VLE), Gas, and, Liquid Types .....	164
Figure 115: Input Parameters for FPHX Modelica Model .....	165
Figure 116: Input Parameters for Fin-and-Tube HX Modelica Model.....	166
Figure 117: Input Parameters for Heat Tube Modelica Model.....	166
Figure 118: Input Parameters for Simple Storage Volume Modelica Model .....	167
Figure 119: Input Parameters for Thermal Capacitor Modelica Model .....	167

## NOMENCLATURE

CD – Clothes Dryer

CFM – Cubic Feet per Minute

CW – Clothes Washer

DHW – Domestic Hot Water

DOE – Department of Energy

DW – Dishwasher

FPHX – Flat Plate Heat Exchanger

HA – Horizontal Axis

HTC – Heat Transfer Coefficient

HVAC – Heating, Ventilation, and Air-Conditioning

HX – Heat Exchanger

RF – Refrigerator/Freezer

VA – Vertical Axis

## ABSTRACT

Author: Caskey, Stephen, L., PhD  
Institution: Purdue University  
Degree Received: May 2019  
Title: (Analysis of Thermally Connected Residential Appliances)  
Major Professor: Groll, Eckhard, A., Dr-Ing.

With the United States being the world's second largest consumer of primary energy, research into areas of significant consumption can provide large impacts in terms of the global energy consumption. Buildings account for 41% of U.S. total energy consumption with the residential sector making up a majority. Household appliances account for the second largest site energy consumption at 27%, after the HVAC system for the U.S. residential sector. Federal appliance standards have been instrumental in improving efficiencies but have been increasing aggressively to where it is unknown what suitable technologies can support this rate of increase. Thermally integrating residential appliances by leveraging waste heat recovery goes outside standards and has not been adequately explored by connecting all residential appliances. Limited studies exist focused only on single appliances connected to waste heat recovery or being thermally integrated. Preliminary modeling on waste heat availability from five major appliances, namely refrigerator-freezer, clothes dryer, clothes washer, dishwasher, and cooking oven was conducted. Conservative estimates predict the total amount of heat recovery to be around 2,000 kWh/year; clothes dryer - 137 kWh/year, clothes washer - 60 kWh/year, 1,500 kWh/year- refrigerator-freezer, 27 kWh/year – dishwasher, and 178 kWh/year – cooking oven. The cooking oven presents technical challenges coupled with safety concerns. The clothes dryer and refrigerator-freezer can deliver useful water temperatures and reduce compressor power consumption, up to 20%. The dishwasher has better opportunity as a heat sink to offset the internal heater, 0.17 kWh of electricity/cycle for heating wash water. The clothes washer drains large volumes of water available for heat recovery and can offset the impact of using high temperature washes with improved wash performance.

Modelica appliance models have been developed for four of these five appliances. The Modelica models capture individual use and the predictions of the RF and DW were compared against available experimental data. The individual models have been connected to a simple storage tank model to simulate the integrated appliance system. An integrated appliance prototype was designed

and fabricated for the collection of experimental data. Comparisons made between the experimental data and the integrated appliance simulation results adjusted the modeling approach and improved agreement with collected data. After tuning, ideal modifications to each appliance are made and reflected in a new integrated model. A parametric study is conducted on ideal improved, thermally capable appliances under a 1-week schedule for two different tank sizes. For 300L and 150 L tank sizes, the appliance total energy for the week is roughly 30.5 kWh compared to a baseline appliance system with no thermal resource sharing at 33.8 kWh. At an electricity cost of \$0.15/kWh, the cost savings for the integrated system is a little over \$0.40/week. Furthermore, the savings is completely diminished when considering the required auxiliary power to support the exchange of heat between each appliance and storage tank. The impact of tank size should be explored further to identify a critical tank size where the system savings is no longer available. Accounting for all the domestic hot water needs of the home would generate an improved picture where integrated appliances have technical feasibility.

## 1. INTRODUCTION

The North American and European continents have historically dominated global energy consumption due to the concentration of advanced technologies utilizing energy dense resources such as fossil fuels. Having access to highly capable means provided a fertile backdrop for numerous improvements to quality of life. Widespread electrification enabled greater access to advanced technologies while growing the demand for fossil fuels to generate the electricity. Other developments producing quicker methods of travel such as the railroad or internal-combustion-engine have also contributed to this existing demand of fossil fuels. The growing demand on a limited resource required these regions to explore new areas of the globe to continue their support for these societal improvements. With the rise of computers and the ease information is spread globally, other regions without these rapid advancements are quickly developing their own countries.

### 1.1 Motivation

Globalization has spurred not only the spread of advanced technology to developing nations, but has also accelerated the rate of adoption. As a result global energy demands are outpacing the population growth as developing nations advance the standard of living to larger percentages of the population. The annual growth rate of global energy and population in 1990-2000 was 1.3% and 1.4% respectively while during the next 10 years, in 2000-2010, this increased to 2.8% and decreased to 1.0% respectively (Buildings Energy Data Book, 2011). More specifically the regions with a significant annual growth of energy were China, India, and Africa at 11.1%, 5.9% and 4.9% respectively. In terms of global population, these regions and countries account for 20%, 18.1% and 14.9% respectively of the total, combining for more than half of the entire population of the Earth. From this high rate of energy growth from the fastest growing population sectors, the U.S. has fallen to second place behind China as the largest consumer of energy in the world, with less than a quarter of the population. The US consumed 103.2 EJ (97.8) quads of primary energy in 2010 or 19% of global consumption (Buildings Energy Data Book, 2011). Reducing the energy consumption of the US provides an effective mechanism to achieve significant reductions to the world total energy consumption. The U.S. Department of Energy breaks down the energy picture

across four sectors: transportation, commercial, residential and industrial. The building sector, which combines both commercial and residential, is the largest consumer at 41% of the U.S. total compared to 29% from transportation and 30% from industry, Figure 1. In broader terms, U.S. buildings, on their own, account for 7% of global primary energy consumption. The dominate energy source was fossil fuels at 75%, while nuclear generation and renewables provided 16% and 9% respectively (Buildings Energy Data Book, 2011).

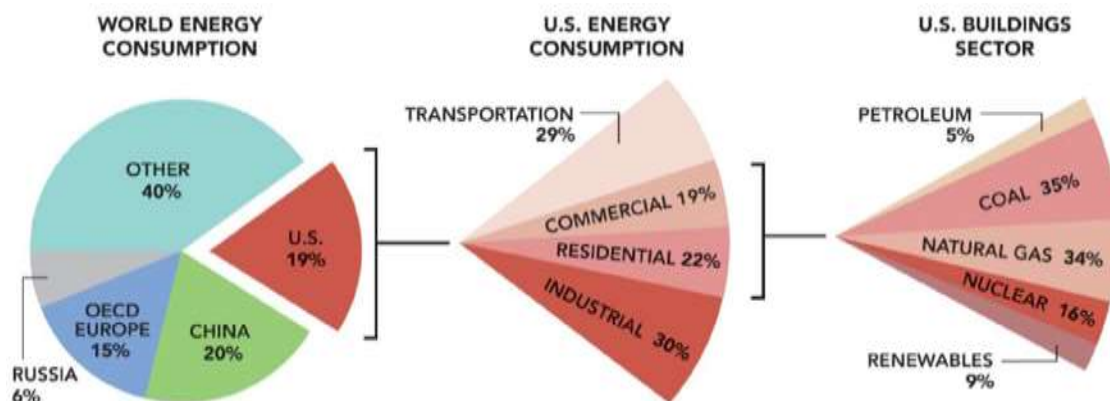


Figure 1: Global Breakdown of World Energy Consumption (Buildings Energy Data Book, 2011)

A further look into the energy consumption of the building sector indicates 41 EJ (39 quads) of primary energy provided only 21 EJ (20 quads) of site energy for an energy loss of 49%. A large source of these losses occurs from site electricity usage. From the production of electricity at the power plant, to the transmission and distribution through the grid, conversion and resistive losses stack-up and compound the inefficiencies present. The impact results in larger than necessary, primary energy consumption to support end-use electricity. Therefore, exploring methods to reduce site electricity will magnify any impact on annual building energy consumption by demanding less primary energy for electricity generation. Addressing residential energy consumption for the building sector is of greater relative importance due to residential buildings accounting for a slightly larger consumption than the commercial buildings, 22% versus 19%.

## 1.2 Scope

The largest percentage of residential, site energy usage is from the heating, air conditioning, and ventilation (HVAC) system, 54%. The next significant percentage is from the household appliances; water heater, refrigerator, wet cleaning (dishwasher, clothes washer and dryer) and

cooking equipment at 27% (Table 2.1.5 Buildings Energy Data Book, 2011). A complete breakdown of each end use percentage of total site energy consumption is presented in Figure 2.

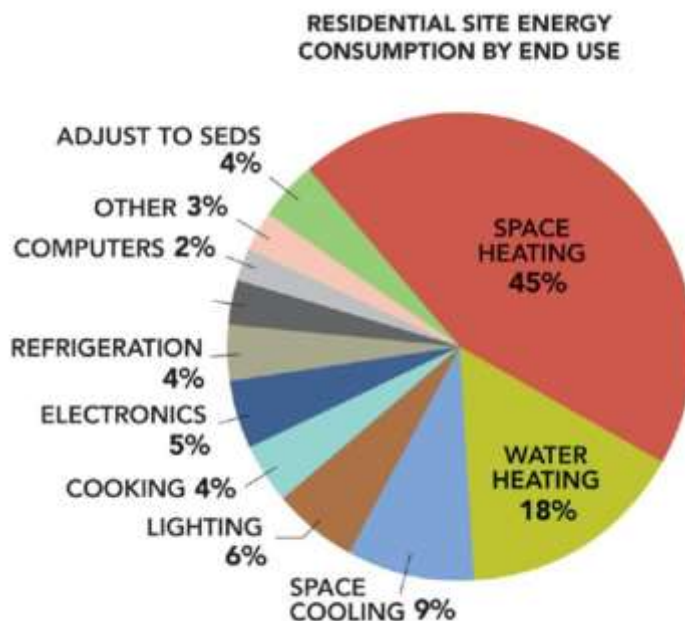


Figure 2: Residential Site Energy Consumption by End Use (Buildings Energy Data Book, 2011)

Countless studies have been conducted to reduce building HVAC energy by exploring various improvements on the HVAC equipment to upgrading building materials obtaining reductions in the thermal demand of the home. For household appliances, the research has mainly been focused only on the appliance itself with some study on benefits from connection to resources available outside the appliance. Legislation is mentioned as a great mechanism to drive energy reductions in household appliances (Bansal et al., 2011). Federal standards have resulted in significant reductions in appliance energy consumption by forcing the industry to explore and adopt new technology. As one example, the average annual electricity use of U.S. household refrigerators in 1980 of about 1,300 kWh drops to about 950 kWh in 1990 and then is under 700 kWh by 1992 due to the introduction of new energy efficiency standards in 1990 and 1993 (Meyers *et al.*, 2003). In spite of legislation demanding appliances to complete the same function with fewer resources, manufacturers have been able to increase the capacity of appliances in the same timeframe. A plot in Figure 3 identifies this effect. The years when new RF standards were applied relative to their annual energy consumption are shaded and compared to the upward trend in the average volume of RF cavities (Bansal et al., 2011). Under a new standard, the RF annual usage decreases and quickly levels off establishing a new baseline. The similar trend is observed in Figure 4 for CWs

when plotting the energy consumption per cycle (Bansal et al., 2011). The standards have become more aggressive and started targeting additional appliances. In the U.S., the following efficiency standards were set in 2010 (Bansal et al., 2011):

- RFs – reduce energy use by up to 30% by January 2014
- CWs – VA save 26% energy and 16% water by 2015, increasing to 37% energy and water savings by 2018; HA reduce energy use by 43% and water use by 52% by 2015
- CDs – increase efficiency by 5% in 2015
- DWs – save 14% energy and 23% water by January 2013

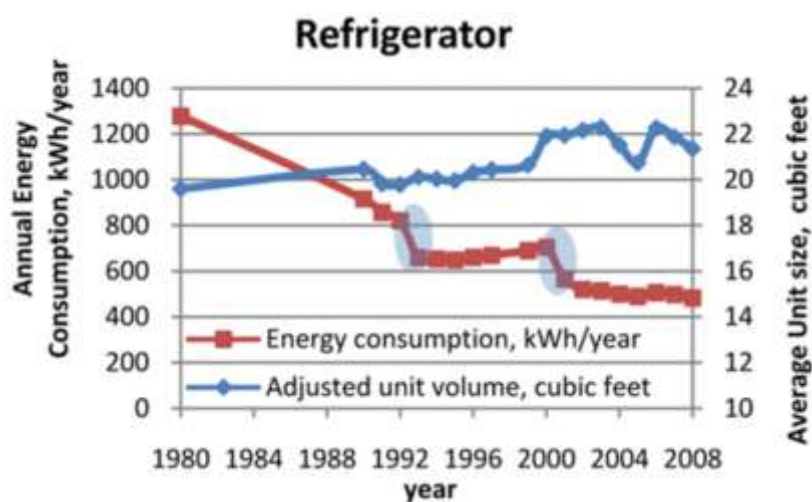


Figure 3: Historic Trend of Refrigerator-Freezer Annual Consumption and Unit Size (Bansal et al., 2011)



Figure 4: Historic Trend of Clothes Washer and Dishwasher Energy Consumption per cycle (Bansal et al., 2011)

While regulation in general provides benefits to consumers, they can create tunnel vision for manufacturers by limiting their scope in adhering to the standards and only considering improvements within the scope of one appliance. This perspective is referenced in literature, “appliances are optimized to meet standards and not actual use, especially when it comes to energy” (Bansal et al., 2011). The authors point to three experimental studies where the best performance of the appliances tested was at the same conditions as their respective standard.

New savings are realized when one considers waste heat streams available from each appliance that is not covered by the standards. The RF rejects internal heat from the cavity to adjacent air behind or beneath the unit. CWs and DWs can drain hot or warm water after each wash and rinse cycle. CDs vent moisture removed from wet clothing as hot, moist air via ductwork to the outside of the building. At the end of a baking cycle, a CO slowly dissipates high temperature thermal energy built-up in the cavity to the ambient air. Identifying the amount of heat available and their associated temperatures from these different waste streams can predict the amount of reuse possible through heat recovery.

### **1.3 Approach**

Early work on waste heat recovery of residential appliances used an RF condenser to preheat supply water to the water heater (Bansal et al., 2011). One study looked at DWs for waste heat recovery but reported a 13 year payback period (Bansal et al., 2011). Water recycling of the CW is one potential means of waste heat recovery. COs vent hot air with the potential for heat recovery (Bansal et al., 2011). One example is the CD exhaust has been used to preheat incoming cold air. A review on technological status of five major residential appliances; RFs, DWs, CWs, CDs and COs identify overall energy use can be reduced by more than, 50%, 17%, 43%, 50%, and 45%, respectively, through several strategies including waste heat recovery and legislative improvements (Bansal et al., 2011).

One barrier to the adoption of new, highly efficient appliances is third-party decision makers, developers, who purchase the equipment but do not pay the utility bills (Bansal et al., 2011). Creating a packaged, integrated appliance system for installation in new construction could appeal to developers with lower labor costs for installation and smaller dead volume in the building layout.

Having all appliances connect to a single, cold water supply, the installation is easier and thus becomes attractive to the installer. Additionally, the standard expectation of homes providing access to all five major appliances makes an integrated approach intuitive. The development of new appliances should be within a connected system instead of individual components operating independently.

To develop an understanding of the waste energy profile of household appliances, their standard operation and typical usage characteristics had to be captured. First, the total number appliances installed in the U.S. are identified. If available, a distinction is made between the different technologies available driving the appliance. For example, CD's heated by gas combustion or electric resistors. Next, the energy usage per appliance is reported as an annual or per cycle energy consumption. Sources listing appliances with only cycle energy consumption usage are combined with their respective usage rates to estimate annual energy consumption. Published or manufacturer data provides typical operational parameters of the appliance; volume and temperature of water being drained by the CW and DW, temperature and humidity of exhaust air by the CD, vapor compression cycle of a household RF, and the metal cavity mass of the CO.

A great point mentioned on implementing waste heat recovery for all appliances is the requirement of energy storage due to the intermittent nature of each appliance operation (Bansal et al., 2011). The authors indicate energy storage would need to be optimized for a range of temperatures; cooling, preheating, and reheating. While projections on energy savings utilizing waste heat recovery are up to 25%, more research is needed: an energy storage system supporting a range of temperatures across all appliances, and investigating the physical approach to extract or deliver heat to each appliance; a combination of HXs, piping, pumps and sensors interfacing with the energy storage system (Bansal et al., 2011). As a reference, the approach that is proposed can be seen in Figure 5. While the amount of sensors would be reduced in a commercial application, the amount of added components to each appliance is realized.

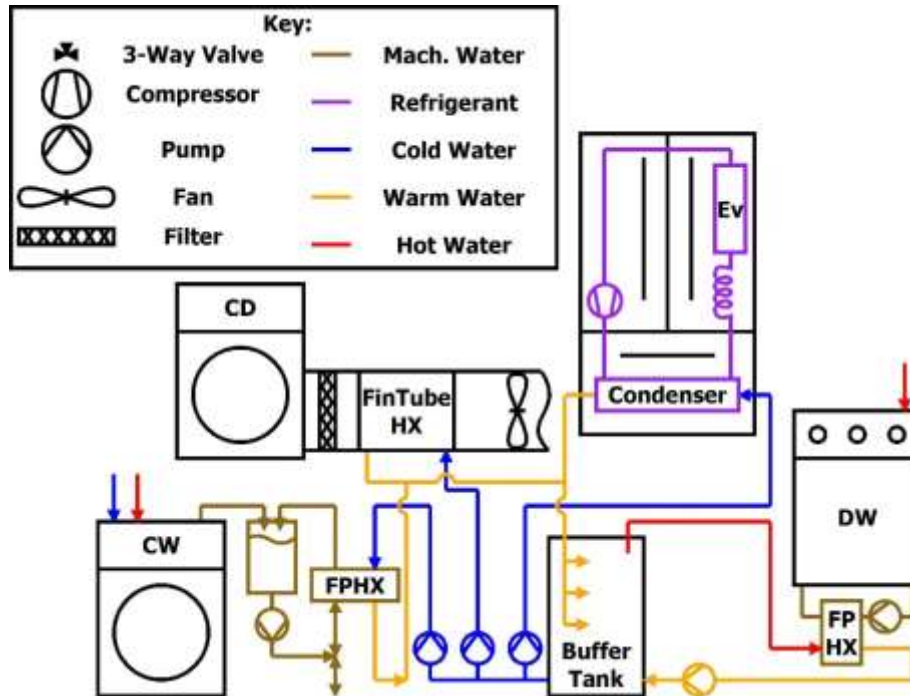


Figure 5: Schematic of Proposed Integrated Appliance Test Stand

#### 1.4 Objectives

To properly investigate thermally integrated appliances and provide useful recommendations, objectives are outlined. The first objective focused on conducting a theoretical and comprehensive analysis assessing the impact of thermal resource sharing between residential appliances through EES and Modelica models. Sub-models are created for each major appliance capturing its operation when running under the standard, standalone mode. Each appliance model can be compared to readily available experimental data collected by the manufacturer for quick verification.

The second objective used the conclusions obtained from this analysis as inputs to design and build a prototype system for an experimental investigation. The previously built Modelica models for each appliance are combined to create an integrated appliance model capturing the physical connections. The experimental data collected under a basic testing procedure is applied to the modeling simulation results to fine tune model inputs and validate results showing improved agreement. Simulations run on validated models estimate any energy savings from thermal integration and scope the requirements to achieve them.

The work culminates in a parametric study on the validated, integrated model by exploring the impact on appliance energy savings with variation in the thermal network temperature and the storage tank. Considerations can be made from multi-family or single-family housing units having different usage levels that are dependent on the respective consumer trends or behaviors from those sectors. The level of energy and operating costs reduced is identified for the respective different input factors to further map the system capabilities.

## 2. APPLIANCE BACKGROUND

The major residential appliances are identified as the clothes washer and dryer, cooking oven, dishwasher, and domestic refrigerator/freezer. From this list, each appliance is investigated thoroughly to identify a number of characteristics or features that define the scope of the appliance; the total number of units installed in the U.S., the frequency of use, and the different technologies driving the appliance function.

Residential lighting, appliances, and miscellaneous electric loads have grown to become significant fraction of total household energy (Eastment et al., 2006). These end uses are all heavily dependent on occupant behavior and product choices (Eastment et al., 2006).

An NREL study created a reasonable method to calculate energy savings for DWs, CWs, and CDs when comparing models with different efficiencies (Eastment et al., 2006). The specifications required are available on Energy-Guide labels, ENERGY-STAR® website, California Energy Commission's Appliance website and manufacturer's literature. The approach enables feedback on the impact of efficient appliances on the whole-building energy consumption. For example, the influence on the annual DW energy consumption from different DHW set-points or main water temperatures can be captured, and then savings by available DW models are compared using their associated efficiency ratings.

The introduction of microprocessors in appliances provides remote control to shift the demand during peak loads (Bansal et al., 2011). PCMs introduced into RFs allow load shifting to be safely used with minimal impact on the cavity temperatures.

### 2.1 Refrigerator-Freezers

Out of 113.6 million American homes, 113.4 are listed as using a refrigerator with 87 million having only one while 26 million have two or more (Table HC3.1 RECS, 2009). Two configurations are the most common: top-mount freezer accounts for 49% of all refrigerators while the side-by-side accounts for 34%. With RFs offering different configurations the fundamental

technologies still stands, a vapor compression cycle operates to maintain a cavity temperature by rejecting the heat to the ambient air.

### **2.1.1 Electrical Consumption**

In 2008 the median volume and annual electricity consumption for the top-mount freezer and side-by-side were 510 liter (18 ft<sup>3</sup>), 454 kWh and 710 liter (25ft<sup>3</sup>), 580 kWh respectively (Refrigerator Market Profile, 2009). A higher annual consumption of 660 kWh is projected when under certain test conditions specified by the Department of Energy (Table 2.1.16 Buildings Energy Data Book, 2011). The refrigerator size for this larger value is not mentioned and the test standard version is unknown, both of which would impact this estimated annual energy consumption. The current EPA Energy Star program requires a 10% reduction from the 2014 federal minimum standards (ENERGY STAR V.5, 2013). As an example, the maximum annual energy consumption under the current standards; a top-mount freezer with no icemaker and a rated capacity of 510 liter (18 ft<sup>3</sup>), can use 403 kWh for the federal standard and 363 kWh for Energy Star. For the other common configuration, a side-by-side with an icemaker and a rated capacity of about 710 liter (25 ft<sup>3</sup>), must have a maximum annual consumption of 705 kWh for the federal standard and 634 kWh for Energy Star. Comparing the median values from 2008 to the 2014 federal standard, a reduction of 11% is reported for the top-mount freezer, while for the side-by-side, an increase of almost 10% is found. One potential reason for the allowable increase for the side-by-side is having an icemaker puts the refrigerator into a different category for the federal standard, and thus provides a higher annual consumption to handle ice making.

### **2.1.2 Efficiency Ratings**

National Appliance Energy Conservation Act in 1987 mandated the Department of Energy to develop and maintain standards on RFs and freezers (Radermacher et al., 1996).

### **2.1.3 Cycle Characteristics**

Experimental data collected by the manufacturer during a standard DOE test run was obtained for a 750 liter (26.5 ft<sup>3</sup>) rated volume, side-by-side refrigerator with ice maker. Referencing an older Energy Star version, the refrigerator was certified with a 552 kWh annual energy usage falling under the federal standard of 737 kWh (references Model WRL767SIA\*0\* EnergyGuide Label)

How was this model selected to represent the experimental data?

Have two sets of data, SN33 with transducers, for GSS26C4XXW03. And a second data set, MM Data with System Specs.xlsx, that is from a similar unit with same compressor. See emails “Fw: SxS Test Data” from 02/11/2014 and “More Refrigeration Data” from 02/11/2014 for more details. Also, a compressor map for EGX70HLC was sent in an email, “Fw: Compressor Map” from 02/14/2014. Compare to the fit made on the other compressor used for the unit modified for TIRA testing.

The data was processed using EES to determine the heat transfer rates and COP of the refrigeration cycle (Klein et al., 2002). Many cycles of the compressor turning on and off are captured during the 48 hour test. The RF is also goes through a defrost cycle after about 18-19 compressor cycles. A calrod heater rated at 160W is run off a timer, lasting 10-30 minutes using 0.027 to 0.08 kWh. The ambient and refrigerated cavity conditions are relatively constant during the testing span and only one cycle is needed to understand the operation of the refrigerator. The ambient and freezer compartment (location of the evaporator) temperatures measured were 32.2°C (90°F) and -16.6°C (2.1°F) respectively. Air flow rates of 85 m<sup>3</sup>/hr. (50 CFM) and 68 m<sup>3</sup>/hr. (40 CFM) were assumed for the evaporator and condenser. Air side measurements were used to obtain an estimated heat transfer rate for each heat exchanger. The temperature difference across the evaporator was 3.9°C (7°F) providing about 148 Watts of cooling. For the condenser, the temperature difference was 5.6°C (10°F) requiring 256 Watts of heat rejection to the ambient. The measured power consumption of the entire refrigerator was 103 watts and the rated compressor displacement was 5.56 cm<sup>3</sup> (0.34 in<sup>3</sup>). Cooling and heating COPs were calculated to be 1.44 and 2.49 respectively. Using the ambient and freezer compartment temperatures for heat sink and source reservoir temperatures, a Carnot COP provides the ideal cycle efficiency for cooling and heating. Dividing the measured cooling and heating COPs by the Carnot COP generates a 2<sup>nd</sup> law efficiency temperature. The data shows a cooling second law efficiency of 27% and a heating second law efficiency of 40%. A refrigerator with the performance characteristics from the experimental data, 552 kWh per year, is referenced for the waste heat analysis. The number of units in the U.S is roughly 38.6 million from 34% of all refrigerators are side-by-side. The total annual energy consumption is therefore 0.077 EJ (0.073 quads) for all side-by-side refrigerators.

### 2.1.4 Controls

The overall control steps assumed for a basic RF are laid out in a flow chart seen on the left in Figure 6. Once the unit is plugged into a power source, it immediately starts monitoring the cavity temperature and compares it against the programmed thermostat temperature. This can be adjusted in some units by the end-user via a dial or programmed input. The HX fans are powered on before the compressor is activated. The diagram also indicates in the sequence when the pump driving the cooling loop would be activated. Once the compressor is ON, the controller checks both the cavity temperature and the defrost condition. If the cavity temperature reaches an OFF threshold, the unit is cycled OFF and continues to monitor the temperature until it reaches the ON threshold again, repeating the cycle. If the compressor is ON and the defrost condition becomes active, the RF goes into the defrost mode. A basic approach relies on a timer during which a calrod heater connected to the evaporator is powered ON diffusing heat and melting the accumulated frost. The duration is often a fixed value dependent on a frost rate as a function of compressor runtime. The right flow chart of Figure 6 shows a basic example of a timer based de frost controller energizing the calrod heater until a time threshold is reached.

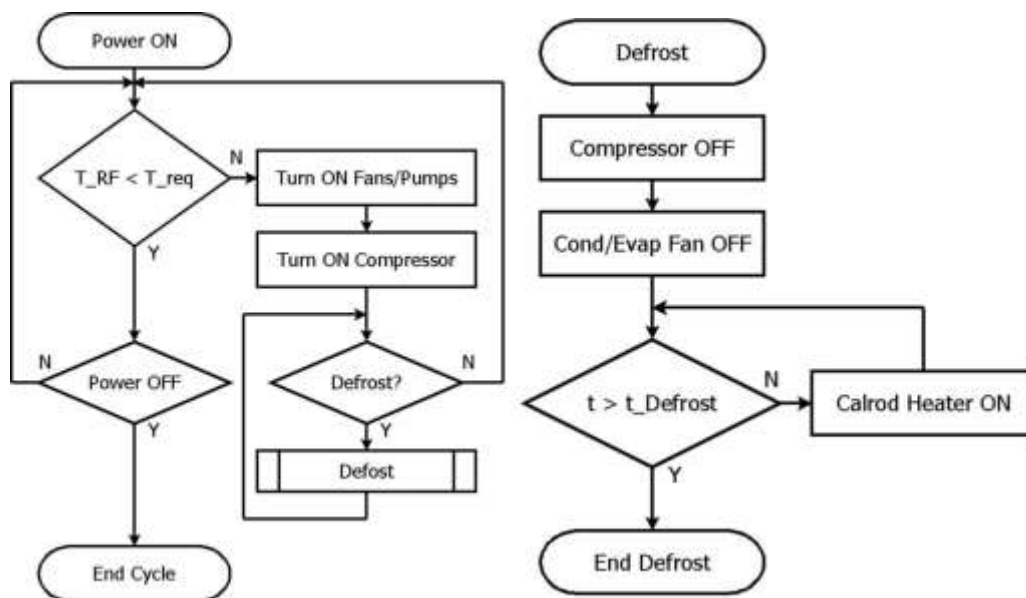


Figure 6: Overall Basic RF Temperature Control Flow Chart (Left) and Basic Defrost Timer Control Flow Chart (Right)

### **2.1.5 Energy Saving Methods**

The refrigerant used, methods to improve the refrigeration cycle efficiency (charge optimization, new compressors, Lorenz-Meutzner), decreasing the cabinet heat load (vacuum insulated panels), reducing parasitic electrical loads (high-efficiency fan motors), and reducing on/off cycling losses (preventing refrigerant migration, defrost) are summarized (Radermacher et al., 1996).

The combination of improved insulation levels, compressor efficiencies, and system optimization, led to energy savings of 25%, 33% and 42% respectively in a chest freezer in Europe (Bansal et al., 2011).

#### ***Refrigerant Migration***

A 4% reduction in the RF power consumption and increased cooling capacity was measured when preventing refrigerant migration during compressor off-cycle (Radermacher et al., 1996).

#### ***Replacement Refrigerants***

During an investigation for a replacement refrigerant for CFCs R11/R22, an HFC, R134a showed lower efficiencies by 4-10% (Radermacher et al., 1996). Hydrocarbons or ammonia due to their zero ozone depletion potential (ODP) are mentioned as an alternative replacement to HFC134a (Radermacher et al., 1996). R152a was also considered to replace R12 having a very low global warming potential (GWP) value compared to other replacement candidates but its flammability was a major drawback (Radermacher et al., 1996). Hydrocarbons such as, propane-R290, have superior transport properties while having comparable thermodynamic properties to CFC12 and 22 (Radermacher et al., 1996). The paper reports of isobutane, R600a, being used in Europe for domestic RFs and freezers with no automatic defrost (Radermacher et al., 1996). Isobutane is used extensively in residential refrigerators outside the U.S., especially in Europe (Bansal et al., 2011). The paper lists drop-in improvements of R290 or R600a having up to 2% improvement (Radermacher et al., 1996). HFC-134a has GWP of 1430 of CO<sub>2</sub> (Bansal et al., 2011). Legislation is being considered to phase out HFCs while they are already scheduled for phase out in Japan and Europe (Bansal et al., 2011). HFOs, R-1234yf or R-1234ze, have been identified by refrigerant manufacturers as replacements for HFCs (Bansal et al., 2011). Offer up to 5% efficiency

improvement with simple cycle modifications (Bansal et al., 2011). Further research is needed to improve HX and compressor efficiencies (Bansal et al., 2011). The U.S. RF market is driven by safety and liability and also has large units using 150-300g of charge (Radermacher et al., 1996). Worldwide, RF sizes are considerably smaller and have lower risks when paired with hydrocarbons (Radermacher et al., 1996). U.S. RFs rely on electric defrost providing another safety risk if hydrocarbons are used.

Correlations on the optimum refrigerant charge based on the capacity of the evaporator and condenser were suggested (Radermacher et al., 1996)-79. Another study explored the impact of the RF ambient temperature on the required charge level (Radermacher et al., 1996)-80. Assuming lower ambient temperatures required lower charge amounts, a water cooled condenser could provide additional environmental benefits from the low temperature heat sink with lower charge amounts. Due to safety regulations limiting the charge of hydrocarbons used in domestic systems, water cooled condensers could enable larger capacity RFs to use low GWP, natural, hydrocarbon refrigerants.

### ***Compressor***

Typical fixed speed compressors cycle often because they operate at 50% of their rated capacity, sized to satisfy a maximum load (Bansal et al., 2011). Cycling leads to losses and impacts overall RF performance. Linear compressors use very efficient linear electric motors, have improved valving and are oil-free, providing benefits over existing reciprocating compressors (Radermacher et al., 1996). Recent advances on oil-free linear compressors have improved the overall RF energy efficiency by 30% (Bansal et al., 2011).

### ***Cabinet***

Vacuum insulated panels, VIPs, were in production over 20 years ago but at that time cost were high (Radermacher et al., 1996). In the mid-1990s, an experimental study on VIPs established an energy savings up to 20.4% depending on the area covered of the RF while recent studies show up to a 25% savings (Bansal et al., 2011).

### ***Fans***

Introducing high efficiency fans requiring only 2-5 watts from a current level of 10-15 watts (Radermacher et al., 1996). Fans within RFs are still reported to 12 W for the evaporator, and 9 W for the condenser while electronically commutated motors, ECMs, only need 2-5 W (Bansal et al., 2011). While readily available, the market penetration of RFs is 50% of evaporators fans and 20% of condenser fans (Bansal et al., 2011). 10% of overall RF energy use can be attributed to the fans (Bansal et al., 2011).

### ***Defrost Control***

RFs have been tested using variable defrost control systems relying on a prediction based off daily energy consumption (Radermacher et al., 1996). While this in practice works well, there is significant opportunity on improving the efficiency of adaptive defrosting with a frost detection sensor (Bansal et al., 2011). Defrost RFs commonly use electrical heater on the evaporator operated by a timer (Radermacher et al., 1996). A further improvement on the energy penalty from defrosting is to cycle the heater on and off and thus minimize the total temperature rise in the cabinet to reduce the post defrost cooling demand (Bansal et al., 2011).

### ***Different Cycle Configurations***

Different approaches on cooling the two RF cavities separately with energy savings from 20% to 40% were reported but introduced more components; a second compressor, a second evaporator, adding to the cost (Radermacher et al., 1996).

Control valve supplying refrigerant to one of two evaporators, with separate capillary tubes report an energy savings over a single-stage RF (Radermacher et al., 1996).

18% improvement on two evaporators in series with cooling controlled to either RF cavity by activating the respective fan (Radermacher et al., 1996).

## ***Alternative Refrigeration Technologies***

Absorption, thermoelectric and Stirling cycles have all been investigated as alternative refrigeration systems (Radermacher et al., 1996). A later review of RF research found eight alternative refrigeration technologies investigated; absorption, adsorption, magnetic, Malone cycle, Stirling/Pulse tube, thermoacoustic, thermoelectric, and thermo-tunneling (Bansal et al., 2011). Only two refrigeration technologies, thermoelectric and magnetic, are mentioned having promise for energy or environmental benefits but require significant breakthroughs to become cost competitive with vapor-compression (Bansal et al., 2011).

### **2.2 Dishwasher**

The market penetration of dishwashers in U.S. households is not as high as other appliances. About 59% or 67.4 million households use a dishwasher (Table HC3.1 RECS, 2009). 65% of U.S. households use DWs accounting for 3.2% of the 2005 residential primary energy consumption (Bansal et al., 2011). Water savings are obtained over traditional hand washing by recirculating same volume of water to remove soils. A calrod heater provides energy input to water to indirectly heat the dishware and cabinet.

#### **2.2.1 Usage Frequency**

The largest number of dishwashing cycles per year is listed at 365 or one per day (Table 2.1.16 Buildings Energy Data Book, 2011). The current Energy Star rating for dishwashers reduced the average, annual number of cycles from 264 to 215 (ENERGY STAR V.6, 2015). From the housing survey, 104 cycles per year covers 67% of all households using dishwashers while higher usage rates, 208 cycles per year only covers 35% (Table HC3.1 RECS, 2009). For a conservative estimate, 215 cycles per year is selected for dishwasher usage covering 35% or 23.7 million households. From the Building America Performance Analysis Procedures, the number of DW cycles per year is dependent on the number of bedrooms in the home,  $N_{br}$ , and the capacity of place settings shown in Equation 1 (Eastment et al., 2006).

$$N_{DW} = 215 * \left[ 1/2 + \left( \frac{N_{br}}{6} \right) \right] * \frac{8}{\text{place setting capacity}} \left( \frac{\text{cycles}}{\text{yr}} \right) \quad (1)$$

### **2.2.2 Electrical Consumption**

To capture the energy impact associated by DWs, three types are categorized based off the water connection and the use of an internal heater; only hot water connection with no internal heating, only hot water connection with internal heating, only cold water connection with internal heating (Eastment et al., 2006).

The energy usage of a dishwasher is heavily weighted by the required heating energy to maintain the water temperature at a high temperature of around 50°C (122°F). One study on dishwasher energy usage reports 88% of a dishwasher cycle energy input of 1.05 kWh is used for heating the inlet water, the dishes and cookware, and the physical cabinet of the appliance (Persson, 2007). Another source that does not include the energy required for water heating lists an annual energy consumption of 120 kWh or by including the associated 365 cycles per year, the energy usage per cycle is 0.33 kWh (Table 2.1.16 Buildings Energy Data Book, 2011). When considering Energy Star requirements, a standard size dishwasher cannot use more than 270 kWh per year or 1.26 kWh per cycle with 215 cycles per year (ENERGY STAR V.6, 2015). And for a compact dishwasher (less than 8 place settings) the annual energy usage must be less than 203 kWh or 0.94 kWh per cycle. A standard size, Energy Star dishwasher with 215 cycles a year, is selected by referencing an annual energy consumption of 270 kWh. With 23.7 million households, the total annual energy consumption of a standard, Energy Star dishwasher is 0.023 EJ (0.022 quad).

### **2.2.3 Water Consumption**

The amount of water used by the dishwasher per cycle is listed in one study at 10.2 liter (2.7 gal) per cycle (Persson, 2007). The current Energy Star requirements for a standard size limits water usage to 13.2 liter (3.5 gal) per cycle and for a compact dishwasher, limits usage to 11.7 liter (3.1 gal) per cycle (ENERGY STAR V.6, 2015). Minor losses of water volume to the ambient through evaporation and being trapped in the dishwasher on cookware or in the sump for the pump are all neglected. The water usage of a standard, Energy Star dishwasher is used for the volume of waste water available. With a working water temperature around 50°C (122°F) being maintained by the internal electric heater, assuming some but minimal losses, result in an estimated drain temperature of 40°C (104°F).

### 2.2.4 Cycle Characteristics

A study was conducted on the DW electric heater developing a mathematical model capturing the variation associated with power input, geometry, and operating strategy (McDonald et al., 1989). During a DW drying cycle the calrod heater is exposed to air, becoming red-hot, reaching temperatures near 1300°F (980°C) (McDonald et al., 1989). As a result the resistance increases with temperature and reduces the power output of the heater as Equation 2 identifies. Parameters for heaters used by one U.S. DW manufacturer are, 0.135 in nominal diameter, power outputs of 600-800 Watts, and heat fluxes from 14-28 W/in<sup>2</sup> (McDonald et al., 1989). European DW versions have higher nominal power due to higher supply voltages but with longer lengths, the surface areas are also larger resulting in comparable heat fluxes, 19-39 W/in<sup>2</sup> (McDonald et al., 1989).

$$W_{elec} = \frac{E^2}{R} = \frac{E^2}{R_o[1+\alpha(T-T_o)]} \quad (2)$$

The water sump temperature and power consumption during a sample DW cycle with a soil sensor is shown in Figure 7. Two different power levels are easily recognized in the graph; one during the water heating periods of the cycle, ~800 W, the second during the drying portion when exposed to air, ~500 W. The control of the electric element pulses the power supply to maintain a safe element temperature and prevent any localized temperature extremes deformations or damaging the DW tub or cabinet.

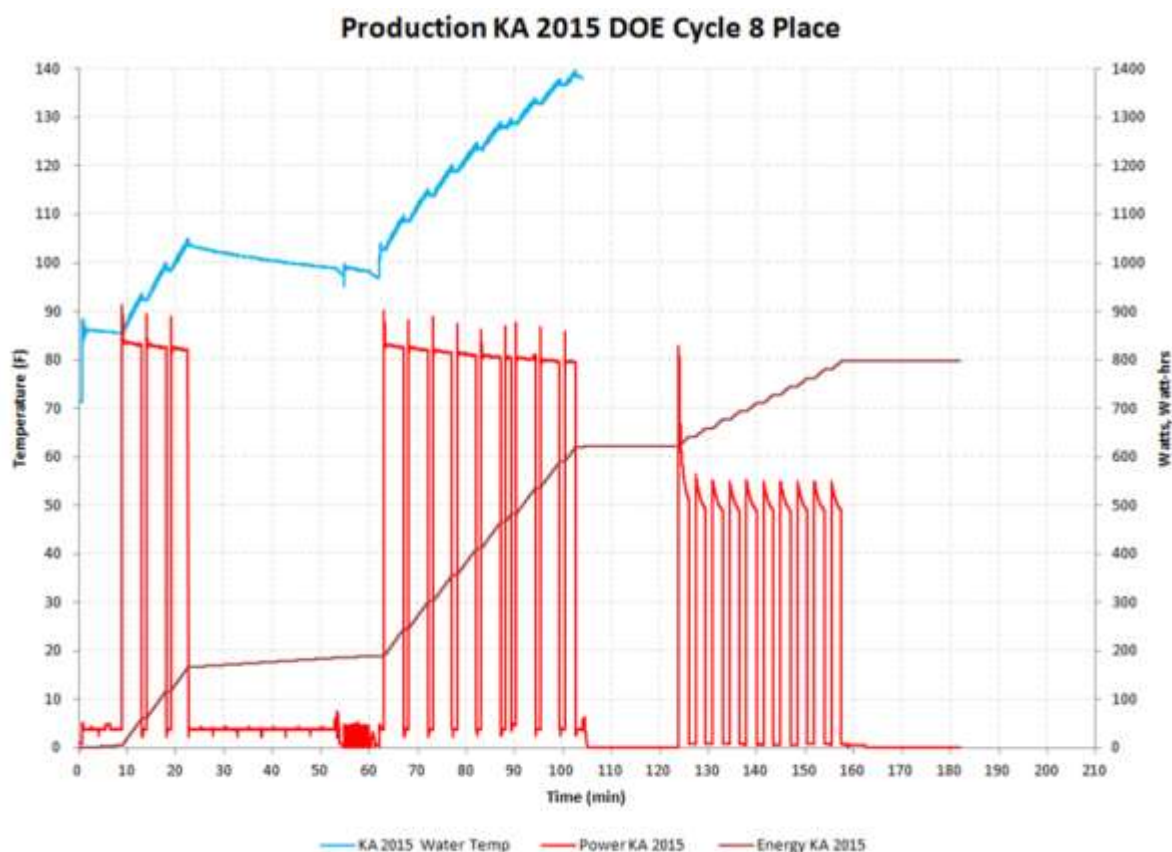


Figure 7: Example DW Sensing Wash Cycle with Sump Temperature and Power Consumption (Whirlpool Corp. 2017)

The thermal capacity for one heater was obtained by closely matching experimental data, temperature versus time, and in this study, the best match was found with 145 W-s/K (McDonald et al., 1989). The authors report for an 800 Watt heater, 619 Watts or 77%, is transferred by radiation and remaining 181 Watts, or 23% by convection (McDonald et al., 1989). Three curve-fits provide the heater temperature, convection heat flux, and fraction of heat flux transferred by radiation, all dependent on the surface heat flux (McDonald et al., 1989). Within the sample cycle shown, Figure 7, 0.8 kWh of electricity is consumed where; ~0.17 kWh heated the wash water volume from 85°F (29°C) to 105°F (40.5°C), ~0.43 kWh heated the rinse water volume from 98°F (37°C) to 140°F (60°C), and ~0.18 kWh for drying the dishware (Whirlpool Corp. 2017). The DOE energy efficiency rating requires accounting for the energy delivered to the DW in the hot water volume, which is not included in the 0.8 kWh cycle total.

The temperature rise in the DW water during the wash and rinse steps can be used to estimate a lumped thermal capacity of the system including the dishware. By taking the total amount of energy delivered during a heating step and dividing by the change in the system or DW water sump temperature, a lumped thermal capacity is found. For a different set of experimental data, ten heating cycles are identified and ten values of thermal capacity are calculated. Figure 8 is plot of the calculated thermal capacity versus the starting temperature of the water sump.

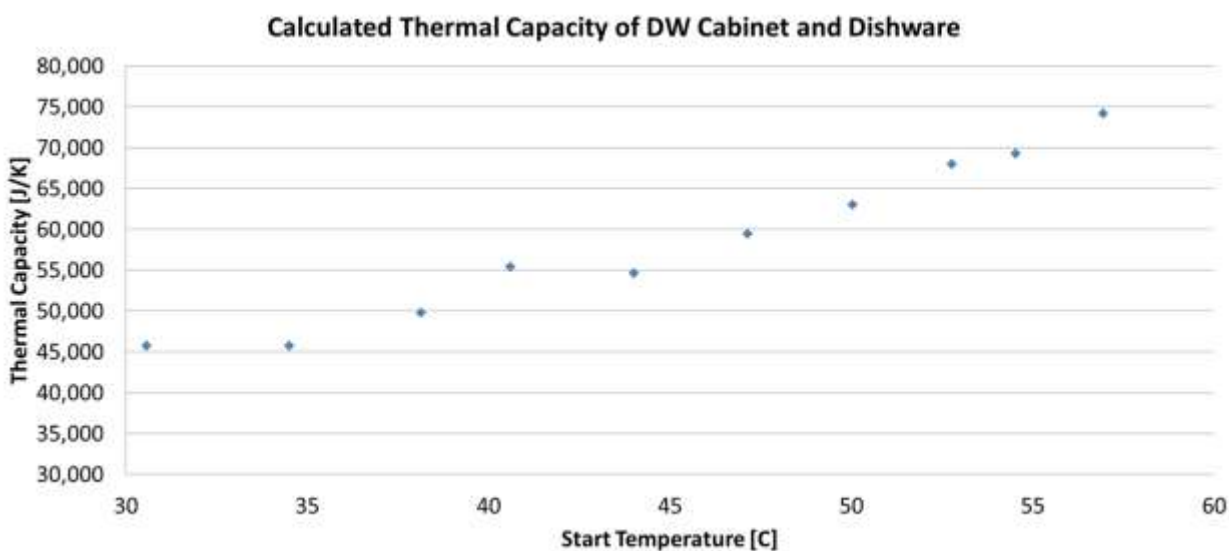


Figure 8: Calculated Thermal Capacity of Entire DW during Water Heating Cycles as a Function of the Starting Water Temperature

### 2.2.5 Controls

A sample DW cycle, Figure 7, was referenced to build a sequence of operations the appliance controller follows. A step was identified by having a unique function for a fixed duration within the cycle. The experimental cycle data obtained from the manufacturer was found to have 8 unique steps possible within one DW cycle, see Figure 9. Depending on the region in the world where the DW is used, some of the steps listed are not used. For example, European DWs do not use a heated dry function and therefore would skip this step in the cycle.

The prewash step draws the initial volume of DHW for the cycle, circulating around the appliance using one spray arm at a time. An optical sensor checks the turbidity of the water in the sump to decide if a new batch of water is needed before proceeding into the main wash. If the amount of soils removed during the prewash is high, the sump is drained to reduce the rate of soil redepositing

on the dishware during the main wash. Next the electric element is energized to heat the water in the sump to the required wash temperature, 40.5°C (105°F). The wash performance is improved at higher temperatures. After reaching the set-point, the DW uses the mechanical action of the spray arms for the main wash by pumping the water. A diverter oscillates the pump outlet to operate one spray arm at a time on each rack. Water reductions required by federal standards have reduced the volume allowed over the whole cycle and not enough volume of water is available to run both spray arms at the same time. The main wash terminates after a timer expires and proceeds into a pre-rinse step. The main wash water is drained and a smaller volume of DHW is drawn to lightly rinse the dishware, removing any soils redeposited from the main wash. Depending on the DW technology for the specific model, this may occur more than once before the rinse step is entered. The electric element is again energized during the rinse step but this time a water sump temperature of 60°C (140°F) is the set-point. One purpose of the high rinse temperature is to raise all the dishware to a high temperature which improves the drying performance by starting the system at elevated temperatures. The rinse water is drained and the DW controller enters the drying steps. A short timed delay to let any water drip off the dishes. The electric element is used one last time to accelerate the drying process and runs for a fixed time interval. The last step holds to air dry the dishware by letting the residual heat remove any remaining moisture.

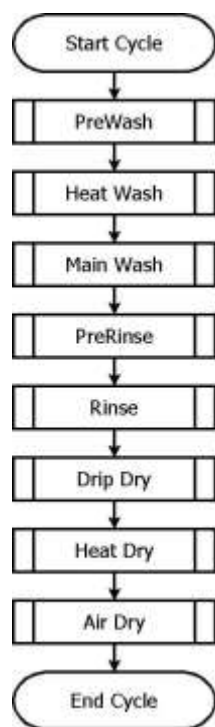


Figure 9: Overall DW Control Flow Chart

### **2.2.6 Energy Saving Methods**

An energy savings of 20% over a residual heat drying system is reported from a DW assisted by sorption (Bansal et al., 2011)-45. The Super Efficient Home Appliances Initiative promotes a DW using a maximum 295 kWh/year and 16L/cycle of water (Bansal et al., 2011). A couple recommended areas of improvement are adaptive control sensing the soil level, improving the food filter to reduce redepositing, using ECM motors, higher levels of cabinet insulation, and an improved dry cycle (Bansal et al., 2011).

#### ***Sense Soil Level***

Depending on the level of soil on the dishware, a soil sensor coupled with filtered recirculation can help reduce unnecessary purges of wash water. A prewash will circulate water to remove any locations with large soil levels and accumulate in the DW sump. Here an optical sensor checks the turbidity of the water and determines if a new batch of water is needed to reduce the rate of soil redepositing before proceeding to the main wash. The DW is able to reduce the volume of water used per cycle by adjusting to the type of load.

#### ***Reuse Waste Water***

As explained previously, Federal standards on DWs regulate both the amount of energy used (including energy required to heat DHW volume) and the volume of water consumption. One approach investigated storing the previous cycle final rinse for the next cycle prewash. Here the DW can reduce the total volume of DHW needed per cycle and thus reduce the associated energy and water penalty. The approach is effective when assuming fairly clean water produced at the final rinse can provide useful cleaning during the highest expected soiled wash step. The concern for redepositing of soils from the previous final rinse is not significant due to the already high expected presence of soils on the dishes. The estimated energy savings from this approach is not quantified.

#### ***Alternative Heating Sources***

Two different approaches were applied to reduce the electricity consumption by offsetting some or all of the internal resistor heating energy (Persson, 2007). The first explored varying the hot

water supply temperature. By increasing the DHW temperature from 49C (120F) to 65C (149F), the amount of electricity can be reduced by 19%, 0.8 kWh to 0.65 kWh with the entire cycle still using about 1.2 kWh of energy in total. The other approach applied an external water loop as a heat source to the internal water and dishware through a custom designed and built HX. Above loop temperatures of 70C (158F), the amount of electricity used plateaus to about 0.1 kWh while around a loop temperature of 50C (122F), about 0.6 kWh of electricity is predicted. Both conditions use similar amounts of total energy, combined electrical and thermal, for the entire cycle.

## **2.3 Clothes Washer**

More than 80% of U.S. households have clothes washers, consuming 3.7% of total residential primary energy (Bansal et al., 2011). The total number of U.S. households having a clothes washer is 93.2 million homes, slightly higher than the number of households with clothes dryers (Table HC3.1 RECS, 2009). In general CWs are first broken down into two designs dependent on the orientation of the drum, vertical axis, VA, top loading, or horizontal axis, HA, front loading (Bansal et al., 2011). The dominate CW orientation is regionally dependent. In Australasia, Canada, the U.S. (81% of all CW), and Latin America the VAs are popular while in Europe and the Middle East, HA dominate the market (Bansal et al., 2011). Another approach classified CWs into four types based off the water connections and use of an internal, electric heater; both hot and cold water connections with no internal heating, both hot and cold water connections with no internal heating but with thermostatically controlled valves, both hot and cold water connections with internal heating, and lastly, having only a cold water connection with internal heating (Eastment et al., 2006).

### **2.3.1 Usage Frequency**

Many sources were found for the number of wash cycles per year. The smallest value reported was 289 for North American in a worldwide study of washing machine usage which is close to the number of dyeing cycles assumed (Pakula et al., 2010). The largest value mentioned, 1.21 loads per day or 442 cycles per year, was obtained from a two-month, field demonstration in Bern, Kansas comparing vertical and horizontal washing machines (Tomlinson et al., 1998). One value was found in two reports, 392 cycles per year, from the Texas Water Development Board and the DOE

(7.2 Residential Clothes Washer, 2013) (Table 2.1.16 Buildings Energy Data Book, 2011). A final source provided a breakdown of the number homes for a range of loads per week (Table HC3.1 RECS, 2009). Converting the weekly total to a yearly value, 43.9 million households use the washing machine at least 260 to 468 cycles per year versus 84.9 million homes using it at least 104 to 208 cycles per year. To be conservative on estimating the waste energy source, assuming an annual number of 289 wash cycles covers at least 43.9 million households and is larger than the annual number of drying cycles assumed.

From the Building America Performance Analysis Procedures, the number of CW cycles per year is dependent on the number of bedrooms in the home,  $N_{br}$ , and the test load weight, TLW, as shown in Equation 3 (Eastment et al., 2006).

$$N_{CW} = 392 * \left[ 1/2 + \left( \frac{N_{br}}{6} \right) \right] * \left( \frac{12.5 \text{ lbs}}{TLW \text{ (lbs)}} \right) \left( \frac{\text{cycles}}{\text{yr}} \right) \quad (3)$$

### 2.3.2 Electrical Consumption

The energy consumption per cycle of clothes washers is sometimes reported with the energy required for generating the hot water used during the wash cycle in spite of the energy being spent externally to the appliance. Low average wash temperatures for North American result in low energy consumption levels due to reduced energy required for heating water, 0.43 kWh per cycle (Pakula et al., 2010). Annual energy consumption at this level with 289 cycles is 124 kWh. On the same magnitude, 110 kWh is reported when excluding energy required to heat water used by the appliance (Table 2.1.16 Buildings Energy Data Book, 2011). If the water heating energy is included, a top loader had an average, measured energy consumption of 2.26 kWh per cycle and a front loader had 0.96 kWh per cycle (Tomlinson et al., 1998). Following the same procedure with 289 cycles per year, the annual energy consumption is 653 kWh for top loading washers and 277 kWh for front loading. Considering only top loading washers covering 76 million households, the total annual energy usage when including water heating energy (653 kWh/yr) is 0.18 EJ (0.17 quad) or excluding water heating energy (110 kWh/yr) is 0.03 EJ (0.028 quad).

### 2.3.3 Water Consumption

The waste stream of clothes washers is the elevated temperature water at the drain of the appliance. To accurately determine the amount of energy available, the volume of water drained and the associated temperature is required. The type of washing machine greatly impacts the volume of waste water leaving due to the different methods employed to agitate the clothing. Top loading washers require larger volumes of water to achieve the desirable cleaning performance compared to front loading machines. With a significant number of CW in the U.S. being top loaders, a value of 144 liter (38 gal) per cycle is provided from one study (Pakula et al., 2010). The extensive field demonstration is able to identify average water usage per cycle for top loaders at 157 liter (41.5 gal) covering a range of 68 liter (18 gal) to 227 liter (60 gal), and for front loaders at 98 liter (25.8 gal) covering a range of 64 liter (17 gal) to 140 liter (37 gal) (Tomlinson et al., 1998). One report lists top loaders at 155 liter (41 gal) per cycle and high-efficient CW between 42 liter (11 gal) and 95 liter (25 gal) per cycle (7.2 Residential Clothes Washer, 2013). A water usage of 155 liter (41 gal) per cycle from top load washers is assumed due to the large percentage, 81%, of all U.S. washing machines used.

### 2.3.4 Efficiency Ratings

The remaining moisture content, RMC, of the clothes at the end of a wash cycle reduces the amount of water supplied to the appliance from making it down the drain. The type of clothes, load size, and maximum spin speed of the washer all impact the RMC. Front load washers operate at much higher spin speeds and result in lower RMC values than their top load counterparts. Comparing the total volume of water remaining in the clothes to the total volume of water used during the entire cycle results in a small percentage, 2-5%, of total volume left in the clothes. Thus the impact of the RMC on the energy available in the waste stream will not be accounted for.

A water factor rating is for CWs captures how water efficient the appliance is relative to the amount of clothes the tub can hold. The value is calculated by dividing the volume of water needed to wash a full load in gallons by the capacity. A standard CW has a 13.3 gallon/ft<sup>3</sup> rating while a tier 3, high efficiency CW has a 4.0 gallon/ft<sup>3</sup>.

### 2.3.5 Cycle Characteristics

The other piece of information needed on the waste stream is the temperature of the water being drained. Two separate steps occur during the entire washing machine cycle, a wash and then a rinse step. 48% of households report selecting warm water, wash cycle and 46% select a cold water wash (Table HC3.1 RECS, 2009). For rinsing, a large majority, 80% of households, report selecting cold water rinse. Similar trends are presented in another study with 58% to 67% of all washing machine cycles using a warm water wash, cold water rinse (Tomlinson et al., 1998). While for a hot water wash, and cold water rinse, the same study showed higher percentages of all washing machine cycles, 17% to 25%. To associate the relative terms: cold, warm, and hot water with temperatures, typical housing water supply temperatures and experimental data from the manufacturer were referenced. Cold water typically is around ground temperatures and is assumed to be 12.8°C (55°F). Hot water supply temperature depends on the water heater set-point used by the homeowner and is assumed to be 49°C (120°F). Appliance testing data from the manufacturer identified warm water used during the wash step at a temperature of 36°C (97°F). The variation of the CW wash and rinse settings as a percentage of all loads is shown in Figure 10. Three different sets of data are plotted. Two are from a study replacing VA with HA CWs and the third references DOE test standards for the time period.

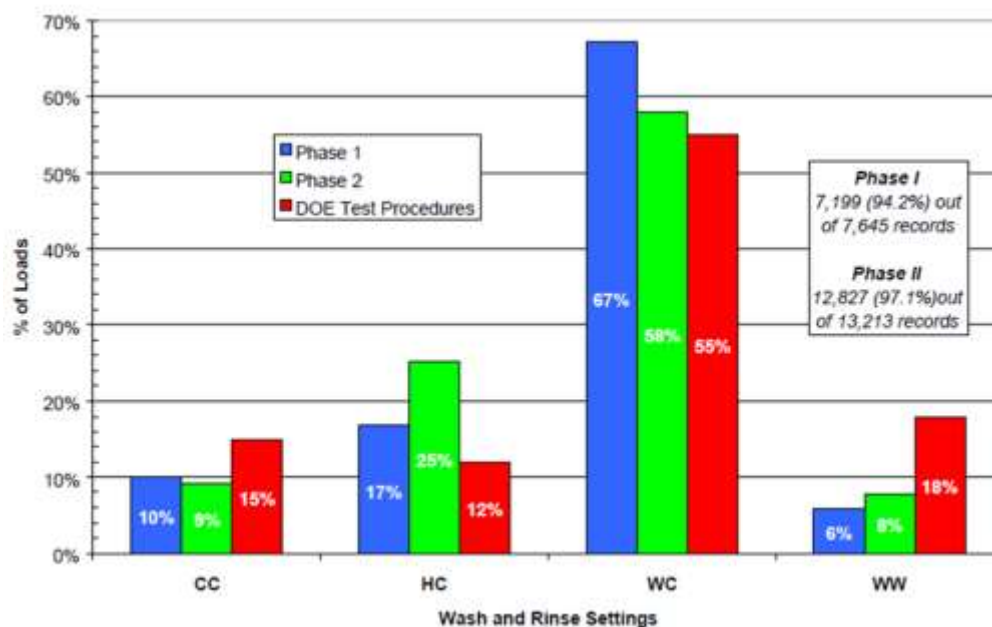


Figure 10: Profile of CW Wash and Rinse Temperature Settings from a VA and HA Study Compared to the Department of Energy Test Procedure (Tomlinson et al., 1998)

### 2.3.6 Controls

A sequence of operation is built for the CW around wash and rinse steps in one cycle. Similar steps are labeled with the same controller. The flow chart outlining the overall control strategy for a CW is listed in Figure 11. One CW cycle goes through two fill steps, two drain steps, two spin steps, and a wash or rinse step corresponding to control on the drum for agitating.

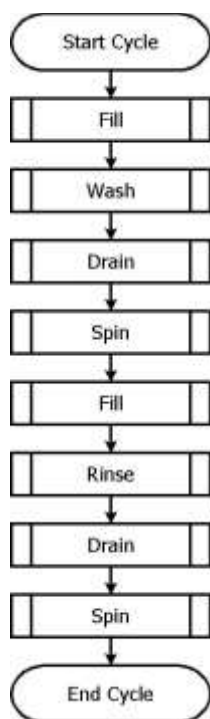


Figure 11: Overall CW Control Flow Chart

### 2.3.7 Energy Saving Methods

Various efforts have been made to improve the energy efficiency of CWs. The focus primarily is around water usage, both the volume and temperature level. Advancements have improved load detection and wash performance enabling the machine to clean with less volume. Using detergents rated for colder water temperatures and external heat sources have reduced CW energy consumption attributed to elevated temperatures. One indirect benefit of increasing the water extraction efficiency of CWs is through reductions in the CD per cycle energy consumption.

### ***Water Temperature***

Majority of CW energy consumption is attributed to the hot water required for the cycle versus the electric motor (Bansal et al., 2011). The quickest savings is to improve the wash performance at lower temperatures. In Europe, research into more efficient detergents has generated significant reductions of CW energy consumption (Bansal et al., 2011).

One study investigated the impact of varying the supply, hot water temperature on the CW electricity consumption. The energy used for the cycle is identified as a combination between electrical and thermal, fluctuating depending on the wash temperature setting and supply, hot water temperature (Persson, 2007). If 60C water is delivered to the CW for a 40C wash temperature, 0.173 kWh of electrical energy is used with 0.783 kWh of thermal energy from the hot water for a cycle. In contrast, by supplying 15C water and thus simulating a cold water supply connection, the use of the internal heater raises the electrical consumption to about 0.52 kWh, accounting for the entire cycle energy use. Hot water fed CWs have the possibility to make use of heat normally wasted and reduce the amount of electricity used per cycle. The benefit becomes mitigated when the wash setting uses only cold water and amplified for very hot wash settings.

### ***Water Extraction***

HA CWs are more efficient than their VA counterparts. Less water and detergent is used, wash performance is higher, and they allow faster spin speeds leading to reduced CD energy consumption (Bansal et al., 2011). Speeds of 1200 RPM are common with new models in Europe reaching speeds of 1800 RPM and in some units, 2000 RPM (Bansal et al., 2011). VA advancements have begun to reach efficiency levels comparable to levels attained with HAs. Using up to 18 gal (68 L) per cycle, improved wash performance, and have higher speed spin cycles resulting in energy cost savings up to 50% (Bansal et al., 2011).

### ***Microprocessor Introduction***

Introduction of microprocessors on CWs have led to 20% reduction of motor electricity and hot water use through detection methods on load size and wash temperature (Bansal et al., 2011).

### ***Wash Performance***

While additional testing is needed, bubble-action cleaning combining air bubbles and swirling water are reported to leave clothes 20% cleaner and may achieve up to 30% savings in water use, hot water, and detergent (Bansal et al., 2011).

### ***Alternative Heating Sources***

Prior work considered explored technologies requiring expensive deviations from the existing appliance. The advancements considered were, heat from another source outside the appliance, heat pump driven internally to the appliance, and even the combination of several appliances. To consider an easier and hence cheaper alternative, the authors experimentally investigate using an HX to extract heat from the ambient to preheat the cold water supply into the appliance. An internal heater energizes after a set-timer and cycles ON-OFF maintaining a wash water temperature. The final temperature before heating is the objective parameter to determine energy savings by the heater. The design maximum water temperature of the cycle is 95°C (203°F). Slow water flow rates through the HX produce low HTC due to the laminar flow (1E-2 kg/s). Traditionally, air-side HTCs are the dominate resistance in air-to-liquid HXs. This results in the relatively modest increase in water temperature given higher air-side flow rates (5.6E-2 m<sup>3</sup>/s to 17E-2 m<sup>3</sup>/s). To address this modest increase, an additional pump is added to provide higher water flow rates (8.5E-2 kg/s). Also a different type of fin, a slit-fin, is explored to address the limiting factor on the air-side HTC. The highest predicted energy savings came with the slit-fin HX having the highest water and air flow rates, ~6% of the total baseline energy usage. (Park, J.S. et al. 2009 ).

### ***Miscellaneous***

Other areas mentioned on future research into energy saving advancements for CWs are component upgrades (increased thermal insulation, reduced thermal mass, high efficiency direct-drive motors), lower water consumption (spray rinse, recirculation), and improved wash performance (drum redesign, plastic particle cleaning, ultrasonic washing) (Bansal et al., 2011).

## 2.4 Clothes Dryer

Over 80% of U.S. households have CDs that account for 4.2% of the total, residential primary energy consumption (Bansal et al., 2011). CDs can be separated into air-vented or condensing units (Bansal et al., 2011). Most CDs in the U.S. are vented by which removed moisture from wet clothes is ducted out of the appliance and blown outside the home. Alternatively, vent-less CDs actively condense removed moisture out of the exhaust airstream using a heat exchanger allowing cooled exhaust be vented directly inside the home. Vented CDs can use the two available heating technologies, electric or combustion driven (Eastment et al., 2006). Within electric CDs, different fundamental technologies exist generating the heat source, conventional electric element or heat pump (vent-less). The number of U.S. households that use a dryer at home is 90.2 million, out of 114 million households, with 80% (71.8 million) having electrically heated ones versus 20% using natural gas (17.5 million) or propane/LPG (1.0 million) (Table HC3.1 RECS, 2009). Only electrically heated clothes dryers are considered due to the small percentage of combustion heated dryers.

### 2.4.1 Usage Frequency

Due to the function of some appliances, they can influence the usage frequency of other, related appliances. Here the clothes washer usage rate has a direct factor on the rate of use of the clothes dryer. 74.4 million households report the dryer is used every time clothes are washed which provides some insight to the correlation between clothes dryer and washer usage (Table HC3.1 RECS, 2009). Other considerations such as clothes type or time of year can reduce dryer usage when air drying is desired. One approach to estimate annual frequency of dryer use is to assume some percentage of the total annual washer use, where 100% or 1.00 reflects every load washed produces a dryer cycle. Any percentage below 100 considers some washed loads to be air dried versus mechanically dried by the appliance. From the Building America Performance Analysis Procedures, the number of CD cycles per year is dependent on the number of CW cycles per year,  $N_{CW}$ , and the dryer use factor,  $DUF$ , which is assumed to be 0.84 from DOE test procedures (Eastment et al., 2006). The approach is shown in Equation 4.

$$N_{CD} = N_{CW} * DUF \left( \frac{cycles}{yr} \right) \quad (4)$$

Until the DOE test procedure was adjusted in 2011, the number of drying cycles a year was assumed to be 416 (ENERGY STAR, 2011). With new data on usage characteristics from housing surveys, the number of cycles a year was adjusted to 283, or 32% less (Table HC3.1 RECS, 2009). This number is also lower than the assumed 359 cycles per year by the DOE, (Table 2.1.16 Buildings Energy Data Book, 2011).

### **2.4.2 Electrical Consumption**

The electrical consumption of clothes dryers depends on a number of inputs; some are specified by user settings on the interface of the appliance and the others depend on the moisture content of the clothes. Different drying cycles can be run: permanent press, delicates, or auto-termination using moisture detection. Low, medium or high temperature heat settings can be selected. The moisture content of the clothes being loaded directly correlates with the required heating energy to evaporate and remove all the stored water. The type of clothing, the amount of clothes or load size, and the water extraction efficiency of the washing machine all determine the clothing moisture content. While all these factors directly impact the amount of heating energy delivered by the electric resistor, the motor electricity consumption will be relatively constant regardless of dryer inputs. One source reports an annual electric consumption of 1000 kWh for electric dryers (Table 2.1.16 Buildings Energy Data Book, 2011). Referencing the previously mentioned 359 cycles per year by the Buildings Energy Data Book, the average power consumption is estimated at 2.78 kWh per cycle.

### **2.4.3 Efficiency Ratings**

CDs are often rated by their moisture extraction rate, MER, a ratio of the drying energy used divided by the wet clothing weight at the start of the drying cycle.

### **2.4.4 Cycle Characteristics**

A typical CD can run a range of different cycles depending on the user settings selected. Each type of cycle can have different fixed settings such as duration or heat level or can be custom run allowing the user to modify the length or air temperature desired. The unknown load, clothing type and moisture level, put into the CD for drying combines with the drying settings for the cycle to output an exhaust airstream profile varying in temperature and relative humidity during the entire

cycle. With a wide-range of clothing load inputs available and a number of possible combinations for the cycle controller, experimental data with CD exhaust air conditions presents an example CD cycle for the waste heat analysis. An electric clothes dryer is first monitored and recorded with no modifications to develop a baseline operation before running different failure mode tests as a safety evaluation (Butturini et al., 2004). Two plots identify the baseline operation for measured temperatures at various locations throughout the dryer starting from the ambient air intake to the exhaust air (Figure 12), as well as the relative humidity of the ambient, interior cabinet, and exhaust (Figure 13). The parameters of interest here are the exhaust air temperature and relative humidity leaving the appliance.

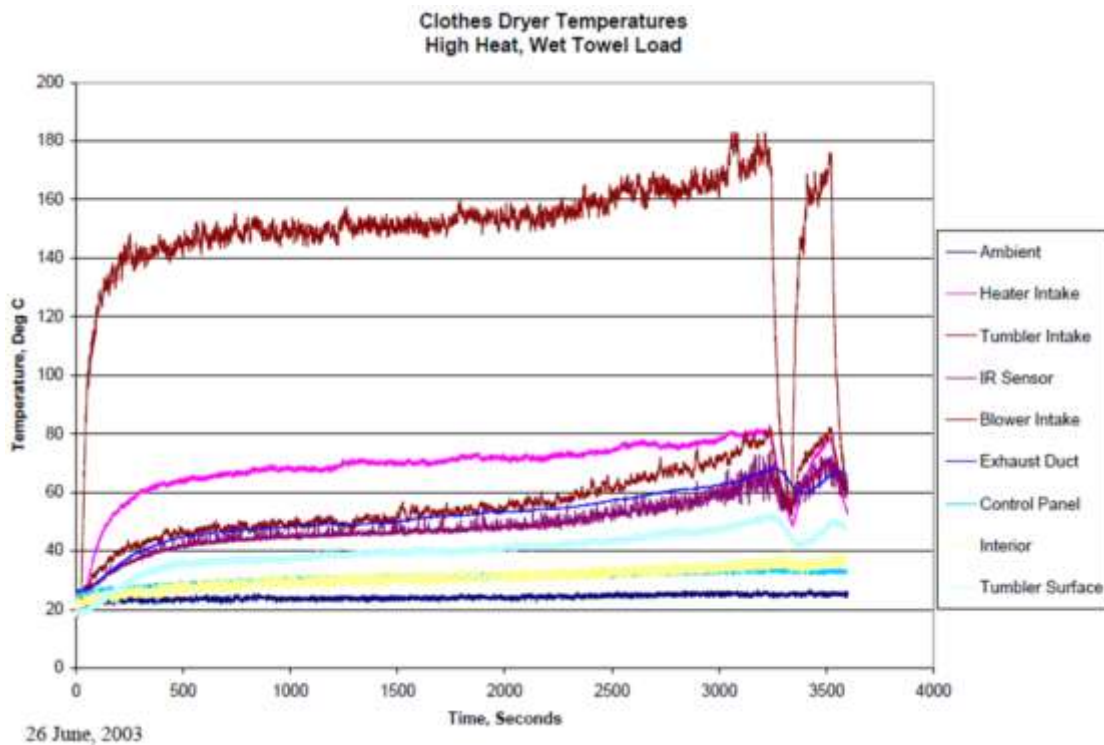


Figure 12: Temperature Readings on Several Locations of a CD during a Sample Drying Cycle (Butturini et al., 2004)

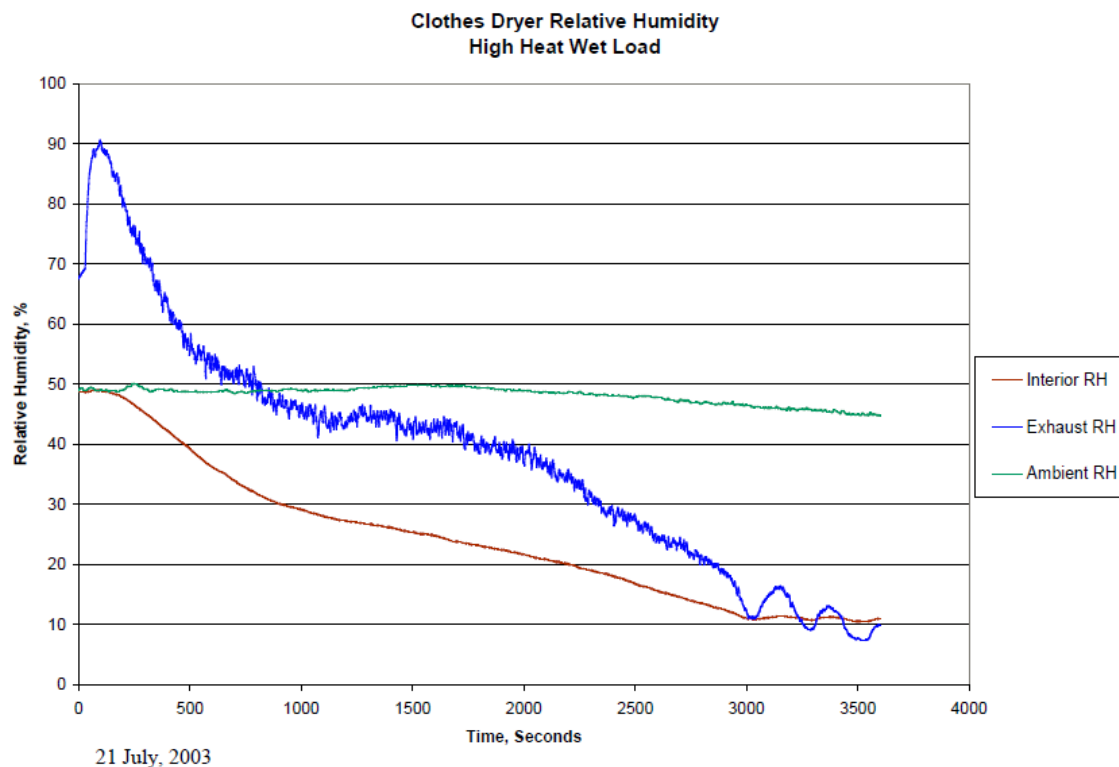


Figure 13: Relative Humidity Readings on Three Locations of a CD during a Sample Drying Cycle (Butturini et al., 2004)

A load of wet towels weighing 10.1 kg (22.2 lbs) is loaded into an electric dryer where 4.5 kg (10 lbs) is removed during the drying process. The average exhaust velocity was measured to be about 6.8 m/s (1337 ft/min). Assuming a 10 cm (4 in) diameter, round exhaust duct, the volumetric air flow rate is 200 m<sup>3</sup>/hr (117 CFM). The heating element drew an average of 22.8 amps while the electric motor drew an average 4.35 amps. The power supply for electric dryers use typically higher voltages, 220 volts, resulting in a lower amp draw. The baseline test lasted 1 hour. With the known power consumption, 5.97 kWh of energy is consumed over the entire CD cycle and a MER value of 0.5914 kWh/kg is calculated. If 283 cycles per year are run with a power consumption of 5.97 kWh per cycle, an annual power consumption of 1,690 kWh is predicted. Applying the number of homes with an electric dryer, the total annual energy consumption with this example drying profile is 0.44 EJ (0.416 quads).

### 2.4.5 Controls

A sequence of operation was developed to capture the major control steps in an electric CD. The created flow chart can be seen in Figure 14.

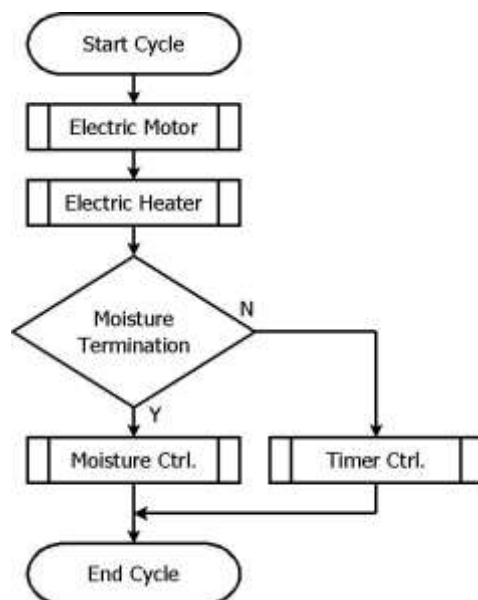


Figure 14: Overall CD Control Flow Chart using Moisture or Timer Condition

#### 2.4.6 Energy Saving Methods

A study compared four different CD types; air vented, closed cycle-condensing, open cycle-condensing, and closed cycle with heat recovery (Bansal et al., 2011)-9. An energy savings of 14% and 7% over an air vented CD were reported for the open cycle-condensing and closed cycle with heat recovery respectively (Bansal et al., 2011).

##### *Cycle Termination*

Moisture sensors on some CDs can save up to 15% energy (Bansal et al., 2011).

##### *Component Improvements*

CD cabinet insulation can provide an additional 6.9% of energy savings (Bansal et al., 2011).

##### *Heat Pump Dryers*

An air heat pump cycle for a CD is predicted up to 40% reduced energy consumption compared to a conventional CD and does not require any venting to the outside (Bansal et al., 2011). One drawback is the size of the HX needed for the required capacity would be excessively large. A

refrigerant HP cycle for a CD offers a 50% energy savings over conventional CDs (Bansal et al., 2011).

### ***Miscellaneous***

Other options available to CDs for energy savings are reverse tumbling, improved drum design, improved air circulation, exhaust heat recovery, microwave electric heating, and reduced stand-by power (Bansal et al., 2011).

## **2.5 Cooking Oven**

The 2006 U.S. residential electric cooking consumes 0.72 quads [760 PJ] of primary energy equivalent to 3.5% of the residential annual primary energy, includes ranges (microwave and electric resistance), ovens, and cooktops (Bansal et al., 2011). The number of U.S. households that have a stove is 102.3 million where 60% are heated by electricity and the remaining 40% are heating by direct combustion (Table HC3.1 RECS, 2009). The cooktop is not considered in the analysis on the CO.

### **2.5.1 Usage Frequency**

The number of cooking cycles a year depends on the usage per day. Only 3.5% of all households are using an oven 3 or more times a day, while 31% are using the oven at least once a day. The largest jump in percentage of households occurs when the oven is only used 2-3 times a week or 104-156 cycles a year. To represent a large percentage of households, an assumption of 104 cycles a year and covers 72.1 million households.

### **2.5.2 Electrical Consumption**

In the U.S. electric ovens annually consumed an average of 444 kWh (Hager et al., 2013). An annual usage of combustion driven ovens could not be found in the literature. Therefore only electrically driven ovens will be considered. With the 104 cycles and 444 kWh per year assumption, the CO is estimated to use 4.27 kWh per bake.

### **2.5.3 Efficiency Ratings**

For standard and self-cleaning electric COs, an average cooking efficiency is listed of 12.15% and 13.79% respectively (Hager, T. et al 2013). Compared to electric COs, gas driven models have lower ratings, 5.92% and 7.13% for standard and self-cleaning respectively. The ratings are similar to another reported thermal efficiency of electric COs, 12.7% (Bansal et al., 2011).

### **2.5.4 Sample Cabinet**

Waste heat recovery of the cooking oven will utilize only the energy from an elevated temperature, metal cavity. Self-cleaning ovens offer the consumer a convenience and for waste heat, a bonus with a higher temperature heat source at the end of the cooking process. To determine the mass of metal creating the oven cavity, a cavity size must be determined. Referencing the local, building supply retailers identifies the most common oven size at about 150 liters (5.3 ft<sup>3</sup>) for a free-standing range having a self-cleaning feature. The rough cabinet dimensions for the oven cavity selected are 71 cm by 66 cm by 33 cm (28 inches by 26 inches by 13 inches). Assuming a wall thickness of 0.635 cm (1/4 inch) and using the calculated surface area of the oven, not including the door, of 1.6 m<sup>2</sup> (17.3 ft<sup>2</sup>), the total estimated volume of the metal oven cavity is 0.0102 m<sup>3</sup> (0.36 ft<sup>3</sup>). Assuming the oven cavity is made from steel with a density of 7,900 kg/m<sup>3</sup> (493.5 lbs/ft<sup>3</sup>); the resultant mass of the cavity is about 80 kg (178 lbs).

### **2.5.5 Cycle Characteristics**

A cooking temperature of 204°C (400°F) is assumed as the initial temperature of the oven cavity at the end of a cooking cycle.

The breakdown of the energy input is as follows: 47% absorbed by CO structure, 25% lost through the walls, and 15% lost from evaporated moisture through the vent (Bansal et al., 2011).

### **2.5.6 Energy Saving Methods**

A high efficiency, low emissivity CO encased the electric heating element in a reflective compartment to reduce heat losses (Bansal et al., 2011). A thermal efficiency of 23% is obtained from this approach. Other modifications improved the cavity insulation level or door seals but

produced modest improvements of 4.9% and 1% respectively for gas COs (Hager, T. et al 2013). On electric COs, the cooking efficiency is only improved by 0.52% with insulation improvements.

### 3. THERMODYNAMIC APPLIANCE MODELICA MODELS

A Modelica model is built for each major appliance identified for thermal integration; CD, CW, RF, and DW. The CO is omitted due to the challenging requirements for a safe, heat recovery approach and compounded with a low usage frequency in the home. Each model attempts to capture the main functions of the appliance that would interact, and thus be impacted by, a thermal loop for heat transfer. A CD exhaust air stream for heat collection having elevated temperatures and humidity ratios during the drying cycle. A CW drains elevated temperature waste water for heat recovery at the end of wash or rinse steps when operating under hot or warm water settings. A RF rejects heat during compressor ON cycles. A DW extracts energy for heating water and dishware during the wash and rinse steps.

Each model references experimental data that was either provided by the manufacturer or extracted from published data in the literature. Ideally, by referencing experimental data directly, each appliance model accurately captures its interaction with a thermal loop.

#### 3.1 TLK-TIL Modelica Thermal Library

The desire to use Modelica as an object-orientated programming language was from having easily built and modified models from quick development times and good simulation convergence. A commercial simulation environment, Dymola, was used but other open-source versions are available, JModelica.org, Modelicac, OpenModelica (Modelica Association). Also many open-source platforms exist within the Modelica community having pre-built models for common equipment, dependent on the purpose of the platform. Often any support on these packages for a specific application is limited and thus can be challenging to implement. Some companies have developed commercial, advanced libraries with detailed component models, a large selection of fluid properties, and prebuilt examples combining several lower level models. Additionally, licensed libraries are often experimentally verified for improved accuracy. A licensed Modelica library TIL from TLK is a well-developed thermal systems library with component models and fluid property functions (TIL Suite, 2016). The library covers all common equipment leveraged in thermal systems; commercial or residential refrigeration, power generation, and building or

transportation HVAC. Being a commercial product, the libraries are updated and new components that capture emerging technologies in the field can be added.

For the modeling effort here, the basic components are to be used over expensive or emerging technologies with the goal of keeping the complexity and cost of the overall system low.

A detailed description of each component used can be found in the Appendix.

## **3.2 Clothes Dryer**

The CD Modelica model is entirely focused on capturing the waste heat recovery approach by specifying exhaust air conditions that represent a load size, type and selected settings on the appliance. Accounting for the drying process would increase the complexity of the model and computational time without significant added value. Experimental results generate curve-fits of dry bulb and relative humidity during a CD cycle under a prescribed load (weight of clothing) and heat setting and/or dryness level or moisture detection.

### **3.2.1 Cycle Controller**

When the controller is triggered, a timer input with curve-fits obtained from literature (high heat, large load) or from experimental data (high heat, small load) provide the dry bulb temperature and relative humidity percentage over a 60-minute cycle. The process is laid out in Figure 15. The individual switches have inputs provided within the Modelica script directly and are not captured in the diagram view with the traditional use of connectors.

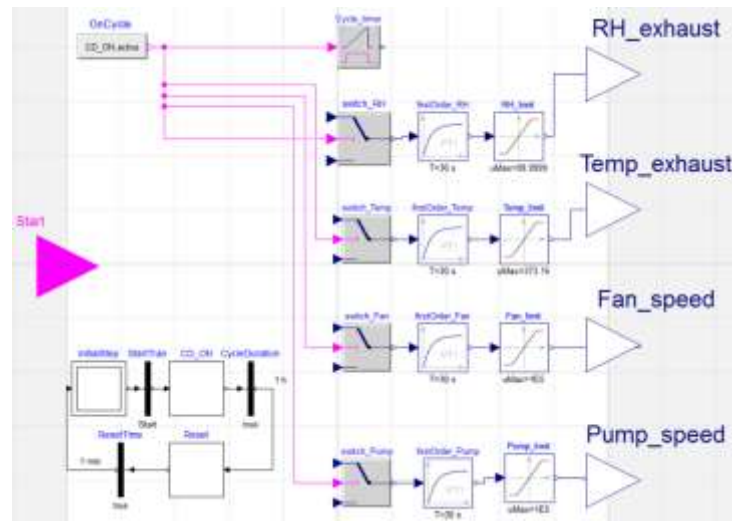


Figure 15: Clothes Dryer Modelica Controller for High Heat-5 kg load

The fan airflow rate is fixed throughout the 60 minute cycle and specified by the same data source for the temperature and relative humidity trends. Without detailed experimental data, a figure from literature was replicated with a discrete number of points to generate a curve fit function as an input for the relative humidity and dry bulb temperature (Butturini et al., 2004). After completing the controller, a tester interacts with the inputs and outputs to verify its operation. An example of a controller tester while connected to the heat recovery components is shown in Figure 16.

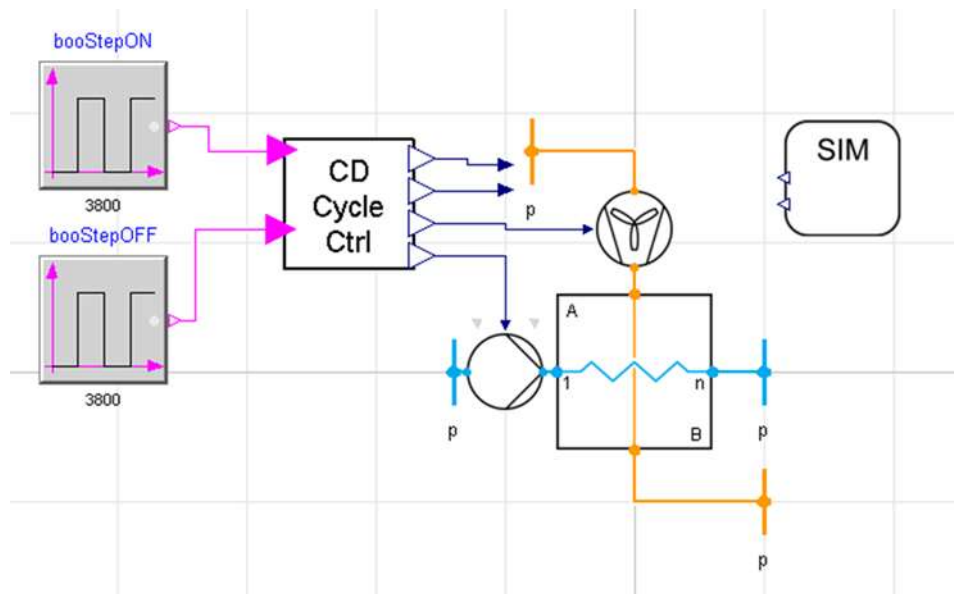


Figure 16: Testing the Clothes Dryer Cycle Controller with the Heat Recovery Components

### 3.2.2 Exhaust Heat Exchanger

The HX type selected is a cross-flow HX. Two different geometries were considered. Both were constrained to fit within the cross-section of the existing, 4", CD exhaust duct. The purpose of the limitation was to explore the performance of a HX that required minimal modifications to the existing appliance. The different geometries were obtained by varying the diameter of the water loop from 1/4" to 3/8" through the HX.

### 3.2.3 External Model

After verifying the CD controller works as intended, the model is then converted to be externally connectable. Binary inputs extend the controller start and reset inputs to the outside. The liquid loop inlet and outlet boundaries are replaced with liquid ports. Similarly the exit boundary for the exhaust stream is replaced with a gas port. The specific changes and the external model diagram are shown in Figure 17. At this point, the CD model can be called during a simulation, the sample drying cycle is executed, and then the model can be reset for the next drying cycle.

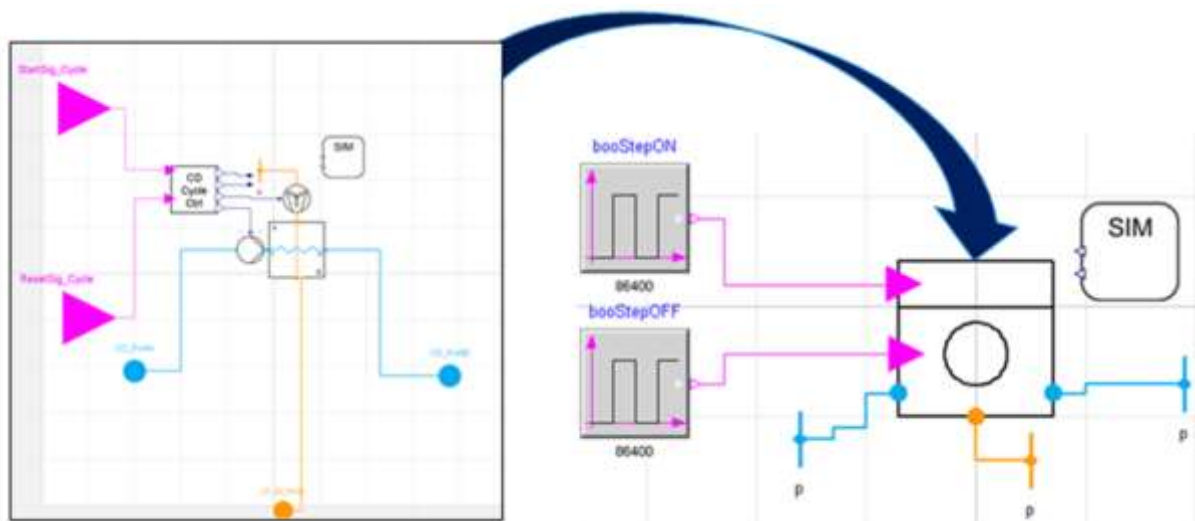


Figure 17: Creating External Connections for Clothes Dryer Model

### 3.2.4 Dymola Simulation Results

With a HX geometry using 3/8" diameter tubing, the breakdown of the heat transfer rate from the air stream is shown in Figure 18. The majority of HT occurs via sensible heat over latent heat and reaches a maximum rate of almost 2 kW and holds steady for most of the cycle.

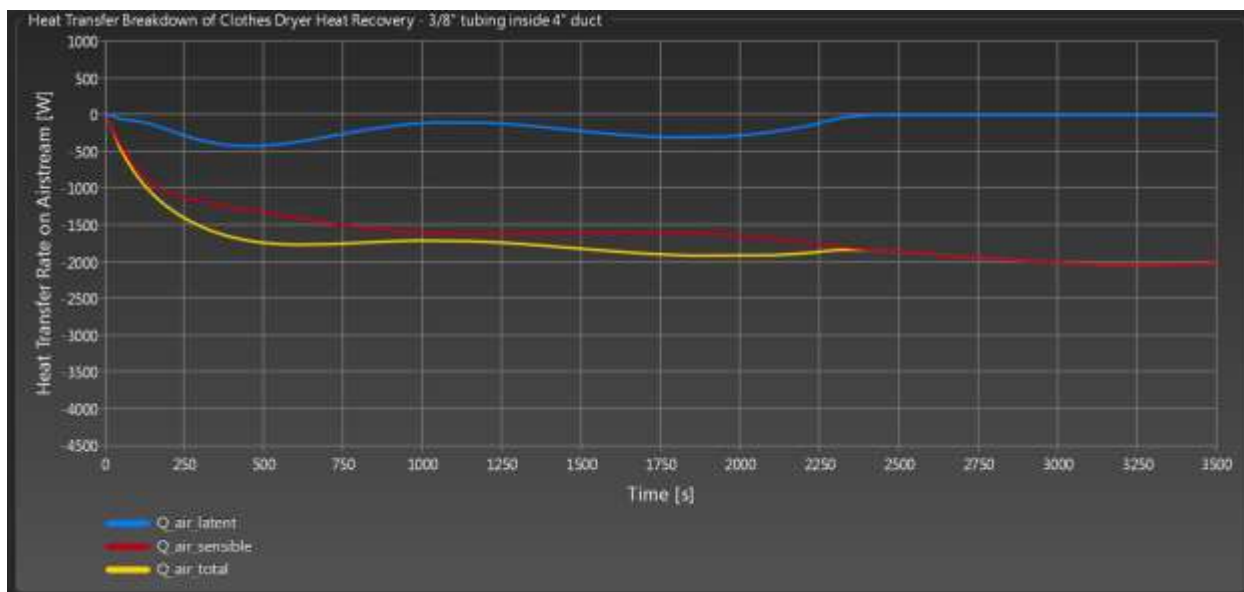


Figure 18: Breakdown of Heat Transfer Rate CD Modelica Simulating 3/8" Diameter

The heat recovery HX temperatures for the same geometry are plotted in Figure 19. The air exit temperatures from the HX are reported to be still high around 42C (113F) and are not suitable for venting into the laundry room.

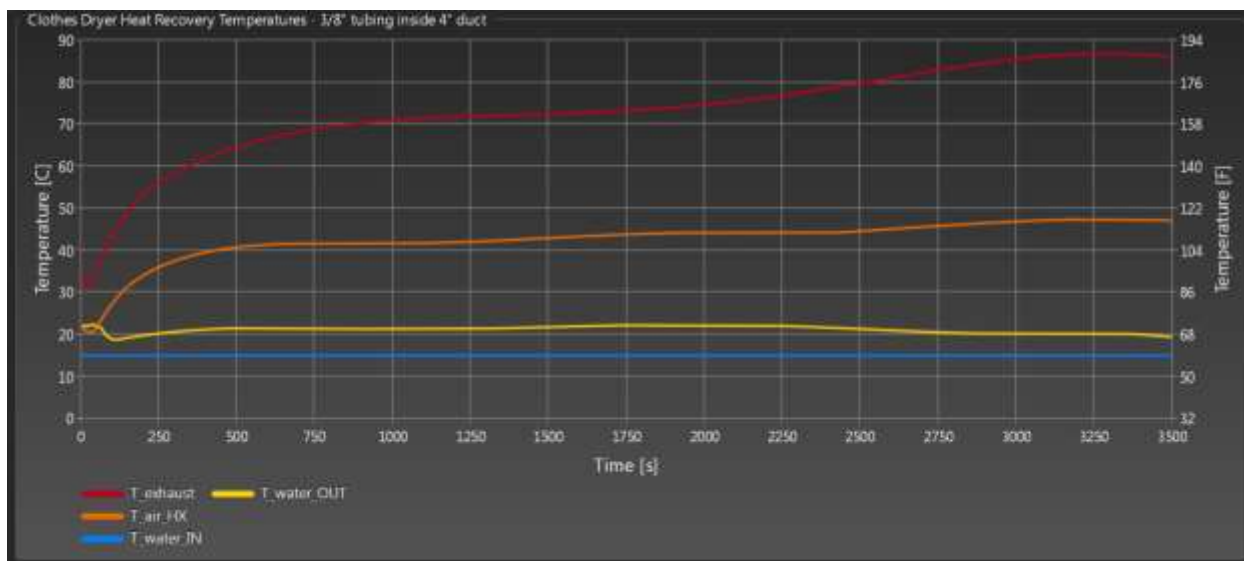


Figure 19: HX Air and Water Temperatures of the CD Modelica Simulating Heat Recovery using 3/8" Diameter

By increasing the HX geometry, an ideal air exhaust steam can be reached from cooling the airstream enough to safely vent the CD exhaust into the laundry room. The breakdown of the heat transfer rate from the air stream is shown in Figure 20. The majority of HT now switches to latent

heat over sensible heat. The HT rate reaches a maximum above 4 kW with almost a 50-50 split between the two HT modes in the HX.

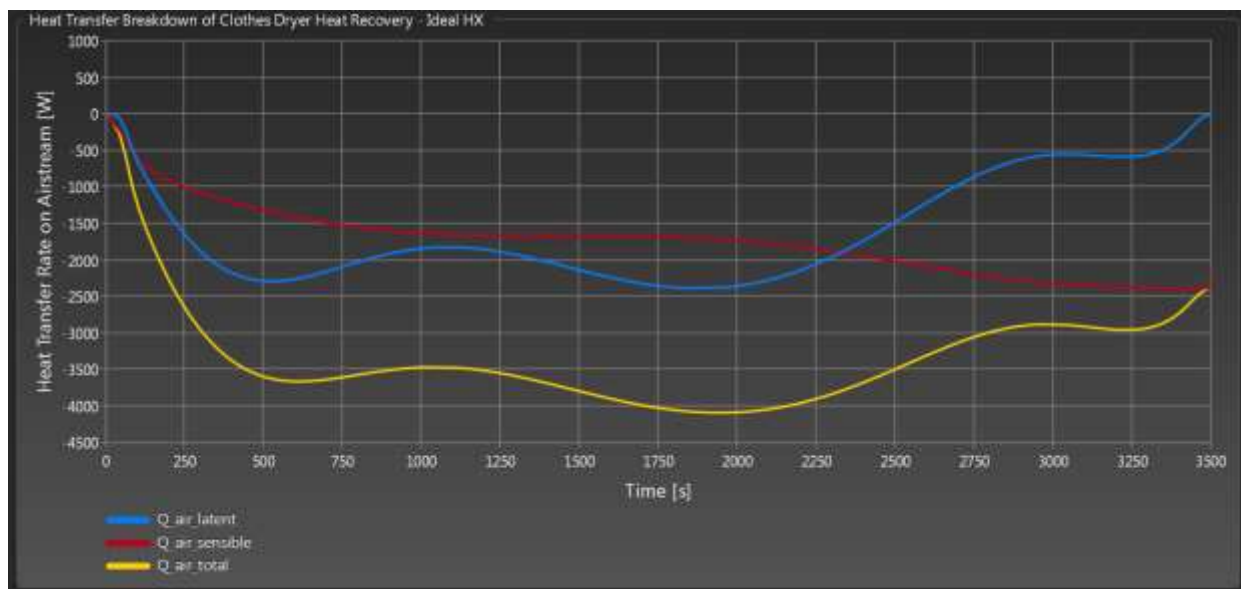


Figure 20: Breakdown of Heat Transfer Rate CD Modelica Simulating Ideal HX Surface Area

The heat recovery HX temperatures for the ideal geometry are plotted in Figure 21. The outlet air temperature is reduced to about 22C (72F).

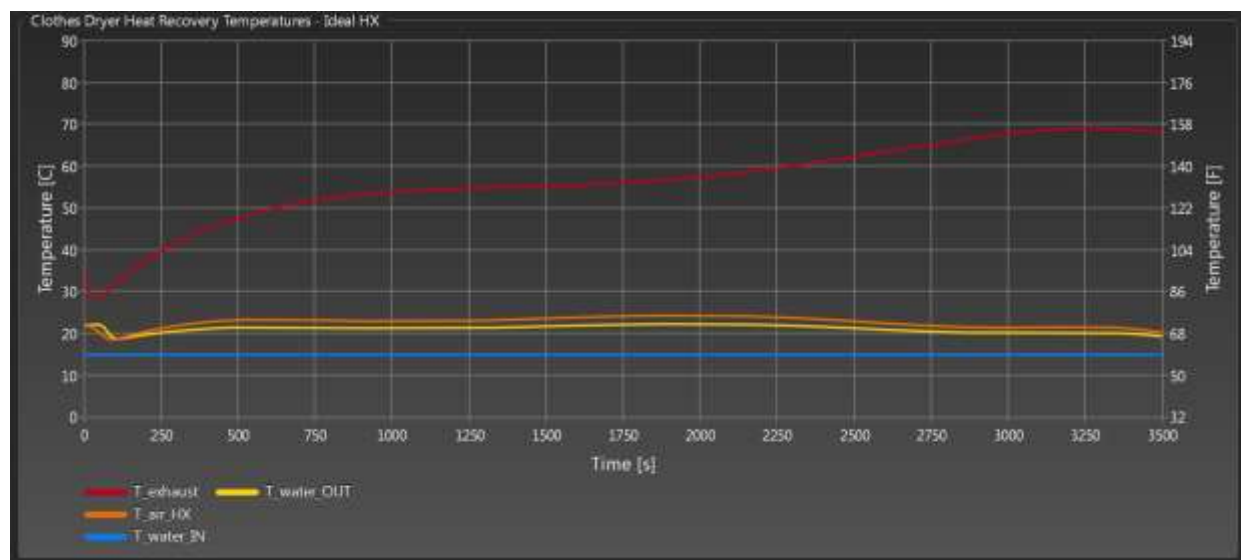


Figure 21: HX Air and Water Temperatures of the CD Modelica Simulating Heat Recovery using Ideal Surface Area

### 3.3 Refrigerator-Freezer

To properly capture the impact of waste heat recovery on the RF energy consumption, the entire vapor compression cycle is to be modeled in Modelica. The working fluid is R-134a to match the experimental data collected. The Modelica model supports other refrigerants and can be easily switched via the dropdown list in the SIM component. R-290, propane, and R-600a, isobutane, are two potential candidates as a drop-in replacement using the same equipment.

#### 3.3.1 Compressor

To model the reciprocating compressor, a simple compressor model assuming a volumetric efficiency, isentropic efficiency, and compressor displacement is used. The initial assumptions for the efficiencies were, an 80% volumetric efficiency and a 70% isentropic efficiency. These are updated depending on the agreement between the predicted power consumption and the measured power consumption. The rated displacement from the compressor manufacturer is  $5.19 \text{ cm}^3$  ( $0.317 \text{ in}^3$ ) per stroke and operates at 60 Hz.

#### 3.3.2 Condenser

For the water cooled condenser, a flat-plate HX Modelica model is programmed with the physical dimensions of the installed HX used during preliminary experimental evaluation (Small, S. 2017). The exact values are shown in Figure 22. The model also requires a HTC. A correlation can be entered or constant value. For the initial phase to reduce model complexity, literature is referenced for a reasonable constant value capturing the condensation of R-134a in a brazed plate HX (Longo, G.A. 2008). Refrigerant fluxes in the span of 10 to 40  $\text{kg/m}^2\text{s}$  start in the range of 1,800-2,000  $\text{W/m}^2\text{K}$  and increase up to 2,200-2,600  $\text{W/m}^2\text{K}$ . To cover most fluxes conservatively, a constant 2,000  $\text{W/m}^2\text{K}$  will be assumed. This value can be adjusted depending on the simulation results or replaced with a physical model to calculate a HTC. During an testing phase to evaluate the Modelica model, a cooling stream of water is maintained at a fixed inlet temperature of  $15^\circ\text{C}$  ( $59^\circ\text{F}$ ) and flow rate of 0.25 L/min (0.066 GPM). The HX model also supports discretizing into cells to separate the analysis into several segments along the HX area.

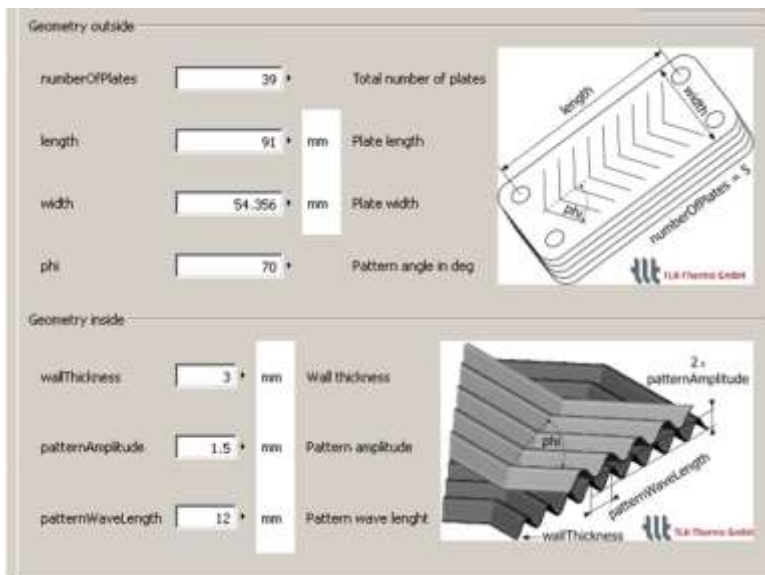


Figure 22: RF Water-cooled Condenser – Modelica Flat-Plate Model Geometric Inputs

### 3.3.3 Expansion

The expansion process in a RF uses a capillary tube with a fixed length and runs along the compressor suction line acting as a suction line HX. To simplify the model, this is represented with a fixed orifice expansion device and an upstream, suction-line sub-cooler. Adjustments to the cross-sectional area control the degree of superheat and pressure levels in the condenser and evaporator. The changes are iterated by observing the response in the simulation output to improve agreement with the available experimental data.

### 3.3.4 Evaporator

The evaporator is modeled as a cross-flow, fin-and-tube HX. Dimensions are measured from the physical HX and entered into a Modelica model representing the type selected. The exact values are displayed in Figure 23. Refrigeration loop is a single circuit having multiple passes. The HTC coefficient is assumed to be a constant value initially to reduce model complexity. From the literature, a study on R-134a evaporation HTCs inside a FPHX report values starting from 1,000-1,500 W/m<sup>2</sup>K at a heat flux of 5 kW/m<sup>2</sup> and increasing up to 3,000 W/m<sup>2</sup>K at a heat flux of 20 kW/m<sup>2</sup> (Longo, G.A. et al. 2007). While an initial value of 1,000 W/m<sup>2</sup>K is assumed, this is to be updated from literature that matches the HX and refrigerant conditions simulated and from the agreement between the simulation and experimental data. The airflow rate assumed to be a

constant 1400 L/min (50 CFM). The freezer cavity has a design temperature of  $-20^{\circ}\text{C}$  ( $-4^{\circ}\text{F}$ ) and the air inlet temperature is set to this level.

finnedTubeLength	<input type="text" value="216"/>	mm	Length of finned tubes
nSerialTubes	<input type="text" value="3"/>		Number of serial tubes
serialTubeDistance	<input type="text" value="25"/>	mm	Distance between serial tubes
nParallelTubes	<input type="text" value="58"/>		Number of parallel tubes
parallelTubeDistance	<input type="text" value="25"/>	mm	Distance between parallel tubes
finThickness	<input type="text" value="1"/>	mm	Thickness of fins
finPitch	<input type="text" value="5"/>	mm	Distance between fins
Tube Side Geometry			
tubeInnerDiameter	<input type="text" value="7.5"/>	mm	Inner diameter of tube
tubeWallThickness	<input type="text" value="0.7"/>	mm	Thickness of tube walls
nTubeSideParallelHydraulicFlows	<input type="text" value="1"/>		Number of parallel tube side flows

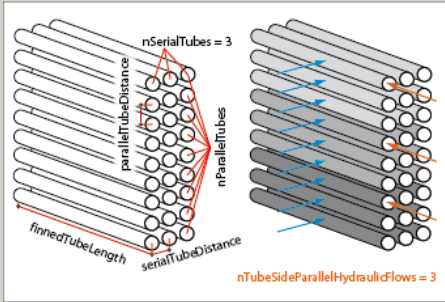


Figure 23: RF Evaporator – Modelica Fin-and-Tube HX Model Geometric Inputs

A charge port is added on the refrigerant loop of the suction line to control the subcooling level in the system. An initial value of 254.8 grams (9.1 oz) of R134a is used and adjusted to obtain a level of 5 K on the outlet of the condenser. Keeping in mind that actual subcooling to the inlet of the expansion process will be higher due to the suction line HX.

### 3.3.5 Steady State Simulation Results

Each Modelica component is connected using a graphical interface shown in Figure 24. Starting with the top right component and working around the schematic in a counterclockwise direction, the compressor is followed by the water-cooled condenser. A tube model represents the liquid side of the suction line HX but is not connected thermally to the suction line. The fixed orifice expansion device provides the pressure drop needed. The evaporator is connected to air side boundaries referencing the assumed temperature and air flow rate. The charging port component follows the evaporator and leads into the gas side of the suction line HX before returning to the compressor inlet. In the same image, several “ph” sensors can be seen and these represent the refrigerant state points of the cycle for overlay on refrigerant property plots. Additional sensors report the superheat or subcooling levels and absolute temperature of the refrigerant. Two pressure state components identify the expected regions of the cycle operating at similar pressures. A reference for either pressure state is also required to be set within the individual component models.

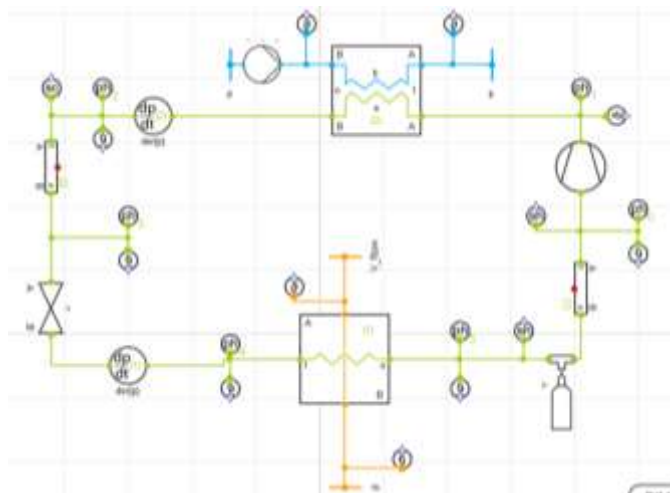


Figure 24: Basic RF Modelica Model with No Control

The initial RF model is simulated for 1,000 seconds (16.7 min) to reach a steady-state response using the previously described conditions. Overlaying the cycle on the property plots of R143a P-h and T-s is shown in Figure 25 and Figure 26. The plots are generated using a software built by the same company creating the TIL Library. They allow for saving of plots from Dymola and are easily updated after running a new simulation. By overlaying the cycle state points on a refrigerant diagram, the operation of the RF model can be quickly reviewed and determine if any improvements are necessary.

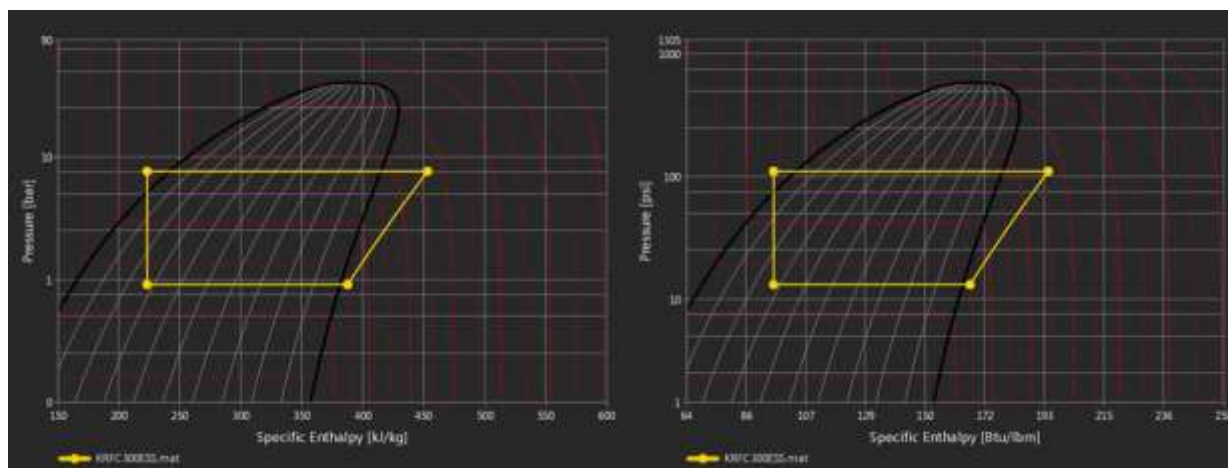


Figure 25: Ph Diagram of Simulated Basic RF Model

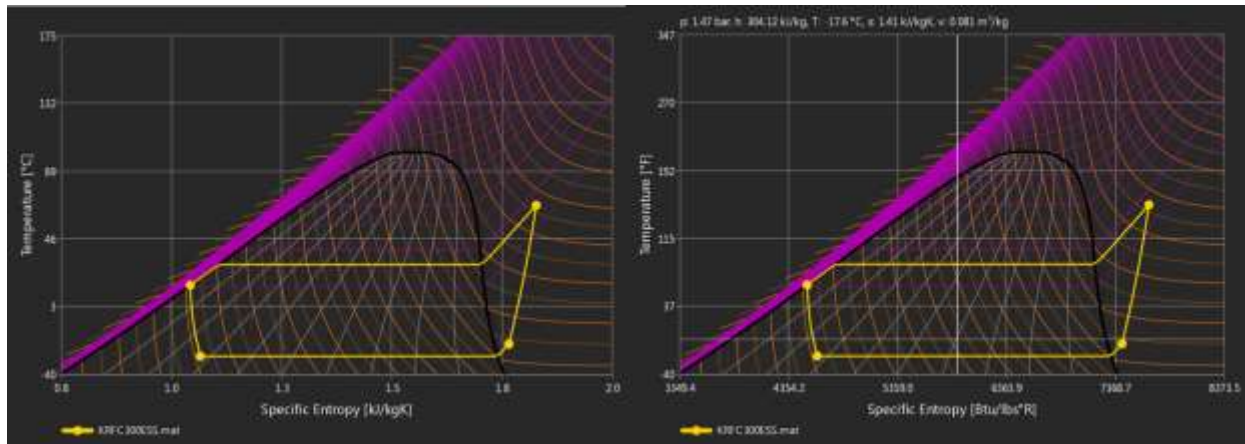


Figure 26: Ts Diagram of Simulated Basic RF Model

Another feature that was mentioned previously is the ability to discretize the HX model into several nodes or cells. The plots shown in Figure 27 compare the refrigerant, HX wall, and working fluid temperatures for each discrete cell within the condenser and evaporator HX models. By comparing temperatures, a quick assessment is on the impact of the HTCs can be visualized as well as locations where superheating, subcooling, or 2-phase HT occurs.

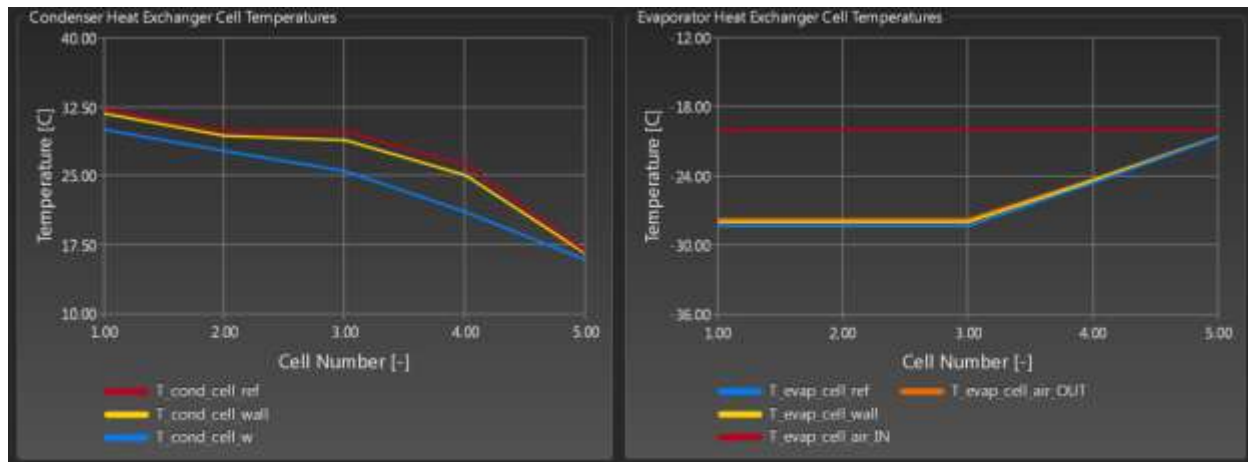


Figure 27: Temperature Plot of Condenser and Evaporator HX Nodes from the Basic RF Model

With the fixed boundary conditions applied to generate the basic RF simulation, the condenser and evaporator steady state capacities were about 250 W and 200W respectively. The compressor steady state power consumption was around 75 W making the cooling and heating COPs around 2.67 and 3.33 respectively. The preliminary results are promising for recovering heat from the RF condenser.

### 3.3.6 Compressor Capacity Controller

After verifying the overall operation of the basic RF model in steady state, the next step required making a controller for the compressor to capture the transient, cycling aspect of the RF. In a standard RF, the compressor control is dependent on the temperature settings for each cavity. The ON frequency of the compressor cycles increase as higher rates of thermal gain are experienced due to; rising ambient temperatures, the number of times the RF door is manually opened, or placing food product in the RF to be cooled to the cavity temperature. Many of these factors are user influenced and are hard to accurately predict. For simplicity, the RF ambient temperature is assumed to be constant, resulting in a fixed rate of heat gain over time from the ambient. The required amount of thermal energy removed to maintain the cavity temperature can also be assumed to be constant under this scenario. The fixed amount of heat gain for the RF cavities results in two control decisions; the first waits on a timer until a threshold is passed to turn ON the compressor and the second turns OFF the compressor after a threshold of energy removed during the entire ON cycle is surpassed. This approach also captures the impact from RF cycle changes on the evaporator capacity which directly influences the compressor duty cycle. The OFF time and ON energy thresholds are both adjusted based off the simulation agreement with experimental data collected. More details on how the controller is programmed can be found in the Appendix.

### 3.3.7 Transient Simulation Results

A 20,000 second (5.56 hr) simulation is run on the completed RF model while connected to a fixed volume of water, 18.9 L (5 gal). The goal is to verify the response of the refrigeration cycle to a heat sink increasing in temperature over time. The RF Modelica model is modified slightly on the condensing side with a recirculating water loop coupled to the fixed volume as shown in Figure 28 on the blue circuit. The junction on the inlet to the water pump provides a pressure state for the liquid circuit (blue), in this case set to water. While the ambient heat loss on the storage tank is neglected in this study, the model can be easily modified. A thermal resistor placed between the tank temperature node and a boundary temperature represents an insulation layer on the storage tank and provides a connection to a lower temperature environment.

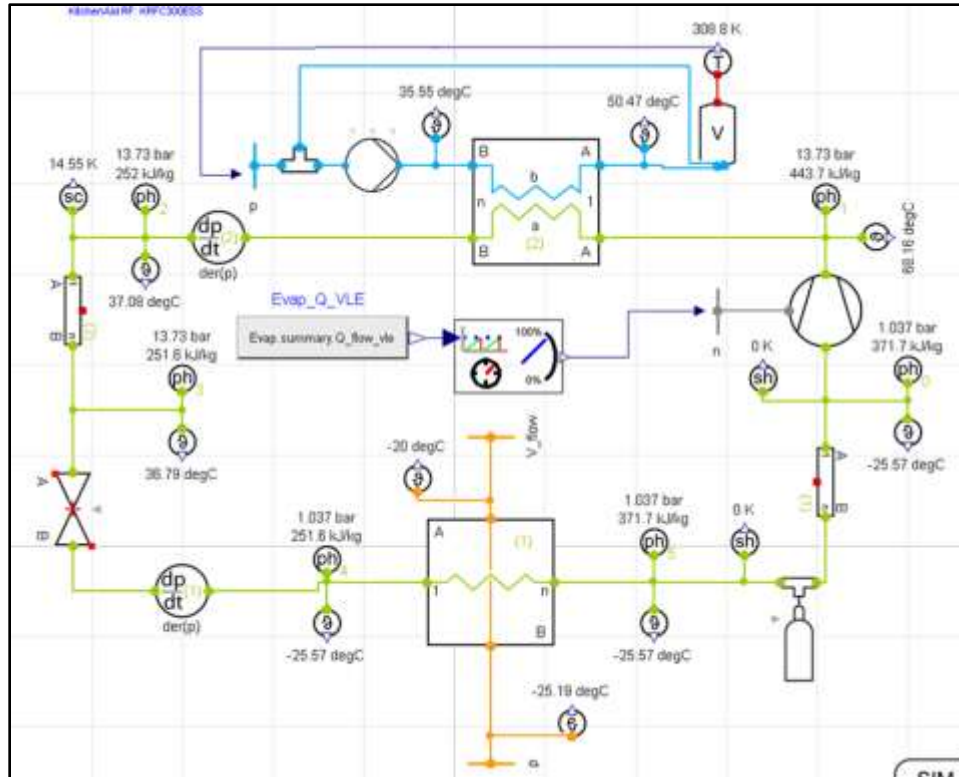


Figure 28: Testing Cooling Loop with Simple Storage Connected to Refrigerator-Freezer Modelica Model

A plot of the compressor power consumption and suction and discharge pressures during the simulation is shown in Figure 29. The compressor experiences higher condensing pressures each ON cycle due to the rising temperature heat sink. The average power consumption also is shown to increase over time, first drawing only 70-75 Watts and by the last cycle is reaching 100 Watts. The simulation result is compared to experimental data collected on a RF with a water-cooled condenser. A sample test run of the RF operation is obtained by rejecting condenser heat to a fixed volume of water over time (Small, S. 2017). The power consumption is shown to increasing over time with every compressor ON cycle as shown in Figure 30.

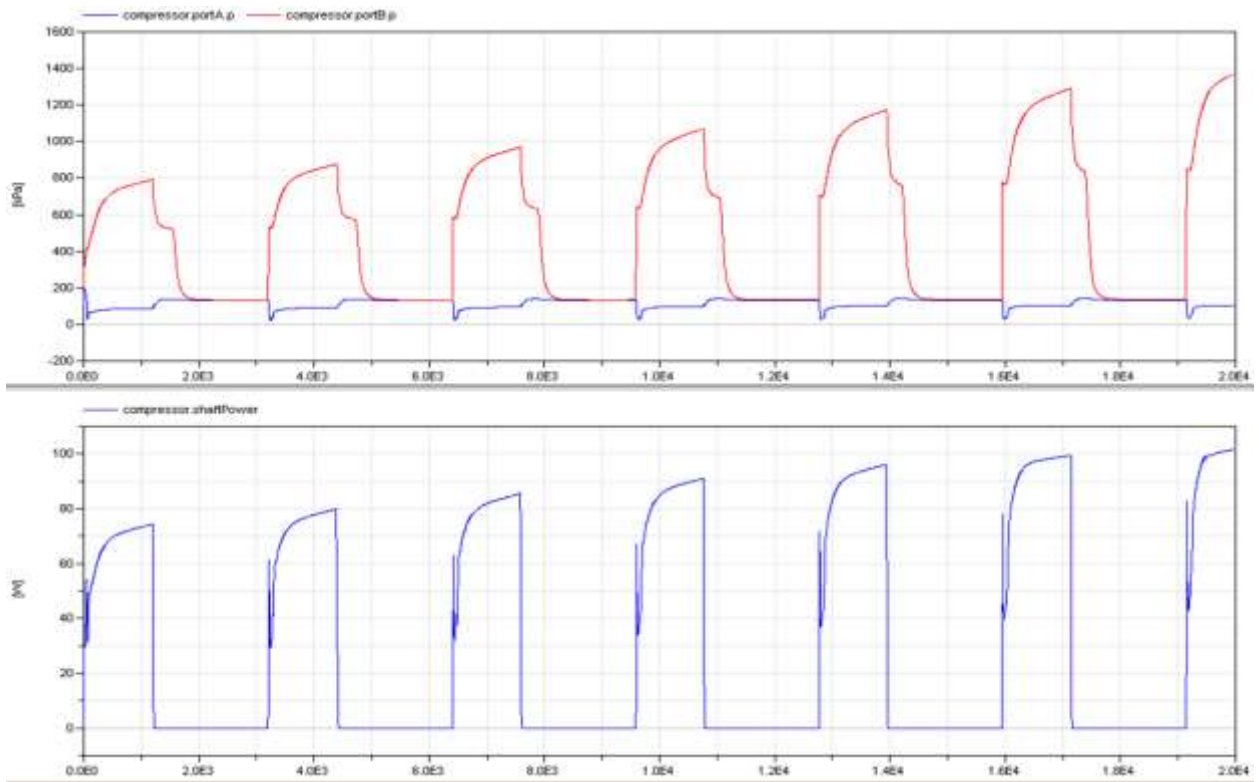


Figure 29: RF Simulated Compressor Suction/Discharge Pressures (top) and Power consumption (bottom) when connected to Water Storage Tank

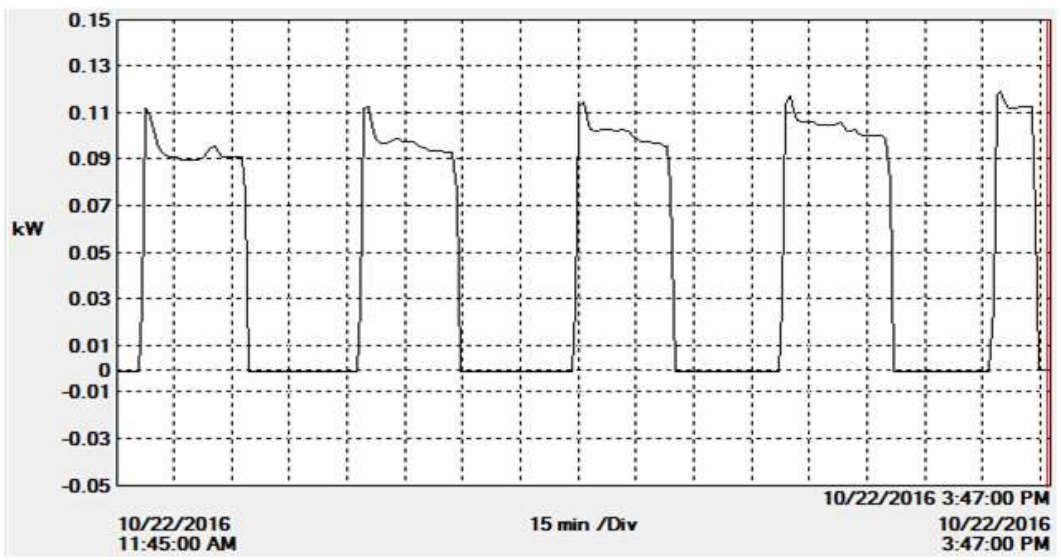


Figure 30: Sample of Experimental RF Power Consumption while Rejecting Heat to Fixed Volume of Water (Small, S. 2017)

The simulated evaporator air inlet and outlet temperatures over time are shown in Figure 31 (top) as well as the cooling capacity (bottom). As the tank is heated, the evaporator capacity is negatively

impacted due to a higher pressure drop creating a lack of superheat control by the fixed orifice. Overall the evaporator capacity averages around 180 Watts during the simulation.

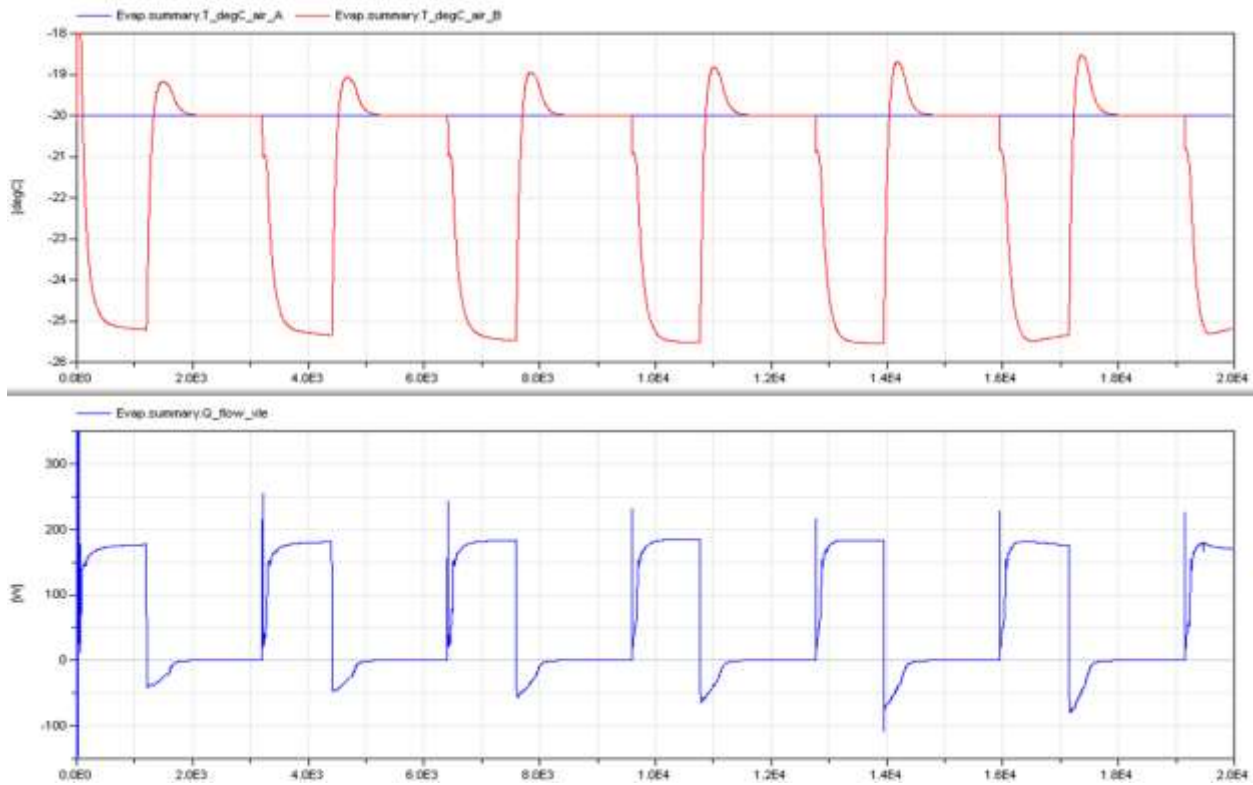


Figure 31: RF Simulated Evaporator Air-side Temperatures (top) and Refrigerant Heat Transfer (bottom) when connected to single volume water tank

The cooling water temperatures during the ON cycles are shown in Figure 32 (top) compared to the compressor discharge temperature. The potential maximum water temperature, compressor discharge, identifies the benefit of using a RF condenser as a hot water source. Also plotted in Figure 32 are the cycle subcooling and superheat levels during the simulation. As the condensing pressure increases, the superheat into the compressor is lost and two-phase compression occurs. The corresponding conditions are identified in the discharge temperature dropping near the end of a compressor ON cycle.

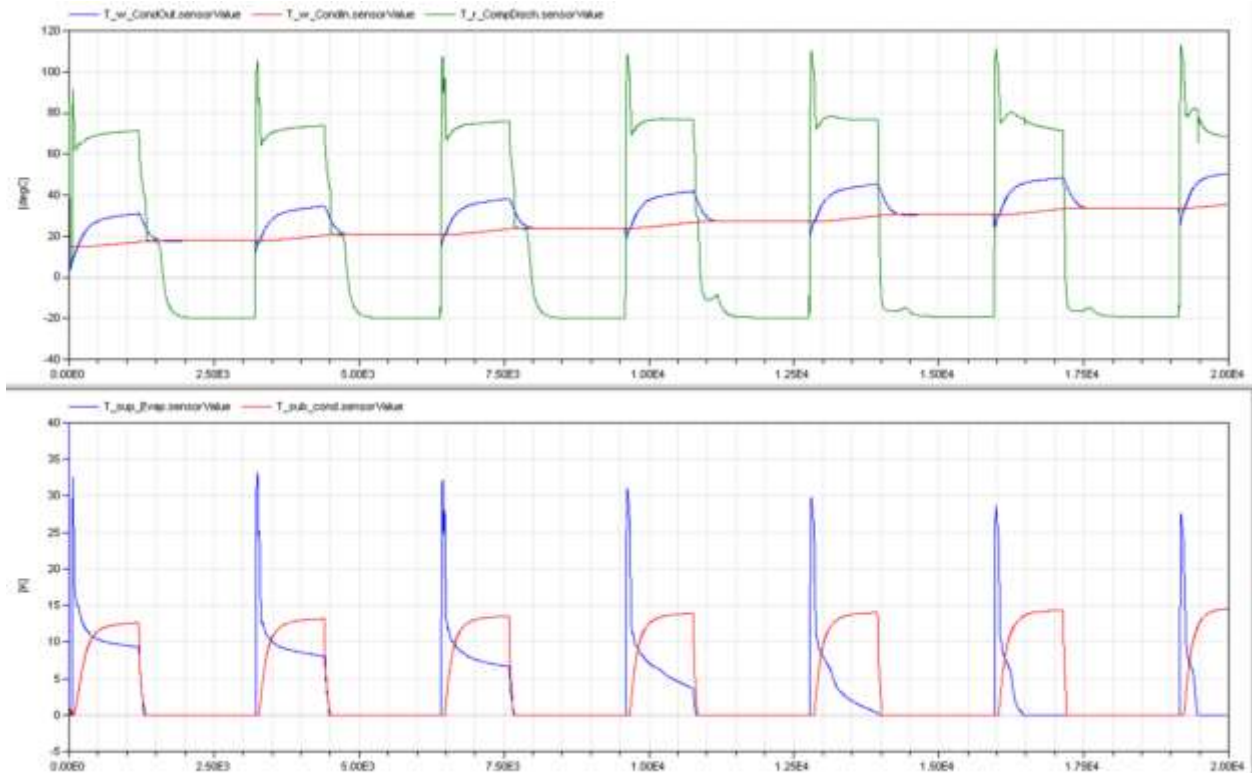


Figure 32: RF Simulated Cooling Water, Compressor Discharge Temperatures (top) and Superheat, Subcooling Temperatures (bottom)

### 3.3.8 Discussion

The RF Modelica model has the functionality to reject heat to water. As the heat sink increases in temperature, the impact on both the compressor power consumption and evaporator capacity is reflected in the results. The introduction of pressure drop within the HX models, at least the evaporator, should be explored due to the real system relying on a single refrigerant circuit. Explore a more robust fixed orifice opening to ensure adequate superheat to the compressor over the range of expected operating conditions. Improving the superheat may also require adjustments on the refrigerant charge in the system. The compressor controller can be improved by expanding the number of output signals to include ON/OFF control of the condenser and evaporator fan(s) and heat sink pump along with the compressor.

### 3.4 Dishwasher

To accurately capture a DW cycle, the Modelica model must follow a sequence of actions seen in typical operation. Separate, unique steps are defined by characterizing experimental data

displaying water sump temperature and overall instantaneous power draw over time. The soil sensing DW cycle shown in Figure 7 is used to generate the flow chart for the DW controller shown in Figure 9. An overall controller is built to simulate all the steps in a DW cycle. To properly represent the response of the DW to a cycle controller, the dynamics of the dishware and other components need to be captured as well. Major parts involved in a DW cycle are a recirculation and drain pump, volume of recirculating water, cabinet heat loss to the ambient, and the thermal capacity of the dishware.

### **3.4.1 Cycle Controller**

Of all the unique steps within one DW cycle, several can be duplicated with minor changes to achieve the same goal. For example, each cycle starts with a pre-wash that only recirculates water and provides no heating until a timer condition is satisfied. The same function is observed during the main wash but operates for a different amount of time. Here a controller for the prewash or main wash step dependent on a timer has the same function but requires different durations. The same similarity is found in the heated wash and rinse steps where the controller heats the water sump to a required temperature but to a different level for the respective steps. The draining and filling steps of the cycle are combined into the same controller due to how the Modelica components have a constant holding volume of water.

Once a controller is built for each major function identified, an overall DW cycle controller is built. The sequence of stepping through each controller capturing each major step is established in this overall cycle controller. A cycle is started by an ON signal then the entered assumptions for various steps are read and the DW marches through each step of the cycle. Modelica model is to also allow for an external heat input reducing the amount of heating required by the electric heating element. The cycle controller is also has as an input, whether to use an external heat loop or not. A heat loop controller modifies the electric element heater control by overriding the output if adequate temperature of water is available. Otherwise the electric element is energized following the pulsing controller and heat is delivered to the water sump.

### ***Timer Control***

The subcomponent to control any timed steps during a cycle accepts two Boolean inputs, has an internally modifiable timer, and generates an output signals. The Modelica icon of the timer and the parameter window to enter the duration is shown in Figure 33. Of the two inputs, the first initiates the controller to start the output while the second input either resets the controller to an OFF state from the END state or overrides the controller by interrupting the timer and ending the controller output independently of the timer. Of the two outputs, the first provides a status value that corresponds to the state of the controller: 0 – controller is off and waiting for a start signal, 1 – the controller is active and waiting for the timer to lapse, and 2 – the controller timer has expired and the step has been completed.

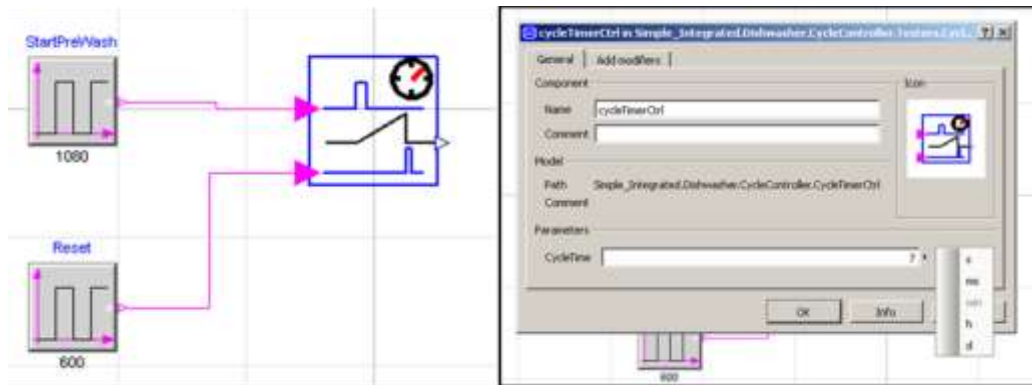


Figure 33: DW Modelica Diagram and Parameter Window for the Timer Controller

### ***Heating Control***

A second subcomponent controls any heating steps required during the overall dishwashing cycle. The overall structure is very similar to the timer step controller but instead of a timer setting, it has a temperature setting.

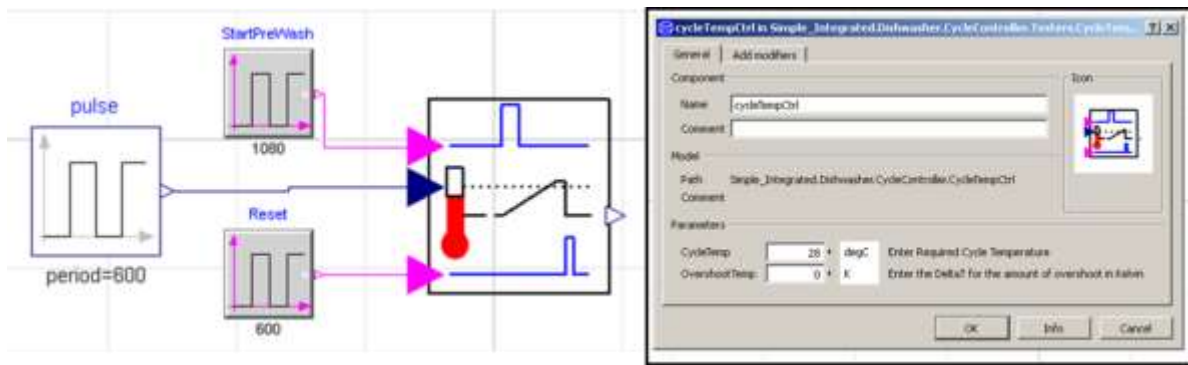


Figure 34: DW Modelica Diagram and Parameter Window for the Temperature Controller

### ***Fill and Drain Control***

The filling and draining steps of the DW are captured within the same controller. In the model, the drain pump results in a draw of DHW into the DW at an equal volume. The drain flow rate is set by quickly charging the assumed volume of water used for a step in the DW cycle.

### ***Heat Loop Control***

When the DW is to use the external heat loop, the source temperature must be higher than the sump temperature for any heating to occur. An input for the source temperature provides the controller feedback to accept a fluctuating temperature source. If the source is not more than 10C higher than the sump temperature, the heat loop pump does not turn on and the normal heating mode is used by energizing the electric element.

### ***Overall Control***

With all the controllers finalized to capture every step of the DW cycle, the overall cycle controller is built. Each controller occurs sequentially representing a step. The available parameters that can be adjusted on the controller to improve agreement with experimental data is shown in Figure 35.

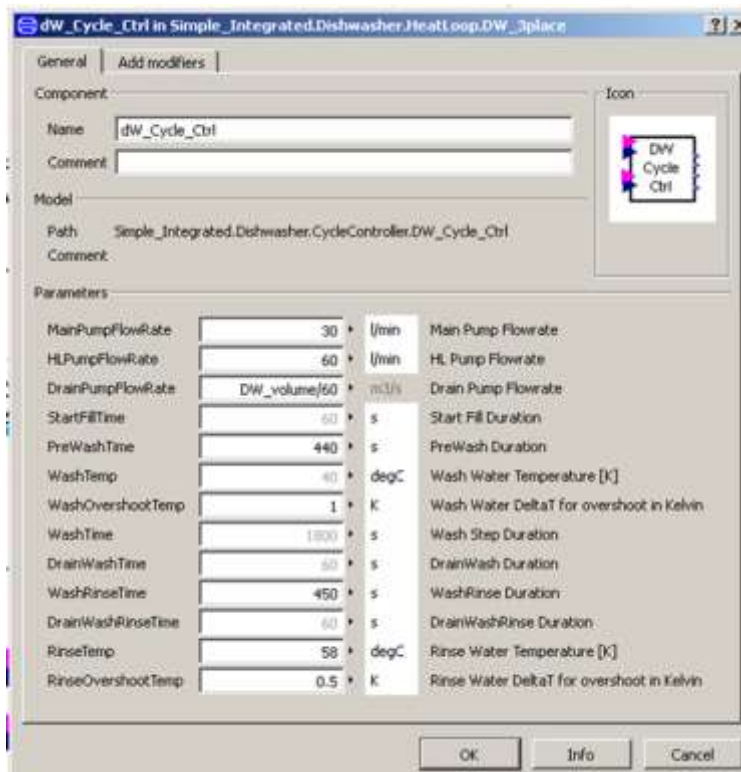


Figure 35: Parametric Inputs for DW Cycle Controller

### 3.4.2 Modelica Components

To capture all the major parts that interact during a DW cycle, the Modelica model uses TIL prebuilt component models. The diagram view of the finalized DW Modelica model is shown in Figure 36. Three simple pump models represent the circulation pump, the drain pump, and the heat loop pump for external heating. Three tube models represent the DW water interacting with the electric element, the thermal capacity of the dishware, and ambient heat losses through the cabinet. A small simple water volume model is connected to account for the mass of water circulating inside the DW during a cycle.

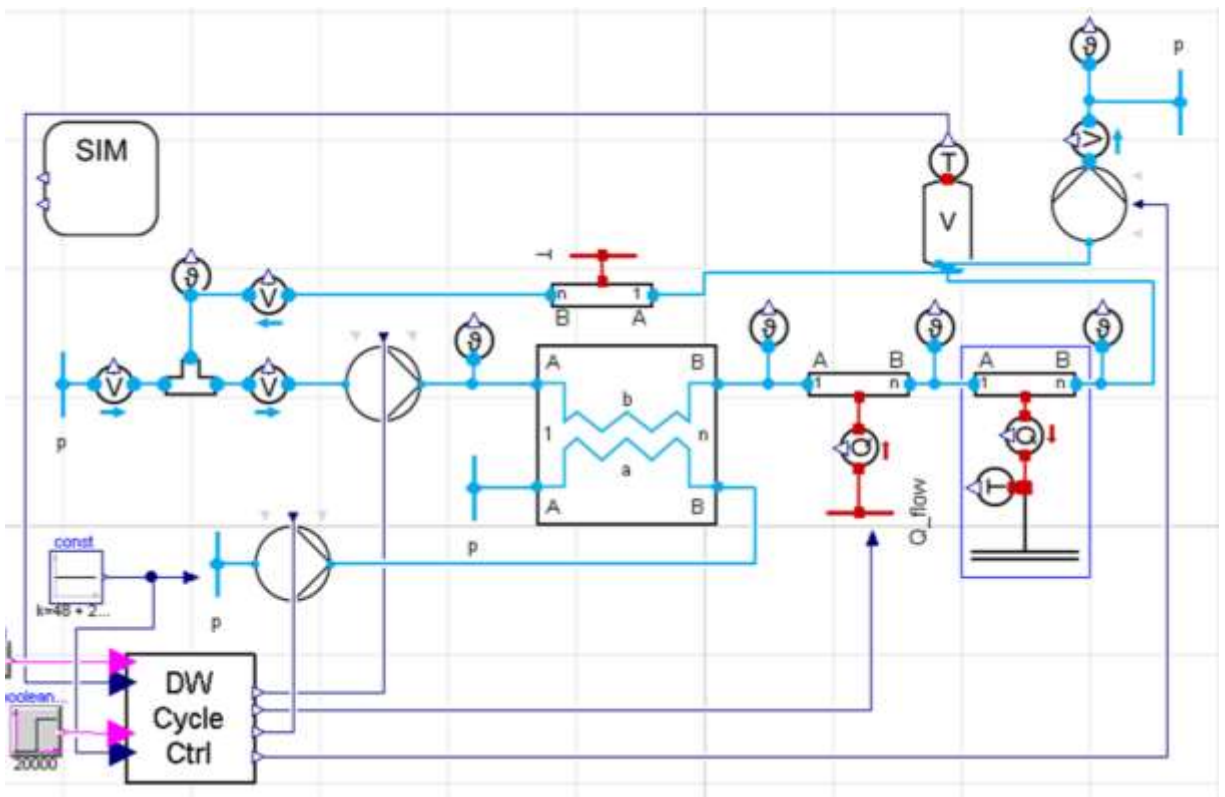


Figure 36: DW Modelica Model Diagram for Testing the DW Cycle Controller

### 3.4.3 External Connection

The boundary conditions replaced in the diagram, Figure 36, are shown in Figure 37 with the external port connections. The DW external model allows for the sump volume to be modified but all other cycle properties shown available in Figure 35 are not accessible from the DW appliance model.

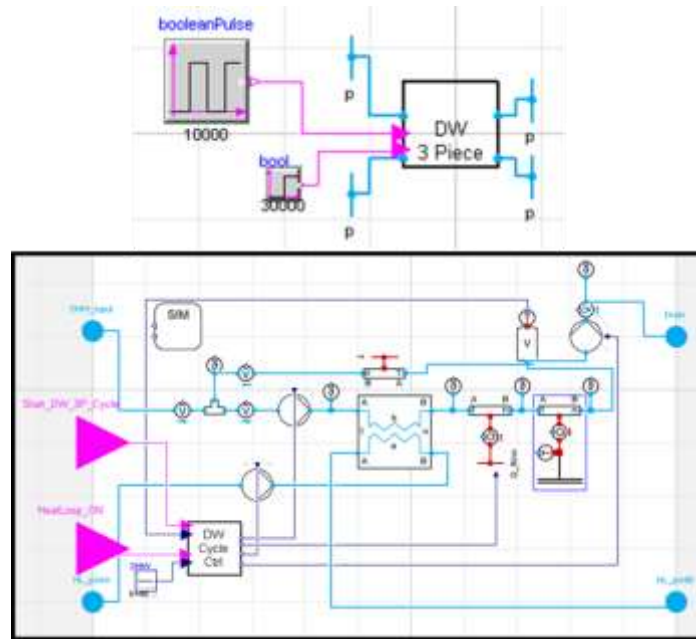


Figure 37: External DW Modelica Model for Integrated System

### 3.4.4 Traditional DW Simulation Results

First the DW appliance model is run in the traditional mode and compared to the experimental data. After some adjustment of the cycle control parameter, better agreement with the data is possible. The comparison to experimental data for the traditional DW is shown for the water sump temperature, Figure 38, and for the power consumption, Figure 39. Good agreement is found on the time required to reach the wash and rinse temperatures. Also the temperature decay during the main wash from recirculating water with no heat input is captured in the model. The pulsing controller for the electric element is also represented well. One improvement possible on the heater controller is to incorporate Equation 2 and modify the power output as a function of the element temperature.

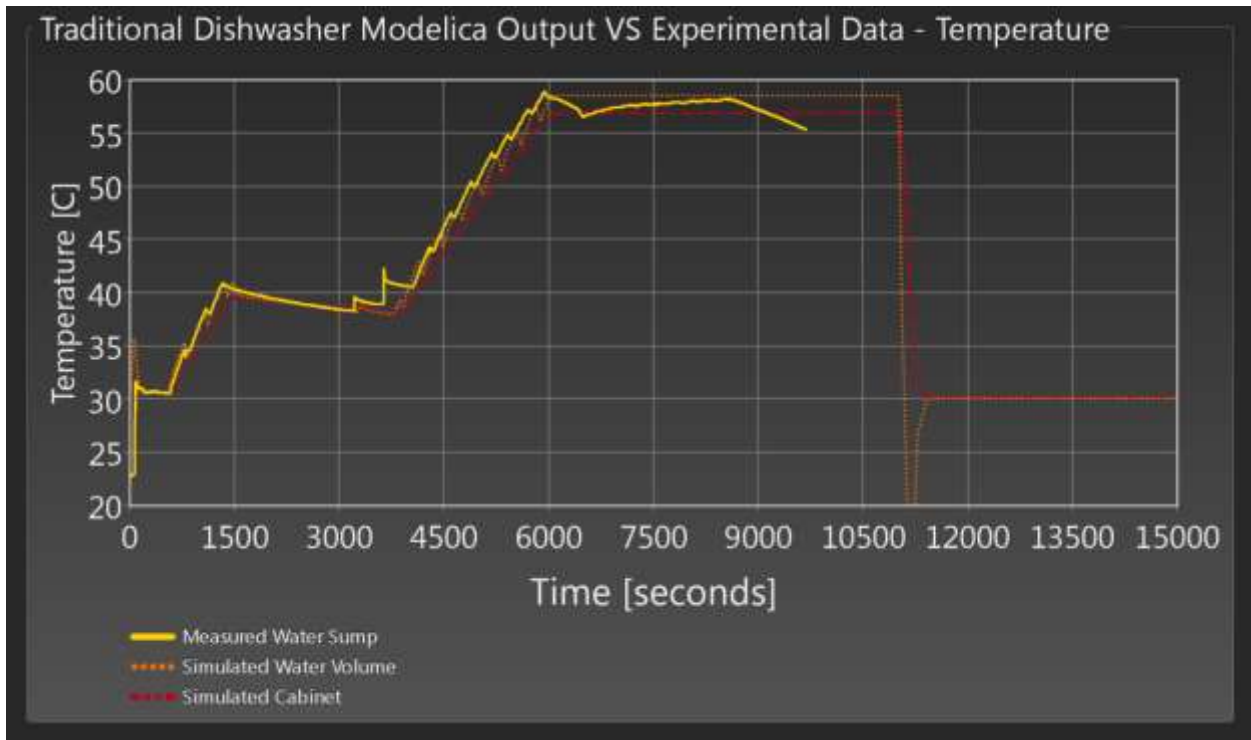


Figure 38: Traditional DW Simulated Temperatures Versus Experimental Data

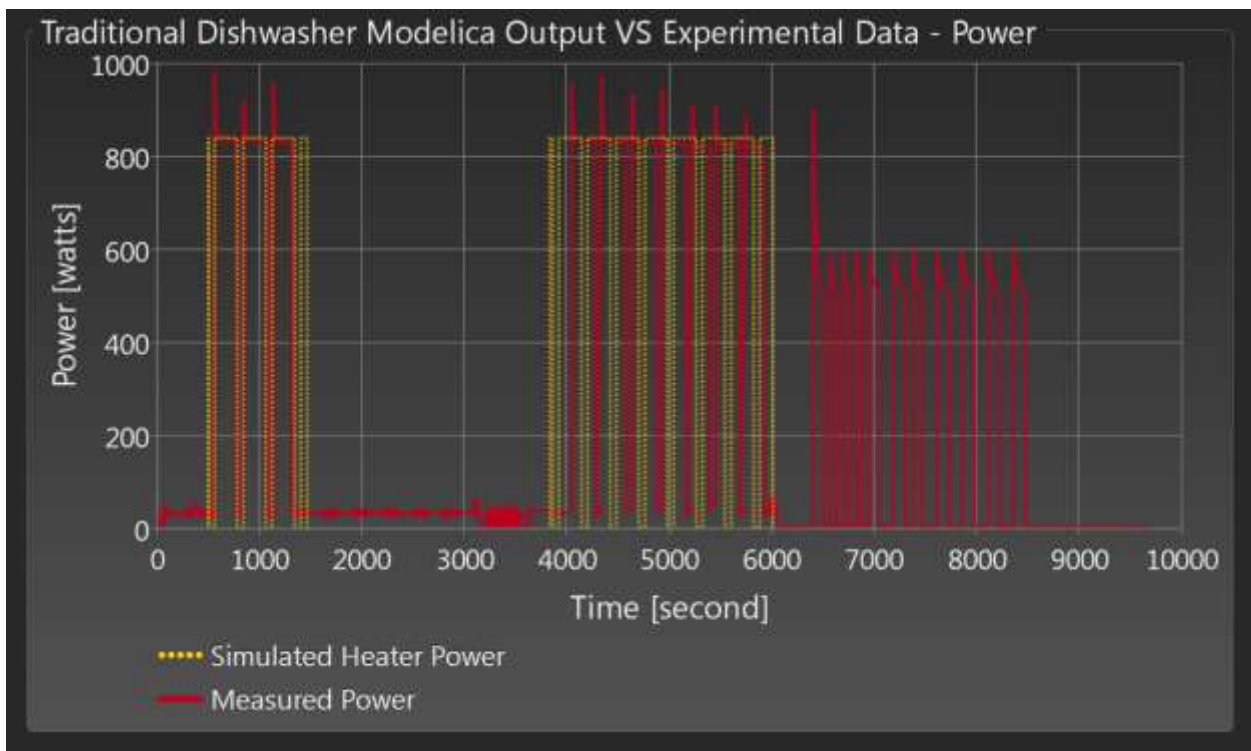


Figure 39: Traditional DW Simulated Electric Element Power Versus Experimental Data

Another plot compares the predicted sump temperature versus the sump temperature from experimental results and identifies a 5% error band to estimate the accuracy of the model prediction. Overall the model shows fairly good agreement. At lower temperatures the model tends to under predict while at high temperatures the model starts to slightly over predict the sump temperature. For the purposes of the initial simulation, this agreement is suitable as a starting point to explore DW cycle impacts from thermal integration.

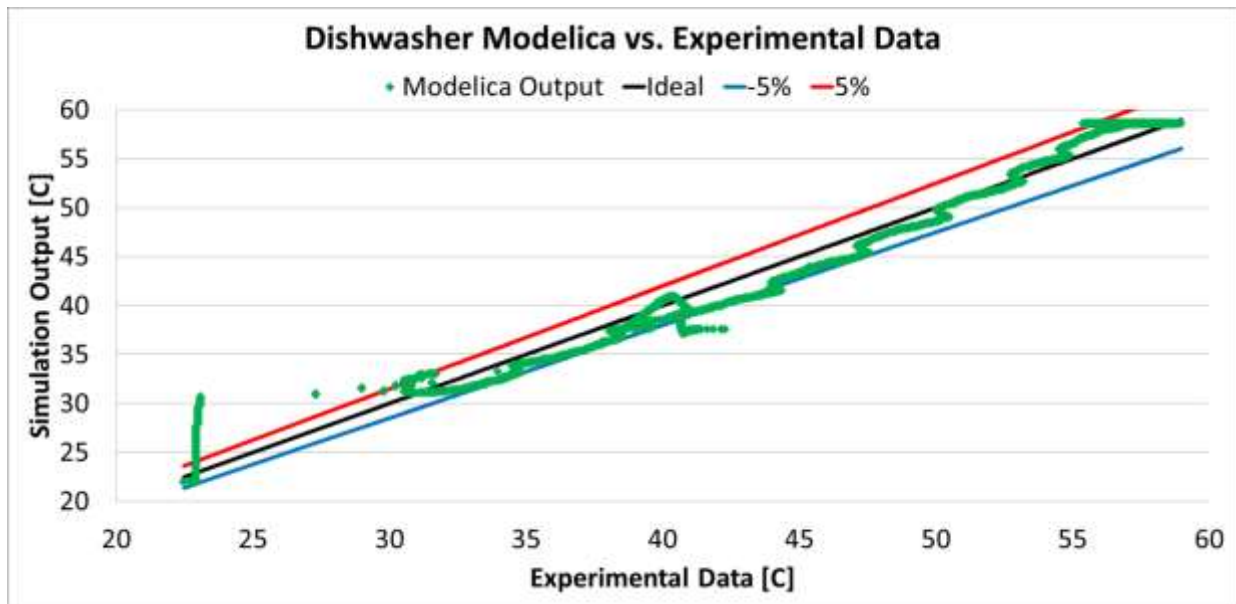


Figure 40: DW Modelica Water Sump Temperature – Simulated versus Experimental

### 3.4.5 Heat Loop DW Simulation Results

The heat loop feature of the DW is simulated and compared to the traditional experimental data as shown in the previous graphs. The plots of the sump temperature and power consumption versus time are viewed in Figure 41 and Figure 42. The heated wash step required more time than the traditional system due to the lower heating capacity of the hot water loop. The number of electric element cycles is reduced as desired by leveraging the external heating loop.

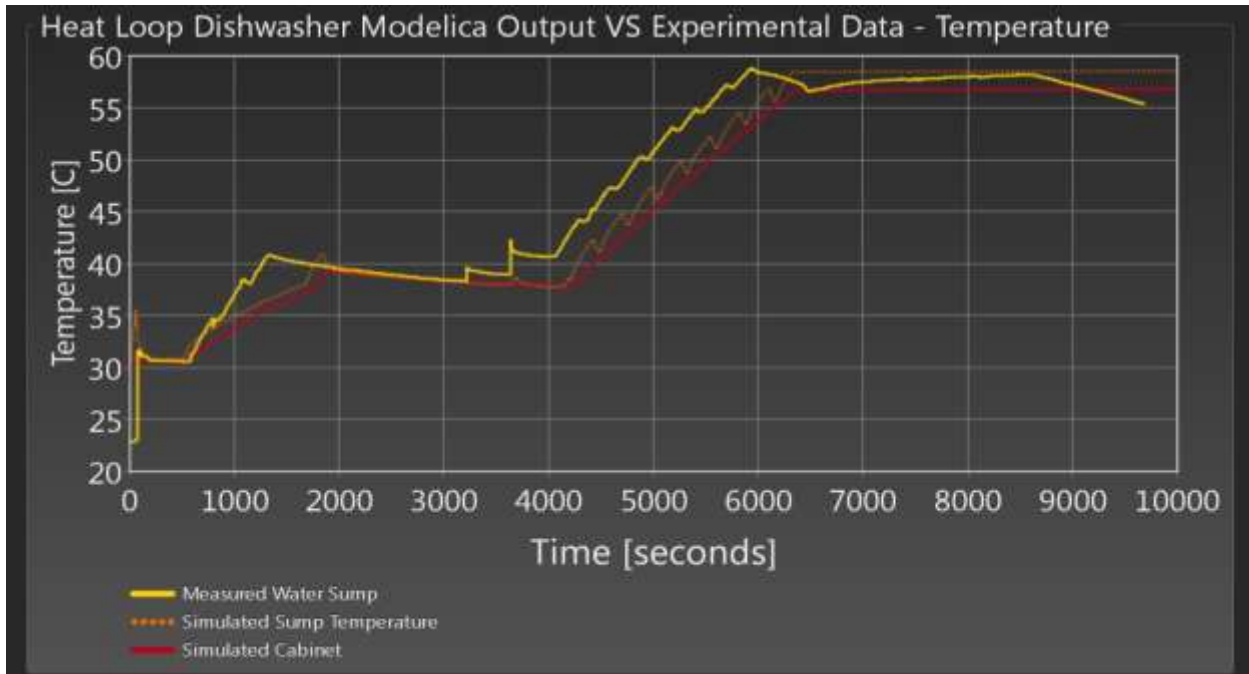


Figure 41: Heat Loop Driven DW Simulated Temperatures Versus Experimental Data

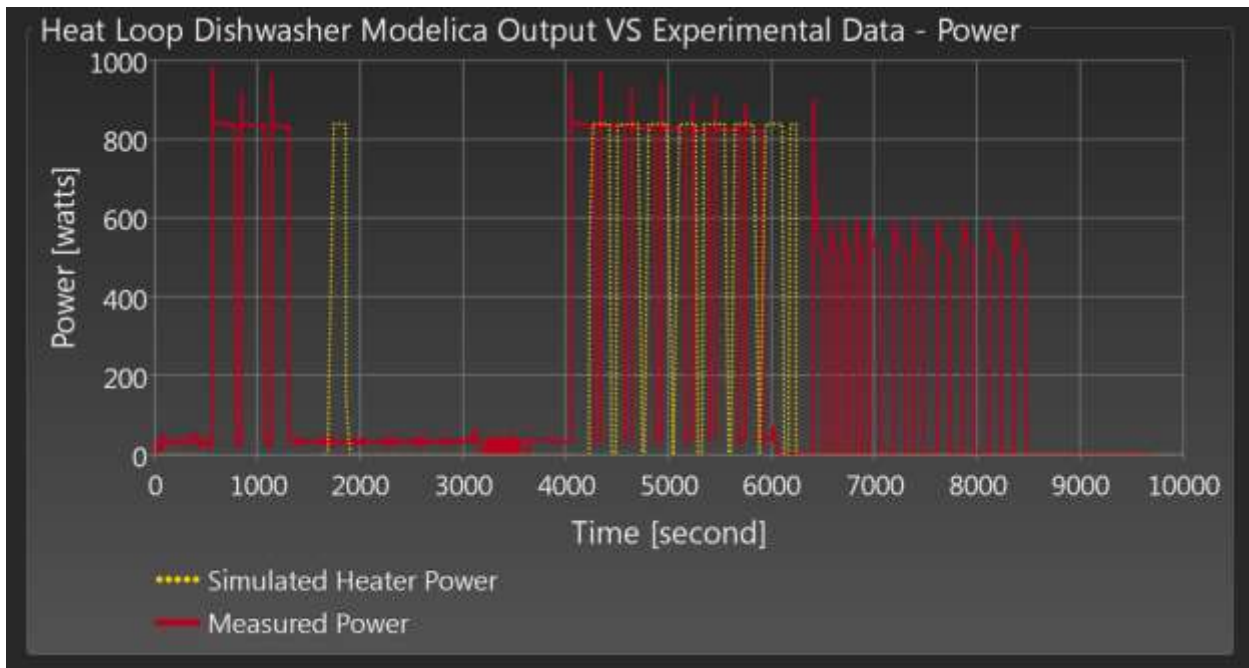


Figure 42: Heat Loop Driven DW Simulated Electric Element Power Versus Experimental Data

### 3.5 Clothes Washer

As identified in the literature and manufacturer data, potential for heat recovery from the clothes washer is from the waste water during the wash cycle. The limited use of an internal heater for temperature control does not justify adding components for the supply of external heat. In contrast, European models are plumbed with a cold water supply instead of a hot water supply and rely entirely on the use of an internal resistor heater to elevate the temperature to required levels based on design settings. Here further energy savings could be realized and could justify the added cost of external connection for a heat loop fed by a central hot water storage tank.

#### 3.5.1 Approach

To represent the CW units today, a pump and a fixed volume tank to capture the drain pump and wash or rinse water in the drum at an elevated temperature. Connect the outlet of the drain pump to a second, fixed volume tank, to hold the warm, waste water for heat recovery. A second pump is connected to this tank for circulating the waste water to one side of a FPHX while on the other side heat is collected by the thermal loop. The pumps are to be controlled with timers to mimic the timing of the wash and rinse drains in a standard CW cycle. The heat recovery pumps then operate in response to the temperature level in both the heat recovery tank and central storage tank. If the drain water is too cool in temperature, a three-way-valve switches the outlet of the pump for heat recovery and activates to dump the waste water down the drain since no heat can be collected.

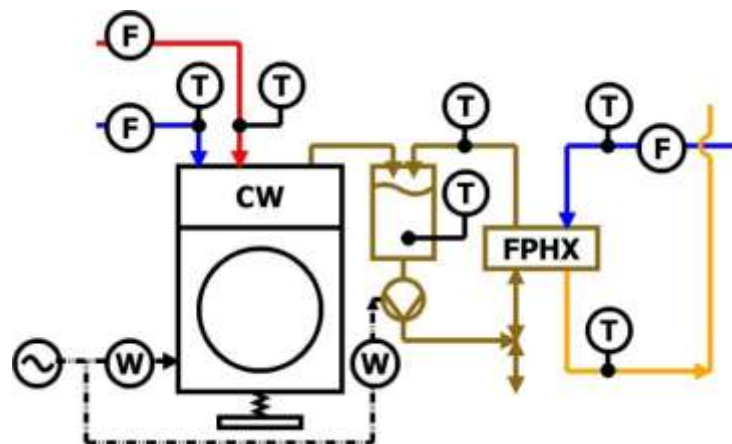


Figure 43: Sample Approach to CW Modelica Model

An expansion tank represents the drain tank that collects water from the waste line of the appliance. The tank is filled by changing opening a valve connected to a pressure boundary with a fixed

temperature. The valve is opened by changing its cross-sectional area and the fixed temperature can be varied to capture different cycle settings resulting in different temperature levels of waste water. The volume of water sent to the expansion tank is controlled by the timing of the valve opening. This can be controlled with a simple PID controller referencing the overall tank volume and filling level. This variation allows for representation of different CW technologies and different load sizes which all impact the amount of waste water generated.

The main areas of interest are the duration between the start of the cycle to the first drain at the end of the wash, and the second duration between the end of wash and end of rinse. The end of these two steps in the cycle is when the heat source is expected. Therefore the Modelica model accounts for the delays between each bulk heat generation to characterize the losses that exist and predict the amount of heat that can be recovered. The volume of water generated is strongly dependent on the CW technology, VA or HA. A figure referenced in the appliance background compared the average volume of cold and hot water used for each CW type, Figure 10. This could be used as a starting point on the amount of elevated temperature waste water that can be expected to be generated per CW cycle.

### 3.6 Integrated Appliance System

To capture the interaction of an integrated appliance system, A simple approach to an integrated appliance system was first modeled by using discrete area HXs for each appliance, interfacing with a single node storage tank volume, and using fixed water source temperatures to replicate the expected temperature levels for each appliance. The results were also published in a conference paper (Caskey et al., 2018).

#### 3.6.1 Approach

A schematic of the simulation interface can be seen in Figure 44**Error! Reference source not found.**, where appliances are identified with the components representing their operation while

connected to a storage tank.

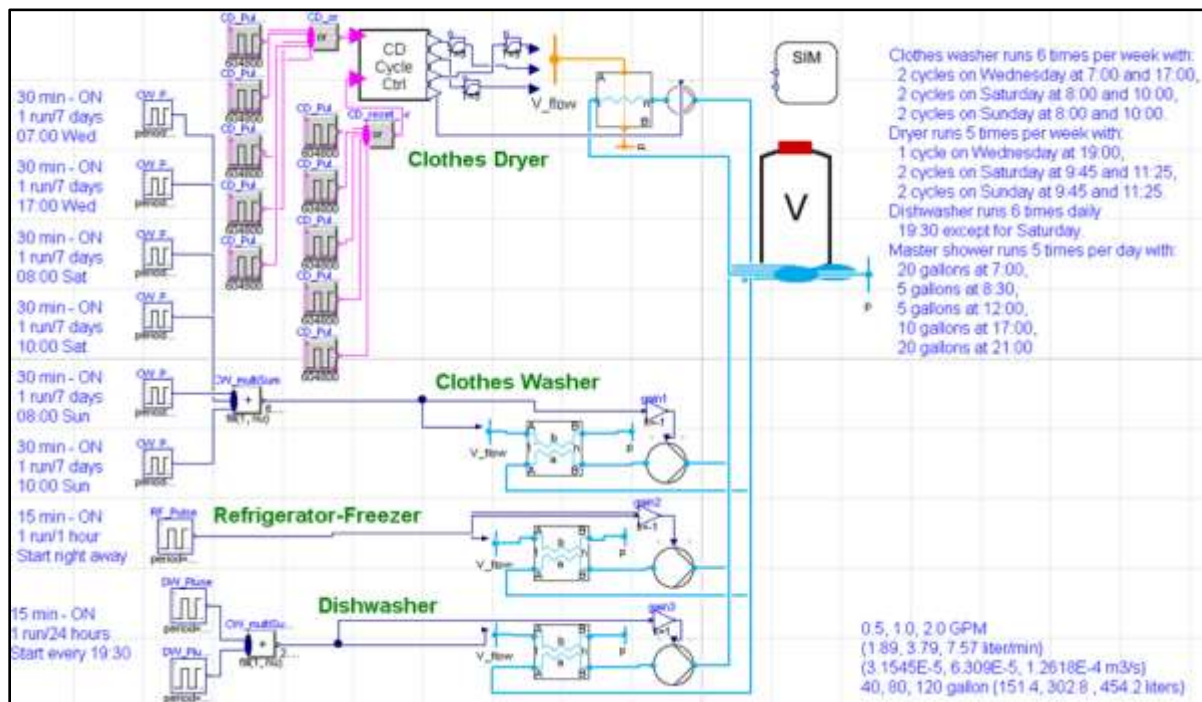


Figure 44: Modelica components representing 4 appliances connected to a central storage tank for heat recovery

### 3.6.2 Appliance Schedule

Significant effort has been made by the DOE on developing a benchmark American home for modeling purposes to support and prove the benefit of using advanced systems in the home (Wilson et al., 2014). The study provides very specific usage characteristics for all systems in the home, including appliances. In one study, a weekly appliance schedule is generated from the 2008 version of the Building America Research Benchmark by Hendron, R., (Boudreaux et al., 2012). From the number of bedrooms and the appliance capacity in the study, an assumed number of cycles per year are calculated for each appliance. With an annual cycle count, the average number of cycles in a week is assumed for each appliance when spreading the annual usage evenly over the 52 weeks in a year. The authors selected six CW cycles, five CD cycles, and 6 DW cycles in a week. The DW is specified to be run every day at 7:30 pm except Saturdays. The CW and CD are used twice on Saturday and Sunday mornings, and two CW cycles to one CD cycle on Wednesdays. During a week simulation, the relative operation of each appliance is shown in Figure 45 with each time step on the grid representing a 24-hour day starting on Monday.

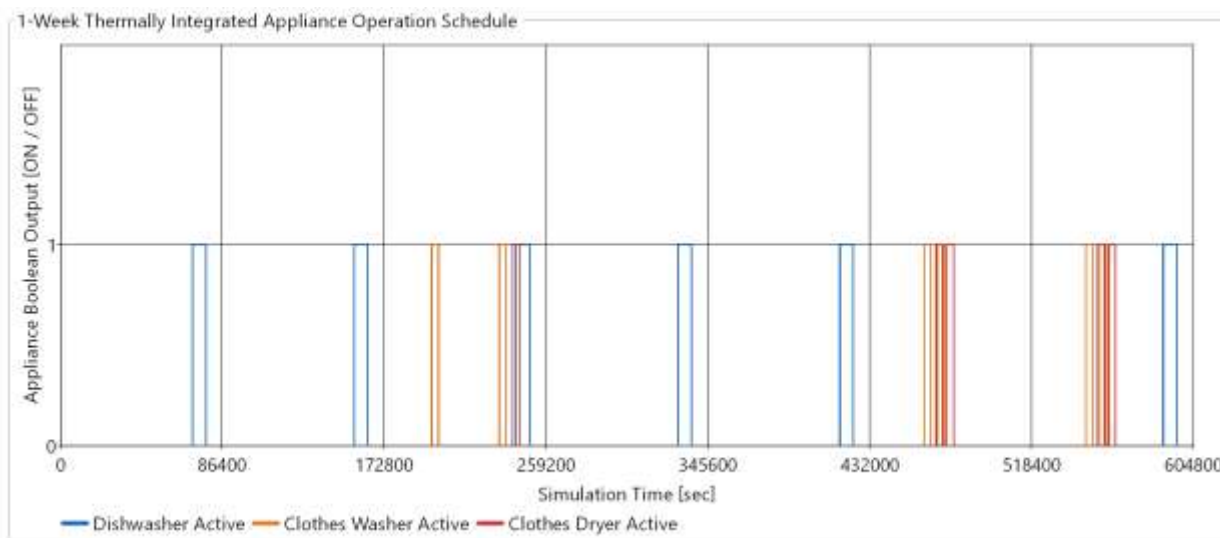


Figure 45: Plot of 1-Week Appliance Schedule for Dishwasher, Clothes Washer, and Clothes Dryer

### 3.6.3 Simple Storage Tank

gallons), 225 liters (60 gallons), and 454 liters (120 gallons) are shown in **Error! Reference source not found.** The collection flow rate was fixed for all appliances at 7.6 liter/min (2 GPM). The rate of temperature rise is higher as expected with the lower volume tank but by the sixth day, the largest tank starts to reach the temperature level of the smallest tank.

### 3.6.4 Simulation Results

The water tank temperature as a function of time for varying tank volumes of 114 liters (30 gallons), 225 liters (60 gallons), and 454 liters (120 gallons) are shown in Figure 46 **Error! Reference source not found.** The collection flow rate was fixed for all appliances at 7.6 liter/min (2 GPM). The rate of temperature rise is higher as expected with the lower volume tank but by the sixth day, the largest tank starts to reach the temperature level of the smallest tank.

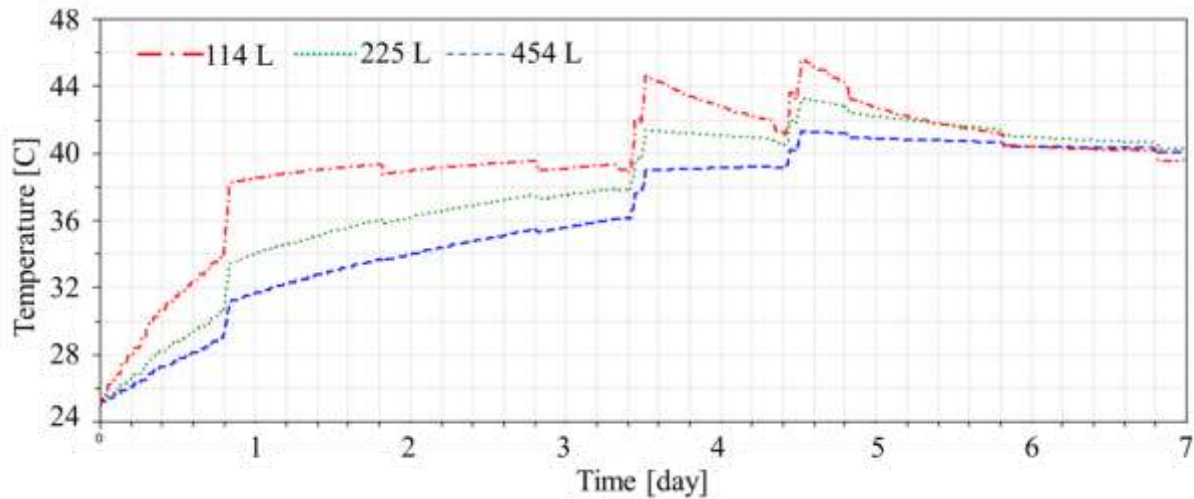


Figure 46: Integrated Appliance Model - Impact of Tank Volume on Temperature over Time

As the tank heats up, the temperature rise impacts the amount of heat possible to extract from each appliance. The trends can be seen in Figure 47 for a tank volume of 454 liters (120 gal.).

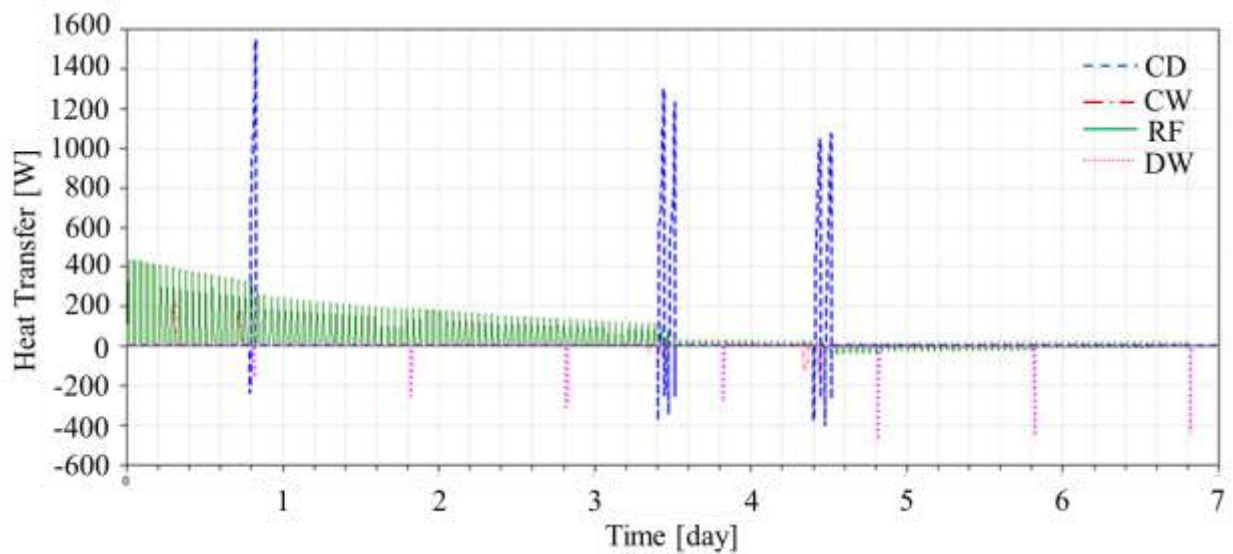


Figure 47: Rate of Heat Transfer between each Appliance and 454 L (120 gal.) Storage Tank

The amount of energy delivered or removed by each appliance by the storage tank is shown in Figure 48.

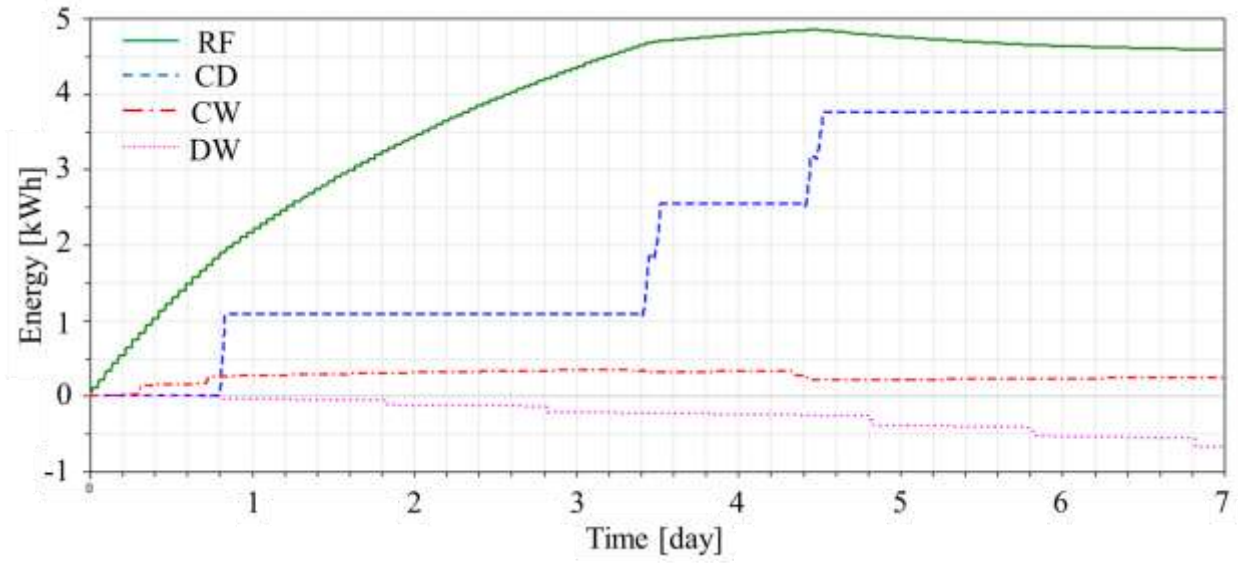


Figure 48: Amount of Energy Collected by Each Appliance with 454 L (120 gal.) Storage Tank

## 4. EXPERIMENTAL TEST STAND

To determine the accuracy of the model and areas for improvement, a functional prototype was designed, fabricated and experimentally tested. The Modelica models provided required capacities and flow rates for the selection of heat exchangers and pumps. The existing RF and DW are modified with a connection to a water loop from a central storage tank. The heat recovery equipment for the CW and CD are attached to the waste heat source of the appliance to avoid any significant modifications. Heat is recovered a similar water loop connected to the central storage. The piping connections, pumps, and central storage tank of water is similar in design to a hydronic HVAC system. A schematic of the built test stand is shown in Figure 49. The instrumentation locations for each major component are also shown.

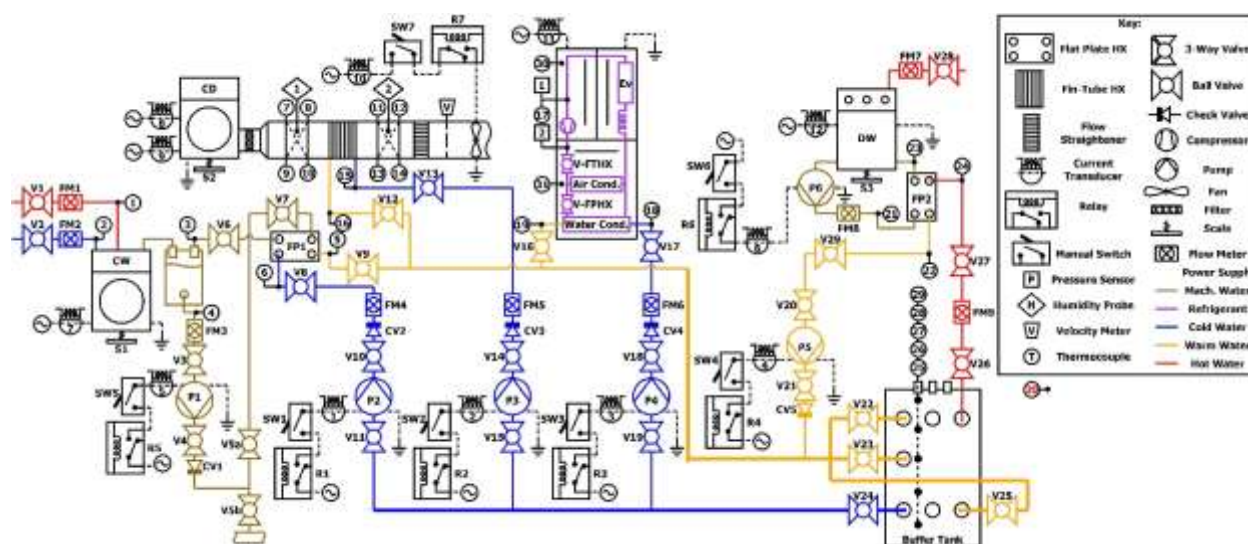


Figure 49: Schematic of Entire Integrated Appliance Test Stand with Instrumentation

### 4.1 Clothes Dryer

An instrumentation system is designed and built to recover heat from the moist, hot air stream being vented out of an electric dryer. Steps are made to accurately quantify the amount of heat recovered and reduce any impact on the drying performance of the dryer. The following sections outline the methods and equipment used to achieve this objective.

### 4.1.1 Overall Approach

A finned heat exchanger is placed in the dryer exhaust duct to extract heat out of the moist, hot air stream using a water loop. A schematic showing the layout of all components and heat exchanger is shown in Figure 50. To reduce fouling on the finned surfaces, an extra lint filter is placed upstream of this heat exchanger. Two sets of a 4-point thermocouple temperature mesh coupled with a single point RH sensor measure the air stream conditions entering and leaving the heat exchanger. A hot wire anemometer downstream of a flow straightener measures the air flow rate of the heat recovery system. The same measurement represents the air flow rate through the dryer drum by the internal blower which has a strong influence on the drying rate of the clothes. To minimize the added pressure drop from both heat recovery and measurement approaches, an auxiliary, variable speed blower is located downstream of all components.

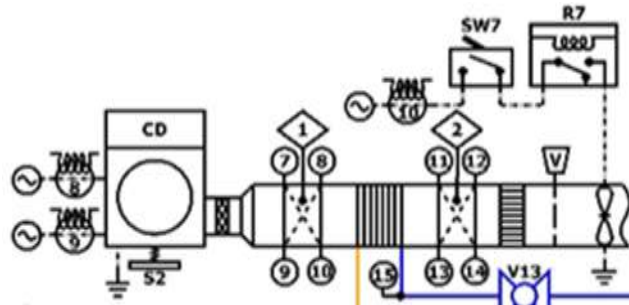


Figure 50: Clothes Dryer Exhaust Duct Layout on Heat Recovery Approach and Measurements

### 4.1.2 Fin-and-Tube Heat Exchanger

A fin-and-tube heat exchanger was selected that could closely fit the existing exhaust duct size, 10 cm (4 in) with minor transitions required. An appropriate unit was found designed for cooling light reflectors within indoor grow rooms for gardening. The HX housing connects to a 15 cm (6 in) round duct. An image of the HX with housing is shown in Figure 51. The level of detail available on the HX capacity from the manufacturer was limited. A rating of 1.31 kW (4,500 BTU/h) was listed but did not provide an associated flow rate or any airside or water side temperatures. Minimum recommended values were listed for supporting equipment, an fan airflow rate of 425 m<sup>3</sup>/h (250 CFM) per 1 kW, and a pump providing 18.9 LPM (5 GPM) at 3.05 m (10 ft) of head. The housing was removed, as seen in Figure 51, to identify the HX circuit layout and measure the fin density for the modeling effort.



Figure 51: Image of Clothes Dryer Fin-and-Tube Heat Exchanger with Geometry Details

#### 4.1.3 Temperature Mesh and Relative Humidity Measurements

A 4-point thermocouple mesh is used to accurately calculate an average inlet temperature for the entire cross-sectional area. The TC beads are located at the center of each 4-part area making up the entire cross-section as shown in Figure 52. A relative humidity probe is located as close as possible to the center of the duct without interfering with the mounting wire holding each thermocouple.



Figure 52: 4-Point Thermocouple Grid and Relative Humidity Probe on Clothes Dryer Duct Before (Left)/After (Right) Heat Exchanger

#### 4.1.4 Hot Wire Anemometer

To measure the airflow rate within the duct a hot wire anemometer is used. The installation requires a separation from any components of several duct diameters upstream and downstream as well as the use of a flow straightener to improve the measurement accuracy. Referencing ASHRAE Standard 41.2 and manufacturer recommendations, a flow straightener of thickness,  $0.45D$  or 6.86 cm (2.7 in), is located at least  $5.25D$  or 78.7 cm (31 in) upstream, and a clear distance downstream of  $3D$  or 45.7 cm (18 in) from the auxiliary blower. The flow straightener is a Plascore crate #19584. Due to these added lengths, the anemometer is located downstream of the HX to minimize heat losses upstream. Two sampling locations are used by the instrument to provide an average airflow value. The installation of both within the duct is shown in Figure 53.



Figure 53: Flow Straightener (Left) and Hot Wire Anemometer (Right)

#### 4.1.5 Auxiliary Fan

A second blower is located at the end of the duct to help overcome the additional pressure drop created by all equipment located in the duct. A variable speed unit rated at 351 CFM with 40 Watts was selected that fit the duct size used. Six different speed settings are available to best match the baseline flow rate measured without HX installed.

#### 4.1.6 Insulation

To ensure the most ideal heat recovery process, all components are insulated downstream of the dryer drum down to the last sensor location. This included insulating the duct within the dryer cabinet, Figure 54. Versamat insulation is used which is rated for the high temperatures seen within ducted clothes dryer.

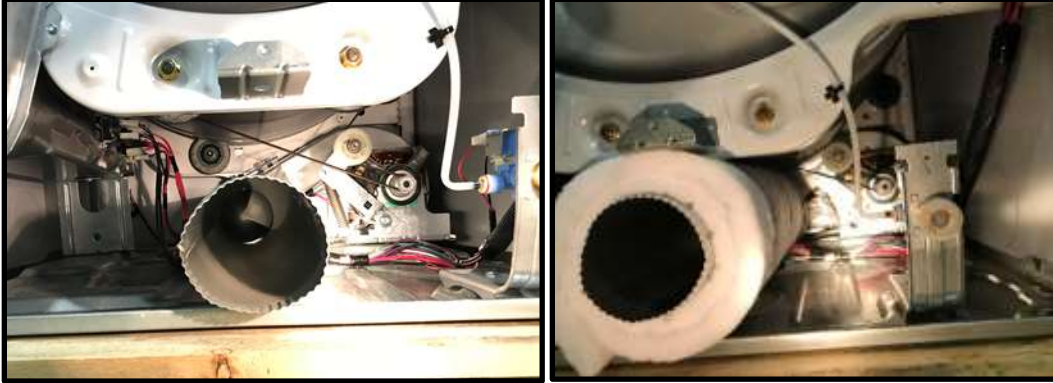


Figure 54: Insulating Internal Duct of Vented Clothes Dryer (Before-left / After-Right)

The entire external duct is also insulated up to the HX and down to the airflow sensor to ensure all sensors are impacted minimally by any heat losses due to the large surface area. The final installation is shown in Figure 55.



Figure 55: Clothes Dryer Duct After Insulation

## 4.2 Refrigerator-Freezer

An instrumentation system is designed and built to recover heat from the moist, hot air stream being vented out of an electric dryer. Steps are made to accurately quantify the amount of heat recovered and reduce any impact on the drying performance of the dryer. The following sections outline the methods and equipment used to achieve this objective.

The RF has the refrigeration circuit modified by replacing the air cooled condenser with a FPHX to reject heat to a water loop. Low temperature water is pumped from the central storage tank to

recover waste heat rejected by the RF during a compressor ON cycle. The amount of heat collected is calculated by measuring the inlet and outlet temperatures and flow rate of the water loop. The only conditions measured on the RF are the refrigerant pressures on the suction and discharge sides of the compressor and the power consumption.

#### 4.2.1 Overall Approach

On a prior project, a bottom-mount freezer, side-by-side refrigerator (KRFC300ESS01) had a water-cooled, flat-plate HX installed in parallel to the existing air-cooled condenser. The U.S. energy guide for this model lists the unit having a rated capacity of 566 liters (20 ft<sup>3</sup>) and an estimated annual energy usage of 563 kWh. Two normally closed solenoid valves located directly after the discharge line control which HX is actively being used for heat rejection. An overall schematic of the refrigerator with instrumentation is shown in Figure 56. With the focus on heat recovery, only the water-cooled condenser is active during testing. A variable speed pump controls the water flow rate and can be varied to explore its impact on compressor power draw and return water temperatures to the buffer tank.

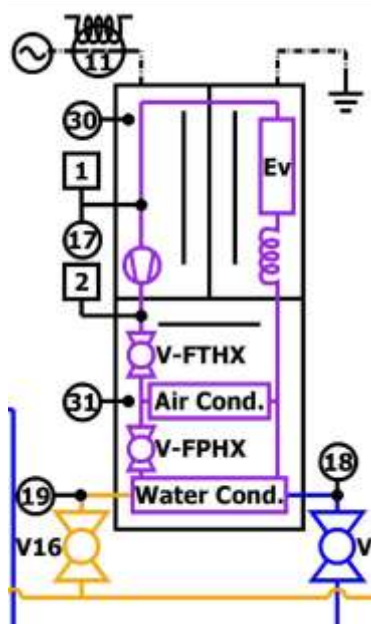


Figure 56: Schematic of Refrigerator Test Stand with Instrumentation

### 4.2.2 Flat-Plate Heat Exchanger



Figure 57: Back of Test Stand Refrigerator with Flat-Pate Heat Exchanger and Instrumentation



Figure 58: Back of Test Stand Refrigerator after Insulation Installed

### 4.3 Dishwasher

The DW measures the temperature and amount of DHW used during the entire cycle. The calculated amount of energy delivered from the DHW along with the measured power consumption combine for the total DW power consumption. The sump pump normally installed on the DW is assumed to require replacement and thus will be separately monitored and accounted to the overall power consumption. The DW machine water loop temperature is measured before and after the FPHX along with the flow rate to calculate the amount of heat supplied by the water loop. This is compared for redundancy to the calculated capacity using the inlet and outlet temperatures on the other side of the FPHX and flow rate.

### 4.4 Clothes Washer

The CW drains into a fixed volume tank that has a pump connected to an outlet port at the base of tank. The pump drives the flow of waste water for heat recovery or drainage as shown in the schematic, Figure 59. Depending on the measured temperature of the CW waste water and the

central storage temperature, the heat recovery pump will activate and the pump on the tank will activate. Both pumps enter opposite sides of a FPHX and heat is recovered by a secondary water loop. The heat transfer on both circuits is measured using four inlet, outlet temperatures and two flow meters. The hot and cold water volumes and temperatures delivered to the CW are also recorded to estimate the amount energy provided by the water stream and total waste water volume.

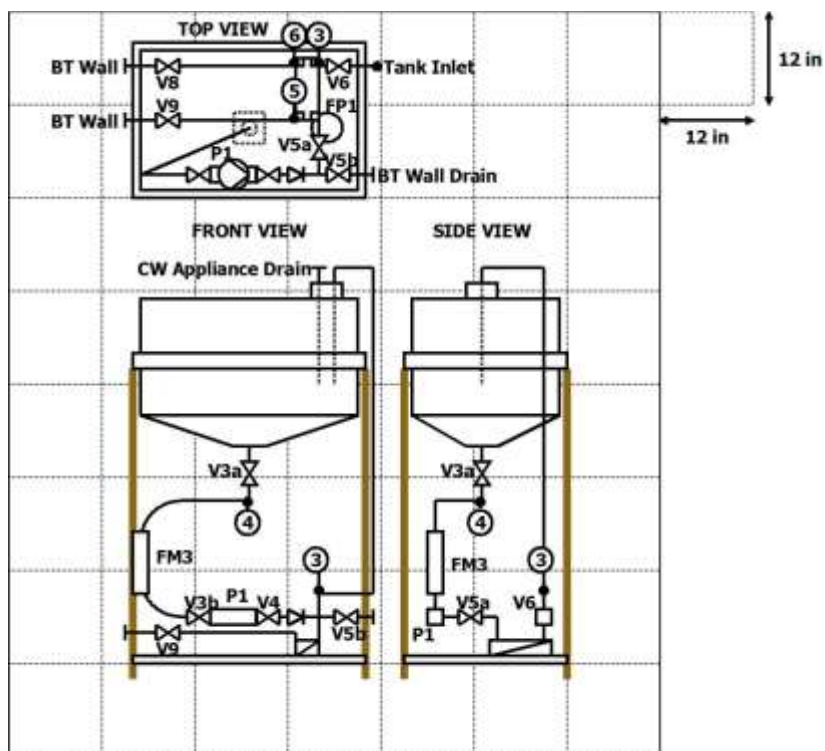


Figure 59: Schematic of Proposed Drain Tank with Heat Recovery for the Clothes Washer

The model appliance used for the test stand was a front load, horizontal axis unit with a rated capacity of X ( $X \text{ ft}^3$ ). The user settings were noted to specify the testing conditions used for each washing cycle. The normal wash was the preferred option since it is assumed to represent most cycles selected by consumers. Three different heat settings were available under the normal wash, cold, warm, and hot. An image of all available options is shown in Figure 60. A medium soil level and extra spin was always selected for all cycles ran. The higher spin speed was desired to provide the lowest water level possible to the CD and thus the lowest moisture content available in the exhaust airstream.



Figure 60: Test Stand Clothes Washer Cycle Setting Front Panel

#### 4.5 Buffer Tank and Piping Backbone

Due to the intermittent operation of the appliances a thermal storage tank is required to hold heat from one appliance heating cycle and deliver heat to another appliance for the next cycle. The approach is very similar to a HVAC hydronic system using a buffer tank interfacing between a source and several building zones. With this well-known system, the original layout started with example hydronic systems and was modified to match any requirements for this specific test stand. Also to properly verify the amount of heat being exchanged as well as control the management of the heat, sensor placement and relay operation was introduced on all piping and equipment connected to each appliance. The process was done iteratively with each step being moved forward starting at a high level and growing in complexity as the design progressed. Having a known space, a layout started by locating all piping connections and buffer tank in the center with the appliances being spread around this center. Appliances consuming water, CW and DW, are to be adjacent to each other for minimizing added piping lengths. The CD had a long profile due to the space requirements between equipment on the exhaust duct for accurate measurements. A scaled diagram shown in Figure 61 identifies the final placement of all components as well as identifying any existing objects such as a tool chest or supporting columns for the building.

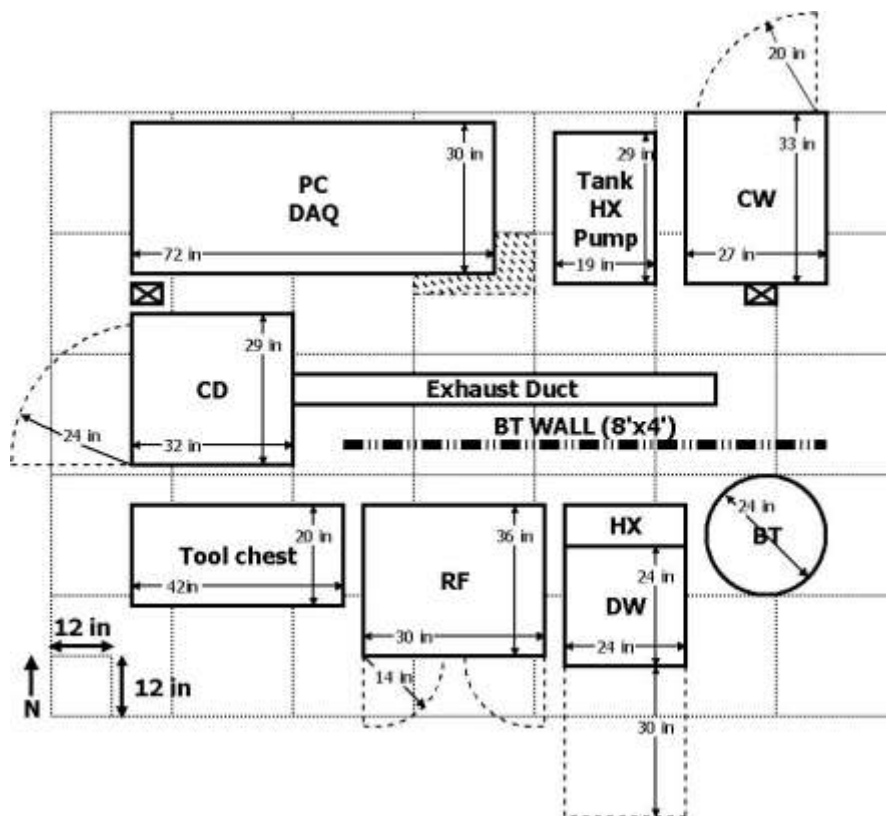


Figure 61: Test Stand Layout for Appliances, Buffer Tank, and Piping Mounting (BT Wall)

Using the finalized layout, the next step was to design the piping connections and sensor positions on a wall at the center of the system. The buffer tank was already known at this point due to its volume capacity and available port locations to charge or discharge. The pulsing, turbine flow meters, FTB4605, for measuring volumetric flow rate required upstream and downstream accommodations for accurate readings. All power controls and measurements were to be located on this central wall as well to simplify the approach and allow for easy replacement of any equipment or appliance. The appliances themselves only required power monitoring and were not connected to any relays for computer control. All pumps, solenoid valves, and fan required both monitoring and control. All electrical connections were made above the plumbing connections to reduce the risk of water contact with any outlet. The final layout of the wall is shown in Figure 62. All labels can be referenced with Figure 49. The line colors correspond with the expected temperature of the water, red for hot, blue for cold, and yellow for warm. Grey indicates required piping distances around the flow meters. Extra distance is required downstream of the pumps since the isolation valves could be used to throttle the delivered flow rate for more control since most pumps selected were fixed speed.

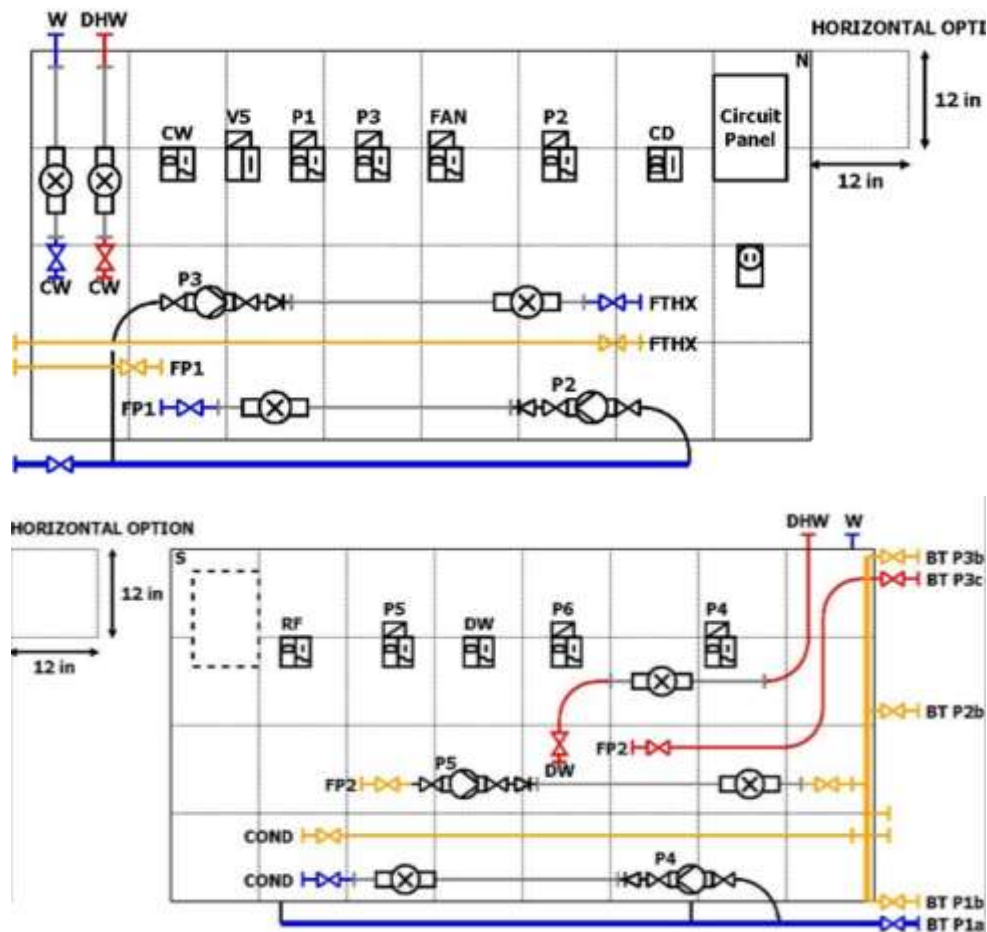


Figure 62: Piping Wall Layout with Pump, Valve, Flow Meter and Power Supply Locations for Each Appliance and Buffer Tank (Top-North Side / Bottom-South side)

#### 4.6 Controls and DAQ System (LabVIEW)

All of the data monitoring, recording and component controls are handled within one LabVIEW program. The structure of the program is a state machine that switches between monitoring selected channels and writing to the CSV for recording.

##### 4.6.1 Front Panel Control

The LabVIEW front panel provides a live display of all monitored channels and can be seen in Figure 63. Three slots are available to choose the mode the DAQ is running in parallel capturing only the flow meter channels associated with the CW, CD, or DW. The minimum sampling time of the DAQ is restricted by the required 1 second per flow meter channel to obtain an accurate flow rate.

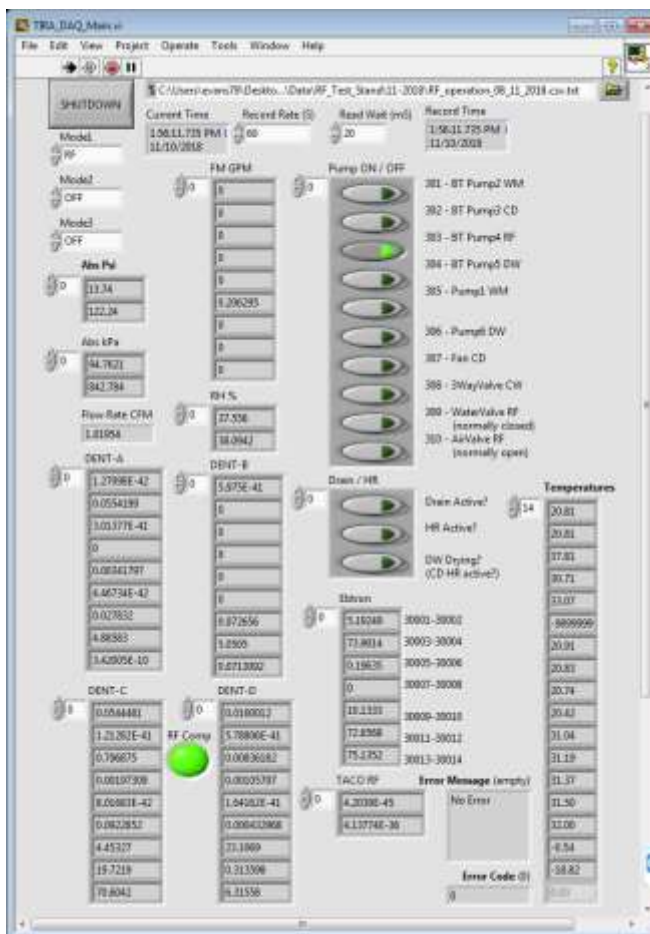


Figure 63: Main Front Panel Display with Monitored Channels and Controls for Different Modes

## 4.7 Cycle Results

The following sections present the experimental data collected from each appliance cycle that best identifies the parameters to be captured in the models and guide any improvements necessary before using them within the integrated appliance system. The raw data required postprocessing using Python and used TIL Media for any fluid property calculations to obtain flow rates or capacities using the measurement data.

### 4.7.1 Clothes Dryer

After completing the baseline measurements to establish the natural operation of the vented dryer, nine drying cycles with the same load size were run with heat recovery.

### *Duct Airflow Rate*

The impact of fouling within the exhaust duct due to the heat recovery components can be understood on Figure 64. The first 4 cycles were collected after establishing the baseline operation without any exhaust duct obstructions. The duct was opened at 3 locations to remove built-up lint on the HX face, flow straightener, and second lint trap.

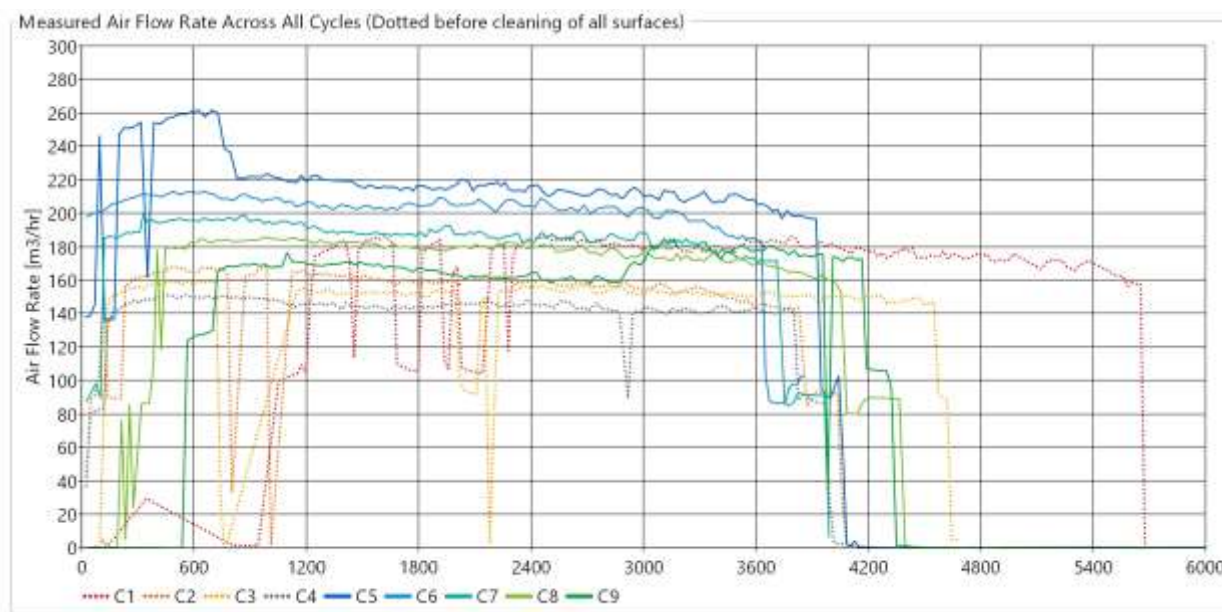


Figure 64: Clothes Dryer Air Flow Across 9 Drying Cycles, Before and After Cleaning

An adjustment of the auxiliary fan speed was required after this cleaning and is evident in the same graph on cycle 6. Here the fan speed was changed from a maximum setting of 6/6 to 4/6 to reach an airflow rate around the baseline measurement of 204 m³/hr (120 ft³/min).

### **4.7.2 Refrigerator-Freezer**

A representative sequence of compressor cycles was used for training the Modelica model. The sample data sets are shown in Figure 65 and Figure 66. The compressor ON/OFF cycling duration is the area of focus and specifically the trends during ON cycles are to be captured in the model.

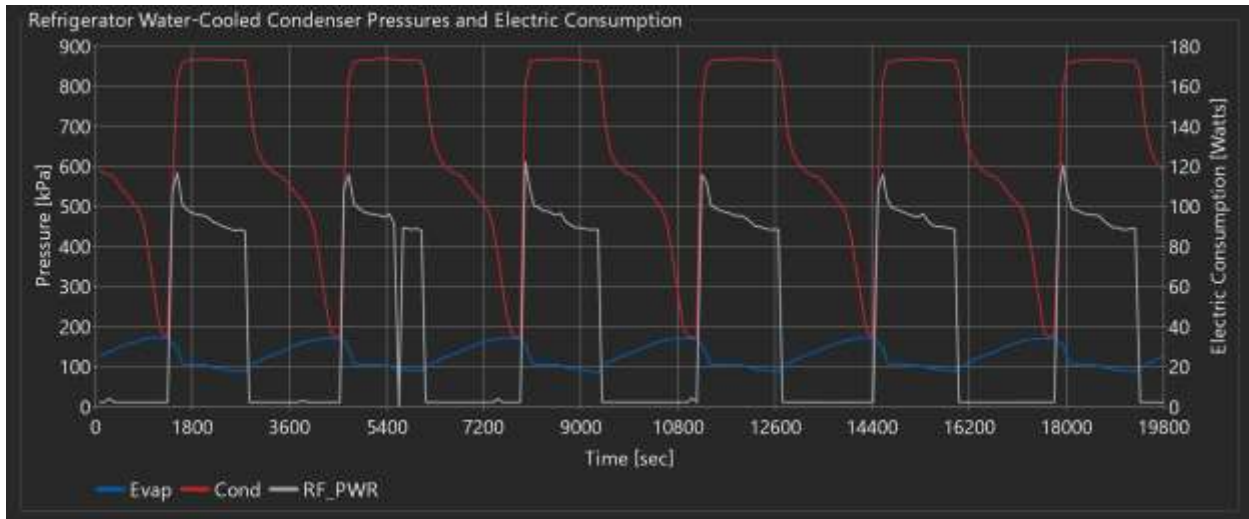


Figure 65: Sample Data Set of Refrigerator Test Stand – Total Power Consumption and Measured Pressures

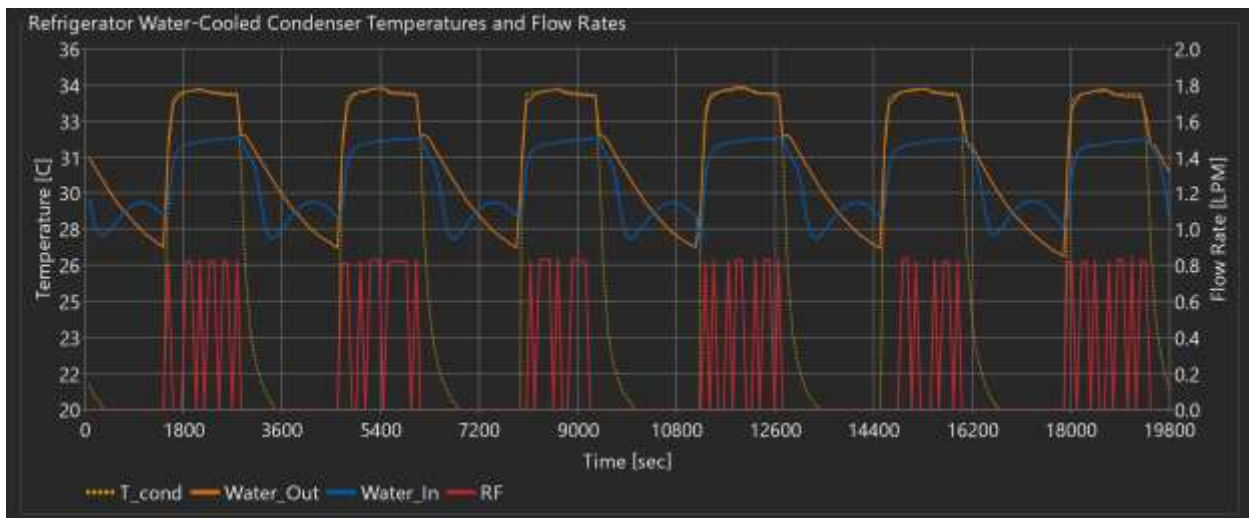


Figure 66: Sample Data Set of Refrigerator Test Stand – Inlet and Outlet Water Temperatures and Volumetric Flow Rate

### 4.7.3 Dishwasher

Four washing cycles of data were collected for the dishwasher with the last cycle run with an external heat input. The first three cycles are run using the newly installed circulation pump at full speed to best reach the baseline flow rate required for the cleaning performance.

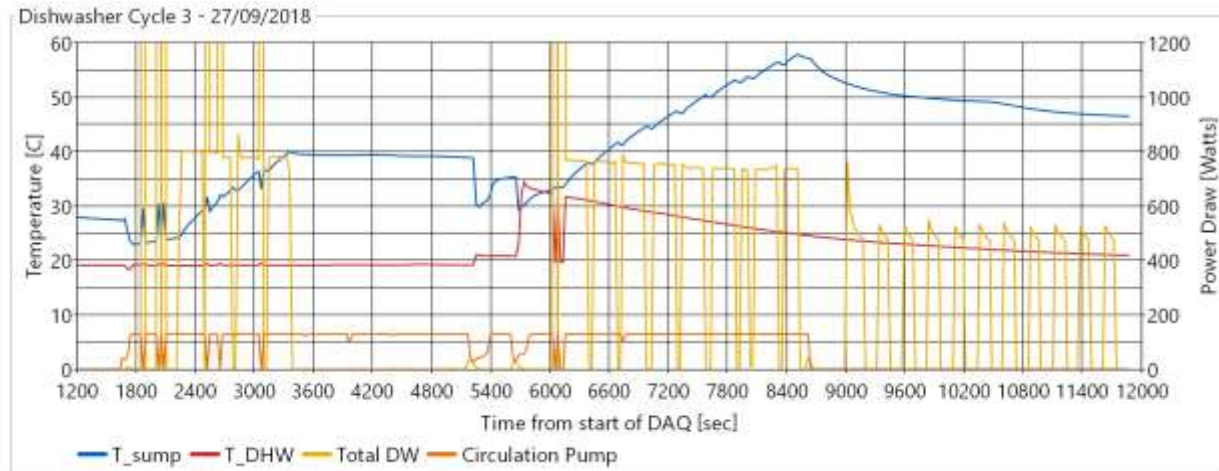


Figure 67: Test Stand Data of Dishwasher Cycle Operation Temperatures and Power Consumption – Cycle 3

#### 4.7.4 Clothes Washer

Nine CW cycles of data were collected to explore the impact of the appliance settings on the waste water temperature and heat recovery process. Due to complications with the drainage strategy not all cycles run with the same settings could be easily compared for repeatable results. Due to the low temperature of waste water measured for the normal/warm cycle, hotter wash cycles were conducted to obtain additional data for comparison, normal/hot and sanitization. With the focus around the recovery of waste heat from the CW, four temperature points on the inlet/outlet conditions of the HX, both flow rates on each circuit, as well as the flow rates into the CW were shown for each cycle.

##### *Normal –Warm Wash*

The temperature and flow rates measured during a normal, warm wash cycle are shown for the first 40 minutes in Figure 69. Roughly 6.1 L ( ) of hot water and 12.9 L ( ) of cold water are drawn for the wash step, and produces a maximum of 19 L ( ) of waste water. The heat recovery is identified in the graph starting shortly after 15 minutes into the start of the cycle, occurring after the first drain.

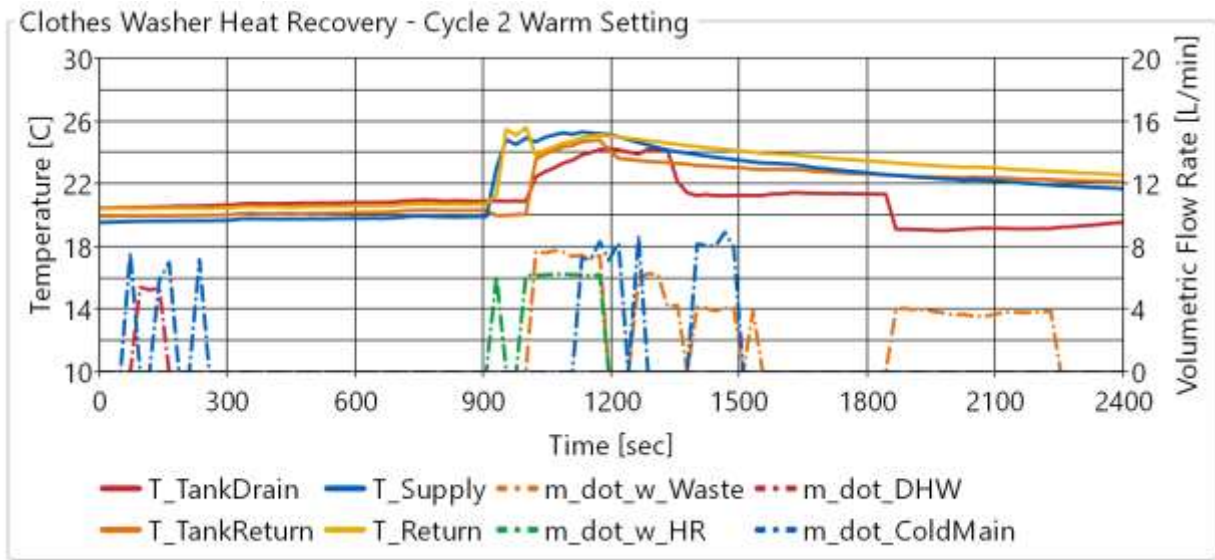


Figure 68: Clothes Washer Cycle 2 with Normal Warm Wash

*Normal – Hot Wash*

The temperature and flow rates measured during a normal, hot wash cycle are shown for the first 40 minutes in Figure 69. About 12.5 L ( ) of hot water and 4.4 L ( ) of cold water are drawn for the wash step and produces a maximum of 16.9 L ( ) of waste water. Heat recovery is also started about 15 minutes from the start of the cycle.

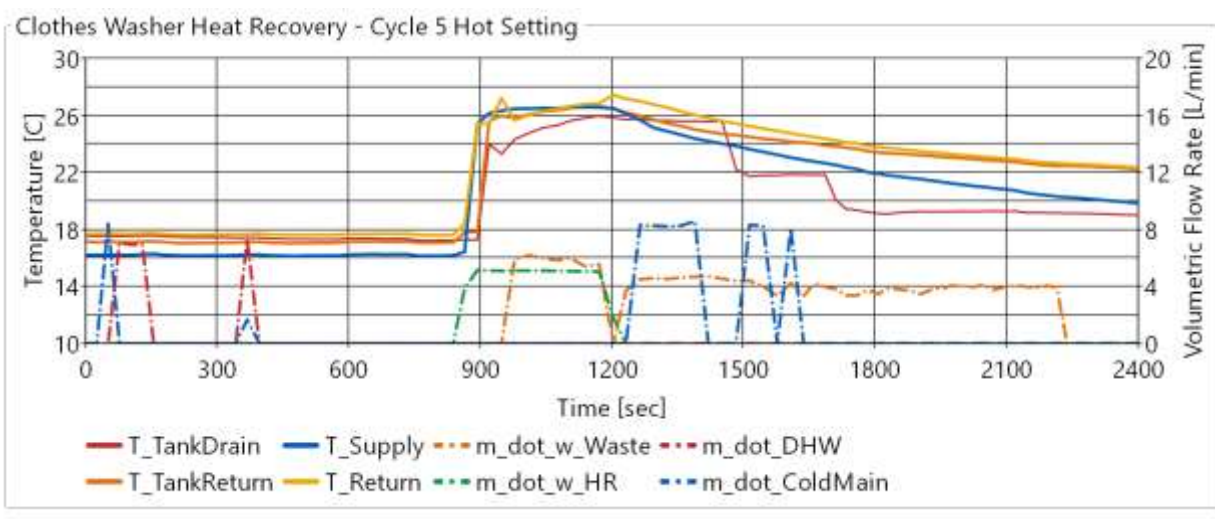


Figure 69: Clothes Washer Cycle 5 with Normal Hot Wash

### Sanitization Wash

The temperature and flow rates measured during a sanitation wash cycle are shown for the first 100 minutes in Figure 70. The cycle produced the highest temperature waste water with 19.5 L (X gal.) of hot water drawn during the wash step for the 3.45 kg (7.6 lbs) load. With a completely different wash setting, the heat recovery process does not start until 45 minutes after the start of the cycle and generates drain temperatures above 38C (F).

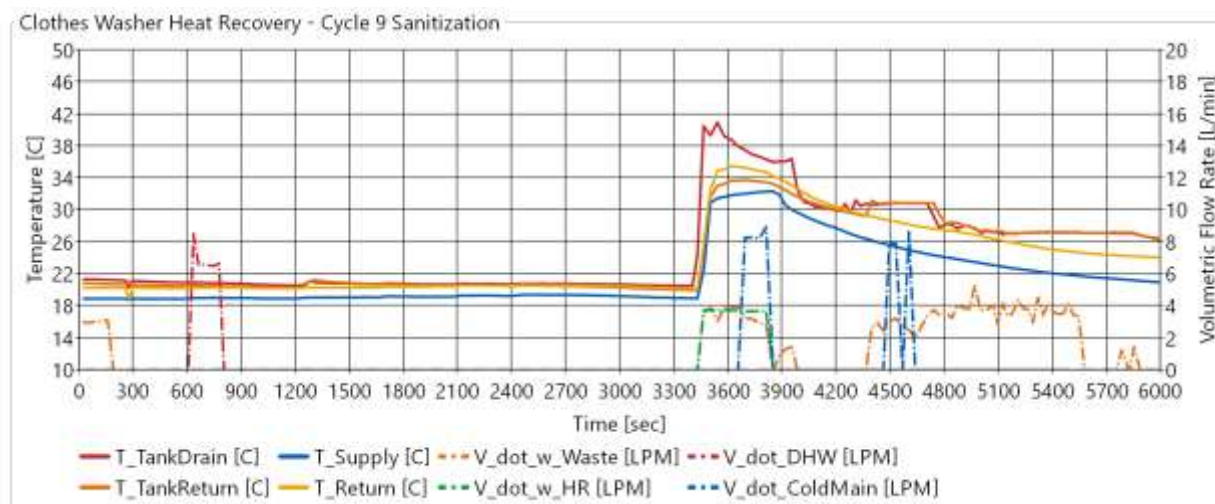


Figure 70: Clothes Washer Cycle 9 with Sanitization

## 5. VALIDATION OF MODELICA APPLIANCE MODELS

The presented models in Section 3 are updated to more accurately represent the real system and improve model stability when solved numerically. Only the clothes washer was added from scratch using the new methods. The specific improvements for each appliance are shown in detail and results of individual operation are presented to demonstrate the benefits.

### 5.1 Clothes Dryer

Heat exchanger geometry of the actual test stand unit was loaded using the available geometric inputs to characterize a fin-tube heat exchanger. The original curve-fits, dry bulb temperature and relative humidity, were updated with cycle 6 data due to having the most comparable air flow rate to the baseline. The raw data and corresponding curves with equations are shown in Figure 71. A spreadsheet program generated a polynomial of minimal degree with reasonable  $R^2$ , greater than 0.9. The average volumetric water-side and air-side flow rates were also updated to best match the experimental data.

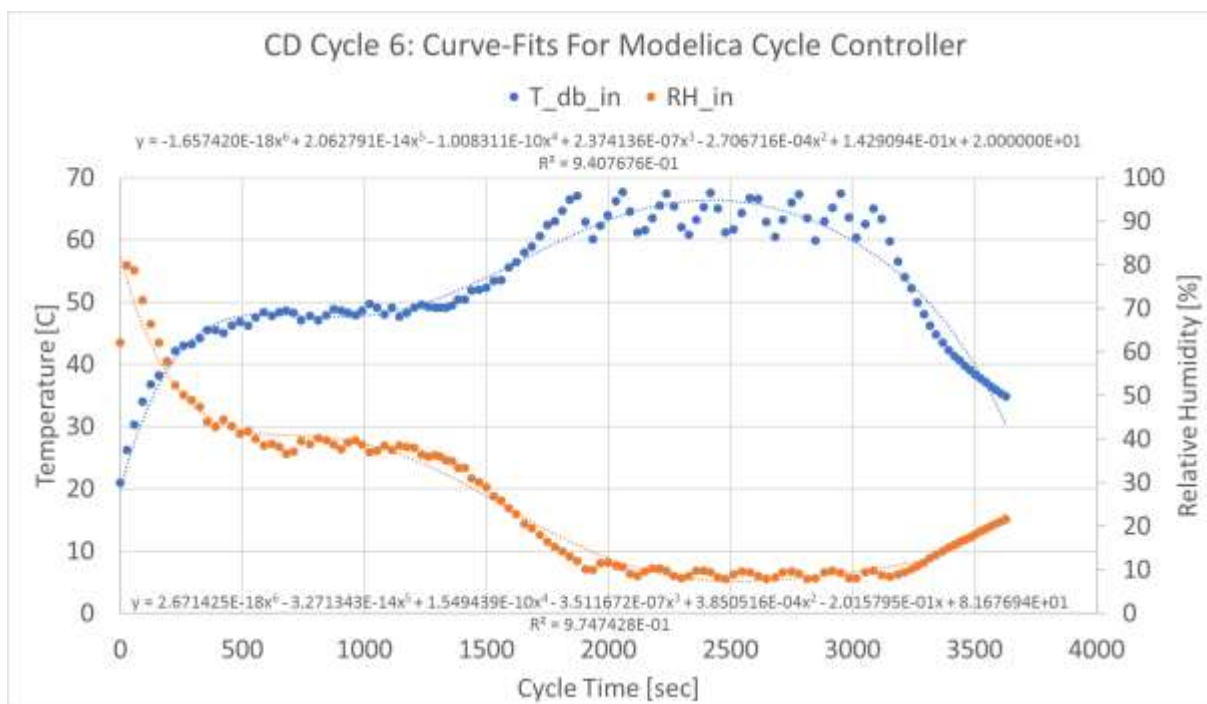


Figure 71: Curve-Fit for Clothes Dryer Exhaust Dry Bulb Temperature and Relative Humidity

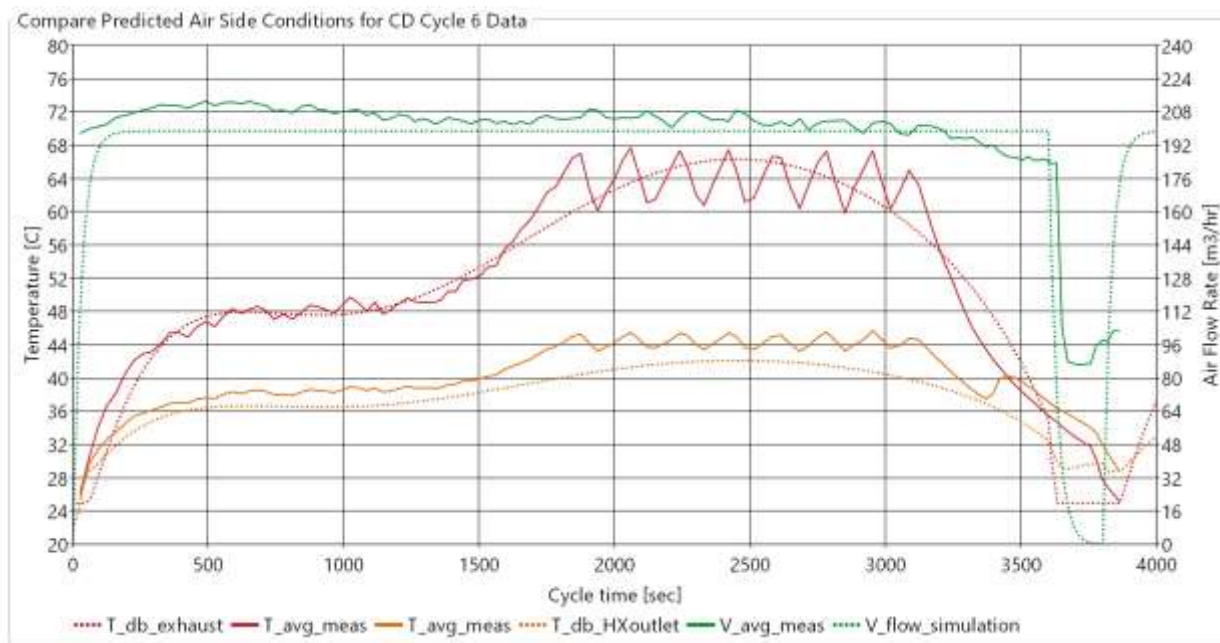


Figure 72: Clothes Dryer Experimental Data of Air Temperatures and Flow Rate – Cycle 6

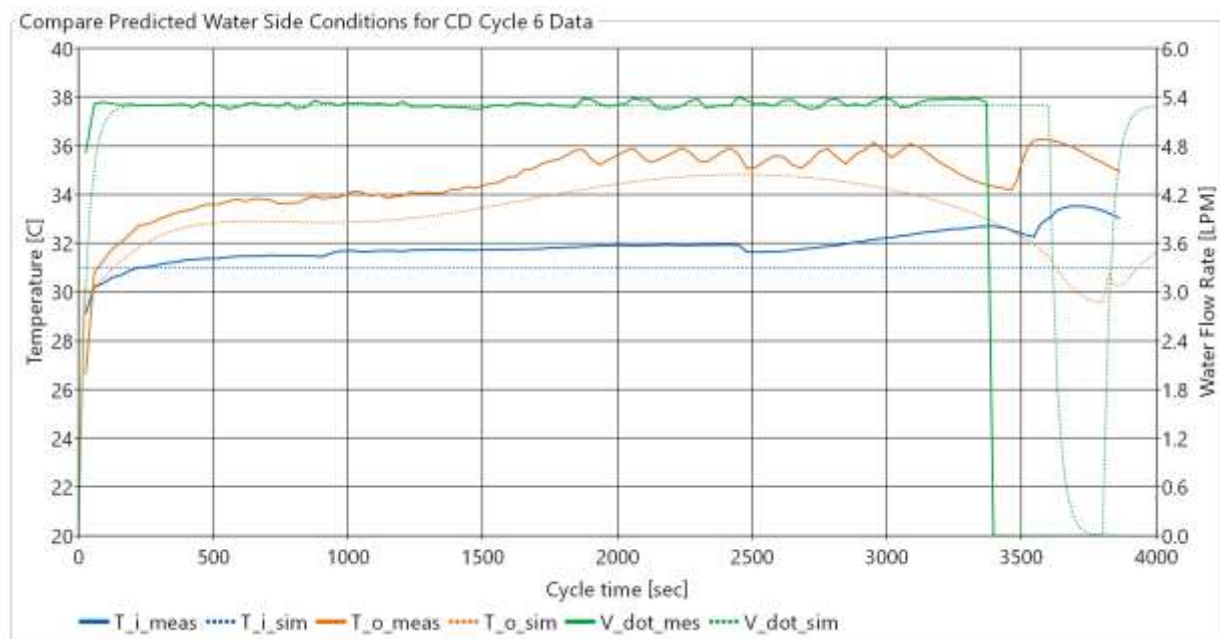


Figure 73: Clothes Dryer Experimental Data of Water Temperatures and Flow Rate – Cycle 6

## 5.2 Refrigerator-Freezer

The original Modelica approach was updated for the Refrigerator-Freezer. The major changes were the introduction of an internal tube-and-tube heat exchanger, liquid separator, a simple insulated cavity model and a new approach on the compressor capacity controller using the Modelica StateGraph library. The icon view of these updates can be seen in Figure 74.

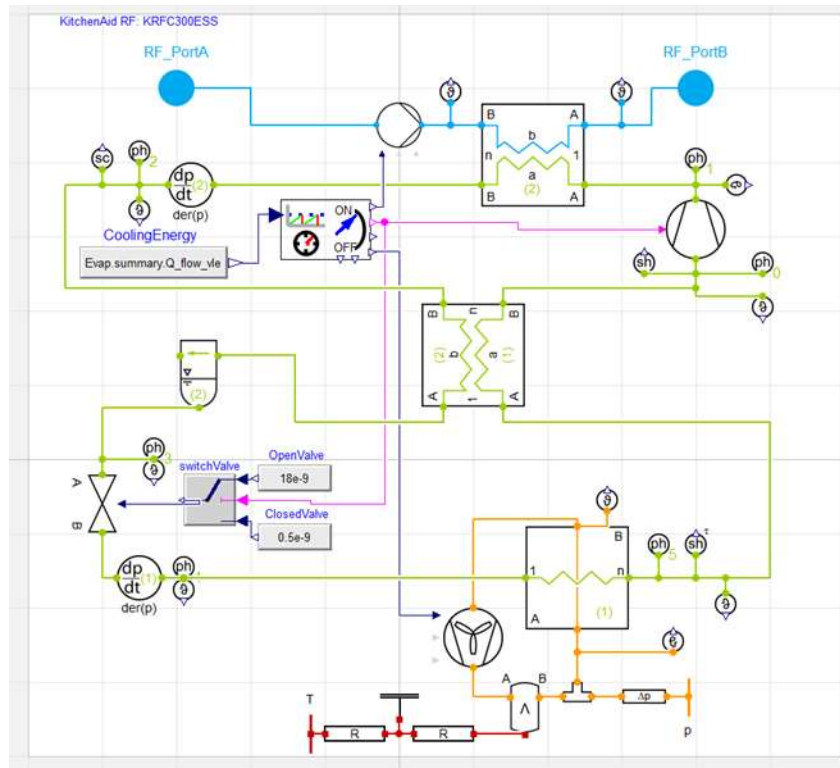


Figure 74: Updated Refrigerator-Freezer Approach in Modelica

The new model is tuned to best match the measured power consumption of the refrigerator and capture the ON/OFF compressor cycling operation. The two main tuning factors are through the prebuilt capacity controller, total evaporator energy during ON cycles and timer setting during OFF cycles. An AHRI compressor map is loaded into the compressor subcomponent and scaled with a factor 0.75 following a reference in literature to account for deviations from the manufacturer rated suction superheat (Dabiri, A.E., et.al., 1981). The developed map is first compared to the available experimental data to verify calculated power consumption is in line with the measured data. A trend of this comparison and the calculated refrigerator mass flow rate is shown in Figure 75. While the dotted line representing compressor power draw is difficult to see, there is a clear trend with the total power consumption measured of the RF during testing. The

on-cycle agreement further confirms the fixed scaling factor is appropriate to obtain an accurate compressor power draw and refrigerant mass flow rate.

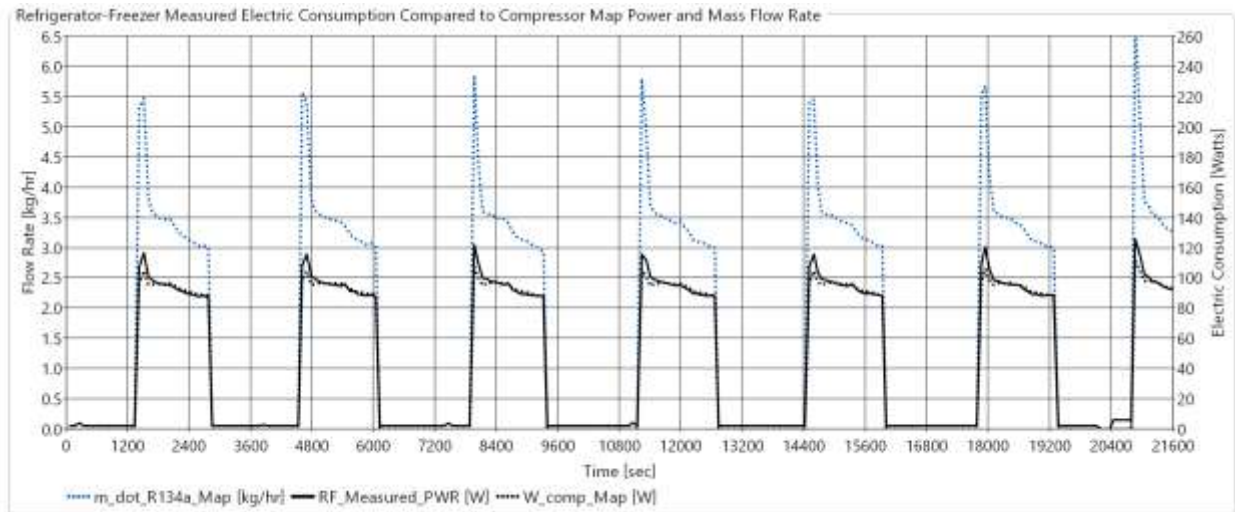


Figure 75: Refrigerator-Freezer Measured Total Unit Power Consumption and Calculated Compressor Power Draw and Refrigerant Mass Flow Rate using AHRI Compressor Map

Using this map within the Modelica refrigerator-freezer provides an accurate representation of the delivered flow rate by the compressor and associated power draw. The final tuned Modelica approach is compared to the experimental data. The simulated compressor power and mass flow rate are shown in Figure 76 for 6-hours, the same duration displayed for the experimental data in Figure 75. Overall the model is not built to accurately capture the dynamic operation of the RF and focuses on the ON/OFF operation of the appliance to represent the intermittent behavior.

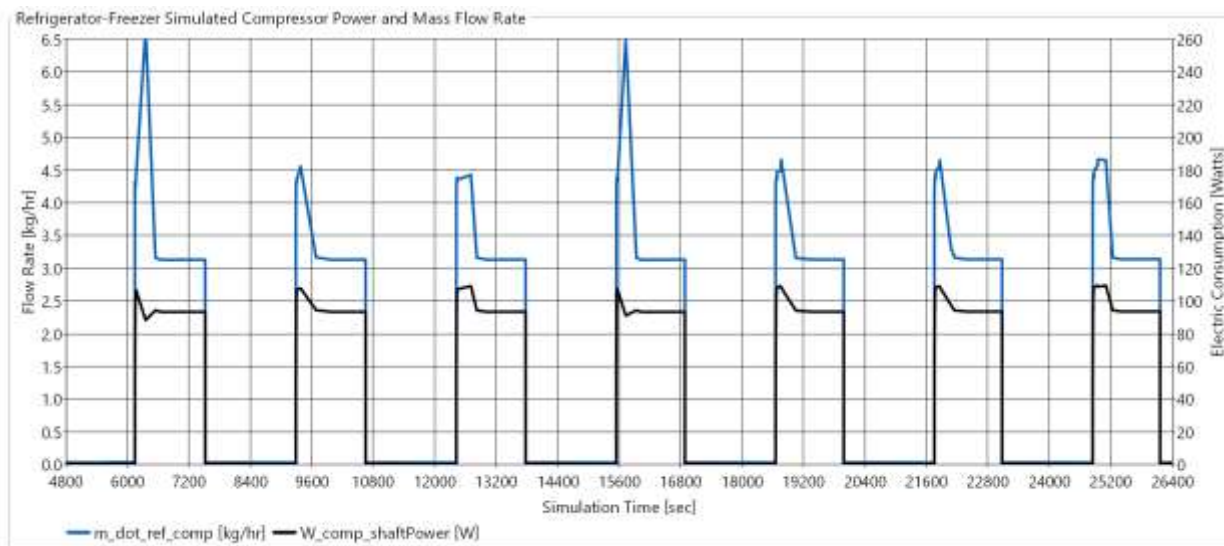


Figure 76: Tuned Refrigerator-Freezer Model Simulated Compressor Refrigerant Mass Flow Rate and Power Draw

The simulated refrigerant flow rate calculated by the compressor map is lower than what is predicted using the experimental data. One explanation is combined impact of the pressure ratio and suction superheat differences between the simulation and experimental data set. To explore this further the measured pressure ratio, total appliance power consumption, and compressor suction superheat is plotted in Figure 77. During a compressor ON cycle, the power draw decreases during over the last 10 minutes. This correlates to an increase in suction superheat which directly reduces the delivered, refrigerant flow rate and results in less work by the compressor.

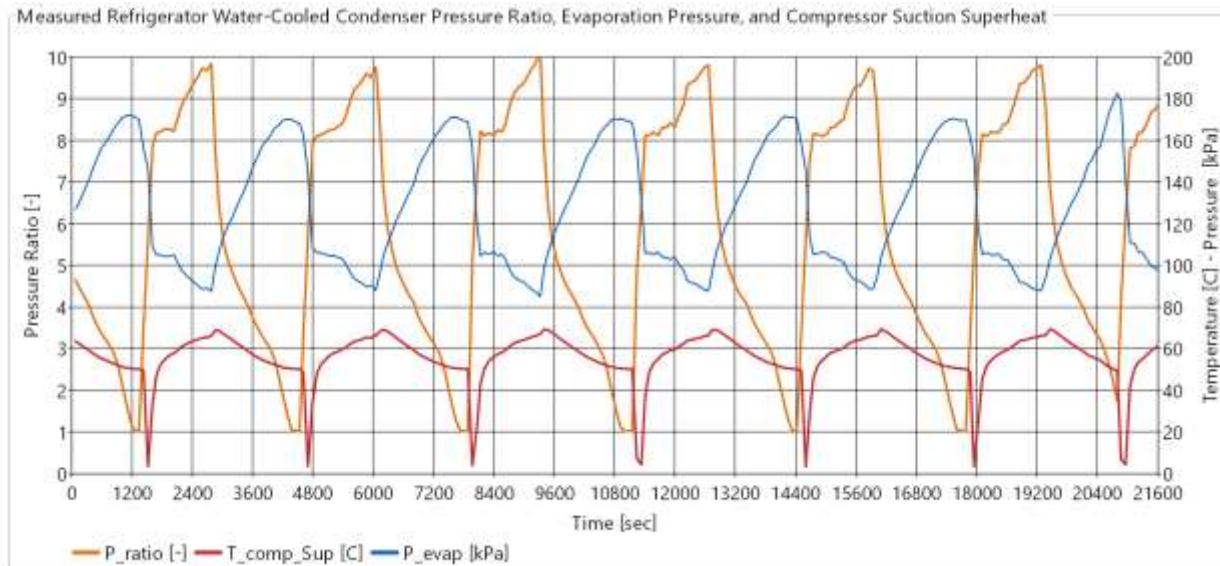


Figure 77: Measured Refrigerator-Freezer Pressure Ratio, Total Electrical Consumption and Compressor Suction Superheat

In the simulation the calculated pressure ratio, compressor power draw and suction superheat temperature is plotted along the same time span in Figure 78. The calculated values are constant during the compressor operation comparable to the other trends shown. As discussed previously, suction superheat has a strong influence on the compressor operation and is assumed to be the main driver of the simulation inaccuracy for the predicted flow rate and power consumption. To better support the numerical solver, no flow rates should be completely zeroed out. During the OFF cycle, the compressor model is imposed with a 1% multiplier of the AHRI-calculated mass flow rate, and a smaller fixed orifice opening to prevent any backward mass flow rates and reduce the rate of refrigerant migration. The resulting OFF cycle accuracy is impacted by this modeling approach and provides an inaccurate description of the built system or expected operation when the compressor is powered off.

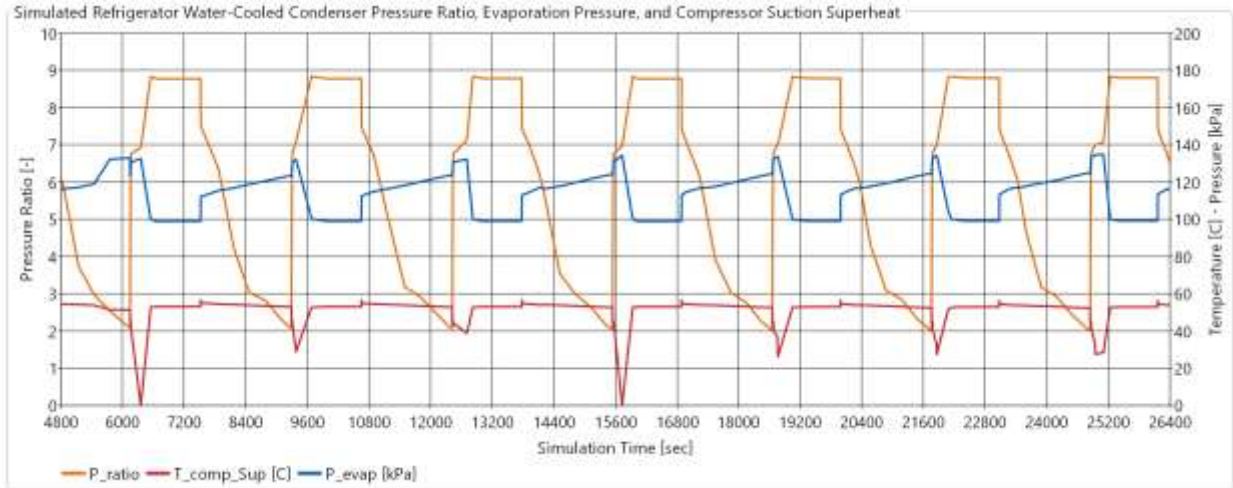


Figure 78: Simulated Refrigerator-Freezer Compressor Pressure Ratio, Electric Consumption and Suction Superheat Temperature

When calculating the water side heat transfer rate measured on the condenser, the corresponding inlet and outlet water temperatures measured during compressor ON/OFF cycles is shown in Figure 79. During one ON cycle, the condenser capacity drops off considerably. The rise in supply water temperature results in the reduced output with the temperature sink becoming closer to the condensing temperature. The reduced water-side capacity also trends with the calculated refrigerant mass flow rate from the adjusted compressor map providing another verification of this decreasing rate of heat transfer during an ON cycle.

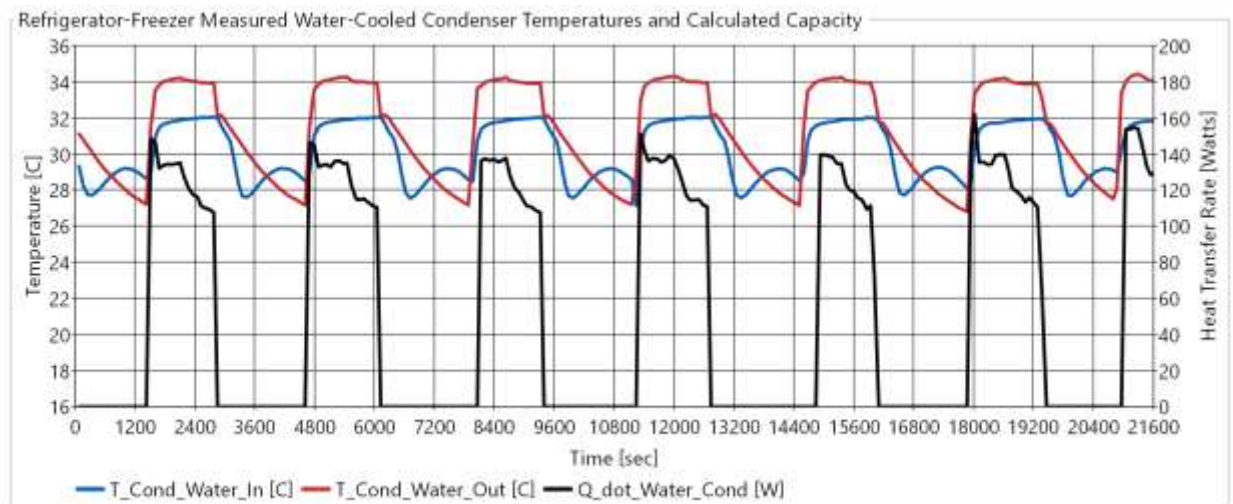


Figure 79: Refrigerator-Freezer Water-Cooled Condenser, Measured Water Temperatures and Calculated Heat Transfer Capacity

The simulation captures the general trend of the measured condenser capacity shown in Figure 80 for a 6-hour span. A quick jump in capacity followed by a quick decay and plateau before the compressor shuts-off. The contrast with experimental data is the steady decline in measured capacity that is not captured in the model. Only the compressor start-up condition is picked-up in the model which identifies the impact of refrigerant migration that collects in the lowest temperature, or evaporator of the refrigerator. The cyclical operation of the temperatures is captured in the model with a high, initial peak return temperature that gradually decays before shutting down.

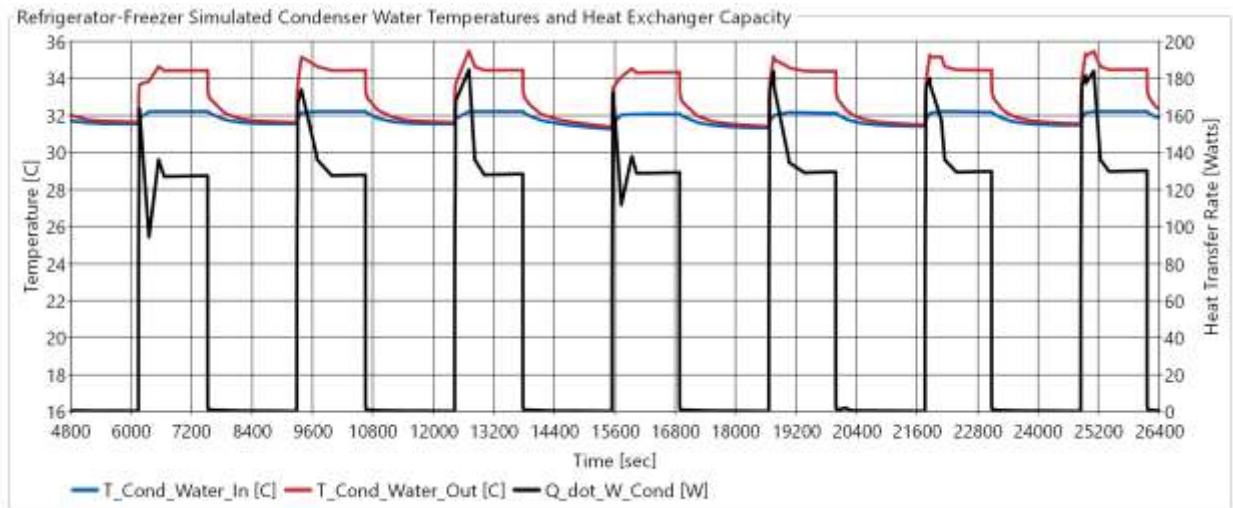


Figure 80: Tuned Refrigerator-Freezer Model Simulated Condenser Water Temperatures and Heat Exchanger Capacity

### 5.3 Dishwasher

The original Modelica approach was updated for the dishwasher. The major changes were the introduction of a fill valve to represent the domestic hot water source, an expansion tank for the sump volume, and a new approach on the controller using the Modelica StateGraph library. The overall changes can be seen in Figure 81.

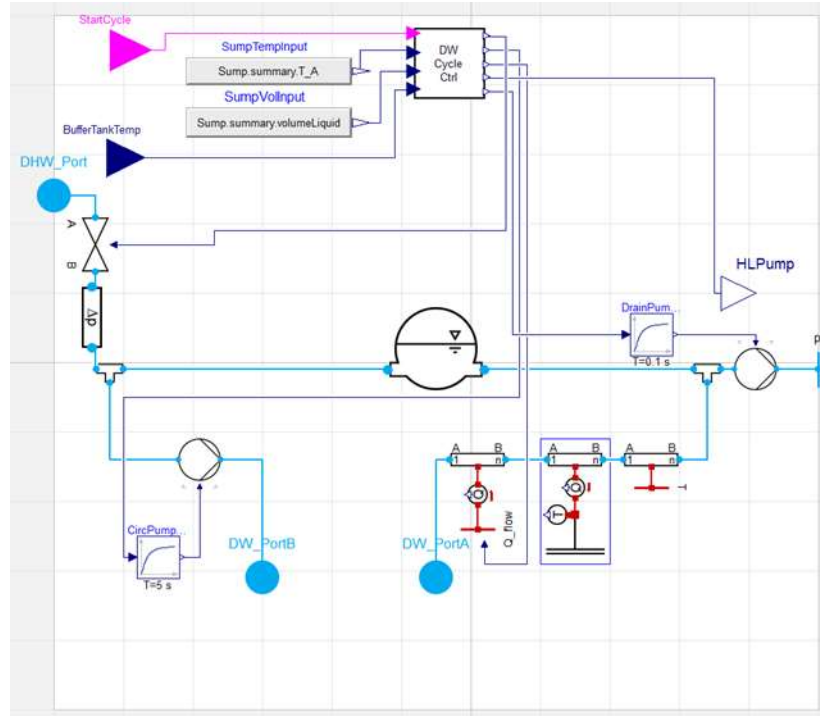


Figure 81: Updated Dishwasher Modeling Approach with DHW Fill Valve, Sump Volume, and Cycle Controller

The updated model is run with a simple connection between sump ports to simulate the baseline operation of the dishwasher. Several runs are conducted to adjust the fixed assumptions of the cycle controller to best match experimental data from the manufacturer. The final model after tuning is shown in

Figure 82 by comparing the simulated sump temperature and internal resistor heater power intervals with the baseline data.

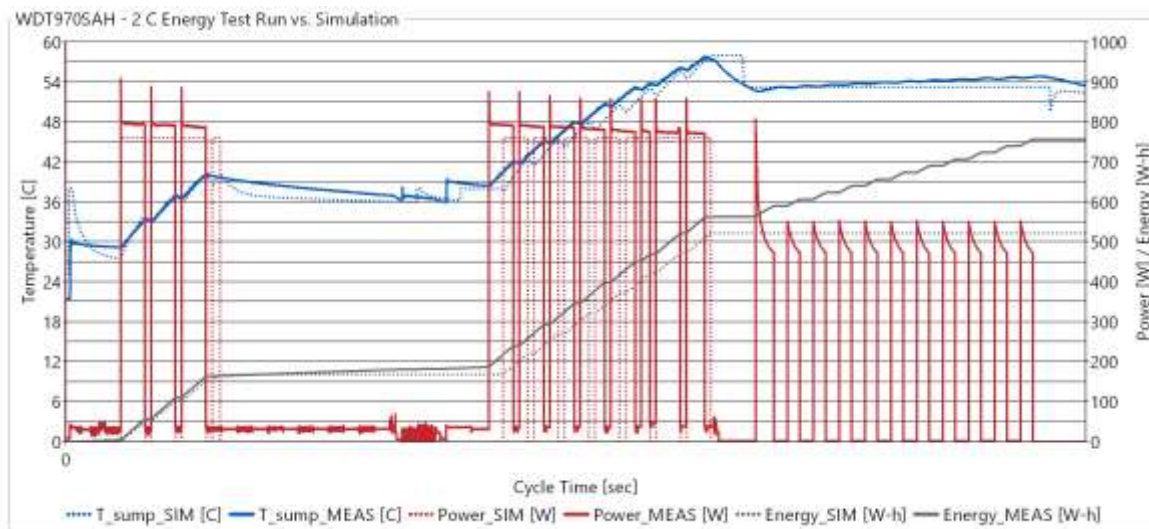


Figure 82: Tuned Dishwasher Modelica Plot of Sump Temperature and Power Consumption

Discuss trends of above graph to identify improved features in this new modeling approach.

#### 5.4 Clothes Washer

The clothes washer model was the only appliance not addressed during the original development. The controller leverages the benefits made when updating the dishwasher approach by using the same controller components, expansion tank for variable liquid volume and DHW fill valve. Based off the experimental results, three different temperature cycles are captured that charge the expansion tank representing the waste, wash water. For the weekly simulation, prior data on consumer cycle behavior is used to define the 6 cycles run in a week. Four warm wash cycles, one hot wash cycle, and one cold wash cycle represent the amount of hot and cold water consumed during the wash step in one week. With CW cycles occurring in groupings of two on three different days during the week, an assumed distribution of cold, warm and hot washes is made. The first two cycles on Wednesday are warm, followed by a warm then cold on Saturday, and the last pair on Sunday is warm then hot. The finalized approach with all Modelica components as icons is shown in Figure 83. To represent the built test stand with a single pump, a 3-way valve directs the waste water drained by the CW to heat recovery or to the overall waste water drain of the home.

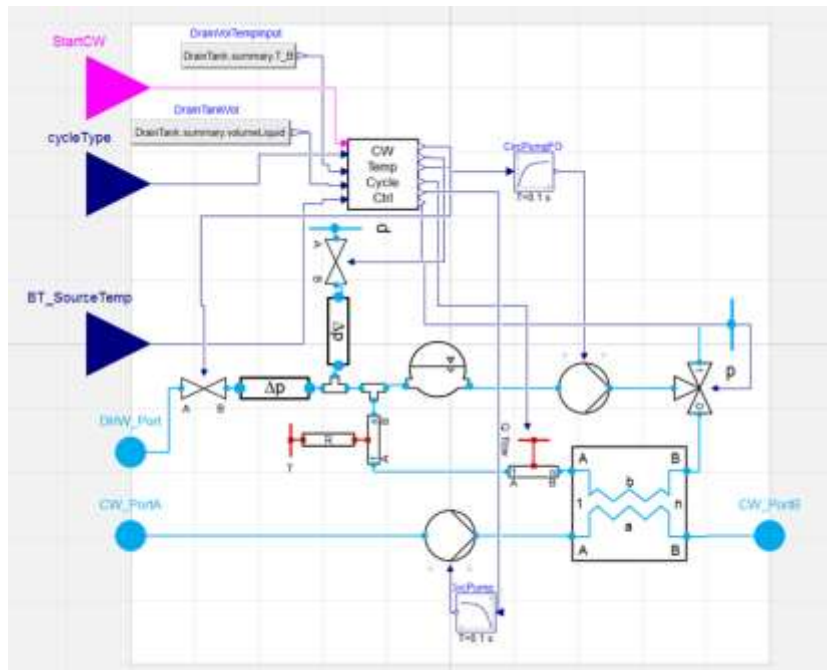


Figure 83: Detailed Clothes Washer Modelica Approach for Waste-Water Heat Recovery

To validate the Modelica approach, experimental data shown in Figure 70 with the best heat recovery potential is shown in better detail in Figure 84.

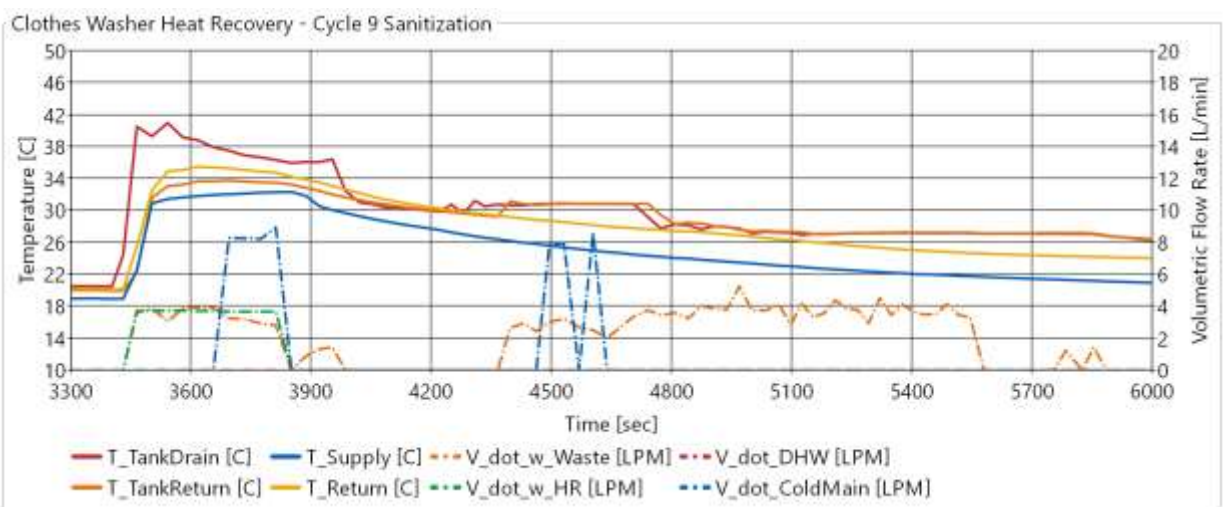


Figure 84: Clothes Washer Cycle 9 Sanitization - Heat Recovery Process

The simulation output, seen in Figure 85, has a lower return temperature to the storage tank due to a lower storage tank temperature.

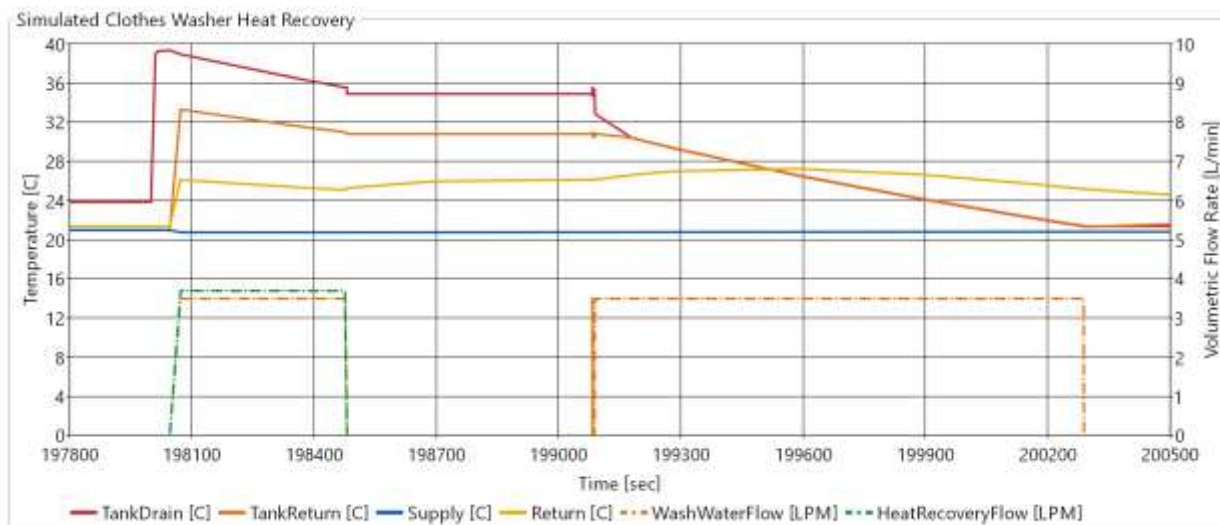


Figure 85: Simulated Heat Recovery Process of Clothes Washer Waste Water for Sanitization Cycle, Water Temperatures and Flow Rates

### 5.5 Integrated Appliance System

Each final appliance model is connected to a stratified storage tank via liquid tube models on both supply and return sides to capture piping heat loss. The icon representation of each model and physical connections is shown in Figure 86. A thermal boundary is also connected to the storage tank to replicate typical standby heat loss experienced in hot water storage systems.

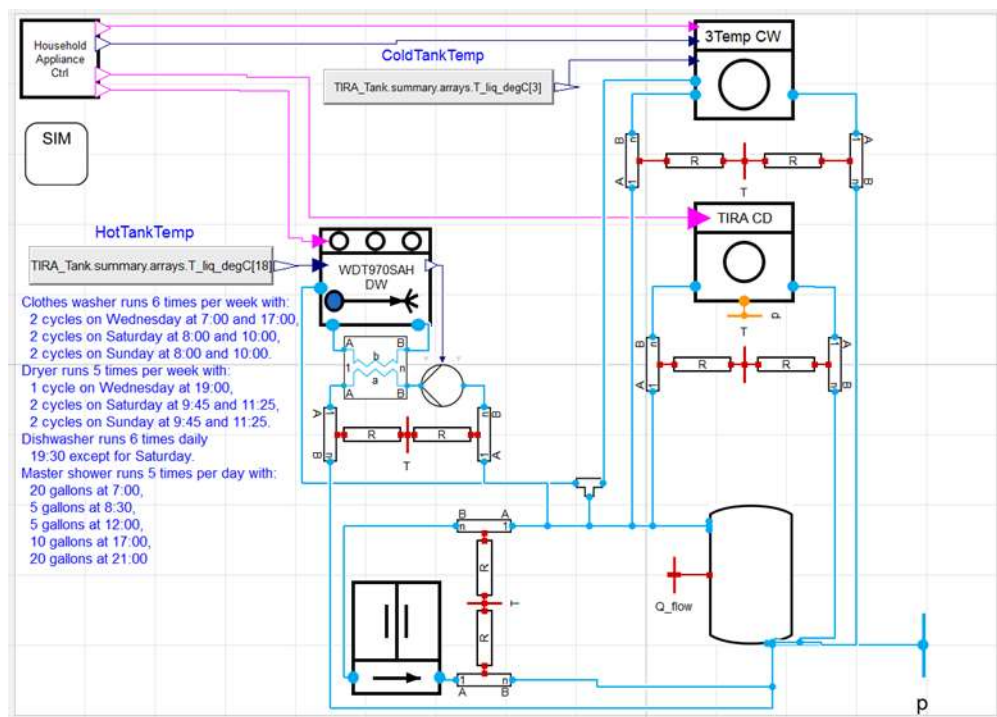


Figure 86: Modelica Icon View of Integrated Appliances System

During the operation of the refrigerator-freezer, the stratified storage tank is captured in the model. The measured tank temperatures during several compressor cycles is shown in Figure 87 during a 6-hour span where the tank started at a temperature of 31C ( ).

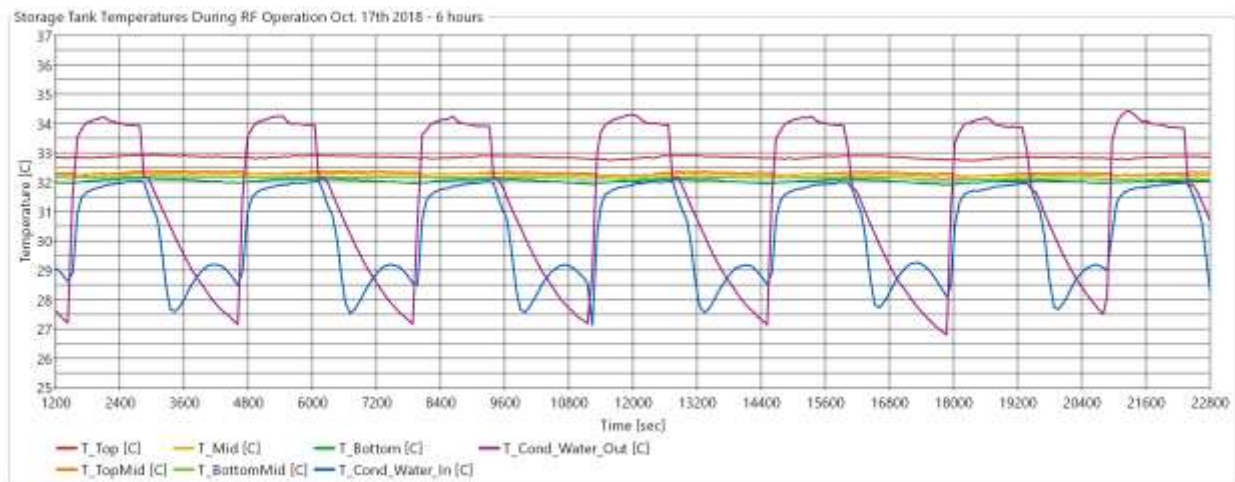


Figure 87: Test Stand Storage Tank Temperatures Compared to Refrigerator Water Supply and Return Temperatures during several Compressor Cycles

With a similar initialization, the simulation is run for only the refrigerator-freezer when connected to the same tank sized used in the test stand. Compressor cycling is observed in Figure 88 with the thermal charging of the top water layer within the storage tank during a six hour window.

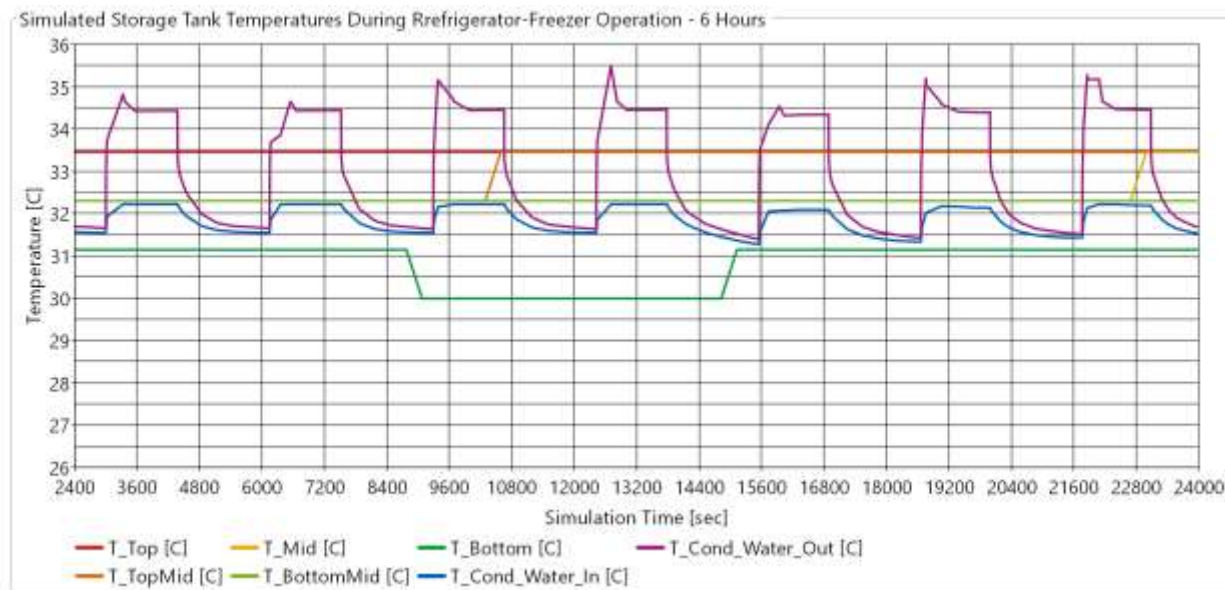


Figure 88: Simulated Storage Tank Temperatures Compared to Refrigerator-Freezer Water Supply and Return Temperatures during Several Compressor Cycles

## 6. PARAMETRIC STUDY

After updating the original models to improve agreement with available experimental data, the integrated appliance system is run through a parametric study to evaluate the energy savings compared to the original individual operation. First the individual operation is quantified for appliances that are impacted by the heat recovery process to provide a benchmark for the integrated system. After this, a final improvement is made to each appliance model before running the parametric study to identify the impact of an ideal configuration by leveraging experience gained from the test stand. To explore the impact of tank temperature, transient heat losses, and appliance cycling operation, two different storage tank sizes are compared using commercially available sizes that would be suitable for domestic hot water storage in a home. The same one-week appliance schedule is run with starting the storage tank at domestic hot water temperature. The identification of available hot water at DHW temperatures

### 6.1 Baseline Operation

With the improvements made to the built system, the individual operation of the appliances is quantified to obtain a predicted energy consumption and performance without thermal integration. The CD is run five times a week using the same cycle settings consuming roughly 4 kWh of electricity per cycle or 20 kWh per week. The DW uses about 0.56 kWh of electricity per cycle for all washing and rinsing steps which excludes energy used for drying. Prior data of the RF operation using the air condenser reported 1 kWh of electricity consumption for a 24-hour period. Using this reference, the RF should use roughly 7 kWh per week. The CW impact is on the DHW consumption with using roughly 38.5 L per week requiring 1.25 kWh of energy to heat from 20C city main temperatures to 49C DHW temperatures.

### 6.2 Ideal Appliance Modifications

Overall the parameters impacting the heat exchanger operation or geometry are altered using experience gained during the operation of the test stand. The clothes dryer switched the heat exchanger to a counter flow from a cross flow. A higher potential outlet water temperature is possible during the heat recovery process and is considered the ideal approach to generate more

useful temperatures. On the refrigerator a simple modification is explored by lowering the flow rate by 40% with the same aim to deliver higher return water temperatures to the storage tank. The dishwasher and clothes washer are updated with identical heat exchanger replacements, a co-axial geometry instead of a flat-plate. Significant pressure drop was observed in the experimental system with a flat-plate HX and required significant pumping power to overcome. Furthermore, the new HX will improve its resilience with expected fouling. The internal water of the appliance, both the dishwasher or clothes washer, will have food or cotton fiber debris resulting in fouling and partial blockage of flow channels. The holding volume of this co-axial heat exchanger is made constant relative to holding volume of the physical flat, plate heat exchanger used during testing. An assumed piping size of the co-axial HX is 1.3 cm (1/2 in) diameter and its length is increased until the internal volume matches that of the waste-water flat-plate HX. The resulting length is 2.15 m (7 ft) for an internal volume of 0.11 L (0.03 gal.).

### **6.2.1 Clothes Dryer**

A comparison is made between the calculated air-side and water-side capacities of the clothes dryer and the model prediction for the test stand HX and counter-flow HX. The plot shown in Figure 89 identifies the amount of heat recovered between the test stand HX and a counter-flow heat exchanger is very similar. And these predicted capacities are much closer to the calculated water-side capacities versus the calculated air-side capacities. The power input to the entire dryer is also visible to provide an indication of how much electricity is used in total compared to the amount of heat recovered from the dryer duct. For this cycle during the drying region at about 10003 seconds, the total power input is 5,421 Watts, and the amount of predicted heat recovered by the TIRA HX is 686 Watts versus 805 Watts for the ideal HX. Giving a percent of heat recovery at 12.6% to 14.8% for each case respectively with a 17.3% increase between the different HX types.

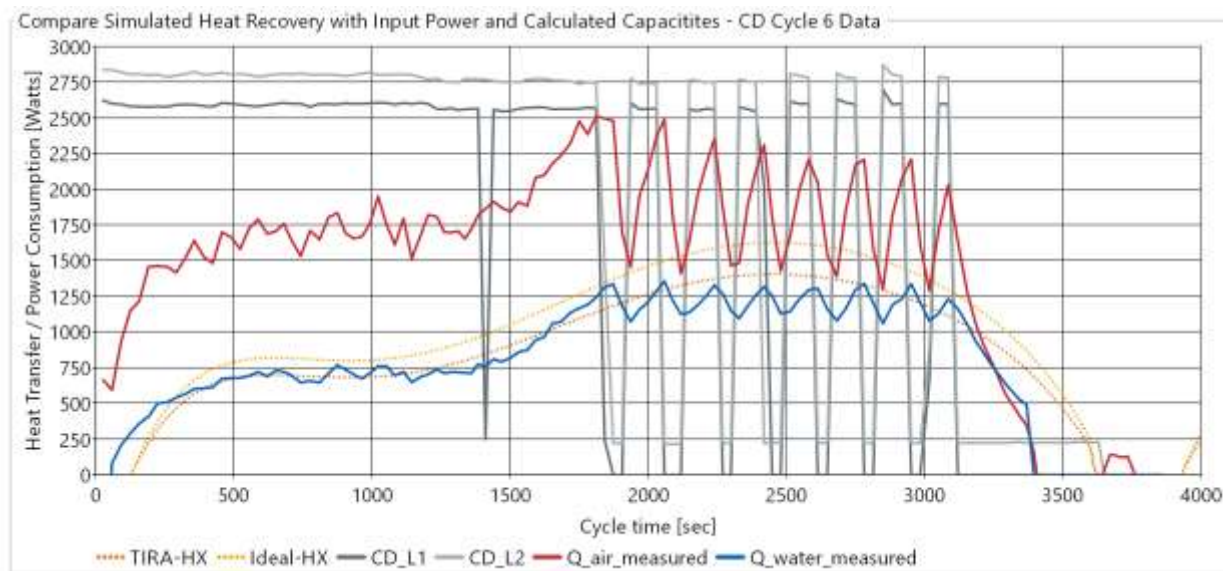


Figure 89: Measurement Versus Simulation of TIRA HX and Ideal HX – Cycle 6

The performance improvement between the two HX is more pronounced when plotting the individual cell temperatures in Figure 90 that represent a fraction of total HX surface area. The cross-flow HX from the test stand did not generate high outlet water temperatures relative to the maximum potential, inlet air temperature. When compared to a counter-flow approach, shown on the right of the figure, a water outlet temperature is predicted above 42°C (108°F) instead of the 33°C (91°F) observed for the test stand.

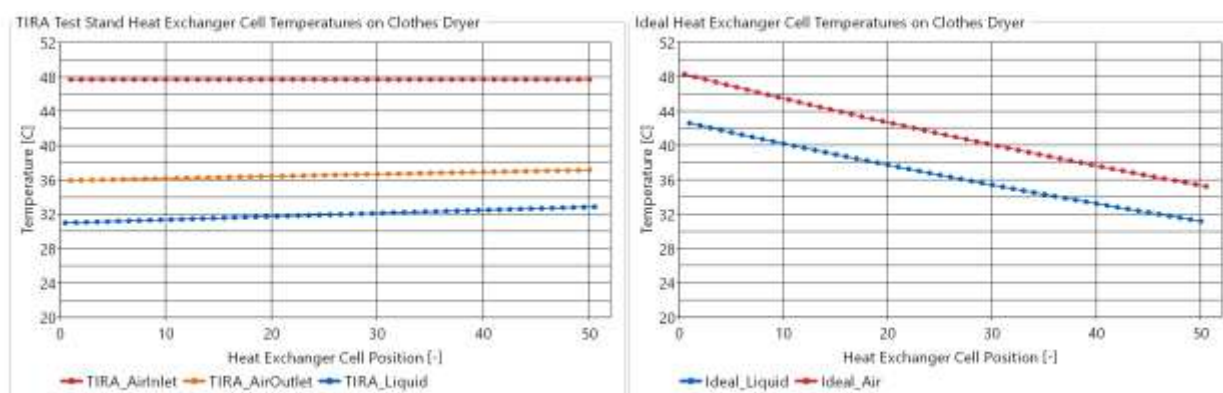


Figure 90: Simulation Comparison between Heat Exchanger Types for Clothes Dryer Heat Recovery at 1000 seconds – Cycle 6 (Left: Test Stand Cross-flow, Right: Ideal Area Counter-flow)

### 6.2.2 Refrigerator-Freezer

The water side volumetric flow rate is lowered to generate a higher return temperature to the storage tank. The trade-off between higher return temperatures and increased power consumption must be considered to quantify the impact on cooling performance. The model has a top-level parameter to vary this flow rate and is constant during a simulation run. A lower rate of 0.5 LPM (0.13 GPM) versus the one measured during testing, 0.83 LPM (0.22 GPM) was explored. The case is considered ideal in the perspective of heat recovery to support another process. A detailed look at this impact is shown in Figure 91 during the final 6-hours of a 24-hour simulation starting with a uniform storage tank temperature of 21C (). The condenser heat transfer rate, compressor power consumption and total energy are compared for both flow rates. While there is some temporal shift on compressor operation between the typical system and ideal case, overall there is not a significant impact on energy recovered or compressor power consumption. One minor point to note is the ideal compressor cycles lead the TIRA configured compressor cycles. The capacity controller of the compressor has a fixed assumed OFF timer and would not be impacted between both scenarios. The shift must be due to a slight increase in evaporator capacity resulting in a shorter ON cycle when using a lower condenser, water side flow rate. With the original purpose to generate higher return temperatures, the water and refrigerant cell temperatures of the condenser are plotted in Figure 92. A slight improvement of 2 C (), is seen on the outlet water temperature of the condenser, 28C () versus ~26C (). The model could be run for 1-week instead of a single 24-hour period to further explore how warm the storage tank can be driven by the RF compressor.

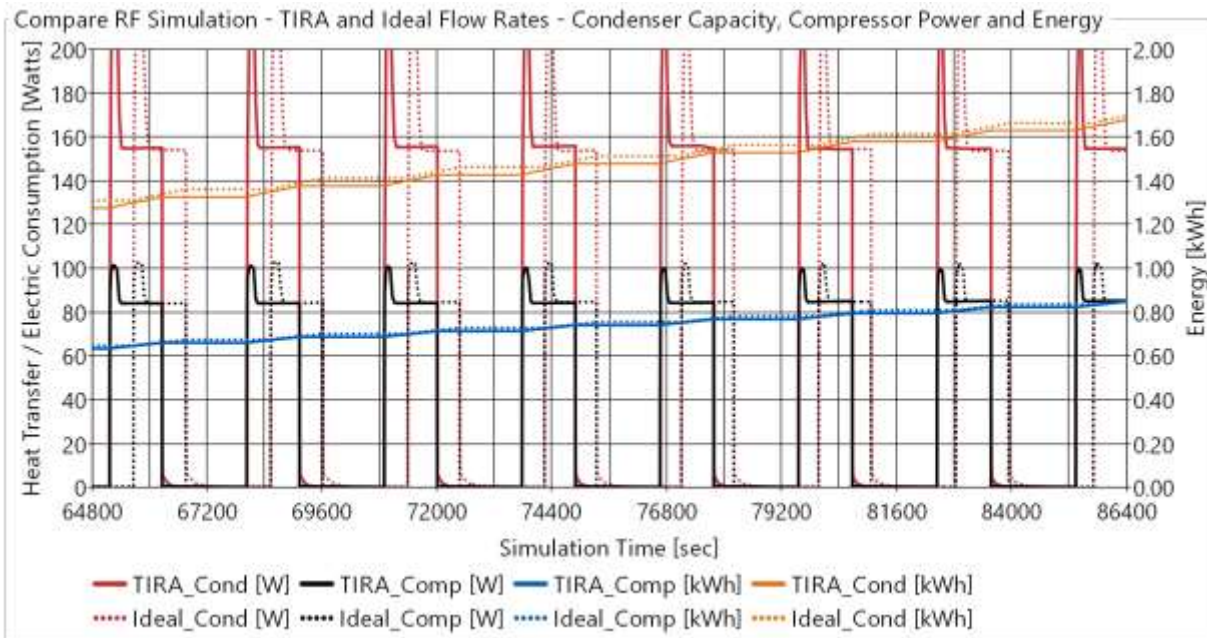


Figure 91: Simulated RF TIRA and Ideal Condenser Flow rate – Heat Transfer, Power Consumption, and Total Energy in 1-Day

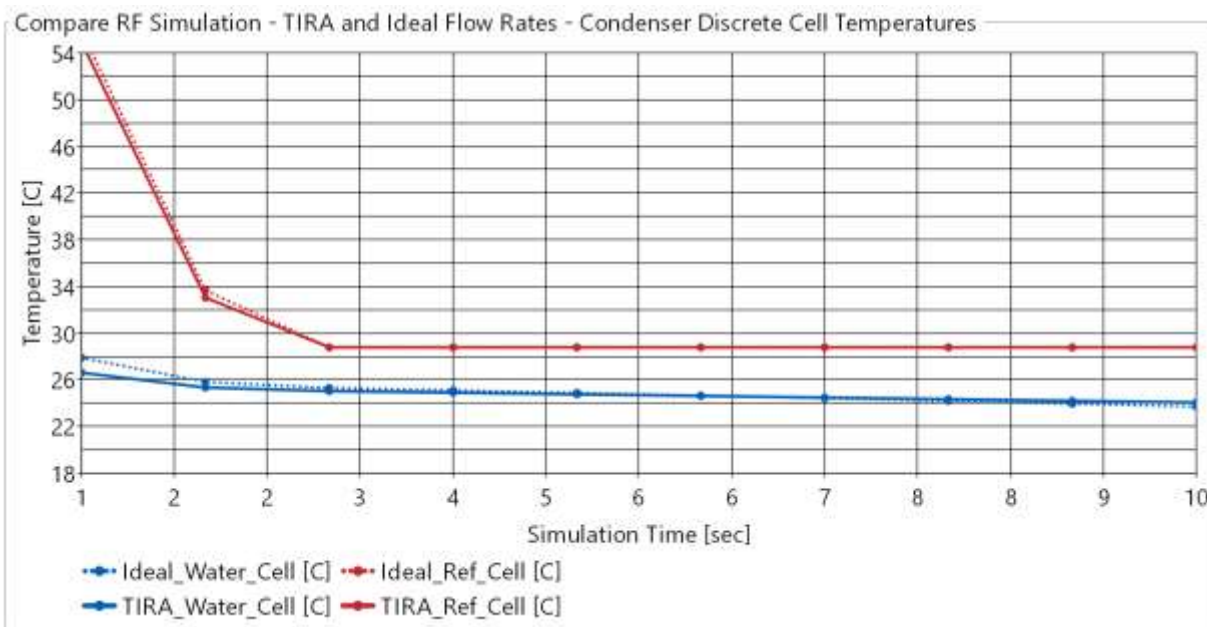


Figure 92: Simulated Refrigerator-Freezer TIRA and Ideal Condenser Cell Temperatures of Water and Refrigerant

### 6.2.3 Dishwasher

Counter-flow, coaxial tube HX that can fit within the existing dimensions of a dishwasher replaced the flat-plate HX. To further reduce the HX pressure drop occurring at the high flow rates, a diameter of 13 mm ( $\frac{1}{2}$ " ) is assumed. The last degree of freedom, HX length, is calculated by keeping the internal volume the same as the original HX installed on the test stand. A constant internal volume between both HXs results in the same DHW volume drawn by the appliance per cycle. The ideal DW is simulated and compared to the TIRA DW as well as a baseline DW using no HX for external thermal input. The connected storage tank was initialized at the DHW temperature and each DW model was connected to their separate tanks. A graph of the first DW cycle called in the simulation is shown in Figure 93 which had access to the warmest tank in the 1-week simulation. Here it is easy to recognize the added cycle time between the three types as well as compare the different amounts of power consumption between each cycle. The TIRA configuration reports the lowest electrical consumption for the heater around 300 W-h while the ideal and the baseline do not show much disagreement here, around 500 W-h in total. As more DW cycles occur, the tank's thermal energy is depleted resulting in the cycles shown in Figure 94. Due to the addition of HXs for both the ideal and TIRA cases to deliver heat from an external source, this thermal mass then results in a higher electrical power consumption when not in use, 700-800 W-h compared to the baseline, 560 W-h.

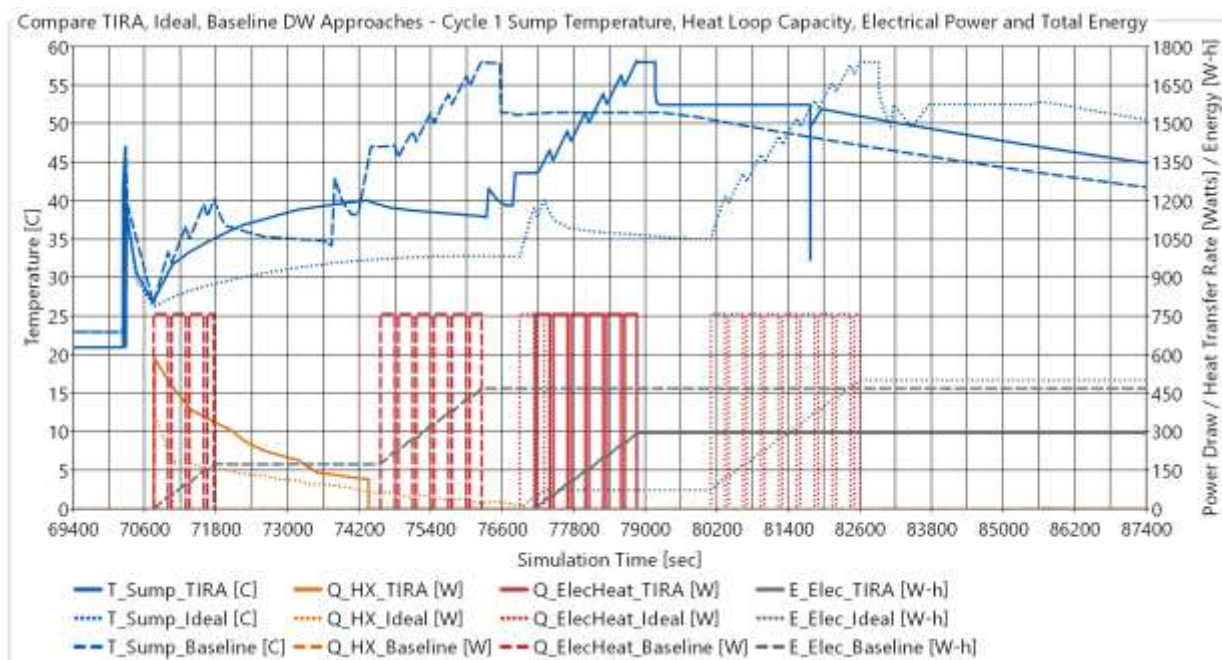


Figure 93: Compare TIRA, Ideal, and Baseline Dishwasher Performance during 1-week Simulation, 1<sup>st</sup> Cycle with 49C Initial Tank Temperature

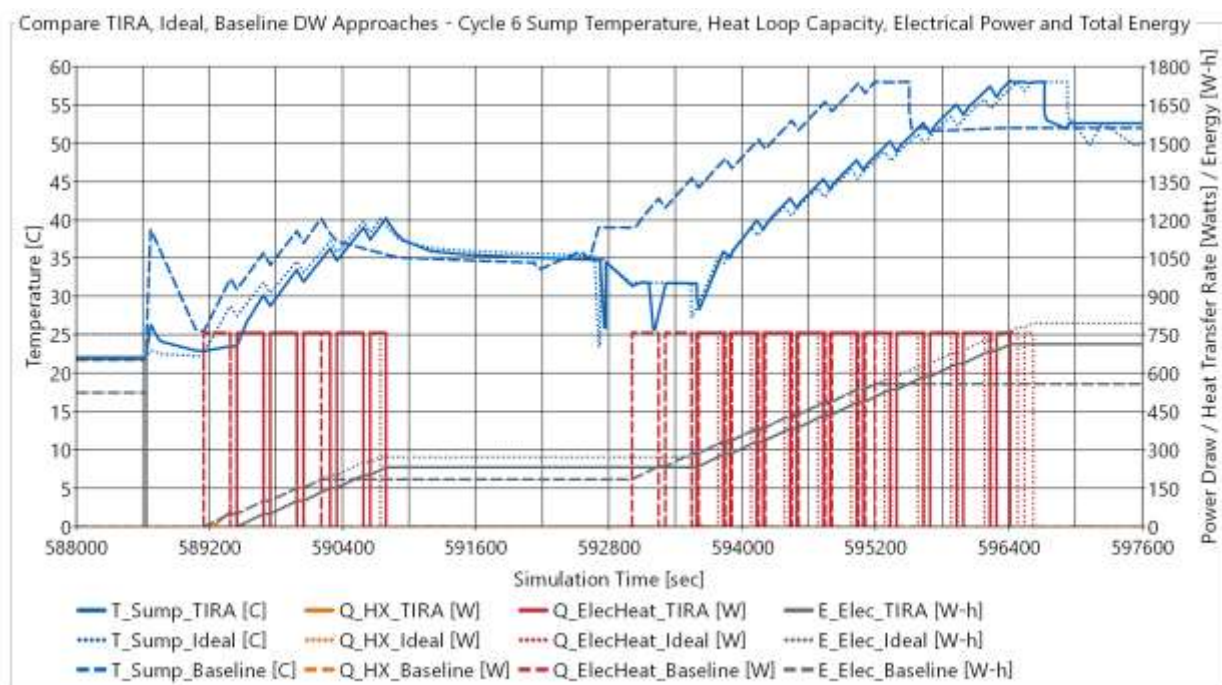


Figure 94: Compare TIRA, Ideal, and Baseline Dishwasher Performance during 1-week Simulation, Last (6<sup>th</sup>) Cycle with 49C Initial Tank Temperature

To further illustrate the impact of different DW configurations on the storage tank temperatures, Figure 95 compares the tank temperatures across 20 points along the height of the tank for 3 different possible DW configurations. The left graph shows the tank temperatures after the first DW cycle of the week, and the right graph shows how much the tank has been cooled after the 6<sup>th</sup> DW cycle. The simulation only has the DWs connected to their respective tanks, all starting at DHW temperatures. The first issue with the ideal configuration is the need for a high flow rate to match the appliance side flow rate on the HX. As a result, the tank is mixed and results in cooling seen in the left graph compared to the TIRA or baseline tank temperatures.

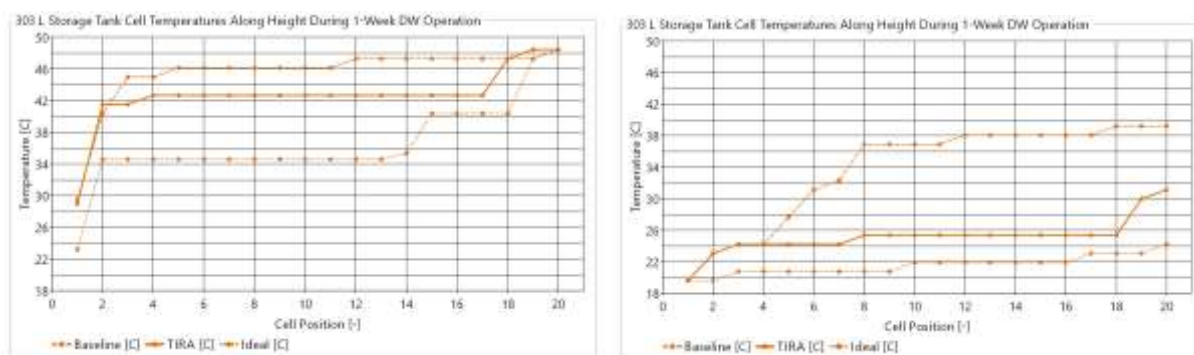


Figure 95: Impact on Storage Tank Temperatures from Dishwasher Operation in 3 Configurations (Left: after first cycle, Right: after the 6<sup>th</sup> cycle)

## 6.2.4 Clothes Washer

Due to the cycle results obtained during experimentation, it is expected the CW does not have much waste heat available for recovery due to the type of cycles typically run by consumers. In situations where a region of the storage tank drops to temperatures below the drained wash water, the heat recovery process is still possible within the Modelica model. The same HX type and geometric assumptions for the DW are extended to this appliance as well. Due to the change in focus of the CW on using waste heat to being a consumer of DHW from the tank, illustrating the different HX approaches in the CW are not beneficial for this study.

## 6.3 Storage Tank Volume

Two different storage tank volumes, 303 L (80 gal.) and 150L (50 gal.) were simulated for the ideal configuration of thermally connected appliances. Both volumes are available from a tank

manufacturer and are common storage volumes for residential DHW. With a goal of supporting the residential DHW demands, the tanks are initialized at, 49C (120F), which represent standard DHW temperatures.

### 6.3.1 300 L Tank

The same tank size used in the test stand, 303 L (80 gal.) was initialized at a temperature of 49C (120F). The impact on the tank temperature over time from all four appliances' operation is shown for five different heights in the storage tank spanning the entire height of the tank. A graph showing these temperatures over time with a 24-hour grid starting on Monday is shown in Figure 96. As different appliances come on and off, the tank temperatures respond depending on the appliance. The DHW required by the CW and DW is also drawn from the same tank connected to all appliances and is replaced with fresh water at a city main temperature of 20C (68F)

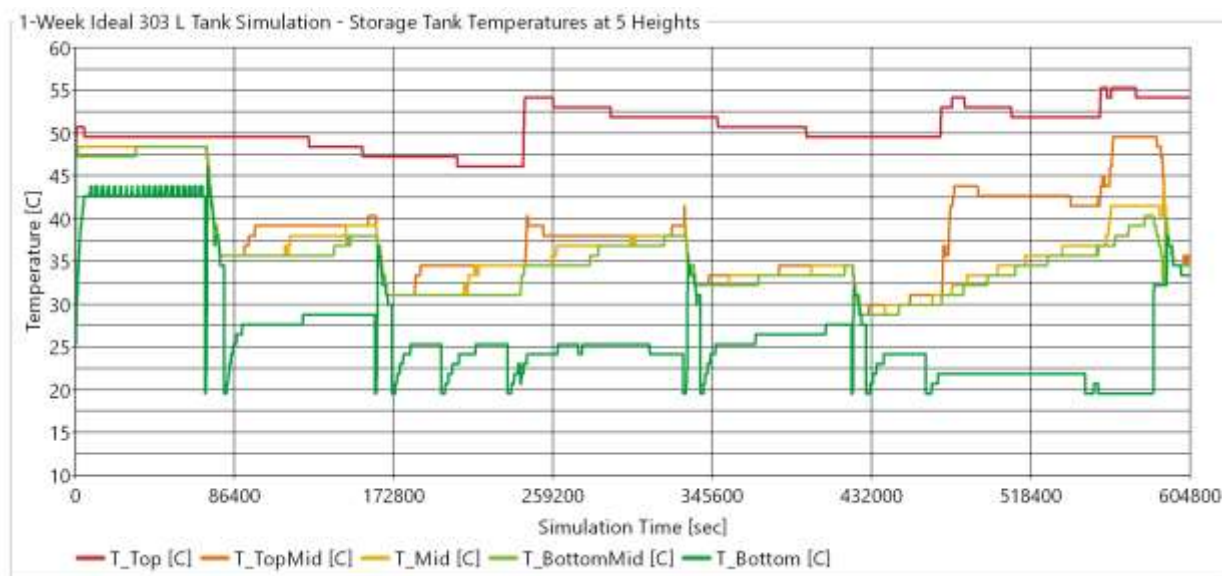


Figure 96: 1-Week 303 L (80 gal.) Ideal Simulation of 5 Storage Tank Temperatures

The only appliance that should see a negative impact with starting at a high tank temperature is the refrigerator-freezer. The compressor power consumption and inlet/outlet pressures are plotted along with the condenser heat rejection rate shown in Figure 97. Here the compressor power is initially higher than levels seen during testing, around 100-110 Watts versus the 85-95 Watts measured. As the week goes on, the compressor power drops to around 60W and maintains this level.

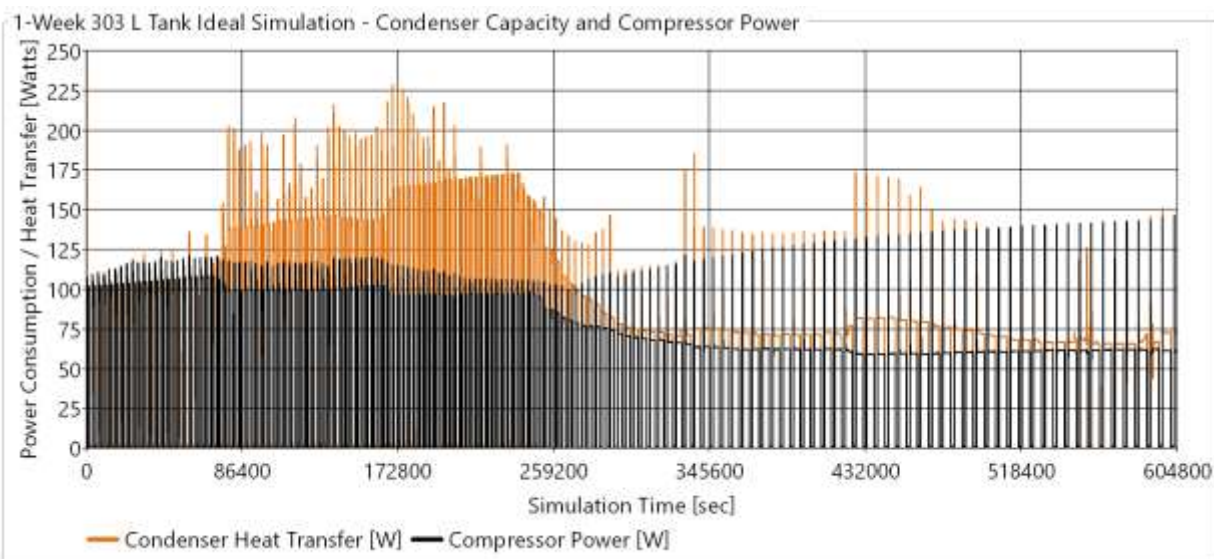


Figure 97: 1-Week 303 L (80 gal.) Ideal Simulation of Refrigerator Condenser Capacity and Compressor Power Consumption

The amount of energy offset by thermal integration for the DW is a function of the stored water temperature at the top of the tank. In Figure 98, the first DW cycle of the week simulation is presented. With a total duration of, 230 minutes, 440 W-h of electricity is used for heating with roughly 190 W-h provided via the external HX. Occurring at the beginning of the week, the first cycle has access to plenty of hot water for heating use.

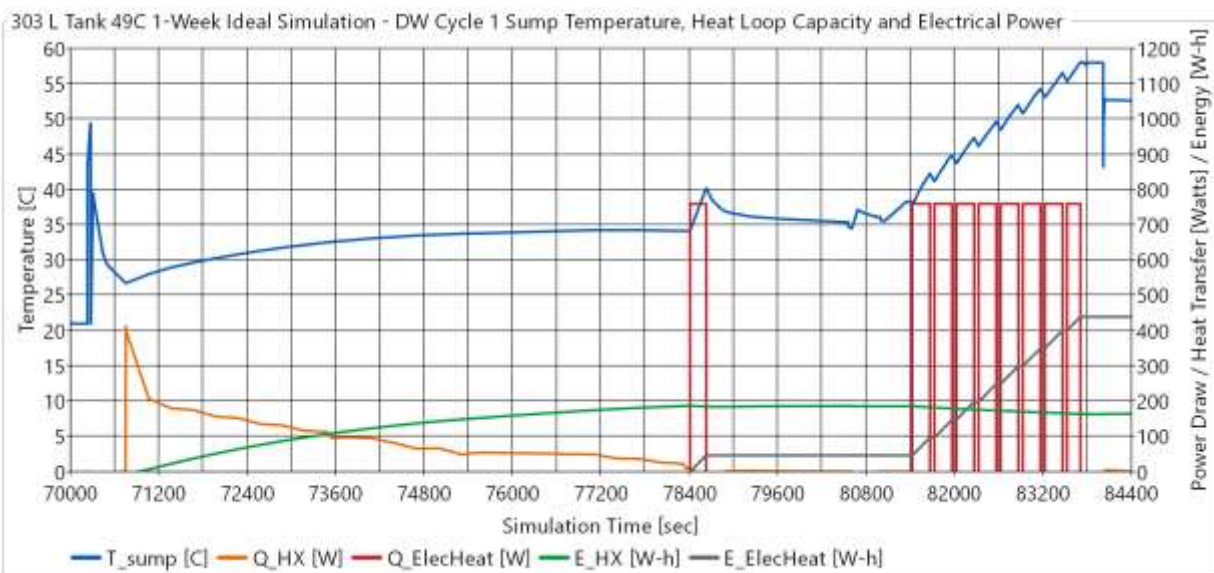


Figure 98: 1-Week 303 L (80 gal.) Ideal Simulation of Dishwasher Cycle 1 Sump Temperature, HX Heat Transfer Rate, Electric Element Power Draw, and Total Energy

Contrasting the first DW with the last DW of the week, Figure 99 displays the sump temperature, heat loop capacity, electric heating and energy delivered or consumed by the DW over time. With a duration of 222 minutes, about 500 W-h of electricity is used for heating and about 130 W-h of heat delivered by the external HX. Both the first and last cycle used a total 630 W-h of energy combined, both electrically and thermally. In the first cycle, the heat loop took 127 minutes to reach the controller cut-off before switching to the electrical heater while in the 6<sup>th</sup> cycle, it took 110 minutes. The model does not capture the required pumping power to support this delivery of external heat. Considering only this duration and the electrical savings associated from offsetting the resistive heater, the pumping power must be below roughly 90 W for cycle 1 and below 70 W for cycle 6. This limitation needs to be kept in mind due to the high demanded flow rate of the DW, 32-36 Liters/minute (8.45-9.51 GPM) and added requirement of passing through a HX requiring more pumping power. The HX heater control can be improved to balance the added time to the DW cycle resulting in more pumping power with offsetting the inefficient calrod heater internal to the appliance.

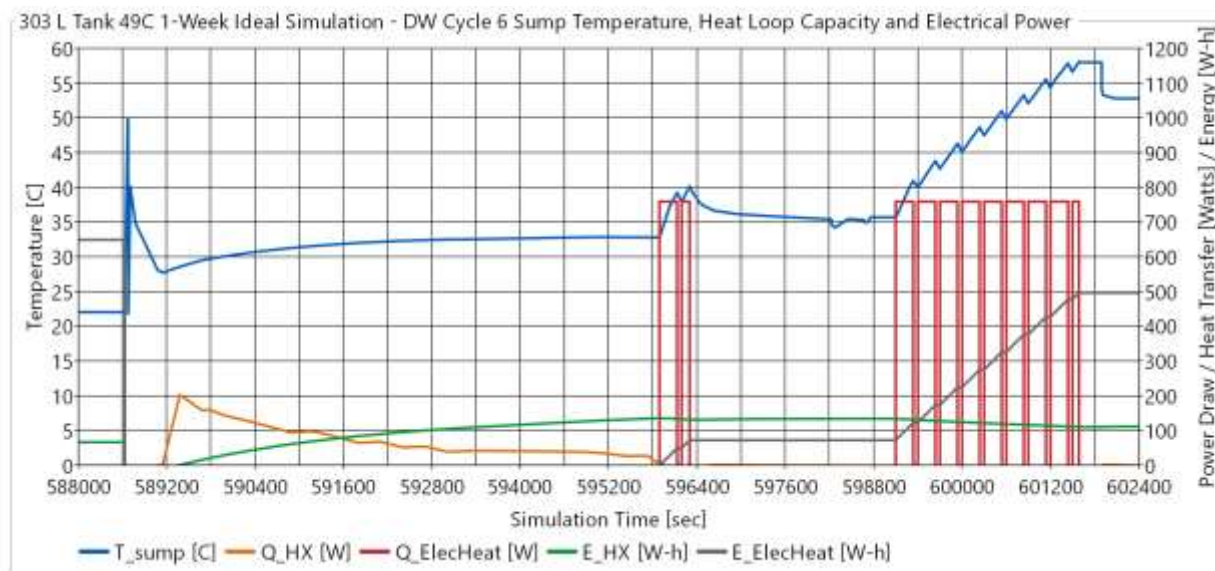


Figure 99: 1-Week 303 L (80 gal.) Ideal Simulation of Dishwasher Cycle 6 Sump Temperature, Heat Loop Heat Transfer Rate, Electric Element Power Draw, and Total Energy

Overall about 9 kWh of heat is collected from the RF and 5 kWh of heat is recovered from the CD over the 5 drying cycles. The CW required 38.5 L (gal) DHW and the DW, 63 L (gal) all provided by the storage tank. With a total tank volume of 300 L, the appliances introduce 100L of city main water, cooling the internal tank volumes on a weekly basis. The use of waste heat for DHW of the

CW and DW offsets about 3.2 kWh of electricity when heating 100L of water from 20C to 48C. The heat from the tank is able to offset roughly 0.67 kWh of heat required by the DW every week. The RF compressor consumed about 7 kWh of electricity during the week simulation. For the 300L tank in 1-week, roughly 14 kWh of heat is recovered from the RF and CD, 3.9 kWh of heat is offset in the DW and overall DHW. The storage tank is also able to maintain DHW temperatures in the upper sections and even exceeding the highest initial temperature of the stored water. The RF used roughly 7 kWh of electricity for the entire week simulation. The pumping power for the RF heat recovery is the smallest while in contrast the DW has a substantial pumping requirement due to the demanded flow rates.

### 6.3.2 150L Tank

The same initial conditions were specified as performed on the 300 L tank simulation. The temperature trends of the storage tank at 5 different heights is shown in Figure 100. When comparing the trends shown on the previous tank, the temperature swings are more pronounced as expected with a smaller storage volume. The amount of heat transfer between each appliance commands a higher percentage of the overall energy stored in the smaller tank size.

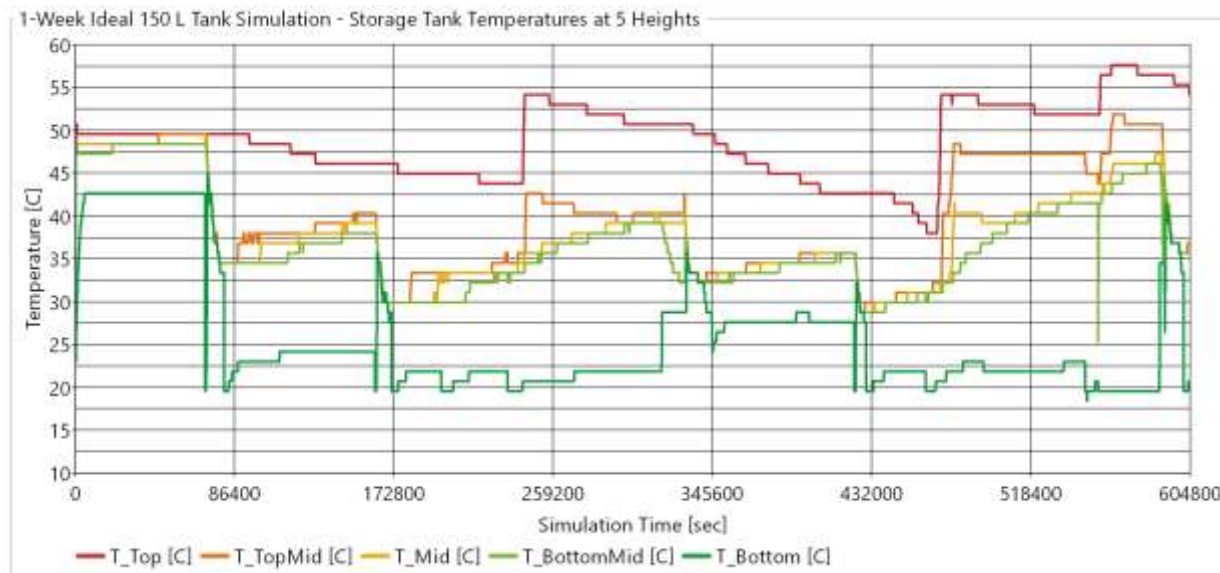


Figure 100: 1-Week 150 L (50 gal.) Ideal Simulation of 5 Storage Tank Temperatures

The impact of a smaller tank size on the RF operation, condenser heat rejected, and compressor power consumption is shown in Figure 101. Again the compressor power consumption follows

closely the temperature at the bottom of the storage tank which is the inlet state for heat rejection by the condenser.

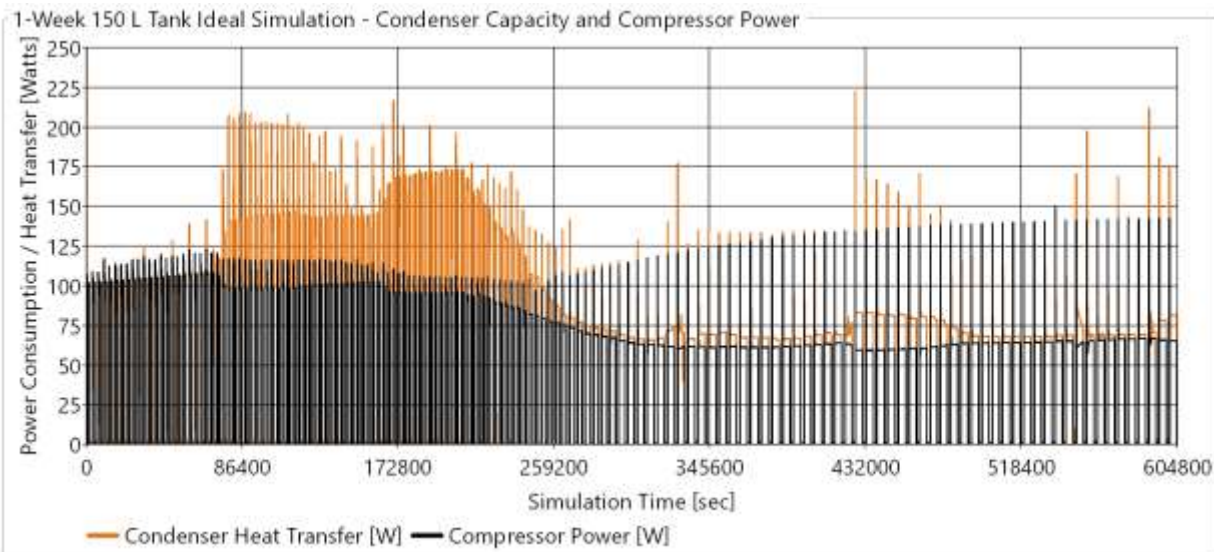


Figure 101: 1-Week 150 L (50 gal.) Ideal Simulation of Refrigerator Condenser Capacity and Compressor Power Consumption

The same two DW cycles, at the beginning of the week and end of the week are shown in Figure 102 and Figure 103.

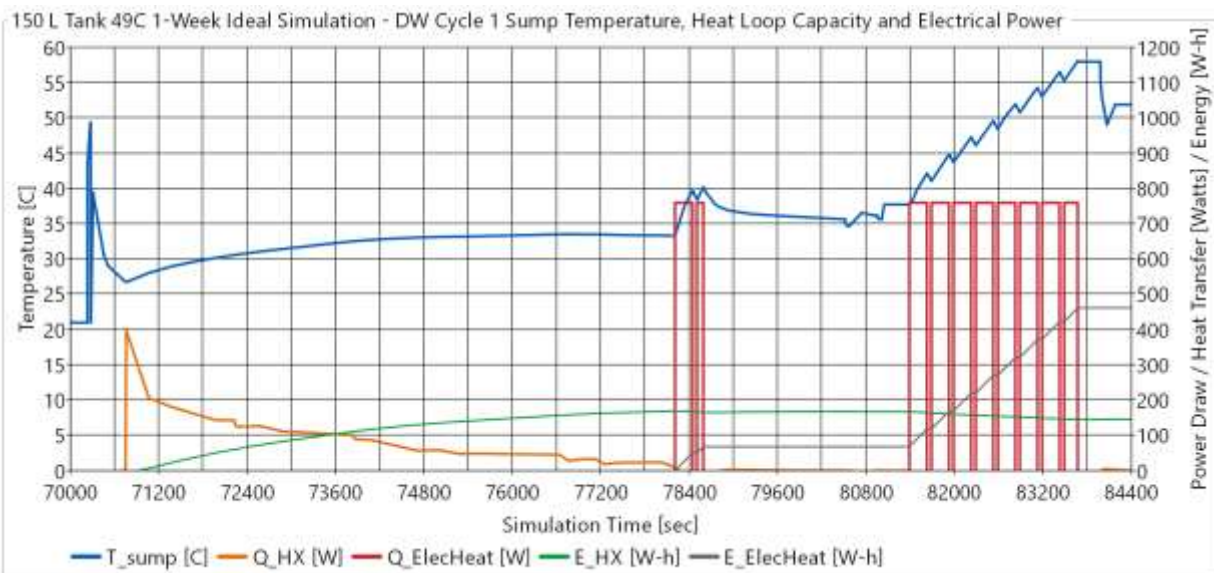


Figure 102: 1-Week 150 L (50 gal.) Ideal Simulation of Dishwasher Cycle 1 Sump Temperature, HX Heat Transfer Rate, Electric Element Power Draw, and Total Energy

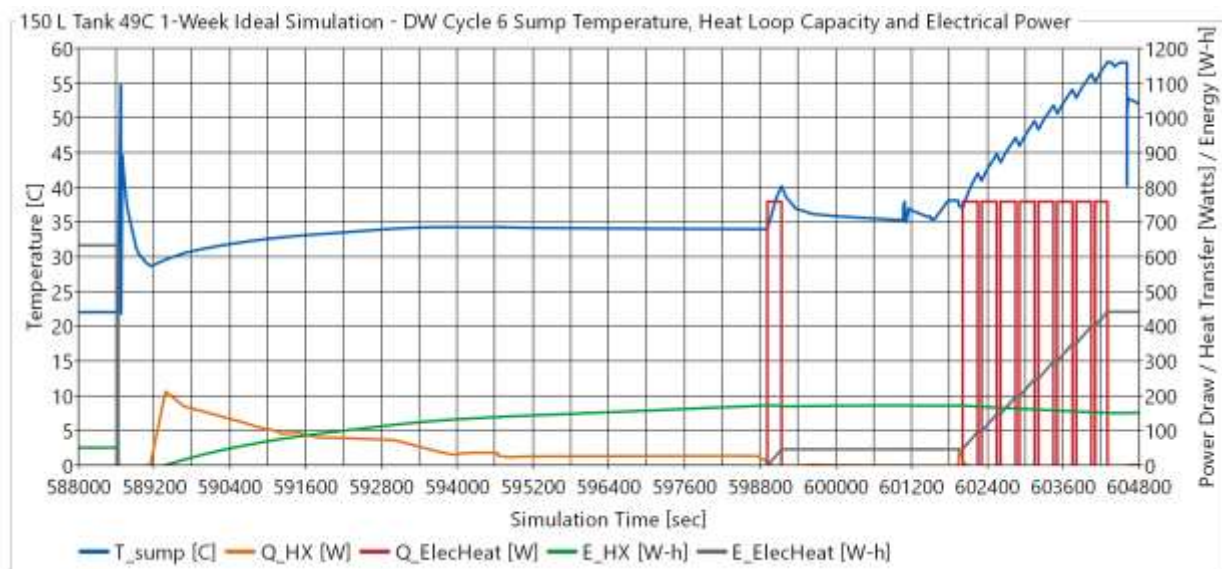


Figure 103: 1-Week 150 L (50 gal.) Ideal Simulation of Dishwasher Cycle 6 Sump Temperature, Heat Loop Heat Transfer Rate, Electric Element Power Draw, and Total Energy

## 7. CONCLUSIONS

The performance of residential appliances relies heavily on thermal energy to achieve their respective end goals and consume high exergy sources such as electricity or fossil fuels directly or indirectly. With every operation occurring within the same building, there exists the opportunity for one appliance to provide some fraction of thermal energy normally wasted to partially offset another's demand of this useful energy source. Prior advancements to appliances have been entirely focused on the individual boxes these units operate within and miss resources that are generated in the waste stream of adjacent appliances. Refrigerator-freezers and clothes dryers reject thermal energy that could heat water for dishwasher and clothes washer cycles. Developing physical models capturing these thermal interactions provide insights on how best to achieve this exchange for the reduction of primary energy consumption. As best as models can be developed, experimental testing is performed to validate the simulation results and adjust initial assumptions for improved agreement with measurement data. A tuned model has a greater degree of confidence in the results and enables a quick exploration of system parameters to be adjusted in the aim of providing the highest energy savings possible when thermally connecting residential appliances.

### 7.1 Contribution to the Field

Prior research has considered waste heat recovery and thermal connections to individual appliances (CD exhaust recovery, heat loop driven CW or DW, water cooled RF) but have not explored the added benefits by connecting all major appliances. The energy savings attainable from any one appliance is very much a function of the magnitude and frequency an appliance is used. A CW could use a hot wash once a week and a cold wash four times a week compared to a warm wash five times a week. The size of the load can vary as well. Exploring the impact of various changes to the overall system of connected appliances could be explored extensively with a comprehensive experimental plan. The difficulty is the time and resources available are most often limited and thus the measurable factors become only snapshots. Building a model dependent on the physical factors of the thermal connections; heat exchangers, flow rates, storage tank volume, and piping, provides a straightforward simulation by avoiding the detailed mechanisms required by the appliance. Prior studies investigating individual appliances would attempt to

capture the internal dynamics. Often these models require tuning factors from experimental results for higher accuracy on the prediction of the system performance.

A dynamic, Modelica model of thermally connected appliances was developed and validated against experimental data collected from a specific test stand. A parametric study explored two different storage tank volumes. Further capabilities of the model could support expansion of the shared thermal resources. Introducing the domestic hot water system for example could be one area of further savings potential. Buildings with hydronic heating and cooling could drive any supplemental demand for or tap any excess thermal energy from the connected appliances.

## **7.2 Overall Findings**

Due to the significant portion of global energy consumption by the U.S., American buildings are one area of great opportunity to achieve meaningful energy savings on a global level. The residential sector having a slightly larger piece of this consumption over the commercial sector is targeted. Significant research exists into the largest percentage of site energy usage, HVAC systems but more work is needed evaluating novel methods for efficiency improvements in residential appliances. Federal standards can help push industry to adopt energy saving technologies but small profit margins make most gambles unable to be considered and limit their focus to gaming the standard for optimal energy savings. Additionally appliance efficiencies have been increasing aggressively to where it is unknown what suitable technologies can support this rate of increase. The thermal integration of residential appliances is one approach that has not been evaluated at a large scale by including all major appliances. Initial projections from the literature estimate up to a 25% energy savings is possible through waste recovery. A preliminary analysis referencing market factors on RFs, CDs, CWs, DWs, and COs as transient and bulk heat sources reported the tradeoffs between percent of waste heat recovered versus a final water temperature attained. Higher percentages resulted in lower water temperatures. The RF is reported having an increase in cooling capacity of about 12% and a reduction of compressor power consumption of about 26%. A sample operation of the CD has the exhaust air stream being cooled down to 30.5°C (86.9°F) or on the other side, is able to heat 19 liter (5 gal) of water up to about 54.5°C (130.1°F). While the DW provided higher heat source temperatures, 40°C (104°F), than the clothes washer, 36°C (97°F), the opposite was true in that the volume of waste water drained is very low compared

to the clothes washer 11.7 L (3.1 gal) to 155 L (41 gal). Thus storage tank water temperatures did not reach above 30°C (86°F) even with low storage volumes. The CO can generate significant water temperatures depending how small of a storage tank is connected but presents technological challenges to safely and efficiently collect this waste heat.

The prototype design of the integrated system was constructed, and several cycles of each appliance operation was collected to obtain experimental data. The tuned models provide guidance on the impact of control decisions during the heat recovery process, how storage tank volume plays a part with increasing waste heat usage in the DHW system, and giving design requirements for the supporting equipment to achieve the explored thermal integration.

Collecting appliance experimental results from the manufacturer and from literature provide references to standard operation characteristics. Modelica models were built by capturing major steps or parameters for each appliance, CD, RF, DW and CW. The available data was used as an input for a heat source to the model and to validation tool to improve the simulation prediction. The tuned individual appliance models interface with a storage tank model to create an integrated appliance model. For a 300L tank, roughly 14 kWh of heat is recovered from the RF and CD, 3.9 kWh of heat is offset in the DW and overall DHW demand. The storage tank is also able to maintain DHW temperatures in the upper sections and even exceeding the highest initial temperature, 48C, of the stored water. The RF used roughly 7 kWh of electricity for the entire week simulation.

### **7.3 Recommended Future Work**

The complexity of the system provides numerous directions to improve the amount of energy recovered and the primary energy reduced. Furthermore other improvements are mentioned to improve the overall simulation performance.

The CD and DW show potential for improved efficiencies compared to the results presented in this work. Updating the CD with a lower density fin pitch and changing the geometry to a counter-flow will reduce the required auxiliary fan power, improve reliance to fouling by lint and generate higher return temperatures to the storage tank and increase the amount of energy possible to offset

for other heat using appliances, CW or DW. The time of the CD operation relative to the start of the CW or DW operation can also further increase this offset energy consumption by minimizing the amount of heat loss during storage.

Changing the HX type on the DW is a crucial improvement to make the possibility for useful heat input a reality. Reducing the significant pressure drop expected at the high flow rates allows for smaller pump power and minimizes the associated energy penalties for running the DW longer to achieve required internal temperatures. With the energy rating of the DW also considering the amount of DHW used per cycle, simulations should be run to explore the benefit of a cold-water supply to the DW instead of a hot-water supply. More heat would be needed of the HX and would be in a better range that can be delivered by the HX instead of unfeasible high temperatures required during the rinsing steps. The Modelica controller of the DW should be improved to increase the threshold for external heating by switching to the electric heater when the heat rise in the DW seems to plateau. The benefit here would balance the overall cycle time to improve customer experience with the energy savings of using an external heat input. Something akin to the eco versus speed mode available on heat pump CDs today.

The RF capacity controller would benefit from operating in two modes, minimizing compressor power and maximizing return water temperatures. The control decision would come from an overall appliance system controller that determines if another appliance will need high temperature water for a cycle. The numerical analysis available from the simulation environment lists many events are generated within the RF HXs during ON/OFF transitions and OFF periods due to switching flow rates between the HX cells. These events slow the implicit DAE solver by requiring small time steps to iterate through. Using Modelica no event declarations around these cell connections or finding other approaches to force a flow rate in one direction throughout the entire simulation could greatly improve the overall weekly simulation.

Supporting the stratification of the storage tank is an important feature of the physical test stand to maintain the hottest water temperatures generated during different appliance cycles. One product was found from a small company in Europe but required custom modifications to the storage tank for installation.

## REFERENCES

ASHRAE Standard 41.2

Bansal, P., Vineyard, E. and Abdelaziz, O. (2011). Advances in household appliances – A review. *Applied Thermal Engineering* 31, 3748-3760.

Boudreaux, P. R., Gehl, A. C., & Christian, J. E. (2012). Occupancy simulation in three residential research houses. *ASHRAE Transactions*, 118, 625.

Buildings Energy Data Book. (2011). Pacific Northwest National Laboratory, Buildings Technologies Program, Energy Efficiency & Renewable Energy, U.S. Department of Energy. Retrieved from <http://buildingsdatabook.eren.doe.gov/>

Butturini, R., Lee, A., & Dunmore, F. (2004). Detection of Abnormal Operating Conditions in Electric Clothes Dryers. U.S. Consumer Product Safety Commission.

Caskey, S.L., and Groll, E.A. (2018). Modelica Analysis of Thermally Connected Residential Appliances. *5<sup>th</sup> International High Performance Buildings Conference*.

Dabri, A.E., and Rice, C.K. (1981). A Compressor Simulation Model with Corrections for the Level of Suction Gas Superheat. *ASHRAE Transactions*, V. 87, Pt. 2.

Eastment, M., and Hendron, R. (2006). Method for Evaluating Energy Use of Dishwashers, Clothes Washers, and Clothes Dryers. *ACEEE Summer Study on Energy Efficiency in Buildings*.

ENERGY STAR Market & Industry Scoping Report Residential Clothes Dryers. (2011). U.S. Environmental Protection Agency. Retrieved from: [https://www.energystar.gov/sites/default/files/asset/document/ENERGY\\_STAR\\_Scoping\\_Report\\_Residential\\_Clothes\\_Dryers.pdf](https://www.energystar.gov/sites/default/files/asset/document/ENERGY_STAR_Scoping_Report_Residential_Clothes_Dryers.pdf)

ENERGY STAR Version 5.0 Specification for Residential Refrigerators and Freezers. (2013). U.S. Environmental Protection Agency. Retrieved from: [https://www.energystar.gov/products/spec/residential\\_refrigerators\\_and\\_freezers\\_specification\\_version\\_5\\_0\\_pd](https://www.energystar.gov/products/spec/residential_refrigerators_and_freezers_specification_version_5_0_pd)

ENERGY STAR Version 6.0 Specification for Residential Dishwasher. (2015). U.S. Environmental Protection Agency. Retrieved from: [https://www.energystar.gov/products/spec/residential\\_dishwasher\\_specification\\_version\\_6\\_0\\_pd](https://www.energystar.gov/products/spec/residential_dishwasher_specification_version_6_0_pd)

- Hager, T.J., & Morawicki, R. (2013). Energy consumption during cooking in the residential sector of developed nations: A review. *Food Policy* 40. 54-63.
- Klein, S. A., & Alvarado, F. L. (2002). Engineering equation solver. F-Chart Software, Madison, WI.
- Longo, G.A., and Gasparella, A., (2007). Refrigerant R134A vaporization heat transfer and pressure drop inside a small brazed plate heat exchanger. *Int. J. of Refrig.* 30. 821-830.
- Longo, G.A., (2008). Refrigerant R134A condensation heat transfer and pressure drop inside a small brazed plate heat exchanger. *Int. J. of Refrig.* 31. 780-789.
- McDonald, A.T., Friskney, S.H., and Ulrich, D.J. (1989). Thermal Model of the Dishwasher Heater in Air. *IEEE Transactions on Industry Applications*, 25, No. 6.
- Meyers, S., McMahon, J.E., McNeil, M., & Liu, X. (2003). Impacts of US federal energy efficiency standards for residential appliances. *Energy* 28, 755-767.
- Park, J.S., and Jacobi, A.M. (2009). A run-around heat exchanger system to improve the energy efficiency of a home appliance using hot water. *Applied Thermal Engineering* 29. 3110-3117
- Pakula, C., & Stamminger, R. (2010). Electricity and water consumption for laundry washing by washing machine worldwide. *Energy Efficiency* 3, 365-382.
- Persson, T. (2007). Dishwasher and washing machine heated by a hot water circulation loop. *Applied Thermal Engineering* 27, 120-128.
- Radermacher, R., and Kim, K. (1996). Domestic refrigerators: recent developments. *Int. J. Refrig.* 19, 61-69.
- Refrigerator Market Profile. (2009). Energy Star Program, U.S. Department of Energy. Retrieved from [http://apps1.eere.energy.gov/states/pdfs/ref\\_market\\_profile.pdf](http://apps1.eere.energy.gov/states/pdfs/ref_market_profile.pdf)
- Residential Energy Consumption Survey (RECS). (2009). U.S. Energy Information Agency. Retrieved from <http://www.eia.gov/consumption/residential/data/2009/>
- Small, S., (2017) TIRA - Thermally Integrated Residential Appliances - Heat Capture Design. Purdue Project Final Report.
- Section 7.2 Residential Clothes Washer Incentive Program. (2013). Texas Water Development Board. Retrieved from <http://www.twdb.texas.gov/conservation/BMPs/Mun/doc/7.2.pdf>
- Tomlinson, J. J., Rzy, D. T. (1998). Bern Clothes Washer Study Final Report. Energy Division, Oak Ridge National Laboratory, U.S. Department of Energy.

- TIL Suite Modelica Thermal Library. (2016). TLK-Thermo GmbH, Braunschweig, Germany.  
<https://www.tlk-thermo.com/index.php/en/software-products/overview>
- Whirlpool Corporation. (2017). Manufacturer experimental data of KitchenAid dishwasher following Department of Energy test procedure. *Personal communication*.
- Wilson, E., Engebrecht-Metzger, C., Horowitz, S., & Hendron, R. (2014). 2014 Building America House Simulation Protocols (No. NREL/TP-5500-60988). National Renewable Energy Laboratory (NREL), Golden, CO.

## **APPENDIX A – WASTE HEAT ANALYSIS**

A preliminary analysis is conducted on the waste heat available from each major residential appliance; RF, CD, CW, DW, and CO. An EES model for each appliance is built and sample cycles are run for each one. Basic heat recovery efficiencies are assumed and the percentage of input energy that can be recovered is calculated. The results indicate the infrequent use of the CO coupled with technological challenges make heat recovery unattractive. The other appliances show promise for designing methods or techniques to collect and reuse the waste heat.

### **A.1 EES Computer Modeling**

The modeling of each appliance in EES is first separated into two different approaches dependent on the heat source. For both the RF and the CD, a transient process is captured for the waste heat steam that is occurring over time. Due to the heat sources from the CW, DW, and CO occurring intermittently and in batches, the available thermal energy is considered as a bulk source.

#### **A.1.1 Transient Energy Analysis**

When the refrigerator compressor turns on, it rejects heat either to the ambient air as in a normal application or is rejected to a cooling water loop with a water-to-refrigerant heat exchanger. For the clothes dryer, the exhaust air is typically sent outside the home, but for heat recovery, a fin and tube heat exchanger is placed in this exhaust stream and a cooling water loop provides an ability to recover the sensible and latent heat leaving the dryer. Curve-fits are generated off the two plots in the study presented in Figure 12 and Figure 13 by picking points evenly along the curves of interest and applying a polynomial fit to the points found using spreadsheet software.

To simplify the analysis, a lumped parameter, heat transfer effectiveness of 80% is assumed for all heat exchangers, waste heat and the vapor compression cycle heat exchangers. The maximum heat transfer is determined by cooling or heating the refrigerant to the inlet conditions of the air or water streams. The experimental data from the manufacturer for the refrigerator is used to provide the compressor displacement and the cycle improvements implemented in a standard household refrigerator. Modeling the suction line heat exchanger attached to the capillary tube was captured

by further cooling the subcooled liquid leaving the condenser with the leaving refrigerant vapor of the evaporator. The expansion process then was assumed to be isenthalpic. The subcooling leaving the condenser and the superheat leaving the evaporator were both assumed to be 5°C (9°F). Due to the suction line heat exchanger, this means additional subcooling is created for a larger evaporator capacity while sacrificing some of the compressor efficiency with higher suction superheat. Additional properties of the compressor were assumed to roughly model the compression process. A volumetric efficiency of 95%, an isentropic efficiency of 80%, and 20% of the input power into the compressor is lost as waste heat to the ambient. The evaporation and condensing conditions are free to move depending on the heat sink and source temperatures being exposed to the respective heat exchangers. For the clothes dryer, the exhaust air stream dew point temperature is checked with the incoming cooling water temperature to determine if the coil is wet or dry. If the inlet water temperature is below the exhaust air dew point, then the exit air temperature of the waste heat exchanger is at saturated conditions. Otherwise when the cooling water temperature is above the dew point, the humidity ratio is kept constant across the waste heat exchanger.

The strategy for measuring the available heat recovery during the transient process is to explore different volume sizes of water storage tanks and cooling water flow rates. The storage tank supplies the waste heat exchanger with cool water where it picks up heat and returns to the storage tank. Over time the tank temperature should rise in temperature depending on amount of heat being rejected to the water stream. Smaller water volume tanks and flow rates should obtain higher temperature at the end of the transient process. While this higher temperature water has more potential to offset energy usage in another location of the home, less total energy is recovered from the waste stream due to the higher sink temperatures for cooling.

### **A.1.2 Bulk Energy Analysis**

To recover the waste heat, a fixed volume of cooling water is brought into contact with the fixed volume of waste water or thermal mass as in the case of the CO, and it brought to thermal equilibrium. Decreasing the volume of cooling water used causes the final temperature to approach the original temperature of the heat source. Maximizing the temperature of cooling water provides a higher availability energy input to another heat demand, and thus reducing the amount of external

energy required. A trade-off exists between maximizing the heat recovery from the waste stream of the appliance with larger volumes of cooling water, and maximizing the supplemental heat provided to another process from smaller cooling water volumes providing higher temperatures.

## A.2 Transient Heat Results

Four different tank volumes were run for the refrigerator model covering a typical cycle time of 50 minutes and a cooling water flow rate of 1.9 liter/min (0.5 gallons/min). A summary of the water tank temperature at the end of the cycle run for each tank volume is shown in Table 1. The tank volume sizes were selected based off a desirable water temperature.

Table 1: Summary of household refrigerator performance with water cooling and air cooling condenser

Cooling Stream	Tank Volume		Maximum Tank Temperature		Total Evaporator Energy	Total Compressor Energy	Avg. Cooling COP
	[liter/gal]		[C/F]		[kJ]	[kJ]	[-]
Water	19	5	28.58	83	753.6	198.4	2.71
Water	15	4	32.5	90	745.8	205.3	2.62
Water	11	3	39	103	730.8	217.8	2.47
Water	7.6	2	55.9	132	694.2	246.8	2.17
Air	-	-	-	-	669.6	267.6	2.20

To see the transient analysis of the tank temperature for the same tank sizes, Figure 104 shows 4 curves with the same conditions shown in Table 1.

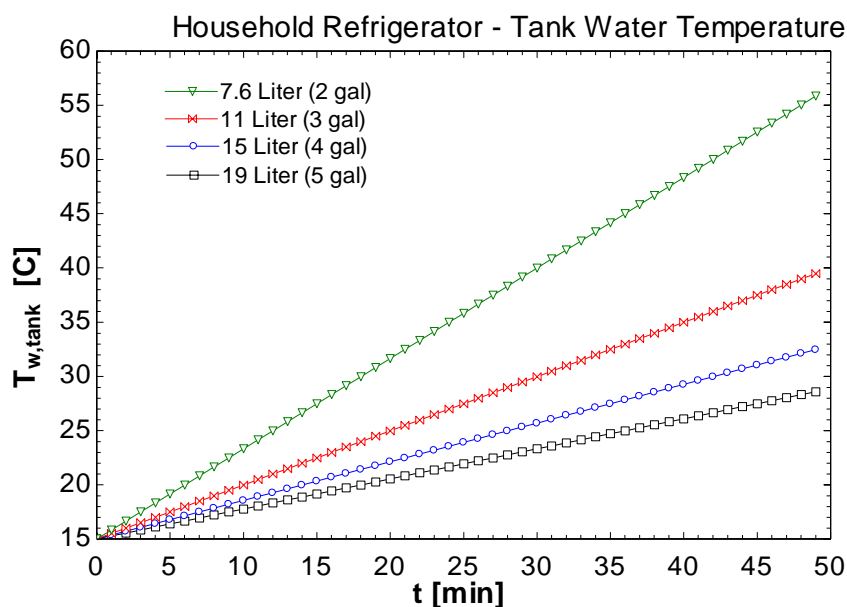


Figure 104: Storage tank temperature for water cooled condenser of household refrigerator

A summary of the clothes dryer simulation runs is shown in Table 2. As the tank size increases the percent of energy recovered increases but the maximum tank temperature decreases. Also the air outlet temperature of the heat recovery process decreases, providing a better possibility of allowing the dryer exhaust to be vented indoors instead of outdoors.

Table 2: Summary of clothes dryer heat recovery

Tank Size [liter/gal]	Start Tank Temperature [C/F]	End Tank Temperature [C/F]	Max Air Outlet Temperature [C/F]	Total Heat Recovered [kJ]	Total Energy Input [kJ]	Percent Energy Recovered
378 100		22.2 72.0	30.5 86.9	11408		51.8%
113 30		33.0 91.4	39.1 102.5	8369		38.0%
76 20	15 59	37.7 99.8	42.9 109.2	6937	22041	31.5%
38 10		45.4 113.7	49.1 120.3	4471		20.3%
19 5		54.5 130.1	56.3 133.4	2668		12.1%

To understand the impact of the storage tank size for the same water flow rate as the refrigerator, 1.9 liter/min (0.5 gallons/min), Figure 105 shows the tank temperature as a function of time. As the volume decreases from 113 liter (30 gallons) to 19 liter (5 gallons), the final tank temperature at the end of the drying cycle goes from 33°C (91.4°F) to 54.5°C (130°F).

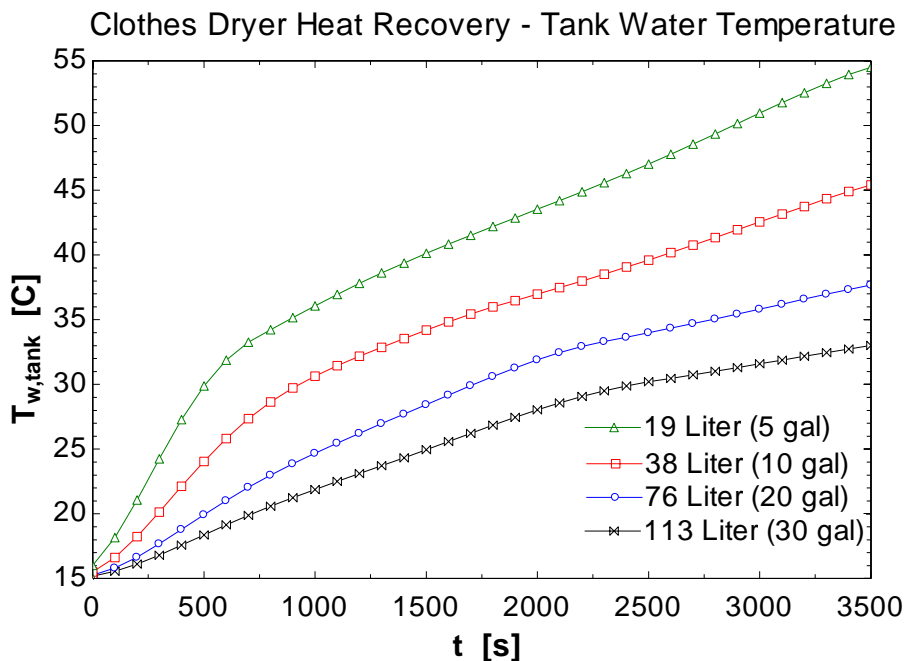


Figure 105: Impact of the storage tank volume size on the water temperature stored in the tank

A secondary benefit of having heat recovery at the exhaust of the dryer is the reduction of the dryer air exhaust temperature and the removal of moisture from the exhaust stream. Figure 106 provides

an indication of the exhaust air stream leaving the heat exchanger changes as the storage tank increases in temperature over time.

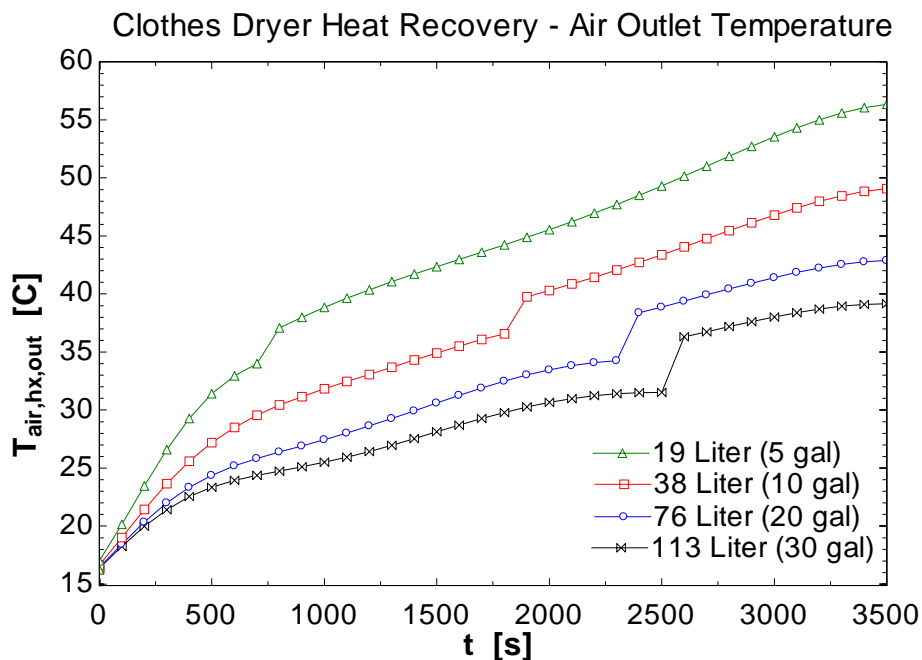


Figure 106: Cooled dryer exhaust air leaving the waste heat exchanger as a function of the storage tank volume

### A.3 Bulk Heat Results

Using the assumed cycle parameters for each appliance providing a bulk energy source, the amount of heat recovered by the cooling water source is calculated for a number of tank volumes. A summary of all the results is listed in Table 3. The assumed cycle energy per cycle presented in the Appliance Background section for each appliance is converted from kWh to kJ to calculate a percent of energy input recovered by the cooling water source.

Table 3: Summary of bulk energy recovery from the clothes washer, dishwasher and cooking oven

Tank Volume [liter/gal]	Clothes Washer [8136 kJ/cycle]				Dishwasher [4536 kJ/cycle]				Cooking Oven [15372 kJ/cycle]				
	Final Temperature [C/F]	Final Temperature [C/F]	Heat Recovered [kJ]	% Recovery [-]	Final Temperature [C/F]	Final Temperature [C/F]	Heat Recovered [kJ]	% Recovery [-]	Final Temperature [C/F]	Final Temperature [C/F]	Heat Recovered [kJ]	% Recovery [-]	
7.6	2	34.9	94.8	700.7	8.6%	30.0	86.1	546.2	12.0%	123.9	255.0	3530	23.0%
15.1	4	33.9	93.1	1339	16.5%	25.4	77.7	799.6	17.6%	90.5	194.9	4923	32.0%
22.7	6	33.0	91.4	1922	23.6%	22.7	72.9	945.8	20.9%	72.3	162.1	5652	36.8%
30.3	8	32.2	89.9	2457	30.2%	21.0	69.8	1041	23.0%	60.9	141.7	6096	39.7%
37.9	10	31.4	88.6	2951	36.3%	19.8	67.6	1108	24.4%	53.2	127.8	6398	41.6%
45.4	12	30.7	87.3	3407	41.9%	18.9	66.0	1158	25.5%	47.6	117.7	6615	43.0%
53.0	14	30.1	86.1	3829	47.1%	18.2	64.7	1196	26.4%	43.4	110.1	6776	44.1%
60.6	16	29.5	85.0	4222	51.9%	17.6	63.7	1226	27.0%	40.0	104.1	6902	44.9%
68.1	18	28.9	84.0	4588	56.4%	17.2	62.9	1251	27.6%	37.4	99.3	7004	45.6%
75.7	20	28.4	83.0	4929	60.6%	16.8	62.2	1271	28.0%	35.2	95.3	7086	46.1%

#### A.4 Overall Predicted Savings from Thermal Connected Suite

There exists a strong trade-off between the tank volume of water used to circulate for heat recovery and the final temperature at the end of the appliance cycle. While smaller tank volumes provide higher water storage temperatures which are useful as a direct input to another appliance cycle, smaller percentages of the energy recovery result due to the higher water temperatures being delivered to the appliance. An improved analysis would be to calculate the availability or exergy of the heat recovered by the water cooled heat exchanger. Most of the input energy for all appliances is pure exergy in the form of electricity since it can be used to perform any task. Once it is converted by the appliance into useful work through refrigeration, cooking or wet cleaning, much of this potential energy is destroyed. The leaving waste stream is now low in availability due to the low temperature and its close to a dead state where no more useful work can be extracted. An improvement of the work presented here would be to have one fixed volume tank and conduct a large transient analysis where different appliances would come on and off. This approach would explore potential benefits or pitfalls when larger storage tanks are used to combine all the waste heat into one location. Additionally, the ability to offset some of the household domestic hot water would be introduced by adding in a hot water schedule relative to the appliance schedule.

While the experimental data referenced for the clothes dryer was very detailed and provided an easy way to calculate the available energy from the waste stream, the drying conditions seen might not be fully representative of a typical cycle. The clothing load was large and the heat setting was

on high. Obtaining exhaust air data for different dryer conditions would properly identify an optimal tank size for circulating the cooling water.

Household appliances account for the second largest site energy consumption, 27%, after the HVAC system for the U.S. residential sector. Many approaches explored in the past to address this area were mainly focused on only the appliance itself. If the scope for improvement also considers factors external to the appliance, there is the potential for greater energy savings. By quantifying the expected energy available in the waste stream for five major appliances; household refrigerator, clothes dryer and washer, dishwasher, and cooking oven, a potential energy source is presented. A cold water cooling stream is applied to the waste stream of each appliance and an estimated amount of energy can be recovered. The household refrigerator is modeled having an increase in cooling capacity of about 12% and a reduction on compressor power consumption of about 26%. A sample operation of the clothes dryer has the exhaust air stream being cooled down to 30.5°C (86.9°F) or on the other side, is able to heat 19 liter (5 gal) of water up to about 54.5°C (130.1°F). A different modeling approach is used for the bulk energy sources. A large volume of water was available by the clothes washer, but due to typical operation characteristics, low wash and rinse temperatures, the waste stream was not high in temperature. The highest temperature of water generated was at 35°C (95°F). While the dishwasher provided higher heat source temperatures, 40°C (104°F), than the clothes washer, 36°C (97°F), the opposite was true in that the volume of waste water drained is very low compared to the clothes washer 11.7 liter (3.1 gal) to 155 liter (41 gal). Thus storage tank water temperatures did not reach above 30°C (86°F) even with low storage volumes. The cooking oven can generate very high water temperature depending how small of a storage tank is connected. There exists a controls risk when preventing the cooling water stream from reaching the boiling point and creating steam. Further work in this area is recommended due to the potential of high water temperatures generated from waste energy streams not currently being captured.

## APPENDIX B - EES CODE

### B.1 Clothes Dryer

```

File:Clothes_Dryer_v4.EES
EES Ver. 10.268: #3045: For use only by students and faculty, Purdue University Campus, West Lafayette, IN
12/9/2017 3:01:25 AM Page 1

1: "clothes dryer"
2:
3: "PROCEDURE Clothes_Dryer(T_wash, T_rinse, V_wash, V_rinse, T_w_drain, T_r_drain, V_w_drain, V_r_drain, W_elec :
   T_clothes, V_clothes, Q_loss, S_gen)"
4: {assume all inputs are in English units, F and gallons}
5:
6: PROCEDURE Tank(delta_t,V_w_tank,T_start,V_dot_w,T_w_return:T_w_tank, u_w_tank)
7:
8: IF(TABLERUN# = 1) THEN
9:   T_w_tank_initial = T_start
10:  u_w_tank_initial = IntEnergy(Water,T=T_start,x=0[-])
11:  rho_w_tank_initial = Density(Water,T=T_start,x=0[-])
12:  T_w_tank = T_w_tank_initial
13:  u_w_tank = u_w_tank_initial
14:
15: ELSE
16:  u_w_tank_initial = TABLEVALUE("Table 1",TABLERUN# - 1, 'u_w_tank')
17:  rho_w_tank_initial = Density(Water,u=u_w_tank_initial,x=0[-])
18:  T_w_tank_initial = Temperature(Water,u=u_w_tank_initial,x=0[-])
19:  h_w_i = Enthalpy(Water,u=u_w_tank_initial,x=0[-])
20:
21:  h_w_o = Enthalpy(Water,T=T_w_return,x=0[-])
22:
23:  Q_dot_hx = V_dot_w*rho_w_tank_initial*(h_w_o - h_w_i)*convert(GPM,m3/s)
24:
25:  u_w_tank = ((Q_dot_hx*delta_t) + V_w_tank*rho_w_tank_initial*convert(gal,m3)*u_w_tank_initial)/(V_w_tank
   rho_w_tank_initial*convert(gal,m3))
26:  T_w_tank = Temperature(Water,u=u_w_tank,x=0[-])
27:
28: ENDIF
29:
30: END {Tank}
31:
32: PROCEDURE Wet_Clothes(T_exhaust_db,m_w_clothes_0,m_w_clothes_mv,m_w_clothes_initial, m_w_clothes,
   u_w_clothes_initial,s_w_clothes_initial)
33:
34: IF(TABLERUN# = 1) THEN
35:
36:   m_w_clothes_initial = m_w_clothes_0
37:   m_w_clothes = m_w_clothes_initial
38:   u_w_clothes_initial = IntEnergy(Water,T=T_exhaust_db, x=0[-])
39:   s_w_clothes_initial = Entropy(Water,T=T_exhaust_db, x=0[-])
40:
41: ELSE
42:
43:   m_w_clothes_initial = TABLEVALUE("Table 1",TABLERUN# - 1, 'm_w_clothing')
44:   T_w_clothes_initial = TABLEVALUE("Table 1",TABLERUN# - 1, 'T_exhaust_db')
45:   u_w_clothes_initial = IntEnergy(Water,T=T_w_clothes_initial, x=0[-])
46:   s_w_clothes_initial = Entropy(Water,T=T_w_clothes_initial, x=0[-])
47:   m_w_clothes = m_w_clothes_initial - m_w_clothes_mv
48:
49: ENDIF
50:
51: END {Wet Clothes}
52:
53: "surrounding temperature to establish the dead state"
54: P_atm = 101.325 [kPa]
55: T_a_0 = T_ambient
56: T_a_0_K = convertTemp('C','K',T_a_0)
57: RH_a_0_per = 50 [%]
58: RH_a_0 = RH_a_0_per*convert(percent,-)

```

```

59: h_a_0 = Enthalpy(AirH2O,T=T_a_0,r=RH_a_0,P=P_atm)
60: s_a_0 = Entropy(AirH2O,T=T_a_0,r=RH_a_0,P=P_atm)
61: T_w_0 = T_main
62: T_w_0_K = convertTemp('C','K',T_w_0)
63: u_w_0 = IntEnergy(Water,T=T_w_0,x=0[-])
64: h_w_0 = Enthalpy(Water,T=T_w_0,x=0[-])
65: s_w_0 = Entropy(Water,T=T_w_0,x=0[-])
66: t_m = t*convert(s,min)
67: delta_t = 100 [s]
68:
69: "ambient air conditions of the environment where the dryer operates"
70: T_ambient = 26 [C]
71: RH_ambient_per = 50 [%] "assumption has minimal impact on the delivered air temperature to the drum"
72: RH_ambient = RH_ambient_per*convert(percent,-)
73: Omega_ambient = HumRat(AirH2O,T=T_ambient,r=RH_ambient,P=P_atm)
74: rho_ambient = Density(AirH2O,T=T_ambient,r=RH_ambient,P=P_atm)
75: h_ambient = Enthalpy(AirH2O,T=T_ambient,r=RH_ambient,P=P_atm)
76: s_ambient = Entropy(AirH2O,T=T_ambient,r=RH_ambient,P=P_atm)
77: e_ambient = (h_ambient - h_a_0) - T_a_0_K*(s_ambient - s_a_0)
78:
79: "electric heater used to increase the ambient air temperature before being delivered to the drum of the dryer"
80: W_dot_acc = 0.957 [kW] "average amp draw of electric motor ~4.35 amps and voltage supply of 220 VAC"
81: W_dot_heater = 5 [kW] "set by average amp draw of electric heater ~22.8 amps and voltage supply of 220 VAC"
82: E_W_dot_heater = W_dot_heater + W_dot_acc
83: Q_dot_heater = W_dot_heater + W_dot_acc "assume ideal electric heater - 100% of input electrical energy converted into
    heat energy"
84: Q_dot_heater = m_dot_a*(h_inlet - h_ambient) "provides the inlet air enthalpy of the dryer to predict the inlet air temperature"
85: Q_heater = Q_dot_heater*delta_t
86: E_Q_dot_heater = (1 - T_inlet_db_K/T_a_0_K)*Q_dot_heater
87:
88: "inlet air conditions to the drum of the clothes dryer"
89: [T_inlet_db = 145 [C] "comment out to use heater input energy for estimating inlet air temperature"]
90: T_inlet_db_K = convertTemp('C','K',T_inlet_db)
91: Omega_inlet = Omega_ambient
92: RH_inlet = RelHum(AirH2O,T=T_inlet_db,w=Omega_inlet,P=P_atm)
93: RH_inlet_per = RH_inlet*convert(-,%)
94: P_inlet_v = RH_inlet*P_inlet_sat_g
95: P_inlet_sat_g = Pressure(Water,T=T_inlet_db,x= 1[-])
96: rho_inlet = Density(AirH2O,T=T_inlet_db,w=Omega_inlet,P=P_atm)
97: h_inlet = Enthalpy(AirH2O,T=T_inlet_db,w=Omega_inlet,P=P_atm)
98: s_inlet = Entropy(AirH2O,T=T_inlet_db,w=Omega_inlet,P=P_atm)
99: e_inlet = (h_inlet - h_a_0) - T_a_0_K*(s_inlet - s_a_0)
100:
101: "initial water conditions of the saturated clothing to be dried"
102: T_clothing_0 = T_ambient
103: rho_w_clothing_0 = Density(Water,T=T_clothing_0,x=0[-])
104: m_w_clothing_0 = 4.5 [kg]
105: V_w_clothing_0 = (m_w_clothing_0/rho_w_clothing_0)*convert(m3,gal)
106:
107: "water conditions of the saturated clothing during drying"
108: T_clothing = T_exhaust_db
109: rho_w_clothing = Density(Water,T=T_clothing,x=0[-])
110: V_w_clothing = (m_w_clothing/rho_w_clothing)*convert(m3,gal)
111: u_w_clothing = IntEnergy(Water,T=T_clothing,x=0[-])
112: h_w_clothing = Enthalpy(Water,T=T_clothing,x=0[-])
113: s_w_clothing = Entropy(Water,T=T_clothing,x=0[-])
114: Q_clothing_req = m_w_CD_rmw*Enthalpy_vaporization(Water,T=T_ambient)
115: e_w_clothing = (h_w_clothing - h_w_0) - T_w_0_K*(s_w_clothing - s_w_0)
116:
117: "exhaust air stream conditions leaving the dryer"

```

```

118: {curve-fit used was generated from Excel spreadsheet "Clothes_Dryer_Operation.xlsx "}
119: T_exhaust_db = -2.52015E-12*t^4 + 1.98456E-08*t^3 - 5.27776E-05*t^2 + 6.08666E-02*t + 2.44562E+01
120: RH_exhaust_per = -5.50527E-18*t^6 + 6.14881E-14*t^5 - 2.58065E-10*t^4 + 4.97191E-07*t^3 - 4.21810E-04*t^2 +
  9.63621E-02*t + 7.18982E+01
121: RH_exhaust = RH_exhaust_per*convert(percent, '-')
122: T_exhaust_wb = WetBulb(AirH2O, T=T_exhaust_db, r=RH_exhaust, P=P_atm)
123: T_exhaust_dp = DewPoint(AirH2O, T=T_exhaust_db, r=RH_exhaust, P=P_atm)
124: Omega_exhaust = HumRat(AirH2O, T=T_exhaust_db, r=RH_exhaust, P=P_atm)
125: rho_exhaust = Density(AirH2O, T=T_exhaust_db, r=RH_exhaust, P=P_atm)
126: h_exhaust = Enthalpy(AirH2O, T=T_exhaust_db, r=RH_exhaust, P=P_atm)
127: s_exhaust = Entropy(AirH2O, T=T_exhaust_db, r=RH_exhaust, P=P_atm)
128: e_exhaust = (h_exhaust - h_a_0) - T_a_0*K*(s_exhaust - s_a_0)
129:
130: "estimated air flow rate delivered by the fan - conflicting result"
131: "either generate realistic supply air temperatures to the drum off the ambient conditions"
132: "or accurately predict the amount of moisture removed during the entire cycle"
133: V_dot_a = 100 [CFM]
134: m_dot_a = rho_exhaust*V_dot_a*convert(CFM, m3/s)
135:
136: "calculated mass of water removed from clothing using air stream conditions before and after the drum"
137: m_w_CD_rmv = m_dot_a*(Omega_exhaust - Omega_inlet)*delta_t
138: V_w_CD_rmv = m_w_CD_rmv*Volume(Water, T=T_exhaust_db, x=0)[-]*convert(m3, gal)
139: CALL Wet_Clothes(T_exhaust_db, m_w_clothing_0, m_w_CD_rmv, m_w_clothing_initial, m_w_clothing_u, w_clothing_initial,
  s_w_clothing_initial)
140:
141: "storage tank of water to be preheated by waste heat recovery heat exchanger"
142: [V_w_tank = 30 [gal]]
143:
144: "water conditions for the waste heat recovery heat exchanger"
145: T_main = 15 [C]
146: V_dot_w = 0.50 [GPM]
147:
148: T_w_i = T_w_tank
149: rho_w_i = Density(Water, T=T_w_i, x=0[-])
150: m_dot_w = rho_w_i*V_dot_w*convert(GPM, m3/s)
151: h_w_i = Enthalpy(Water, T=T_w_i, x=0[-])
152: s_w_i = Entropy(Water, T=T_w_i, x=0[-])
153: e_w_i = (h_w_i - h_w_0) - T_w_0*K*(s_w_i - s_w_0)
154:
155: "air side parameters needed for the waste heat recovery heat exchanger"
156: T_a_i = T_exhaust_db
157: T_a_i_dp = T_exhaust_dp
158: Omega_a_i = Omega_exhaust
159: h_a_i = h_exhaust
160: h_s_o = Enthalpy(AirH2O, T=T_w_i, r=1[-], P=P_atm) "saturation enthalpy of air at inlet cold side temperature"
161: h_d_o = Enthalpy(AirH2O, T=T_w_i, w=Omega_a_i, P=P_atm) "enthalpy of air at inlet cold side temperature"
162:
163: "heat exchanger properties"
164: epsilon_HX = 0.8 [-]
165:
166: "outlet conditions of the waste heat recovery heat exchanger"
167: Q_dot_hx_max_wet = m_dot_a*(h_a_i - h_s_o) {wet coil analysis}
168: Q_dot_hx_max_dry = m_dot_a*(h_a_i - h_d_o) {dry coil analysis}
169: wet_coil = IF(T_w_i, T_a_i_dp, 1[-], 0[-], 0[-]) {check cold water inlet with inlet air dew point if coil is wet}
170: Q_dot_hx_max = wet_coil*Q_dot_hx_max_wet + (1-wet_coil)*Q_dot_hx_max_dry
171: Q_dot_hx = epsilon_HX*Q_dot_hx_max
172: Q_hx = Q_dot_hx*delta_t
173:
174: h_a_o = h_a_i - Q_dot_hx/m_dot_a
175: T_a_o = wet_coil*Temperature(AirH2O, h=h_a_o, r=1[-], P=P_atm) + (1-wet_coil)*Temperature(AirH2O, h=h_a_o, w

```

```

=Omega_a_i,P=P_atm)
176: s_a_o = wet_coil*Entropy(AirH2O,h=h_a_o,r=1[-],P=P_atm) + (1-wet_coil)*Entropy(AirH2O,h=h_a_o,w=Omega_a_i,P
=P_atm)
177: e_a_o = (h_a_o - h_a_0) - T_a_0_K*(s_a_o - s_a_0)
178:
179: h_w_o = h_w_i + Q_dot_hx/m_dot_w
180: T_w_o = Temperature(Water,h=h_w_o,x=0[-])
181: s_w_o = Entropy(Water,h=h_w_o,x=0[-])
182: e_w_o = (h_w_o - h_w_0) - T_w_0_K*(s_w_o - s_w_0)
183:
184: CALL Tank(delta_t, V_w_tank, T_main, V_dot_w, T_w_o:T_w_tank, u_w_tank)
185:
186: "Exergy analysis"
187:
188: "attempts to quantify the loss of energy during one clothes drying cycle"
189: Q_CD_org_loss = (W_dot_heater + m_dot_a*h_ambient - m_dot_a*h_exhaust)*delta_t + m_w_clothing_initial
*u_w_clothing_initial - m_w_clothing*u_w_clothing
190: "maximum amount of heat available"
191: Q_CD_org_max = W_dot_heater*delta_t - Q_clothing_req
192: {only consider the air side of the dryer when adding the HX}
193: Q_CD_hx_loss = (m_dot_a*h_exhaust - m_dot_a*h_a_o + m_dot_w*h_w_i - m_dot_w*h_w_o)*delta_t
194:
195: "entropy production during standard drying cycle"
196: sigma_CD_org_tot = (m_dot_a*s_exhaust - m_dot_a*s_ambient)*delta_t + Q_CD_org_loss/T_a_0_K + m_w_clothing
*s_w_clothing - m_w_clothing_initial*s_w_clothing_initial
197:
198: "energy recovery from waste HX"
199: eta_CD_HX = Q_hx/Q_heater

```

## B.2 Refrigerator-Freezer

File:Refrigerator\_v2.EES

12/9/2017 3:02:41 AM Page 1

EES Ver. 10.268: #3945: For use only by students and faculty, Purdue University Campus, West Lafayette, IN

```

1: PROCEDURE Tank(delta_t,V_w_tank,T_start,V_dot_w,T_w_return:T_w_tank, u_w_tank)
2:
3: IF(TABLERUN# = 1) THEN
4:   T_w_tank_initial = T_start
5:   u_w_tank_initial = IntEnergy(Water,T=T_start,x=0[-])
6:   rho_w_tank_initial = Density(Water,T=T_start,x=0[-])
7:   T_w_tank = T_w_tank_initial
8:   u_w_tank = u_w_tank_initial
9:
10: ELSE
11:   u_w_tank_initial = TABLEVALUE('Table 1',TABLERUN# - 1, 'u_w_tank')
12:   rho_w_tank_initial = Density(Water,u=u_w_tank_initial,x=0[-])
13:   T_w_tank_initial = Temperature(Water,u=u_w_tank_initial,x=0[-])
14:   h_w_i = Enthalpy(Water,u=u_w_tank_initial,x=0[-])
15:
16:   h_w_o = Enthalpy(Water,T=T_w_return,x=0[-])
17:
18:   Q_dot_hx = V_dot_w*rho_w_tank_initial*(h_w_o - h_w_i)*convert(GPM,m3/s)
19:
20:   u_w_tank = ((Q_dot_hx*delta_t) + V_w_tank*rho_w_tank_initial*convert(gal,m3)*u_w_tank_initial)/(V_w_tank
   *rho_w_tank_initial*convert(gal,m3))
21:   T_w_tank = Temperature(Water,u=u_w_tank,x=0[-])
22:
23: ENDIF
24:
25: END {Tank}
26:
27: P_atm = 101.325 [kPa]
28: T_amb_C = ConvertTemp('F','C',T_amb) {Convert ambient temperature in F to C}
29: T_cab_C = ConvertTemp('F','C',T_cab) {Convert cabinet temperature in F to C}
30: T_water_C = ConvertTemp('F','C',T_water) {Convert water temperature in F to C}
31:
32: T_c_in = T_water_C*f_w + T_amb_C*(1-f_w) {inlet temperature of the condenser depends if water cooling is enabled}
33: T_e_in = T_cab_C
34:
35: t_m = t*convert(sec,min)
36:
37: "water properties of heat sink for condenser"
38: rho_w = Density(Water,T=T_water_C,x=0 [-])
39: cp_w = Cp(Water,T=T_water_C,x=0 [-])
40: V_dot_water = V_dot_w_GPM*convert(gal/min,m3/s)
41: m_dot_w = rho_w*V_dot_water
42: h_w_c_in = Enthalpy(Water,T=T_water_C,x=0[-]) {enthalpy of water entering the condenser for cooling}
43: h_w_c_surface = Enthalpy(Water,T=T_cond,x=0[-])
44:
45: "air properties of heat sink for condenser"
46: omega_amb = HumRat(AirH2O,T= 21[C],r=0.95 [-],P=P_atm) {assume the humidity ratio is unchanged from baseline
   conditions}
47: rho_a = Density(AirH2O,T=T_amb_C,w=omega_amb,P=P_atm) {density of inlet air to the condenser for cooling}
48: cp_a = Cp(AirH2O,T=T_amb_C,w=omega_amb,P=P_atm)
49: V_dot_air_CFM = 60 [ft3/min]
50: W_dot_fan_cond = 0.005 [kW] {need to verify fan power}
51: m_dot_a = rho_a*V_dot_air_CFM*convert(ft3/min, m3/s)
52: h_a_c_in = Enthalpy(AirH2O,T=T_amb_C,w=omega_amb,P=P_atm) {condenser air inlet enthalpy}
53: h_a_c_surface = Enthalpy(AirH2O,T=T_cond,w=omega_amb,P=P_atm)
54:
55: h_c_surface = h_w_c_surface*f_w + h_a_c_surface*(1-f_w)
56: h_c_in = h_w_c_in*f_w + h_a_c_in*(1-f_w) {inlet enthalpy of cooling stream to the condenser}
57: cp_c = cp_w*f_w + cp_a*(1-f_w)
58: m_dot_c = m_dot_w*f_w + m_dot_a*(1-f_w) {supply flow rate of cooling stream for the condenser}
59:

```

```

60: "air properties of heat source for evaporator"
61: omega_cab = HumRat(AirH2O,T=T_cab_C,r=0.95 [-],P=P_atm) (assume the air humidity ratio is at saturation inside
    refrigerator cabinet)
62: rho_a_evap = Density(AirH2O,T=T_cab_C,w=omega_cab,P=P_atm) (density of inlet air to the evaporator for heating)
63: cp_e = Cp(AirH2O,T=T_cab_C,w=omega_cab,P=P_atm)
64: V_dot_air_evap_CFM = 45 [ft3/min]
65: W_dot_fan_evap = 0.005 [kW] (need to verify fan power)
66: m_dot_e = rho_a_evap*V_dot_air_evap_CFM*convert(ft3/min, m3/s)
67: h_e_in = Enthalpy(AirH2O,T=T_cab_C,w=omega_cab,P=P_atm) (evaporator air inlet enthalpy)
68: h_e_surface = Enthalpy(AirH2O,T=T_evap,w=omega_cab,P=P_atm)
69:
70: "-----"
71:
72: "compressor operation"
73: T_suc = Temperature(R134a,P=P_evap,h=h_suc)
74: s_suc = Entropy(R134a,P=P_evap,h=h_suc)
75: rho_suc = Density(R134a,P=P_evap,h=h_suc)
76:
77: eta_comp_vol = 0.95 [-]
78: V_comp_disp = 5.56 [mL/rev]
79: N_dot_comp = 3500 [rev/min]
80: Q_dot_loss_comp = 0.2*W_dot_comp
81:
82: m_dot_r = rho_suc*eta_comp_vol*N_dot_comp*convert(1/min,1/sec)*V_comp_disp*convert(mL,m3) (compressor
    volumetric efficiency provides the flow rate)
83:
84: eta_comp_isen = 0.80 [-]
85:
86: h_disch_isen = Enthalpy(R134a,P=P_cond,s=s_suc)
87: h_disch = h_suc + ((h_disch_isen - h_suc)/eta_comp_isen)
88: T_disch = Temperature(R134a,P=P_cond,h=h_disch) (compressor discharge refrigerant temperature)
89:
90: W_dot_comp = m_dot_r*(h_disch - h_suc) - Q_dot_loss_comp (compressor isentropic efficiency and heat loss determine
    power input required by compressor)
91:
92: "condenser operation"
93: T_cond = 40 [C]
94: P_cond = Pressure(R134a,T=T_cond,x=0.5[-])
95:
96: T_r_cond_in = T_disch (inlet condenser refrigerant temperature equal to compressor discharge temperature)
97:
98: epsilon_cond = 0.8 [-] (only expect to need one HX property, either effectiveness percentage or pinch point delta T)
99: {delta_T_cond = 5 [C]}
100: {Q_dot_cond = m_dot_r*(h_disch - h_r_c_out)*epsilon_cond (HX efficiency reduces the maximum amount of heat transfer
    possible)}
101: {h_r_cond_out = h_r_cond_in - Q_dot_cond/m_dot_r (determine exit enthalpy of refrigerant leaving condenser from actual
    heat transfer occurring)}
102: Q_dot_cond = m_dot_c*(h_c_surface - h_c_in)*epsilon_cond
103: h_r_cond_out = h_disch - (Q_dot_cond/m_dot_r) (determine exit enthalpy of refrigerant leaving condenser from actual
    heat transfer occurring)
104: T_r_cond_out = Temperature(R134a,P=P_cond,h=h_r_cond_out) (refrigerant temperature at the outlet of the condenser)
105: Q_dot_cond = m_dot_c*(h_c_out - h_c_in)
106: T_c_out = IF(f_w,0,0, Temperature(AirH2O,h=h_c_out,w=omega_amb,P=P_atm), Temperature(Water,h=h_c_out,x=0[-]))
107: delta_T_cond = T_cond - T_c_out
108: T_sub = 1 [C]
109: T_sub = T_cond - T_r_cond_out
110:
111: "heat exchange on heat loop"
112: h_heat_loop_in = h_r_cond_out (inlet to heat loop is connected to outlet of condenser)
113: delta_T_heat_loop = 1 [C] (expected amount of temperature drop during heat transfer in the heat loop that runs the perimeter

```

```

of the cabinet doors)
114: T_heat_loop_out = T_r_cond_out - deltaT_heat_loop (calculates the outlet temperature of the heat loop before entering the
suction line HX)
115: h_heat_loop_out = Enthalpy(R134a,T=T_heat_loop_out,P=P_cond)
116: Q_dot_heat_loop = m_dot_r*(h_heat_loop_in - h_heat_loop_out)
117:
118: "suction line heat exchanger - attempt to capture heat transfer occuring during expansion process
119: counter flow heat exchanger - inlet streams are h_heat_loop_out and h_r_evap_out, outlet streams are h_r_evap_in and
h_suc"
120: h_slhx_in = h_heat_loop_out
121: T_slhx_in = T_heat_loop_out
122: epsilon_slhx = 0.2 [-]
123:
124: h_slhx_out_max = Enthalpy(R134a,T=T_r_evap_out,P=P_cond)
125: Q_dot_slhx = m_dot_r*(h_slhx_in - h_slhx_out_max)*epsilon_slhx (percentage of maximum heat transfer available by
cooling hot inlet to cold inlet)
126: Q_dot_slhx = m_dot_r*(h_suc - h_r_evap_out)
127: Q_dot_slhx = m_dot_r*(h_slhx_in - h_slhx_out)
128: T_slhx_out = Temperature(R134a,h=h_slhx_out,P=P_cond)
129:
130: T_sup = 5 [C]
131: T_sup = T_r_evap_out - T_evap
132:
133: "expansion valve - assume isenthalpic expansion after suction line HX"
134: h_r_evap_in = h_slhx_out
135:
136: "evaporator operation"
137: T_evap = -30 [C]
138: P_evap = Pressure(R134a,T=T_evap,x=0.5[-])
139:
140: epsilon_evap = 0.8 [-] (only expect to need one HX efficiency property, either HX effectiveness or pinch point deltaT)
141: (deltaT_evap = 10 [C])
142: (Q_dot_evap = m_dot_r*(h_r_e_out - h_r_evap_in)*epsilon_evap (HX efficiency reduces the maximum amount of heat
transfer possible))
143: Q_dot_evap = m_dot_e*(h_e_in - h_e_surface)*epsilon_evap
144: h_r_evap_out = h_r_evap_in + (Q_dot_evap/m_dot_r)
145: T_r_evap_out = Temperature(R134a,P=P_evap,h=h_r_evap_out) (refrigerant temperature at the outlet of the evaporator)
146:
147: Q_dot_evap = m_dot_e*(h_e_in - h_e_out)
148: (h_e_out = Enthalpy(AirH2O,T=T_e_out,w=omega_cab,P=P_atm))
149: T_e_out = Temperature(AirH2O,h=h_e_out,w=omega_cab,P=P_atm)
150: delta_T_evap = T_e_out - T_evap (calculate pinch point of condenser when using the effectiveness-HX method)
151:
152: "total fan power"
153: W_dot_fan = W_dot_fan_evap + W_dot_fan_cond*(1-f_w) + W_dot_water*f_w
154:
155: T_L = convertTemp('C','K',T_cab_C)
156: T_H_a = convertTemp('C','K',T_amb_C)
157: T_H_w = convertTemp('C','K',T_w_tank)
158: COP_cooling = (Q_dot_evap-W_dot_fan_evap)/(W_dot_comp + W_dot_fan)
159: COP_c_cooling = (T_L/(T_H_w - T_L))*f_w + (T_L/(T_H_a - T_L))*(1 - f_w)
160: eta_2nd_cooling = COP_cooling/COP_c_cooling
161: COP_heating = Q_dot_cond/(W_dot_comp + W_dot_fan)
162: COP_c_heating = (T_H_w/(T_H_w - T_L))*f_w + (T_H_a/(T_H_a - T_L))*(1 - f_w)
163: eta_2nd_heating = COP_heating/COP_c_heating
164:
165: CALL Tank(delta_t, V_w_tank, T_main, V_dot_w_GPM, T_c_out:T_w_tank, u_w_tank)
166:
167: T_cab = 5 [F]
168: T_amb = 90 [F]

```

```

1: PROCEDURE Tank(delta_t,V_w_tank,T_start,V_dot_w,T_w_return:T_w_tank,u_w_tank)
2:
3: IF(TABLERUN# = 1) THEN
4:   T_w_tank_initial = T_start
5:   u_w_tank_initial = IntEnergy(Water,T=T_start,x=0[-])
6:   rho_w_tank_initial = Density(Water,T=T_start,x=0[-])
7:   T_w_tank = T_w_tank_initial
8:   u_w_tank = u_w_tank_initial
9:
10: ELSE
11:   u_w_tank_initial = TABLEVALUE('Table 1',TABLERUN# - 1, 'u_w_tank')
12:   rho_w_tank_initial = Density(Water,u=u_w_tank_initial,x=0[-])
13:   T_w_tank_initial = Temperature(Water,u=u_w_tank_initial,x=0[-])
14:   h_w_i = Enthalpy(Water,u=u_w_tank_initial,x=0[-])
15:
16:   h_w_o = Enthalpy(Water,T=T_w_return,x=0[-])
17:
18:   Q_dot_hx = V_dot_w*rho_w_tank_initial*(h_w_o - h_w_i)*convert(GPM,m3/s)
19:
20:   u_w_tank = ((Q_dot_hx*delta_t) + V_w_tank*rho_w_tank_initial*convert(gal,m3)*u_w_tank_initial)/(V_w_tank
   rho_w_tank_initial*convert(gal,m3))
21:   T_w_tank = Temperature(Water,u=u_w_tank,x=0[-])
22:
23: ENDIF
24:
25: END {Tank}
26:
27: P_atm = 101.325 [kPa]
28: T_amb_C = ConvertTemp('F','C',T_amb) {Convert ambient temperature in F to C}
29: T_cab_C = ConvertTemp('F','C',T_cab) {Convert cabinet temperature in F to C}
30: T_water_C = ConvertTemp('F','C',T_water) {Convert water temperature in F to C}
31:
32: T_c_in = T_water_C*f_w + T_amb_C*(1-f_w) {inlet temperature of the condenser depends if water cooling is enabled}
33: T_e_in = T_cab_C
34:
35: t_m = t*convert(sec,min)
36:
37: "water properties of heat sink for condenser"
38: rho_w = Density(Water,T=T_water_C,x=0 [-])
39: cp_w = Cp(Water,T=T_water_C,x=0 [-])
40: V_dot_water = V_dot_w_GPM*convert(gal/min,m3/s)
41: m_dot_w = rho_w*V_dot_water
42: h_w_c_in = Enthalpy(Water,T=T_water_C,x=0[-]) {enthalpy of water entering the condenser for cooling}
43: h_w_c_surface = Enthalpy(Water,T=T_cond,x=0[-])
44:
45: "air properties of heat sink for condenser"
46: omega_amb = HumRat(AirH2O,T= 21[C],r=0.95 [-],P=P_atm) {assume the humidity ratio is unchanged from baseline
   conditions}
47: rho_a = Density(AirH2O,T=T_amb_C,w=omega_amb,P=P_atm) {density of inlet air to the condenser for cooling}
48: cp_a = Cp(AirH2O,T=T_amb_C,w=omega_amb,P=P_atm)
49: V_dot_air_CFM = 80 [ft3/min]
50: W_dot_fan_cond = 0.005 [kW] {need to verify fan power}
51: m_dot_a = rho_a*V_dot_air_CFM*convert(ft3/min, m3/s)
52: h_a_c_in = Enthalpy(AirH2O,T=T_amb_C,w=omega_amb,P=P_atm) {condenser air inlet enthalpy}
53: h_a_c_surface = Enthalpy(AirH2O,T=T_cond,w=omega_amb,P=P_atm)
54:
55: h_c_surface = h_w_c_surface*f_w + h_a_c_surface*(1-f_w)
56: h_c_in = h_w_c_in*f_w + h_a_c_in*(1-f_w) {inlet enthalpy of cooling stream to the condenser}
57: cp_c = cp_w*f_w + cp_a*(1-f_w)
58: m_dot_c = m_dot_w*f_w + m_dot_a*(1-f_w) {supply flow rate of cooling stream for the condenser}
59:

```

### B.3 Bulk Heat Appliances

File: Bulk\_energy\_analysis.EES

12/9/2017 3:03:54 AM Page 1

EES Ver. 10.268: #3945: For use only by students and faculty, Purdue University Campus, West Lafayette, IN

```

1: T_main = 55 [F]
2: T_main_C = convertTemp('F','C',T_main)
3: rho_main = Density(Water,T=T_main_C,x=0[-])
4: u_main = IntEnergy(Water,T=T_main_C,x=0[-])
5: h_main = Enthalpy(Water,T=T_main_C,x=0[-])
6: {V_tank_gal = 5 [gal]}
7: V_tank_liter = V_tank_gal*convert(gal,liter)
8: V_tank_CW_gal = V_tank_gal
9: V_tank_DW_gal = V_tank_gal
10: V_tank_CO_gal = V_tank_gal
11:
12:
13: V_tank_CW = V_tank_CW_gal*convert(gal,m3)
14: m_tank_CW = rho_main*V_tank_CW
15:
16: T_drain_CW = 36 [C]
17: V_drain_CW_liter = 155 [liter]
18:
19: V_drain_CW = V_drain_CW_liter*convert(liter,m3)
20: V_drain_CW_gal = V_drain_CW_liter*convert(liter,gal)
21: m_drain_CW = rho_drain_CW*V_drain_CW
22:
23: rho_drain_CW = Density(Water,T=T_drain_CW,x=0[-])
24: h_drain_CW = Enthalpy(Water,T=T_drain_CW,x=0[-])
25:
26: u_final_CW = (m_drain_CW*h_drain_CW + m_tank_CW*u_main)/(m_drain_CW + m_tank_CW)
27: T_final_CW = Temperature(Water,u=u_final_CW,x=0[-])
28: T_final_CW_F = convertTemp('C','F',T_final_CW)
29:
30: Q_recov_CW = m_tank_CW*(u_final_CW - u_main)
31: W_cycle_CW_low = 0.43 [kWh]
32: per_recov_CW_low = Q_recov_CW/(W_cycle_CW_low*convert(kWh,kJ))
33: W_cycle_CW_high = 2.26 [kWh] {includes water heating energy}
34: per_recov_CW_high = Q_recov_CW/(W_cycle_CW_high*convert(kWh,kJ))
35:
36: n_cycl_CW = 289 [cycle]
37:
38:
39:
40:
41: V_tank_DW = V_tank_DW_gal*convert(gal,m3)
42: m_tank_DW = rho_main*V_tank_DW
43:
44: T_drain_DW = 40 [C]
45: V_drain_DW_liter = 13.2 [liter]
46:
47: V_drain_DW = V_drain_DW_liter*convert(liter,m3)
48: V_drain_DW_gal = V_drain_DW_liter*convert(liter,gal)
49: m_drain_DW = rho_drain_DW*V_drain_DW
50:
51: rho_drain_DW = Density(Water,T=T_drain_DW,x=0[-])
52: h_drain_DW = Enthalpy(Water,T=T_drain_DW,x=0[-])
53:
54: u_final_DW = (m_drain_DW*h_drain_DW + m_tank_DW*u_main)/(m_drain_DW + m_tank_DW)
55: T_final_DW = Temperature(Water,u=u_final_DW,x=0[-])
56: T_final_DW_F = convertTemp('C','F',T_final_DW)
57:
58: Q_recov_DW = m_tank_DW*(u_final_DW - u_main)
59: n_cycl_DW = 215 [cycle]
60: W_cycle_DW = 1.26 [kWh]
61: per_recov_DW = Q_recov_DW/(W_cycle_DW*convert(kWh,kJ))

```

```
62:
63:
64:
65: V_tank_CO = V_tank_CO_gal*convert(gal,m3)
66: m_tank_CO = rho_main*V_tank_CO
67:
68: T_CO = 400 [F] {assumed cooking oven temperature}
69: T_CO_C = convertTemp('F','C',T_CO)
70: V_drain_CO_liter = 13.2 [liter]
71:
72: m_CO = 80 [kg]
73: u_CO = IntEnergy(Carbon_steel, T=T_CO_C)
74:
75: m_tank_CO*u_tank_final_CO + m_CO*u_final_CO = m_tank_CO*h_main + m_CO*u_CO
76:
77: u_final_CO = IntEnergy(Carbon_steel, T=T_final_CO)
78: T_final_CO = Temperature(Water,u=u_tank_final_CO,x=0[-])
79: T_final_CO_F = convertTemp('C','F',T_final_CO)
80:
81: Q_recov_CO = m_tank_CO*(u_tank_final_CO - u_main)
82: n_cycl_CO = 215 [cycle]
83: W_cycle_CO = 4.27 [kWh]
84: per_recov_CO = Q_recov_CO/(W_cycle_CO*convert(kWh,kJ))
```

## APPENDIX C – CUSTOM MODELICA COMPONENTS

To build the required functionality into each appliance Modelica model, cycle controllers are designed and programmed for the RF, DW, and CD. In the following sections, the specific details on the various Modelica codes created are provided in greater detail to clarify the exact approach used.

### C.1 CD Cycle Controller

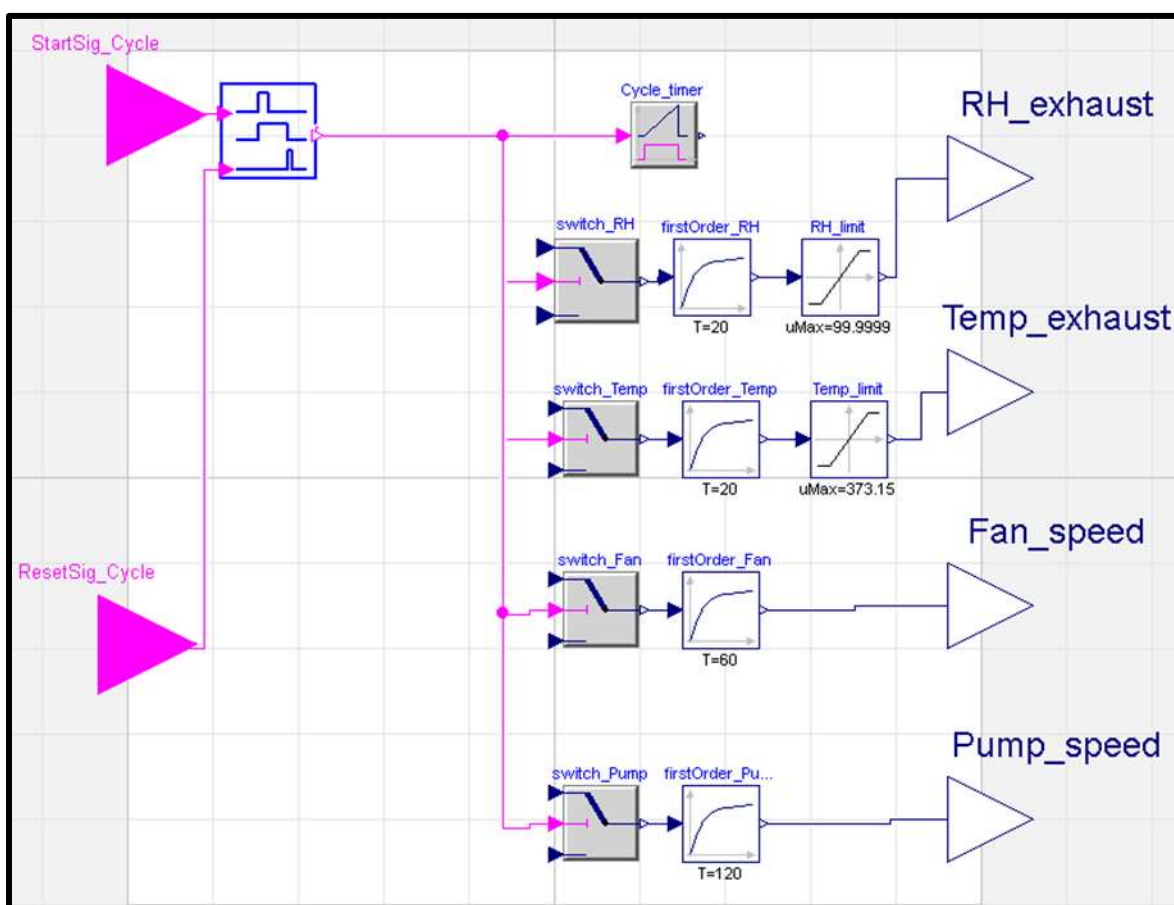


Figure 107: Diagram View of CD Cycle Controller

```

model HighHeatCD_Ctrl "High heat load for clothes dryer controller "

parameter TILMedia.Internals.Units.RelativeHumidity RH_exhaust_OFF = 20;
TILMedia.Internals.Units.RelativeHumidity RH_exhaust_ON;

parameter Modelica.SIunits.Temperature T_exhaust_OFF = 293.15;
Modelica.SIunits.Temperature T_exhaust_ON;

Modelica.SIunits.VolumeFlowRate V_fan_OFF = 1E-10;
parameter Modelica.SIunits.VolumeFlowRate V_fan_ON = 18878E-5;

Modelica.SIunits.VolumeFlowRate V_pump_OFF = 1E-10;
parameter Modelica.SIunits.VolumeFlowRate V_pump_ON = 1E-4;

equation

RH_exhaust_ON = -5.50527E-18*Cycle_timer.y^6 + 6.14881E-14*Cycle_timer.y^5
T_exhaust_ON = - 2.52015E-12*Cycle_timer.y^4 + 1.98456E-8*Cycle_timer.y^3

switch_RH.u3 = RH_exhaust_OFF;
switch_RH.u1 = RH_exhaust_ON;

switch_Temp.u3 = T_exhaust_OFF;
switch_Temp.u1 = T_exhaust_ON;

switch_Fan.u3 = V_fan_OFF;
switch_Fan.u1 = V_fan_ON;

switch_Pump.u3 = V_pump_OFF;
switch_Pump.u1 = V_pump_ON;

end HighHeatCD_Ctrl;

```

Figure 108: Modelica Code for CD Cycle Controller

## C.2 RF Compressor Capacity Controller

The internal features of the capacity controller used for the RF compressor is shown in Figure 109. From the diagram, it can be noticed many of the components have missing inputs needed. This provides a good example of when the graphical approach to building Modelica models breaks down. Modelica code has to be manually entered instead of relying on the auto-generated code from the diagram view to provide more details to the solver on how to handle the different conditions. The completed code is copied from the Dymola environment and displayed in Figure 110.

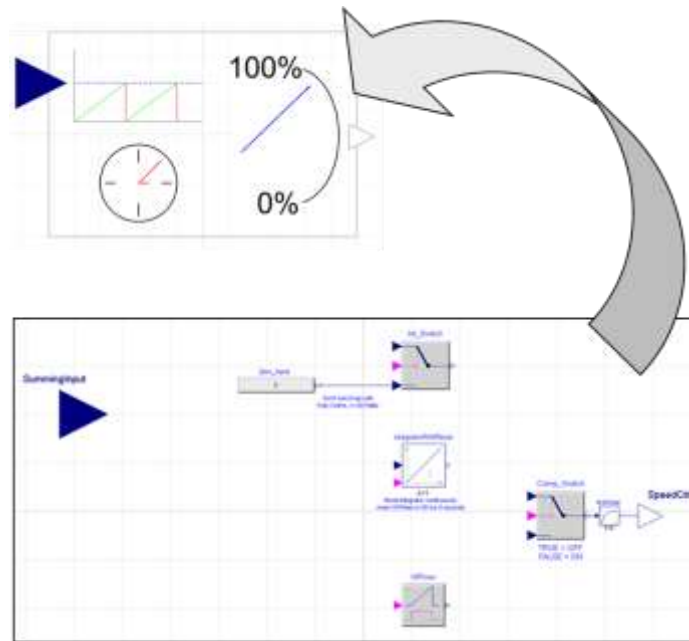


Figure 109: Diagram View of RF Capacity Controller Components



```

model CapacityCtrl_Input
  "Monitor HX capacity to execute control output "
  Boolean IntON(start = true, fixed = false) " start with compressor ON";
  Boolean IntReset(start = true, fixed = false) " start with compressor ON";
  Boolean OffTimer_CTRL(start = false, fixed = false);
  Boolean EvapOFF(start = false, fixed = false);
  parameter Modelica.SIunits.Frequency Zero_Speed(start=0.001) = 0.001 "Off Speed";
  parameter Modelica.SIunits.Frequency Full_Speed(start=60) = 60 "Full Speed";
  parameter Modelica.SIunits.Energy EvapCoolingOffThreshold(start=1000) = 1000 "W-s";
  parameter Modelica.SIunits.Time OffTimerThreshold(start=500) = 500 "seconds";
  parameter Modelica.SIunits.Power EvapCoolingOnThreshold(start = 2) = 2 "Watts";

  //Modelica.Blocks.Sources.RealExpression EvapCoolingOffThreshold(y = 1000) "W-s";
  //Modelica.Blocks.Sources.RealExpression OffTimerThreshold(y = 500) "seconds";

equation
  Comp_Switch.u1 = Zero_Speed;
  Comp_Switch.u3 = Full_Speed;
  Int_Switch.u1 = SummingInput;

  IntON = SummingInput > EvapCoolingOnThreshold;

  integratorWithReset.u = Int_Switch.y;

  EvapOFF = EvapCoolingOffThreshold < integratorWithReset.y;

  OffTimer_CTRL = OffTimer.y > OffTimerThreshold;

  IntReset = OffTimer.y > 5 and OffTimer.y < 10;
algorithm
  //Sum Evaporator cooling capacity
  //when the evaporator has reached expected cooling capacity, Watts
  when pre(IntON) then
    integratorWithReset.reset :=false;
  end when;
  when pre(IntON) then
    Int_Switch.u2 :=true "Evap.summary.Q_flow_vle";
  elseif not pre(IntON) then
    Int_Switch.u2 :=false "zero watts capacity - EvapOFF";
  end when;

  //Reset the integrator - zero out the total Evap cooling capacity
  //when the OffTimer has been on for 5 seconds and less than 10
  when pre(IntReset) then
    integratorWithReset.reset :=true;
  end when;

  //Turn OFF the OffTimer when compressor is ON
  when pre(OffTimer_CTRL) then
    OffTimer.u :=false;
  end when;

  //Turn ON the OffTimer to record the amount of time compressor is OFF
  when pre(Comp_Switch.u2) then
    OffTimer.u := true;
  end when;

  //Turn ON the compressor when the elapsed OFF time has passed
  when pre(OffTimer_CTRL) then
    Comp_Switch.u2 :=false "compressor turns ON";
  end when;

  //Turn OFF the compressor when the integrated amount is surpassed
  when pre(EvapOFF) then
    Comp_Switch.u2 := true "compressor OFF";
  end when;

```

Figure 110: Modelica Code for RF Capacity Controller

### C.3 DW Cycle and Step Controllers

The details for the major step controllers and the assembly of the overall cycle controller are presented below.

#### C.3.1 Wash Step Controller

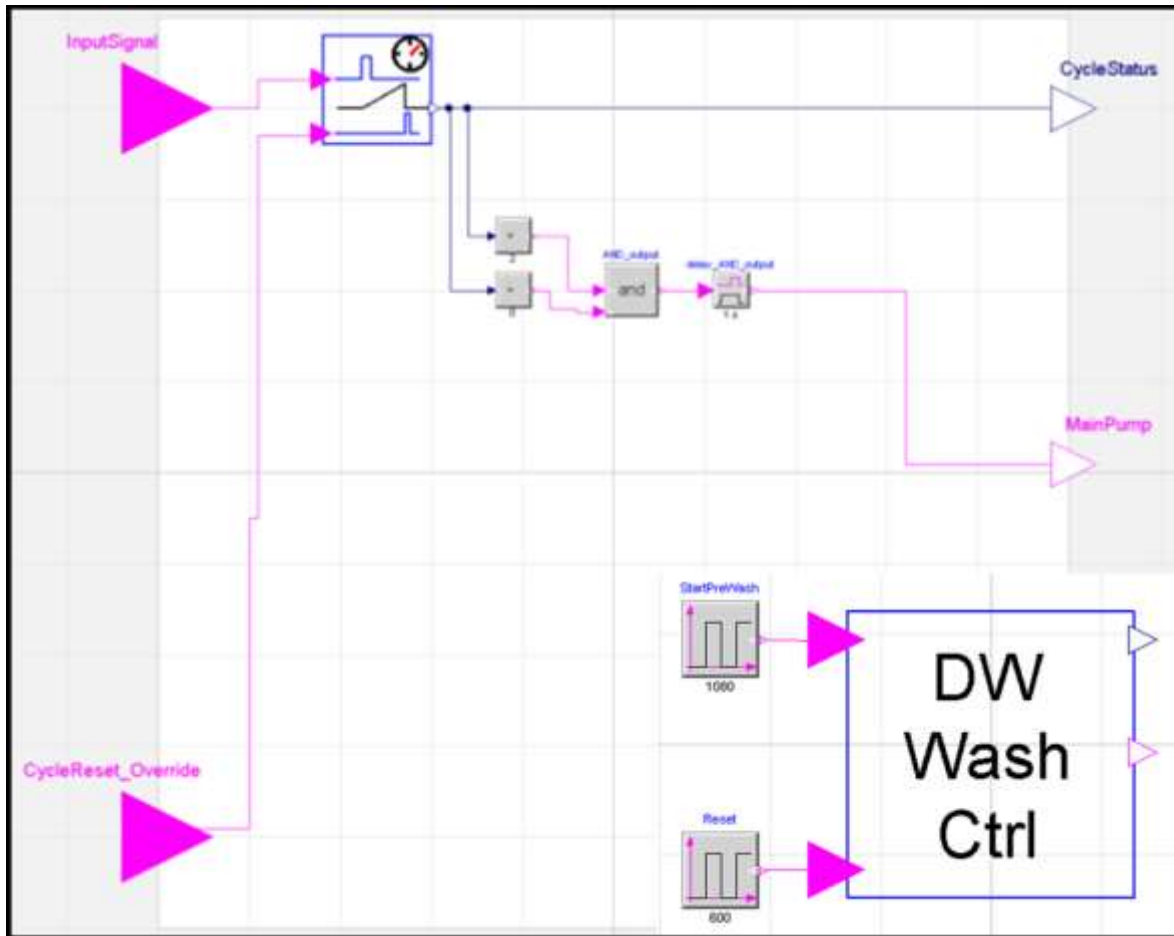


Figure 111: DW Modelica Diagram of Wash Step Controller

### C.3.2 Heat Step Controller

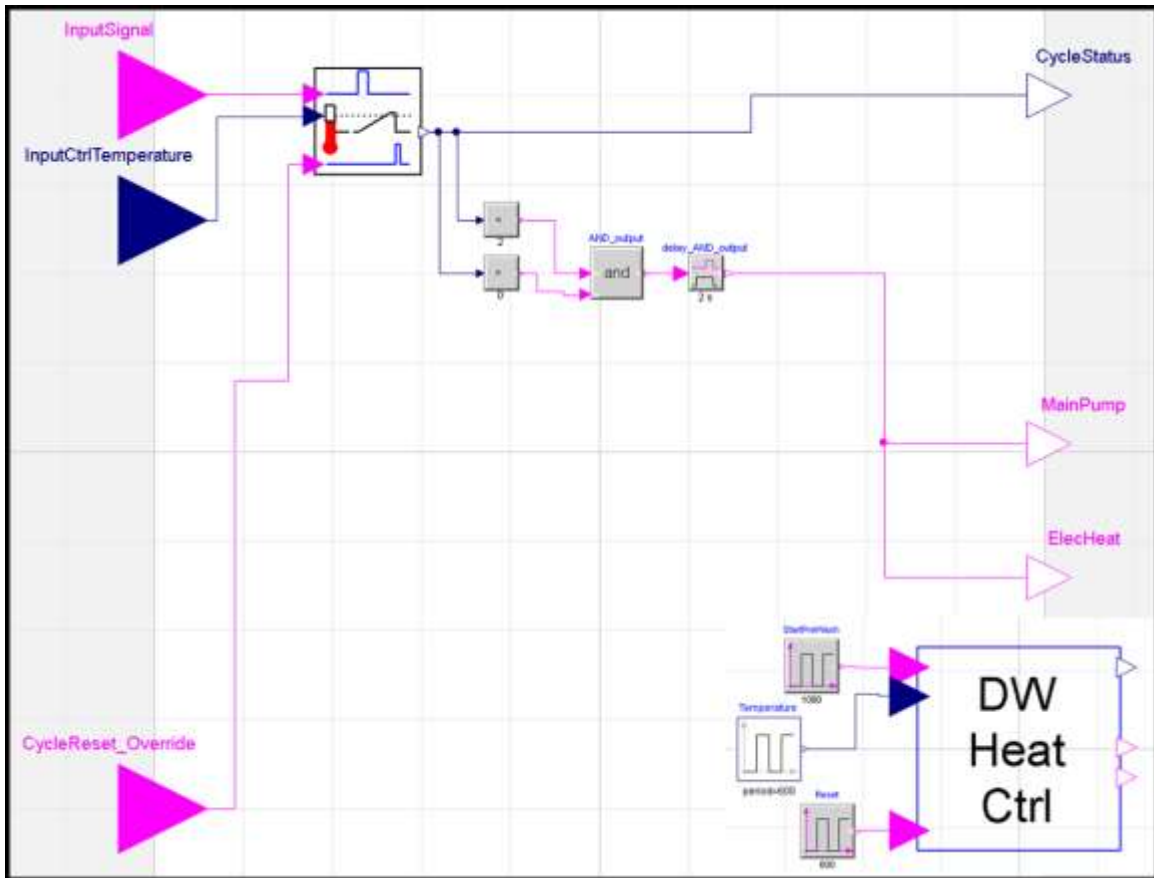


Figure 112: DW Modelica Diagram of Heat Step Controller

### C.3.3 Overall Cycle Controller

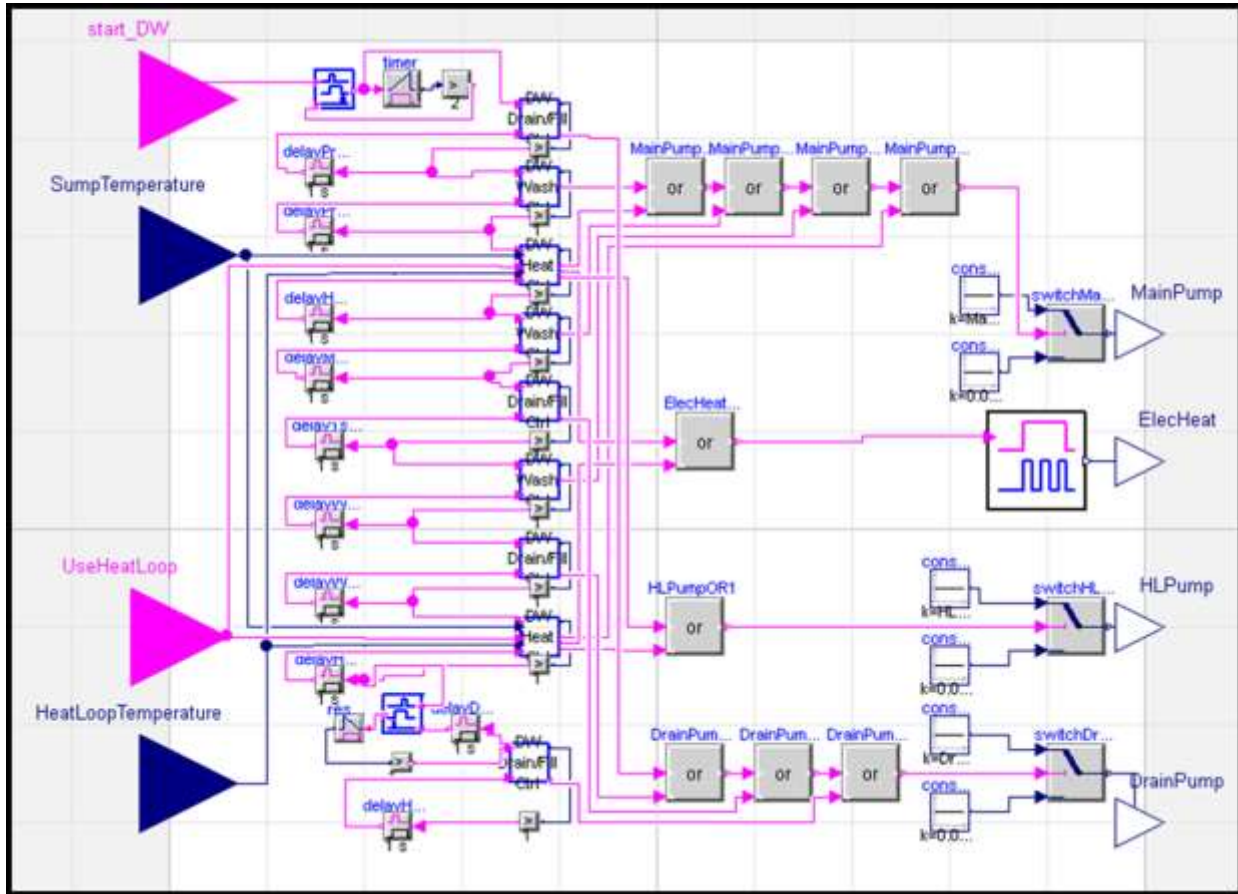


Figure 113: DW Modelica Diagram of Overall DW Cycle Controller

## APPENDIX D – TIL LIBRARY MODELICA COMPONENT DESCRIPTIONS

### D.1 SIM Component

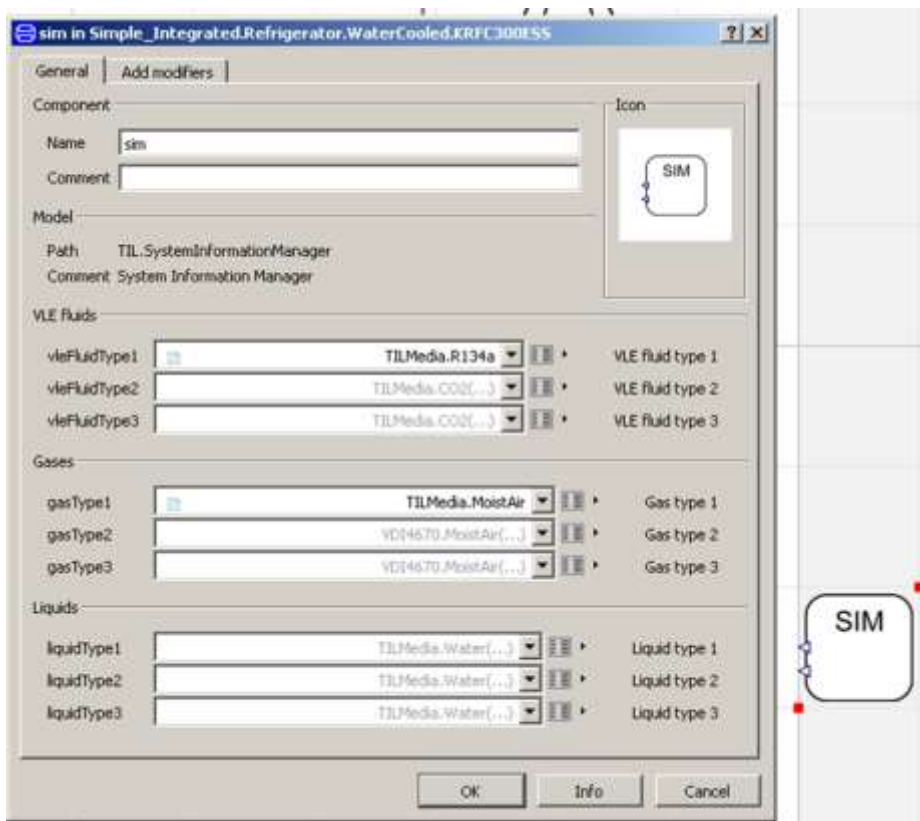


Figure 114: TIL SIM Component for Selecting the Refrigerant (VLE), Gas, and, Liquid Types

## D.2 Flat-plate Heat Exchanger

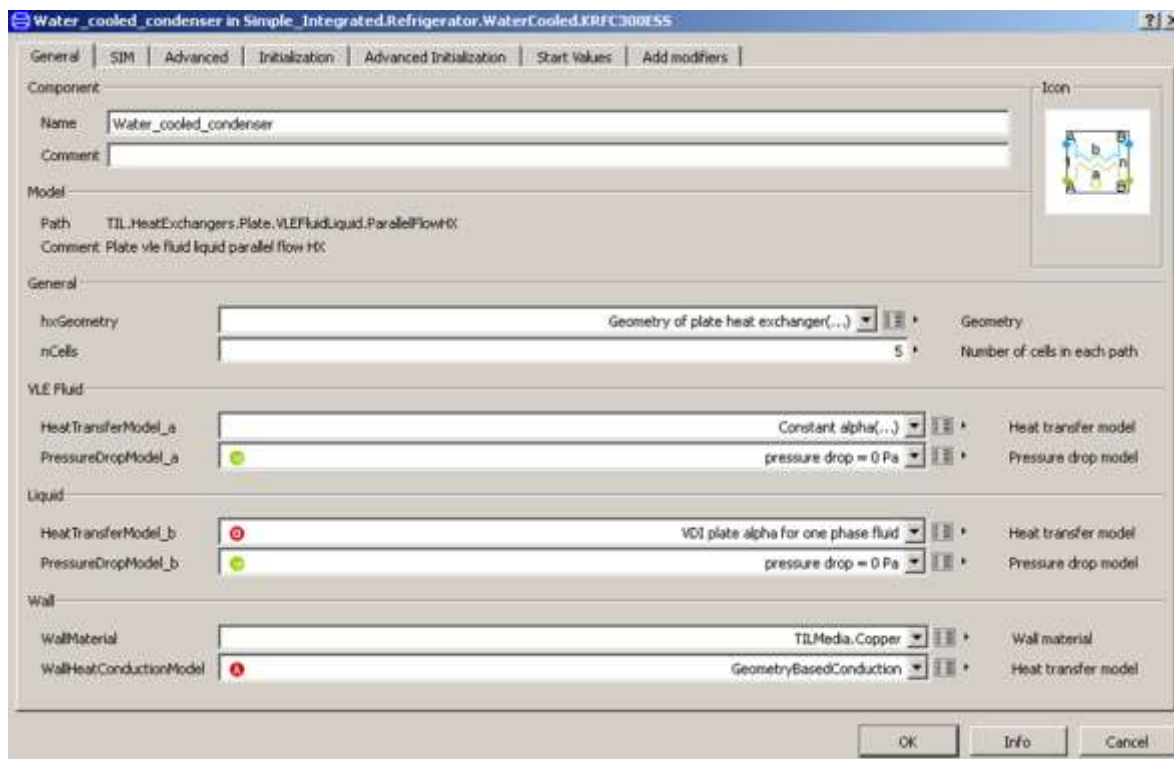


Figure 115: Input Parameters for FPHX Modelica Model

### D.3 Cross-flow, Fin-and-Tube Heat Exchanger

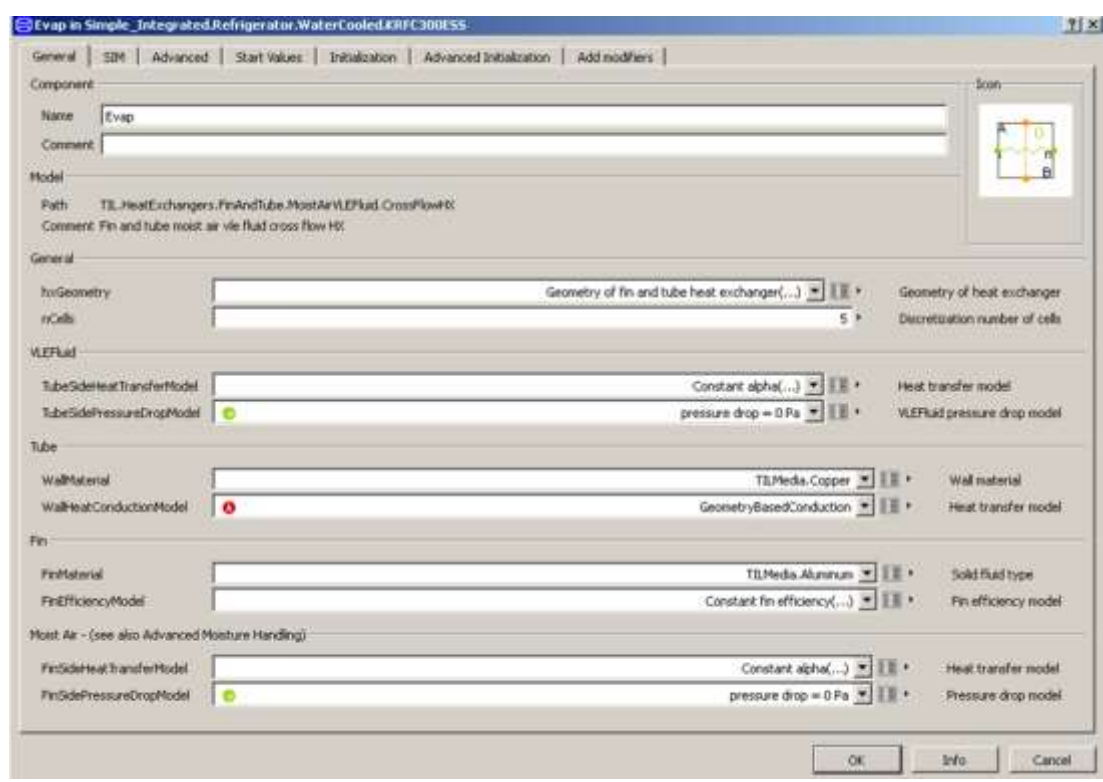


Figure 116: Input Parameters for Fin-and-Tube HX Modelica Model

### D.4 Heat Tube

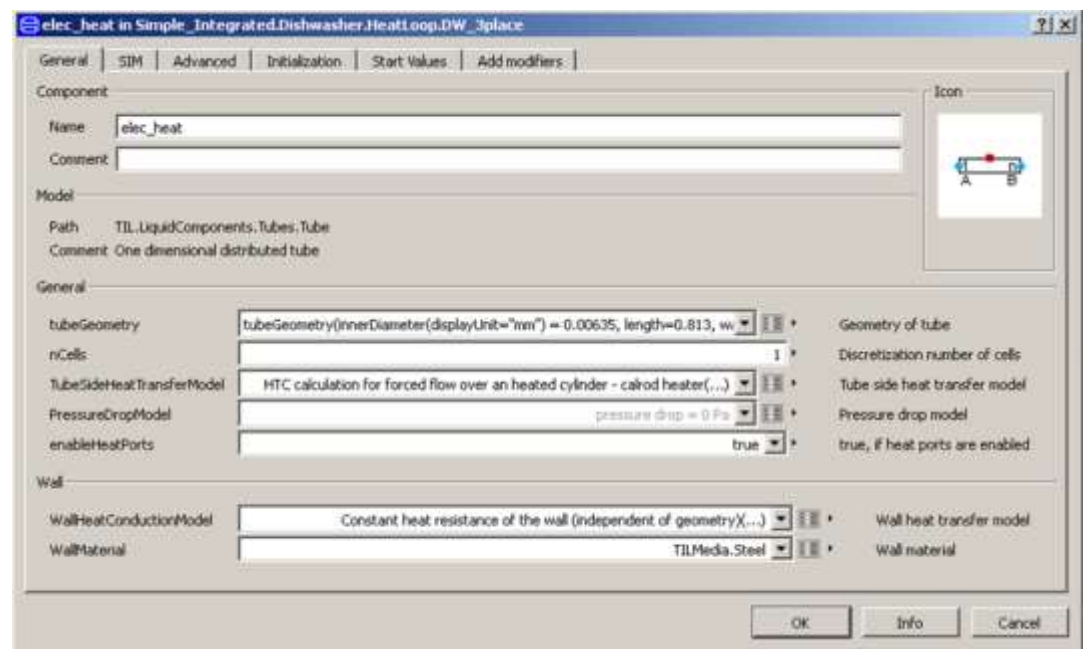


Figure 117: Input Parameters for Heat Tube Modelica Model

### D.5 Simple Storage Volume

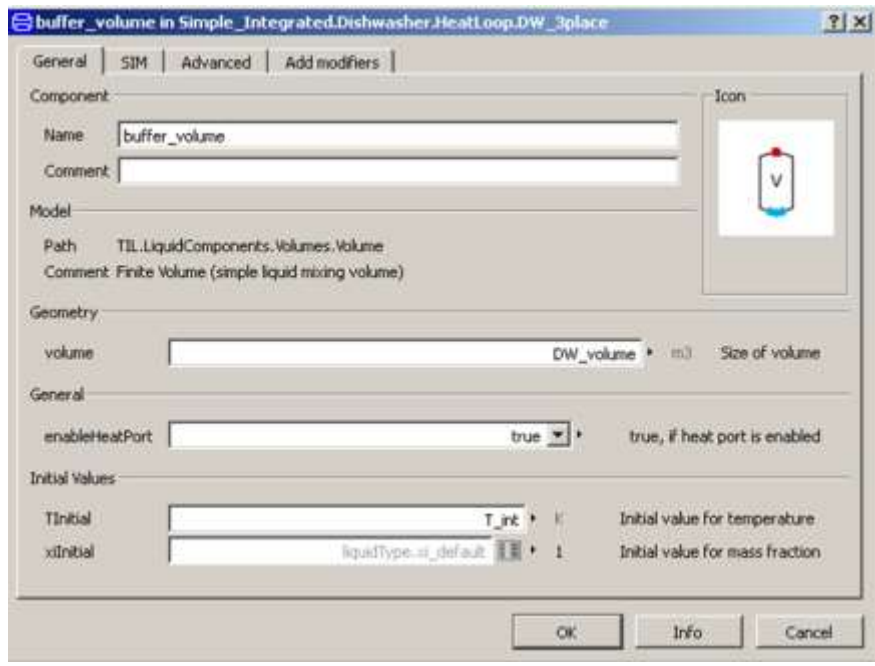


Figure 118: Input Parameters for Simple Storage Volume Modelica Model

### D.6 Thermal Capacitor

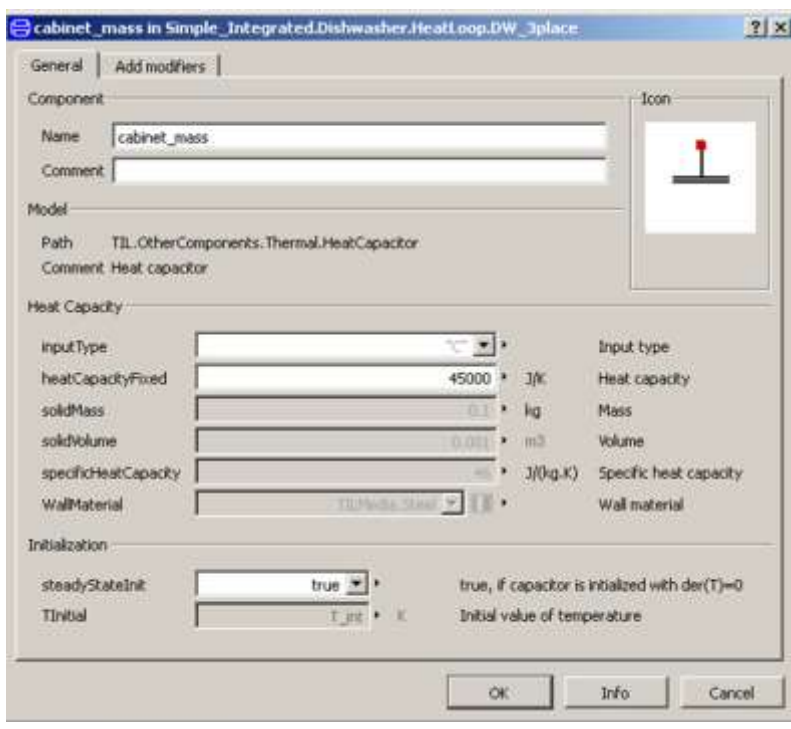


Figure 119: Input Parameters for Thermal Capacitor Modelica Model

## PUBLICATIONS

*Science and Technology for the Built Environment* (2016) 22, 1060–1073  
 Copyright © 2016 ASHRAE  
 ISSN: 2374-4731 print / 2374-474X online  
 DOI: 10.1080/23744731.2016.1216226



## Analysis on a net-zero energy renovation of a 1920s vintage home

STEPHEN L. CASKEY<sup>1,\*</sup>, ERIC J. BOWLER<sup>2</sup>, and ECKHARD A. GROLL<sup>1</sup>

<sup>1</sup>*Ray W. Herrick Laboratories, School of Mechanical Engineering, Purdue University, 177 S Russell St., West Lafayette, IN 47907, USA*

<sup>2</sup>*Whirlpool Corporation, Benton Harbor, MI, USA*

A 1920s vintage home was renovated with the goal of becoming net-zero energy over a 12-month period. The project was performed over a period of two years. The first phase quantified the energy profile of the house in the original state. The second phase included a deep energy retrofit to improve the thermal insulation of the building envelope and an installation of a photovoltaic-thermal solar system. The annual heating demand was reduced by almost 50% from 38,000 kWh to 19,000 kWh. Adjustments made to the annual demand considered missing occupancy during the first phase, gaps in monitoring data, and the heating system used. The thermal comfort of the home was improved by increasing the mean surface temperature of the indoor environment. The net-zero energy target was not obtained during the first year after the renovation, but the solar system did generate 60% of the site electricity consumed. The solar monitoring system was not online 100% of the year for Phase II, and additional adjustments on the HVAC controls in the house, reducing the HVAC energy consumption, will increase the percentage of site energy use being offset by solar.

### Introduction

In 2011, buildings accounted for 41% of the total U.S. primary energy consumption, with the residential sector at 19% of this total (U.S. Department of Energy [DOE] 2011). Due to high energy consumption by the residential sector, research into different approaches to reduce this total is of importance. One big push is for newly constructed homes to be net-zero energy. Title 24 of California's building energy efficiency standard is pushing building efficiencies to reach a goal of all new residential buildings by 2020 being net-zero energy (California Energy Commission 2007). Various studies have been published on how best to define homes that are net-zero energy. The scope can be restricted to site energy usage or expanded to include primary energy consumption. Different balancing periods are considered. The home is grid-tied or off-grid with on-site storage via batteries. The electricity generation is on-site, or the home utilizes large scale renewable energy sources available off-site but can be credited to the home. (Marszal et al. 2011) While different approaches exist to define exactly how a home can be net-zero energy, the overall goal remains to be how a home can best satisfy its energy needs through re-

newable energy sources. Incorporating advanced technologies into new construction is an approach that allows for considerations to be made at the design stage for a goal of net-zero energy. Since the home has yet to be built, many options are available to the designer before settling on a final design. Some options include building orientation, amount of fenestration, etc. However, there are 114 million homes already existing in the United States, and only 15.6 million were built in the years 2000–2009, or only 14% are relatively new construction (U.S. DOE 2009). For the remaining number of homes, 64.7 million, or more than half, were built before 1980. The higher energy intensity of these older homes contributes a significant impact on the total residential primary energy consumption. If much of the focus is spent only on new construction, gains in the reduction of the housing energy footprint will be mitigated, unless the new construction replaces an older home. By exploring approaches to address existing buildings becoming net-zero energy, these inefficient consumers can be greatly improved—if not entirely offset—with renewable energy.

### Project background

In the spring of 2013, the project was started with a search for an older home that would eventually be renovated to achieve net-zero energy. Selecting a home with a significant age provides a fair representation of the effort required for a retrofit and the associated results. The project had additional pillars to reach net-zero water and net-zero waste during future phases occurring in separate years. The first phase officially started in October 2013 and spanned an entire year. A net energy

Received January 24, 2016; accepted July 20, 2016

**Stephen L. Caskey**, Student Member ASHRAE, is a Graduate Student Research Assistant. **Eric J. Bowler** is a Senior Engineer. **Eckhard A. Groll, Dr-Ing**, Fellow ASHRAE, is a Mechanical Engineering Professor.

\*Corresponding author e-mail: scaskey@purdue.edu

Color versions of one or more of the figures in the article can be found online at [www.tandfonline.com/uhvc](http://www.tandfonline.com/uhvc).



Fig. 1. House at the start of Phase I, initial condition.

profile of the home in its original state was generated through a comprehensive data monitoring system. At the end of the first phase, between June and August of 2014, significant renovations were made to the home: from improving the building insulation levels to installing a high-efficiency HVAC system. The goal was to reduce the overall energy consumption of the home as much as possible. After addressing energy consumption, on-site electricity generation was enabled by installing a combined photovoltaic-thermal (PV-T) solar system on the home. To reduce costs and installed system complexity, the solar panels were connected to the grid with a net electric meter provided by the utility. The Phase II period started in September 2014 and ended at the end of August 2015.

### Original condition

The building selected was a detached, single-family home built in 1928. An image from the rear (northwest corner) of the house during Phase I is shown in Figure 1. The site was located in West Lafayette, IN, directly next to the Purdue University campus. The house had three levels—two above and one below ground. On the second floor there were three bedrooms and one full bathroom. The first floor had another full bathroom, a fireplace in the living room, a dining room, kitchen, and a spare room. The total conditioned area, 2864 ft<sup>2</sup> (266 m<sup>2</sup>), was originally heated by an 80% annual fuel utilization efficiency (AFUE) rated, natural gas, forced-air furnace with a rated capacity of 80,000 BTU/h (23.4 kW). The concrete slab, basement walls, and most of the above-grade walls were all uninsulated. The attic had blown vermiculite insulation to approximately a factor of R-4 ft<sup>2</sup>·°F·h/BTU (0.7 K·m<sup>2</sup>/W). The windows appeared to be original to the home and were single-pane, wood-framed, with attached exterior storm windows providing a second layer of glazing. A blower door test performed measured 11 air exchanges per hour over a 50 pascal (0.2 in. H<sub>2</sub>O) pressure differential, 11 ACH<sub>50</sub>. To quantify further the original condition of the home, a Residential Energy Services Network (RESNET) Home Energy Rating System (HERS) Index was completed (RESNET 2013). Receiving a

Table 1. Recommended and installed renovations on the house.

	BEopt Recommendation	Installed
Exterior walls	R-13 fiberglass	R-20.5 closed-cell spray foam
Wall sheathing	R-5 extruded polystyrene	R-3 insulated siding
Attic	R-25 fiberglass	R-41 closed-cell spray foam
Basement	R-13 fiberglass	R-13.7 closed-cell spray foam
Windows	Triple-pane, high gain, low-e, non-metal frame	Triple-pane, SHGC 0.17, low-e, insulated vinyl frame
Air leakage	1 ACH <sub>50</sub>	2 ACH <sub>50</sub>

score of 177, the house in its original condition was 77% less energy efficient than a standard new home, according to 2006 International Energy Conservation Code (IECC) standards, which is the baseline of the RESNET standard.

### Deep energy retrofit

The design process for the retrofit started with the development of a building energy optimization (BEopt) model of the original house (Christensen et al. 2006). First, a 3D model was created where the type of windows, level of insulation at all locations, performance of the HVAC equipment, and other features of the house were selected. From the geometry and physical properties, an annual energy profile was generated using the site weather conditions and assumptions on occupant behavior. The software then ran an optimization and provided a recommendation on the most cost-effective improvements. The simulation predicted 42,322 kWh of site energy was required for heating before the retrofit (Marinello et al. 2014), while after running the optimization on only the envelope, appliances, and lighting, the cost-effective retrofit reduced the heating energy required to 11,966 kWh, predicting an almost 70% reduction in site energy. The details of the envelope recommendations from BEopt and the actual measures installed are listed in Table 1. In almost every category, the recommended insulation levels were matched or exceeded.

### Windows

The approach for replacing windows was straightforward: If the frame was square and in good condition, the existing sashes were removed and replaced with sashes of the same size but a higher thermal resistance. Unfortunately, this approach had a high cost associated with the increased labor to first remove the original windows before installing the new ones. The simulation results from BEopt recommended a high insulation requirement of the windows and demanded triple-pane glazing over double-pane due to the number of windows and the local weather conditions.

*Wall and roof cavities*

For upgrading the wall and roof cavity levels, a couple of different approaches were available. If direct access to the cavity was possible, such as exposed studs on the inner wall or in the attic with exposed ceiling joists, batt or spray insulation could be used, or, on horizontal cavities, batt, loose-blown, or spray insulation could be used. Typically, the wall cavity is covered on both sides for existing buildings and requires different approaches. The most common and affordable option requires drilling holes into each cavity and filling with an insulating material. Any obstructions within the wall cavity, electrical boxes or wires, reduce the effectiveness of the method by blocking sections of the cavity from the blown-in insulation. One proposed solution is to blow the insulation in under high pressure. Another approach drills several small holes instead of one in a cavity and injects foam into each one, which expands inside. From all the mentioned approaches, there is no guarantee the entire cavity will have a uniform level of insulation throughout. A higher cost route, but achieves the ideal level of confidence, is to completely remove the exterior sheathing and directly expose the wall cavity. Although labor costs are significantly higher with this approach, it allows for all insulation options to be available to the designer. Another consideration made was that the house, being of advanced age, had all interior walls finished with plaster. The cavity surface on the unfinished side of the plaster had many raised contours. This would have caused additional complications with effectively filling the cavity with blown insulation. Once de-

cluding to expose the wall cavities from the exterior, advanced, closed-cell spray foam was selected as the insulation.

*Infiltration*

The use of a closed-cell spray foam throughout the exterior walls and attic provided two benefits: a high thermal resistance within a small cavity depth of 3 in. (7.6 cm), and created an excellent seal to minimize infiltration. In spite of these efforts, the infiltration recommendation was not reached, but a significant reduction was achieved from 11 to 2 ACH<sub>50</sub>. One potential reason for the shortfall was the presence of a fireplace. An attempt to seal the chimney flue used a removable bladder by inflating with air to create a temporary seal when not in use. Due to the inability to plug every gap along the perimeter of the chimney, this did not create a perfect seal. Further, with the home being over 86 years old, many potential leakage points existed, and all were probably not addressed. In most homes, enough infiltration exists naturally due to the construction methods that no additional system is required to bring in make-up air. Due to the Phase II upgrades, the house was considered airtight, and an energy recovery ventilator (ERV) was installed to maintain proper air quality through the intake of preconditioned outside air. Another HERS Index measurement was taken of the house, this time after the renovation, and the score obtained was a 2, meaning the house is 98% more efficient than a standard new home, according to the baseline of the RESNET standard. To see the step-by-step process of the exterior renovation, Figure 2 shows the siding



Fig. 2. Step-by-step exterior renovation of the home, clockwise from the top left: removal of exterior wood sheathing, application of spray closed-cell foam, installation of new OSB sheathing, and final exterior finish with insulated siding.

and exterior sheathing being removed for the application of the spray foam insulation.

#### *Solar system*

The BEopt simulation was also referenced to select the total capacity needed for the PV solar array. The annual predicted electrical demands were over 12,000 kWh, using a geothermal heat pump as the HVAC system. The orientation of the home was not ideal for solar generation, with the largest roof area facing due west. Taking this into account, if a 1.33-kWp array is on the south roof and a 10-kWp array is on the west roof, a solar production of about 12,000 kWh was calculated (Marinello et al. 2014). Shading was not accounted for in this prediction, and a fixed roof angle of 25° was assumed. The actual roof angle was measured to be about 22°. To maximize the utilization of available solar energy on-site, a combined solar PV-T system was selected for the roof with the largest area, while, for the southern roof, a smaller, traditional photovoltaic (PV) array. Due to the area limitations for an array install on the western roof, the installed PV capacity was 7.3 kWp, and on the southern roof it was 1 kWp. The material type of the PV panels was monocrystalline with an efficiency of 19%. The benefits from cooling the array are two-fold. The PV panels achieve increased electrical efficiencies by minimizing elevated operation temperatures, and useful thermal energy is generated to supplement the domestic hot water (Tripanagnostopoulos et al. 2002). An additional benefit during the winter months is hot water can be pumped up to the PV-T array to remove any snow accumulation by elevating the panel temperatures above freezing. The PV array was connected directly to the electrical grid instead of opting for on-site storage. The utility provided a net-meter (one meter that can spin in both directions) and credited generation by one-to-one to electric consumption at retail rates. As electricity was generated and used, a monthly difference was calculated. If more electricity was generated by the PV-T system than the house used, an electricity usage credit was given. When monthly usage outpaced generation, the utility charged normal retail rates for the difference.

#### *HVAC system*

A heat pump provides the ideal solution for a very efficient, electrical driven heating and cooling system. Two configurations are available: air and water source. Due to higher efficiencies possible with ground-source heat pumps, this technology was pursued in spite of the associated higher installation costs. The lot size of the house restricted the loop configuration to be vertical instead of horizontal, which further increased the installation cost of the system. A vertical loop geothermal heat pump connected to a hybrid hydronic system replaced the forced-air, natural gas furnace for heating and air source conditioner for cooling. Three wells were drilled to a depth of 250 ft (76 m). The rated heating capacity of the heat pump was 44,100 BTU/hr (~13 kW) at full load with a coefficient of performance (COP) of 3, and, at part load was 35,700 BTU/hr (10.5 kW) with a COP of 3.1. A buffer tank with a storage volume of 20 gallons (75.7 L) held conditioned water being supplied to five zones and was

recharged by the heat pump. In heating mode, the set-point temperature was 105°F (40.6°C), while, in cooling mode, the conditioned water was set to 40°F (4.4°C). Four pumps delivered conditioned water to three wall-hung terminal units in each of the three bedrooms on the second floor and to a water coil in the air handler. Two dampers were installed on the supply duct of the air handler to separate the basement and first floor into two individual zones. The house is considered a hybrid hydronic system because three zones were conditioned by water directly in the space, while two zones were conditioned air via a water coil indirectly. Due to the interconnection between all zones, one zone thermostat had to be specified as the master, controlling when the buffer tank was storing hot water during heating or chilled water during cooling. The first floor thermostat had the master role for the house.

#### *Weather conditions*

A summary of the weather conditions measured during the two testing phases can be seen in Table 2. The monthly average outdoor temperatures were calculated from 30-minute readings recorded at a weather station in West Lafayette (Indiana State Climate Office 2015). The average monthly temperature was slightly higher for Phase II over Phase I. Comparing the number of heating degree days (HDD) can also provide an indication of the heating requirements. A base temperature of 65°F (18.3°C) was used to take the difference from the mean outdoor temperature over a 24-hour period. Table 2 compares the monthly sum of HDD from measured weather conditions during each phase and compares a 25-year average from the ASHRAE climate data for the location (ASHRAE 2009). The outdoor conditions during Phase I had an increase of over 20% in the annual HDD compared to the 25-year average, while Phase II had a 12.5% increase.

### **Experimental design**

#### *Phase I*

A whole-home monitoring system was designed and installed to document the thermal conditions throughout the living spaces, as well as the energy consumption of the home. T-type thermocouples were installed in several rooms measuring air temperature and, at a couple of locations, measuring surface temperature. Two were located on the interior and exterior surfaces of a south facing, exterior wall. The same approach was applied to a window adjacent to the location of the exterior wall measurements. The thermal conditions of the attic were measured with a thermocouple projecting 12 in. (30.5 cm) into the attic space from the ceiling joists as an air temperature, and a second located directly on the underside of the roofing material as a roof surface temperature measurement. Five thermocouples were located in different rooms, having at least one on each level to measure air temperatures in the basement, kitchen, living room, bedroom, and second floor bathroom. At each location, excluding the basement, a relative humidity sensor was installed, totaling

**Table 2.** Average monthly outdoor temperature and monthly heating degree days.

	Outdoor temperature				HDD65				ASHRAE HDD65	
	Phase I		Phase II		Phase I		Phase II		25 year average—2009	
	°F	°C	°F	°C	°F-day	°C-day	°F-day	°C-day	°F-day	°C-day
October	53.2	11.8	52.8	11.6	391	217	384	213	339	188
November	38.6	3.6	35.1	1.7	793	441	897	498	659	366
December	27.6	-2.4	33.0	0.5	1,160	644	993	552	1,051	584
January	18.4	-7.6	24.1	-4.4	1,445	803	1,269	705	1,169	649
February	19.0	-7.2	18.5	-7.5	1,288	716	1,301	723	934	519
March	33.5	0.8	36.7	2.6	977	543	876	487	758	421
April	51.6	10.9	52.5	11.4	403	224	378	210	402	223
May	63.3	17.4	65.0	18.3	160	89	106	59	153	85
June	72.4	22.4	70.7	21.5	1	0	16	9	24	13
July	68.5	20.3	72.4	22.4	15	9	5	3	1	1
August	71.1	21.7	70.8	21.5	6	4	3	2	6	3
September	62.6	17.0	68.1	20.1	131	73	47	26	81	45
Average/Total	48.3	9.1	50.0	10.0	6771	3762	6276	3486	5577	3097

four sensors. Channel space on the data acquisition system allowed for additional relative humidity sensors to be installed. Five more were located in all three of the bedrooms on the second floor and in the remaining two rooms on the first floor, the dining room and office. To quantify the amount of available heat leaving the home as waste water, four thermocouples were installed in the drain lines after the point of use. Only locations with high expected water usage were instrumented: the first and second floor bathroom showers, kitchen (including the dishwasher), and the clothes washing machine. See Table 3 for a complete listing of Phase I measurement locations.

To measure the energy consumption of the home, an electrical monitoring system and two natural gas meters were installed, one for the furnace and the other on the water heater. A custom programmed computer data acquisition (DAQ) system recorded the gas consumption, temperature, and relative humidity readings every minute. A second DAQ system provided a complete package: monitoring and recording the current of each electrical circuit and uploading the associated power consumption via a wireless connection to a server. The electrical monitoring system proved to be beneficial due to the ease of installation and capability to access historical data at month, day, or minute resolution. See Table 4 for a complete listing of the electrical monitoring circuits.

### Phase II

The same monitoring objective used in Phase I was implemented for Phase II. The DAQ channels expanded to include temperature monitoring of the geothermal heat pump: one vertical well at 50 ft (15m) depths and the supply and return piping of the three ground loops. During the installation, the supply and return lines from the heat pump to the ground loops were flipped by mistake. Temperature probes installed for the three return temperatures of each ground loop became

three supply temperatures. The one supply temperature probe turned into a return temperature for one of the ground loops.

The electrical monitoring system had to be expanded due to upgrades on the electrical system of the home and the incorporation of a PV array. The number of circuits increased to allow major appliances, HVAC components, lighting, and plug loads to have separate circuits. Here, the electrical consumption throughout the home would have better resolution on monitoring the various end uses. For example, the household refrigerator power consumption could be read separately to easily recognize different power levels during operation: cooling, defrost, and standby. See Table 4 for additional details on the separation of the electrical circuits. The PV-T system used two different monitoring systems. The first recorded the power generation of each panel in the entire array, and the second recorded the amount of thermal energy generated when rejecting heat to the domestic hot water system.

### Measurement uncertainty

All thermocouple probes installed were T-Type and had a standard limit of error, 1°C or 0.75%, whichever is larger. During the experimental phases, the measured temperature never reached higher than 50°C, meaning the standard limit of error would always be 1°C for all temperatures recorded. The natural gas meters had an uncertainty of  $\pm 0.5\%$  of the full scale setting. The furnace had a full scale of 120 standard cubic feet per minute (SCFM; 3.4 m<sup>3</sup>/minute), resulting in an uncertainty of  $\pm 0.6$  SCFM (0.02 m<sup>3</sup>/minute). The stand-alone electrical monitoring system had an uncertainty of  $\pm 2\%$  of the current transducer (CT) rating. The main lines of the panel had 150-A CTs, with a majority of the remaining circuits having CTs of 20 A, unless being a major appliance or on a double-pole breaker, and then a 50-A CT was used. For the 150-, 50-, and 20-A CTs, the uncertainty is  $\pm 3$  A,  $\pm 1$  A, and  $\pm 0.4$  A, respectively.

**Table 3.** Temperature, humidity, and natural gas monitoring points.

Location	Phase I		Phase II		Both Natural gas
	Air	Water	Surface	Humidity	
Water heater					X
Furnace					X
Second-floor bathroom	X	X		X	
First-floor bathroom		X		X	
North bedroom	X			X	
South bedroom				X	
East bedroom				X	
Office	X			X	
Living room	X			X	
Dining room				X	
Kitchen	X	X		X	
Basement	X	X			
Attic	X				
Roof interior, tar paper			X		
Wall interior, plaster			X		
Wall exterior, siding			X		
Window interior, glazing			X		
Window exterior, glazing			X		
Exterior wall, cavity			X		
Geothermal well, 50 ft (15 m)			X		
Geothermal well, 100 ft (30 m)			X		
Geothermal well, 150 ft (40 m)			X		
Geothermal well, 200 ft (61 m)			X		
Geothermal well, 250 ft (76 m)			X		
Geothermal supply well 1			X		
Geothermal supply well 2			X		
Geothermal supply well 3			X		
Geothermal return well			X		

**Raw data availability**

A summary of the number of data points recorded for each month is provided in Table 5 from both temperature and electrical data collection systems. The amount of data were also shown as a percentage of the month to indicate which time periods during each phase had a high number of points available. Installation delays and complications encountered with the custom programmed data acquisition system led to periods of time where the system was offline. The most notable periods were during the early months of Phase I, awaiting system installation, and in the second half of Phase II, when the next stage of renovations began. The electrical monitoring system was stand-alone and captured many of these unaccounted time frames. Phase I had electrical data for over 60% of the year, and Phase II had almost 100% of the year covered. Additional data were available from the monthly utility bills of the home. The gas bill provided a second measurement of the natural gas consumption to compare the calculated heating energy requirements during Phase I.

**Thermostat scheduling**

Between the two phases, two different thermostat types were used. During Phase I, this was a standard programmable thermostat with four modes: wake, leave, return, and sleep. The

thermostat also provided the ability to have different schedules between weekdays and weekends. The actual time and temperature for each mode established during Phase I are shown in Table 6. To improve upon the programmable thermostat, a smart, learning thermostat was installed for Phase II. The thermostat monitored real time occupancy via a motion detector. One feature was disabled where a HVAC schedule was developed and adjusted by learning occupant behavior. This was needed to match the Phase II set-points and schedule used for Phase I for a direct comparison. The only monitoring feature enabled on the smart thermostat was the auto-away, recognizing when the home is unoccupied, and thus relaxes the set-point until occupancy is resumed. The programmable thermostat during Phase I was set to mimic real occupancy in spite of no one actually living at the house during this time frame. During Phase II, two students occupied the home but often left the house vacant on weekends. The thermostat auto-away feature helped to conserve energy during these vacancies when the home was unoccupied.

**Human occupancy**

The level of occupancy in the home was different between phases—no occupation versus two occupants for Phase I and Phase II, respectively. To estimate the impact of occupancy on the required building heating energy during Phase I, internal

**Table 4.** Electrical monitoring points.

Channel	Phase I	Phase II	CT Rating
2	Main	Main	150
3			
4	Oven	Flash water heater	50
5		Geothermal heat pump	50
6	Furnace closet light	Kitchen outlet right	20
7	Office outlet	Kitchen outlet left	20
8	Basement outlets/lights	Both bathroom outlets	20
9	Office outlet	First-floor lights	20
10	Dining room outlets	Kitchen lights	20
11	Basement closet light	Dishwasher	20
12	Basement lights	Washing machine	20
13	Living room outlet	ERV	20
14	Air conditioner	Forced air fan	50
15		Empty	20
16	Basement outlet	East basement lights	20
17	Basement lights	West basement lights	20
18	First-floor lights/outlets	Utility sink outlets	20
19	Kitchen outlet	Buffer tank	20
20	Clothes dryer	Clothes dryer	50
21			
22	Second-floor lights/outlets	Bedroom space conditioners	20
23	South bedroom outlet	Refrigerator	20
24	First-floor outlets/lights	Second-floor lights	20
25	East bedroom outlets	East basement outlets	20
26	Second-floor outlets	South/north bedroom outlets	20
27	Refrigerator	Living room outlets and closet light	20
28		Hallway/dining/kitchen outlets	20
29		West basement outlets	20
30		Oven	50
31			
32		Light new utility closet	20
33		Office outlet	20
34		Smoke detector	20
35		Solar	20
36			

**Table 5.** Number of raw data points collected each month.

	Temperature data				Electrical data	
	Phase I		Phase II		Phase I	Phase II
	Minutes	Percent of month (%)	Minutes	Percent of month (%)	Days	
October	0	0	14,704	33	0	16
November	0	0	12,201	28	11	30
December	0	0	5176	12	31	31
January	0	0	8181	18	31	31
February	5636	14	13,310	33	28	28
March	43,350	97	6	0	31	31
April	42,897	99	0	0	30	30
May	42,036	94	4051	9	31	31
June	8758	20	0	0	30	30
July	0	0	15	0	8	31
August	0	0	0	0	0	31
September	0	0	0	0	0	30
Total	142,677	27	57,643	11	231	350

**Table 6.** Thermostat schedule for the heating system during both phases.

	Phase I				Phase II	
	Monday—Friday		Saturday—Sunday		Everyday	
	Time	Temperature	Time	Temperature	Time	Temperature
Wake	6:30 a.m.	70°F (21.1°C)	9:00 a.m.	70°F (21°C)	8:00 a.m.	70°F (21.1°C)
Leave	8:00 a.m.	64°F (17.8°C)	—	—	AUTO	55°F (12.8°C)
Return	5:30 p.m.	70°F (21.1°C)	—	—	AUTO	70°F (21.1°C)
Sleep	10:00 p.m.	64°F (17.8°C)	11:00 p.m.	64°F (17.8°C)	11:45 p.m.	65°F (18.3°C)

loads generated by different human activities were referenced (ASHRAE 2013). High and small-impact scenarios were considered here. The high-impact scenario simplified all occupant behavior to an office activity, lifting or packing, generating a high output of 216 watts during periods of occupancy listed in Table 6 for the thermostat. The small-impact scenario considered 72 watts while sleeping, 207 watts from cooking during the wake hours in the morning, and 216 watts, the same as the high impact scenario, during any other occupied periods. The occupancy schedule in Table 6 covers an entire week; thus, these scenarios are applied on a weekly basis. The heating season did not cover the entire year, and 39 weeks were used, instead of 52, to calculate an annual heat output for two occupants. The high-impact scenario predicted an annual heat output of 2030 kWh versus the low-impact scenario, which predicts 1322 kWh.

### Calculation method

To understand the thermal and energy improvements made to the home, both the required energy for heating and the associated primary energy consumed were calculated. A reduction in the amount of heat delivered indicated the level of improvement to the building envelope. Calculating primary energy consumed during the heating season directly accounted for the amount of energy saved by both envelope upgrades and the introduction of an energy efficient HVAC system.

### Heating requirement

During Phase I, natural gas consumption by the furnace was totaled for each day and converted from SCF to BTU. The heat content of natural gas is listed annually by the U.S. Energy Information Administration (EIA) for each state. The 2013 and 2014 values for Indiana were 1015 and 1021 BTU per cubic foot (~10.5 kWh per cubic meter, U.S. EIA 2014). Taking this factor, and multiplying by the total SCF of natural gas measured by the meter, the amount of energy delivered to the furnace was calculated. The AFUE rating of 80% was multiplied with the energy delivered to the furnace to obtain the amount of heat dumped into the duct and delivered to the home. The product was then considered the daily heating requirement of the home. For Phase II, the heating requirement was calculated by first summing the power consumption of the geothermal heat pump over each day. The daily electrical

power consumption measured is then multiplied by a rated COP factor of 3 to obtain an estimate of the daily heating output by the heat pump and, hence, the heating requirement of the home. The actual COP of the system could fluctuate depending on the ground temperature of the vertical loops. During Phase II, ground temperature measurements varied from 55°F (12.8°C) to 32°F (0°C), and the manufacturer had associated COP ratings between 4 and 2.2, respectively. An average COP of 3.1 could be used, but the rated COP of 3.0 provided a more conservative estimate.

Due to lapses in data collection and intermittent occupancy, a second approach was used to estimate the annual heating requirement of the home. Daily average outdoor temperatures were calculated using the weather data available. Next, daily heating energy required by the home were plotted against daily average outdoor temperatures. Only days with guaranteed occupancy, such as weekdays, were used to generate the plot for a clear picture of energy requirements during occupancy. A linear curve-fit to the data provided a prediction of daily heating energy required during each phase as a function of daily average outdoor temperatures. Applying the created function to weather conditions measured during each phase, an estimate could be generated of the annual heating requirement that spanned time gaps in the data collected for each phase. Due to these time gaps, the curve-fit only provided a prediction of daily energy consumption trained with data covering about a quarter of the heating season for Phase I. The approach could lead to an underprediction of the heating energy required with a smaller number of days during extreme weather conditions. To verify the prediction, the Phase I monthly heating requirements were compared with two other predictions from the natural gas consumption. For Phase II, the curve-fit had data covering a large percentage of the heating season but only considered occupied days for an accurate prediction of heating energy required. This approach overpredicted the heating energy required, but was more conservative when calculating the energy savings.

### Primary energy

The natural gas consumption of the furnace can be taken directly as primary energy for heating. The electric consumption of the furnace blower must be converted back to primary energy before being added to the primary energy from gas consumption. The DOE utilizes a multiplier to convert site electrical energy back to source energy, accounting for pri-

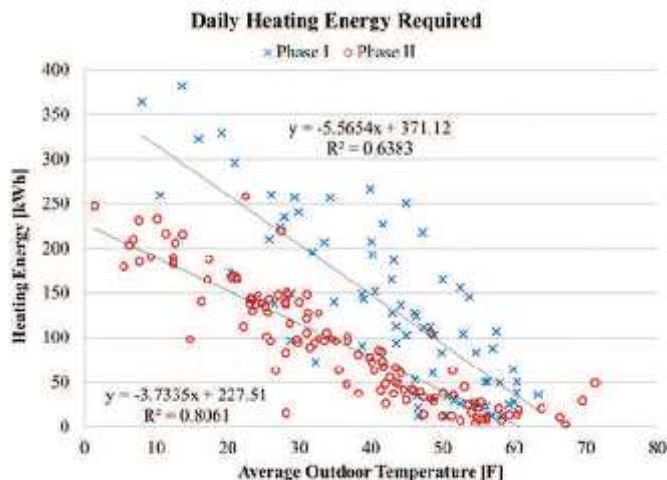


Fig. 3. Daily heating energy required by the home as a function of the average outdoor temperature.

primary energy conversion losses during generation, and delivery losses during transmission (U.S. DOE 2011). A multiplier of 3.1 was referenced from the U.S. DOE using 2010 data. The value was representative of the entire United States and could have better conversion rates when considering local factors such as different primary sources for generation, coal, natural gas, hydroelectric, etc., and site proximity to power plants.

The primary energy for heating calculation during Phase II only required converting the electricity consumption. An energy total was calculated from the sum of the individual power consumptions, kWh, for the geothermal heat pump, air handler, buffer tank, water circulation pumps, and room space conditioners. Due to the ERV being part of the ventilation system, it was not included as part of the primary energy consumption associated with the heating system.

## Results

### Heating requirement

In Figure 3, the calculated daily heating energy required for each phase was plotted against the daily average outdoor temperature. A linear curve-fit was applied and provided with the function and R-squared value for each fit. The Phase I curve-fit had an R-squared of 0.638, while Phase II had a fit of 0.806. The curve-fit function can also provide the balance point, an outdoor temperature when the building heating demand is zero. For Phase I, the balance point is 67°F (19°C), and for Phase II it is 61°F (16°C).

Table 7 lists the monthly heating requirements for both phases. Three different methods were used to calculate the heating demand for Phase I. The furnace efficiency was applied

to the monthly volume of natural gas, either billed by the utility or totaled from the DAQ with a minute sampling rate. The third method applied the linear curve-fit off generated in Figure 3 to the daily outdoor temperature from the weather data. If the outdoor temperature was above the balance point, the heating demand was set to zero. For Phase II, only two methods were available: converting the measured heat pump power consumption with the COP, and the curve-fit method used for Phase I. Overall, the annual heating demand could be shown to be reduced by almost 52% from roughly 40,000 kWh during Phase I to a little over 19,000 kWh during Phase II. The predicted savings would be reduced if the impact of occupancy was considered for Phase I.

For Phase I, the discrepancy between the gas bill and monthly measured heating energy requirements were due to the large periods of time the data acquisition system was offline. On an annual basis, the heating energy required showed a good agreement between the gas bill and the curve-fit method. With a difference of only 626 kWh, the percent error on the gas bill total was 1.6%. The small difference provided confidence in the curve-fit prediction of the building heating demand during Phase I. The months of April and May had heating requirements that were within range of each other across the three different calculation methods. Data recorded by the furnace natural gas meter covered 99% of April and 94% of May. Some monthly gas meter readings were estimated by the utility, but for April and May they were read. The curve-fit prediction had good agreement in April and May due to a high percentage of data points available during these outdoor conditions to generate the fit. During the months of January and February, the heating requirement from the gas bill was not representative of true demand due to the meter reading being estimated by the utility. The heating requirement from the curve-fit had better agreement with the gas bill during the later months of phase I.

**Table 7.** Monthly heating requirements calculated from the natural gas bill, home monitoring system, and a linear curve-fit off the outdoor temperature.

	Gas bill Phase I (kWh)	Measured		Calculated	
		Phase I (kWh)	Phase II (kWh)	Phase I (kWh)	Phase II (kWh)
October	1333	0	475	2419	948
November	3546	0	2774	4696	2814
December	7449	0	2038	6744	3154
January	3758	0	3486	8332	4176
February	13717	1307	4467	7433	4345
March	6104	6024	2413	5731	2721
April	2585	1963	677	2516	927
May	934	819	183	1043	229
June	72	0	0	40	19
July	0	0	0	178	2
August	0	0	0	64	0
September	0	0	0	927	52
Total	39,497	10,113	16,513	40,123	19,387

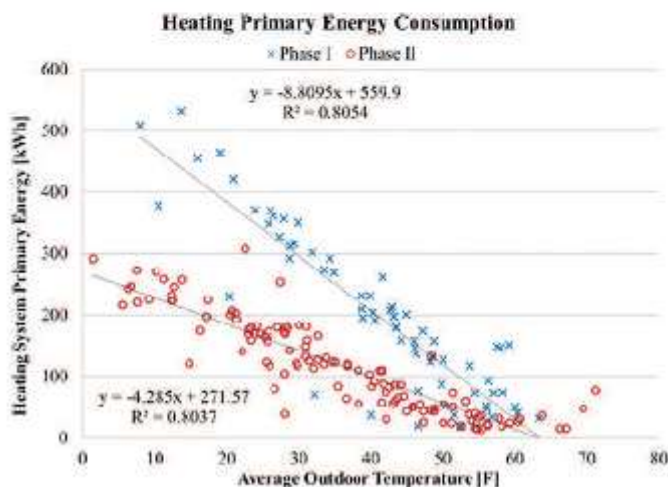
One interesting point is that the months of October and April had very similar HDD amounts, but there was almost double the amount of heating energy delivered when looking at the gas bill. The heating system could have had a lower thermostat setting during these months, or the meter readings by the utility were inaccurate.

For Phase II, the discrepancy was a bit more inconsistent from month to month. Comparing the annual heating requirement better matched the expected result since the calculated values were from a curve-fit of occupied data only. The measured heating requirements had both occupied and unoccupied periods, and, hence, required lower heating energy with a

lower thermostat set point during the away mode. In the month of December, for example, the difference was quite high. The occupants in the home were students, and the month was only occupied for roughly half the time due to the holiday break. Therefore, the measured heating energy would be less than the curve-fit predicted heating requirement referencing the entire month as occupied.

#### Primary energy

In Figure 4, the primary energy required to satisfy the building energy demand was plotted as a function of the

**Fig. 4.** The primary energy consumed by the home as a function of the average outdoor temperature.

**Table 8.** Amount of primary energy used by the home during the heating season.

	Measured		Calculated	
	Phase I (kWh)	Phase II (kWh)	Phase I (kWh)	Phase II (kWh)
October	0	472	3118	1362
November	0	2518	6607	3542
December	0	1279	9821	3945
January	0	2418	12335	5123
February	1895	4222	10995	5288
March	8505	2517	8217	3435
April	2791	750	3183	1328
May	1173	203	1212	344
June	0	0	0	42
July	0	0	60	12
August	0	0	31	0
September	0	0	938	110
Total	14,363	14,379	56,516	24,531

average outdoor temperature. The improvement between the two phases was more significant with this comparison due to both the upgrades of the envelope and the heating system. Both generated curve-fits had *R*-squared values of 0.8.

The primary energy consumption during the heating season for both phases was listed monthly in Table 8. The discrepancy trends between the measured and calculated values month to month were similar to the differences shown for the monthly heating requirements. For the calculated annual total, there was a higher savings of heating primary energy than the heating requirement savings, with a 57% reduction.

#### Exterior wall performance

Figure 5 is a plot of the measured temperature difference between the inside and outside surface of a southern facing exterior wall compared to the measured exterior surface temperature. The first point to note is the range of temperature differences in Figure 5. During Phase II, the temperature difference across the wall reached  $-60^{\circ}\text{F}$  ( $-33^{\circ}\text{C}$ ) during exterior temperatures of  $10^{\circ}\text{F}$  ( $-12^{\circ}\text{C}$ ). This means that the inside surface temperature was around  $70^{\circ}\text{F}$  ( $21^{\circ}\text{C}$ ), which is the heating set-point. During Phase I, the temperature difference was not lower than  $-25^{\circ}\text{F}$  ( $-14^{\circ}\text{C}$ ), with an exterior temperature around  $35^{\circ}\text{F}$  ( $2^{\circ}\text{C}$ ). The associated inside surface temperature

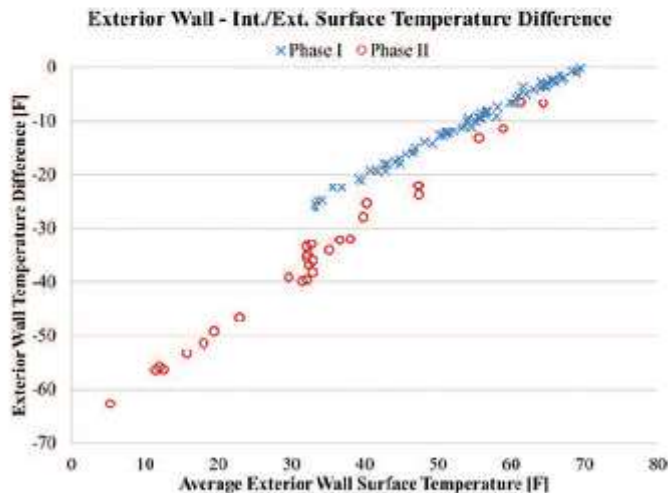


**Fig. 5.** The temperature difference across the interior/exterior surface of the southern exterior wall as a function of the exterior surface temperature.

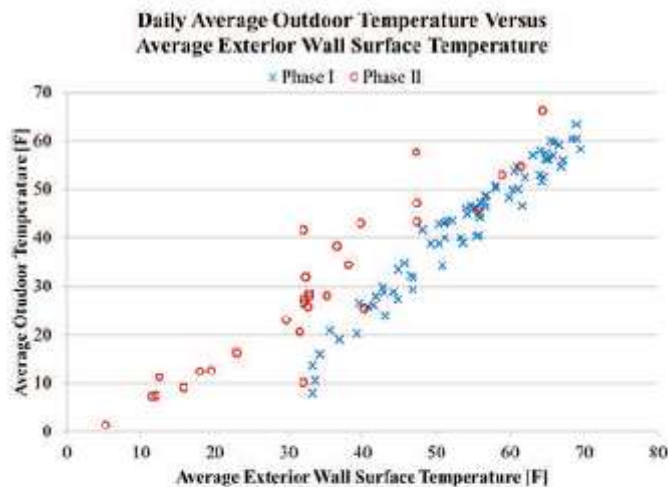


Fig. 6. The daily average outdoor temperature as a function of the exterior surface temperature.

for this case was 60°F (16°C), which is about 10°F (5°C) lower than the set-point. The thermal comfort of a space is negatively impacted by lower mean radiative surface temperature when air temperatures are constant (ASHRAE 2004). One implication of this is, with improved temperature differences due to envelope upgrades, lower set-points are possible for the heating system without sacrificing thermal comfort.

Figure 6 shows, for the same points in Figure 5, a plot of the average outdoor temperature compared to the measured exterior surface temperature. When comparing the two plots, the exterior wall temperature during Phase I only spanned a small range of temperatures, while the outdoor temperature had larger extremes, meaning enough heat was lost from the

building to elevate the exterior wall temperature almost 20°F (11°C) from the outdoor temperature. During Phase II, this difference was not more than 10°F (6°C). Using both plots, the reduction of heat loss between the two phases could be realized.

#### Electrical consumption and production

The monthly electrical consumption of the house is listed in Table 9, along with the solar electricity production measured during Phase II. The annual electric consumption measured increased between the two phases, but was due to occupancy during Phase II and the lack thereof during Phase I. Also, in

Table 9. Amount of electricity billed, used, and generated during both phases.

	Electric bill		Electric consumption		Solar production Phase II (kWh)
	Phase I (kWh)	Phase II (kWh)	Phase I (kWh)	Phase II (kWh)	
October	424	739	0	483	0
November	417	1413	158	1543	100
December	453	1109	471	1174	142
January	478	1399	504	1613	179
February	649	1854	616	2000	297
March	890	559	484	1400	563
April	285	0	203	667	685
May	401	0	315	349	772
June	1043	0	1141	79	809
July	216	0	283	84	831
August	365	0	0	127	833
September	350	0	0	283	627
Total	5971	7073	4173	9804	5839

Phase II, an electric heat pump was used to meet the heating demands instead of the gas furnace used in Phase I. The electric bill did not report any consumption after March during Phase II because the solar system at this point was able to completely satisfy the monthly energy demand. A positive credit builds as long as monthly production is higher than consumption. The total solar production accounted for 60% of the electricity used during Phase II. The percentage should be higher since solar production was not recorded until the monitoring system was online in November. The low amount of electrical use during the summer months of Phase II was due to the start of construction work for the next phase of the project—net-zero water. The power supply to the house was interrupted to install the net-meter; therefore the power supply was temporarily offline. The house was unoccupied during the summer since the spring semester finished in May.

### Discussion

Renovating a home built in 1928 to reach net-zero energy is a challenging task. The difficulty does not lie as much with selecting the best improvements and what technologies are feasible but with the commissioning and day-to-day use of the home. The BEopt software provided a great platform to predict the energy savings with respect to building improvements. The accuracy of the program can be shown by comparing the annual predicted and measured heating energy required during Phase I. BEopt predicted the house would require roughly 42,000 kWh of site energy compared to the 39,000 kWh when referencing the gas bill. One point to remember is that the house was unoccupied during Phase I. Using the high-impact scenario on the thermal gain from two occupants, the annual heating energy demand would be reduced by roughly 2030 kWh. A more accurate heating energy requirement would be 37,000 kWh using the gas bill, or 38,000 kWh when using the curve-fit annual prediction. A 10% to 14% error signals a good confidence in the BEopt model for estimating the heating energy required in light of the many uncertainties provided to the model. Phase II had two students occupying the home with fluctuating schedules of vacancy around semester breaks and weekends. Also, the home had poor insulation and high rates of infiltration during Phase I, leading to a poor thermal comfort. Any significant impact of the occupants in this type of home might be reduced due to the high rate of heat loss to the ambient conditions and the change of occupant behavior in response to lower thermal comfort.

In spite of many BEopt recommendations being met or exceeded for envelope upgrades, the heating demand decreased by about 50%, 38,000 to 19,000 kWh, but still was 7000 kWh short of reaching the savings predicted by the model. One area of potential improvement was with the different control platforms of the HVAC system. A ground source heat pump was connected to a hydronic system with five zones. Each bedroom had a thermostat on the wall-hung space conditioner and generated a signal to a pump on the buffer tank of when to condition the zone. A thermostat on each floor sent a signal

to the air handler which set the dampers and relayed the signal to the buffer tank. As heat was used by different zones, the buffer tank fluctuated in temperature at different rates. The heat pump was controlled to maintain a temperature range in the buffer tank. When commissioning the heating system, there were periods of short-cycling due to the temperature settings on the buffer tank being incompatible with the heat pump. Instead of keeping the buffer tank at a temperature range, the heat pump would turn on during any zone call for heating. Relaxing the temperature setting on the buffer tank helped reduce this coupling. Additional testing is needed to ensure the buffer tank temperature settings are suitable over most or the entire heating season.

The only recommendation from BEopt not reached was minimum infiltration rate. As one would expect, the predicted heating requirement will increase as a result of higher infiltration rates. The fixed schedule of the ERV operation also introduced a constant heating load. Ideally, the ventilation system for fresh air would only run when the home was occupied to avoid introducing unconditioned outside air when indoor air quality was not a concern. Finally, the BEopt model assumed a constant insulating value (U-value) for the entire building envelope, when, in reality, the U-value varies depending on quality of insulation installation and other irregularities, such as the uninsulated fireplace in the building envelope. These three factors combine to reduce the accuracy of the BEopt model prediction on the savings of the annual heating demand. Even though the predicted savings was not reached, the overall heating demand was still cut in half, which is significant when one considers the original state of the home. As the HERS Index measures, the renovated 1920s home is 98% more efficient than a standard home built today, 90 years later.

The electricity production of the solar system was significantly lower than what was predicted. The location of the west panels experienced more shading than what was expected, and the snow removal strategy was not as effective as planned. A three-story apartment building was located on a lot west of the house, and, since the building is tall, it casts a shadow over the panels during the later hours of sun exposure. The snow removal technique employed only worked effectively on half of the west-facing array. Both of these factors had a part in the underproduction of the solar system. In spite of a poor performance of the solar system, 60% of the annual electrical demand was satisfied. After Phase II, changes were introduced to the piping connections between the thermal storage tanks used for heat rejection and the PV-T panels to improve their snow melting capabilities, and thus its effectiveness.

During Phase I, the house was unoccupied; thus, the heating energy required would be impacted due to the lack of additional heating sources from human activities. During both phases, the house was used as a laboratory, increasing the electricity consumption (e.g. for the data monitoring equipment, etc.). In addition, at the start of Phase II, student research projects began to be hosted in the house, causing further increases in electricity usage. The net result of the extra "research related" electricity use reduced the annual im-

pact of the solar PV system on the total annual electricity consumption.

### Conclusions

Significant renovations were made to a 1920s vintage home with the goal of reaching net-zero energy over a 12-month period. The work presented was conducted over two phases. The first phase established a baseline condition of the home. The gas consumption of the furnace and the electrical consumption of the home were monitored and recorded with two data acquisition systems. A 3D model of the house was built inside a simulation model, BEopt, to generate recommendations of the most cost-effective improvements on the building envelope for higher energy efficiency. All recommended insulation levels were exceeded. The original infiltration rate was reduced from 11 to 2 air exchanges per hour at a pressurization of 50 Pascal. The house went from a HERS Index of 177 to 2. A PV-T solar system with a total peak generation capacity of 8.3 kWp was installed on the south and west-facing roof to generate on-site electricity and was grid-tied to eliminate storage needs. The heating energy demand was reduced by almost 50%, when considering the impact of occupancy and associated primary energy consumption of the house was reduced by at least 50% during Phase I. The thermal comfort of the indoor environment was improved by elevating the mean interior surface temperature from higher insulation levels in the envelope. During the first year after renovations, the home was not able to reach net-zero energy, but still was able to offset its electrical consumption by 60% with solar power. Further investigations are ongoing to adjust the heating system control and locate high end-uses of electricity for potential reductions in order to achieve the net-zero energy goal.

### Funding

The authors thank Whirlpool Corporation for funding the research project.

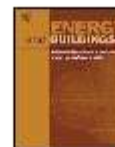
### References

- ASHRAE. 2004. *ANSI/ASHRAE Standard 55-2004, Thermal Environmental Conditions for Human Occupancy*. American Society of Heating, Refrigerating and Air-Conditioning Engineering, Atlanta.
- ASHRAE. 2009. *Standard 169-2013, Climatic Data for Building Design Standards, ASHRAE Handbook—Fundamentals*. Atlanta: ASHRAE.
- ASHRAE. 2013. *ASHRAE Handbook—Fundamentals, Chapter 9, Thermal Comfort*. Atlanta: ASHRAE.
- California Energy Commission. 2007. Integrated energy policy report summary. <http://www.energy.ca.gov/2007publications/CEC-100-2007-008/CEC-100-2007-008-CMF-ES.PDF>
- Christensen, C., R. Anderson, S. Horowitz, A. Courtney, and I. Spencer. 2006. BEopt software for building energy optimization: Features and capabilities, Version 2.6. National Renewable Energy Laboratory. <https://beopt.nrel.gov/home>.
- Indiana State Climate Office. 2015. 30-Minute Purdue automated weather data. [www.iclimat.org](http://www.iclimat.org).
- Marinello, G., S.L. Caskey, E.J. Bowler, and E.A. Groll. 2014. Energy simulation and optimized retrofit practices applied to a real dwelling. *3rd International High Performance Buildings Conference 2014, West Lafayette, Indiana, July 14–17*. <http://docs.lib.purdue.edu/ihpbc/>.
- Marszal, A. J., P. Heiselberg, J. S. Bourrelle, E. Musall, K. Voss, I. Sartori, and A. Napolitano. 2011. Zero energy building—a review of definitions and calculation methodologies. *Energy and Buildings*, 43(4), pp. 971–79.
- Residential Energy Services Network (RESNET). 2013. *Mortgage Industry National Home Energy Rating Systems Standards, Chapter 3, Home Energy Rating System, HERS Index Standard*. [http://www.resnet.us/standards/RESNET\\_Mortgage\\_Industry\\_NationalHERSStandards.pdf](http://www.resnet.us/standards/RESNET_Mortgage_Industry_NationalHERSStandards.pdf).
- Tripapanagostopoulos, Y., T.H. Nouis, M. Souliotis, and P. Yianoulis. 2002. Hybrid photovoltaic/thermal solar systems. *Solar Energy* 72(3):217–34.
- U.S. Department of Energy (DOE). 2009. *Residential energy consumption survey (RECS): Housing characteristics 2009 (Table HC2.1)*. Washington, DC: Energy Information Administration (EIA) and U.S. DOE.
- U.S. Department of Energy (DOE). 2011. *The 2011 building energy data-book*. Washington, DC: U.S. DOE.
- U.S. Energy Information Administration (EIA). 2014. Heat content of natural gas consumed. Table compiled from monthly reports EIA-176, EIA-895, EIA-906, EIA-920, and EIA-923. <https://www.eia.gov/dnav/ng/ng.cons.heat.a.EPG0.VGTH.btucf.a.htm>



Contents lists available at ScienceDirect

Energy and Buildings

journal homepage: [www.elsevier.com/locate/enbuild](http://www.elsevier.com/locate/enbuild)

## Hybrid air-hydronic HVAC performance in a residential net-zero energy retrofit



Stephen L. Caskey\*, Eckhard A. Groll

Ray W. Herrick Laboratories, School of Mechanical Engineering, Purdue University, 177 S. Russell St., West Lafayette, IN 47907, USA

### ARTICLE INFO

#### Article history:

Received 1 January 2017  
 Received in revised form 23 May 2017  
 Accepted 1 October 2017  
 Available online 9 October 2017

#### Keywords:

Net-zero energy renovation  
 HVAC  
 Hydronic  
 Ground-source heat pump  
 ERV  
 Buffer tank

### ABSTRACT

While the United States is no longer the global leader in primary energy consumption, it still represents a significant percentage of global consumption. Residential buildings account for 22% of U.S. national primary energy consumption. Research efforts improving efficiency of existing U.S. homes will have opportunity to greatly impact national energy consumption by addressing a significant energy savings potential. Driving towards net-zero energy buildings provides an ideal scenario where homes produce all energy demands on-site. A joint research project, the ReNEW House, captured an approach of renovating a home to net-zero energy. An efficient and advanced, hybrid air-hydronic HVAC system was installed. During the first heating season, excessive heat pump short-cycling occurred from improper buffer tank controls by default manufacturer settings. Modifications to the temperature control strategy recorded lower energy use through an improved heating system effectiveness. Results were collected over two heating seasons from in-field measurements. During the first heating season, the heat pump used 5440 kWh of electricity at annual heating degree day (HDD) of 6080 °F-day. The second season measured 3920 kWh of electricity at annual HDD of 4800 °F-day. The effectiveness for the heating season increased from 0.89 kWh/°F-day for the first season to 0.82 kWh/°F-day for the second.

© 2017 Elsevier B.V. All rights reserved.

### 1. Introduction

The United States is no longer the global leader in primary energy consumption but still plays a significant role. The U.S. building sector accounts for 41% of the national primary energy consumption while specifically residential buildings are 22% nationally compared to 19% for commercial buildings [1]. Research efforts are needed to address the significant energy consumption from the built environment and the residential sector provides one area of great potential. Some approaches are to improve the energy efficiency of new buildings through the introduction of higher insulation levels, replacement of advanced, high efficiency equipment, and integrating on-site solar generation to reduce demand on external energy sources. The state of California passed a residential building energy efficiency standard, Title 24, with a goal of all new residential buildings to be net-zero energy by 2020 [2]. While energy efforts addressing new construction are excellent in terms of reducing the problem, they do not address the heavy hitters in residential energy consumption; existing buildings. In the United

States, there are 114 million existing homes. 15.6 million, or 14% are relatively new construction, built between the years of 2000 and 2009, while homes built before 1980 account for more than half of the U.S. building inventory or 64.7 million homes [3]. Older homes have significantly higher energy consumption for the same floor area relative to new construction [3]. Developing methods to improve the efficiency of existing buildings is a challenging effort. The structure is already constructed and some energy efficient technologies are difficult to implement due to physical limitations of the building. To investigate these challenges from improving existing buildings, a 1920s era home was renovated over several phases to reach net-zero energy, then net-zero water, and lastly, net-zero waste-to-landfill. The project title is the ReNEW House; a retrofitted, net-zero energy, water, and waste-to-landfill house. Specific details on the first phase of renovations to reach net-zero energy can be referenced in literature [4] and highlights are presented in Section 2. The focus here is on the heating, ventilation, and air conditioning, HVAC, system installed during the net-zero energy retrofit to replace the originally installed natural gas furnace and split-system air conditioner.

A numerical study was performed focusing on existing residential buildings to investigate upgrading a traditional HVAC system [5]. The amount of new construction relative to the total existing building stock is very low, and the authors argue building envelope

\* Corresponding author.

E-mail addresses: [scaskey@purdue.edu](mailto:scaskey@purdue.edu), [Stephen.L.Caskey@gmail.com](mailto:Stephen.L.Caskey@gmail.com) (S.L. Caskey).

upgrades can reduce the heating load to enable lower supply temperatures from the HVAC system and thus enabling heat pump (HP) coupling. The impact on HVAC system performance was explored for an existing building from the 1970s by comparing an identical building, renovated to reduce the nominal heating load by 40%. Three systems were investigated: a HP only, a HP supplemented with a boiler, and a boiler only. An air-to-water heat pump, AWHP, operated with two capacity modes and used R410A. The impact of domestic hot water, DHW, production on the HVAC systems was not considered though commonly provided in hydronic systems. The HP only in the renovated case had a seasonal performance factor, SPF, of 3.25 while when coupled with a boiler, the SPF increased to 3.88 and reduced the number of HP cycles by almost 25%.

A similar study by the Department of Energy reported on field measurements showing the efficiency benefits of AWHPs installed in low-load homes when replacing residential air conditioners with ducted air delivery [6]. Heating SPFs of 3.26 and 4.18 are reported for two homes located in Northern California and Arizona, respectively. TRNSYS modeling from the same study indicated up to 28% annual HVAC energy saving from using AWHP versus an air-to-air HP using ductwork. Another study reported up to a 22% savings when replacing traditional forced air equipment (ducts, air handler, air-to-air HP) with hydronic piping, pumps and smaller distributed fan coils [7]. Ductless hydronic systems have reduced space requirements for ducting, eliminate thermal losses along ductwork, and provide an easy ability to zone [7]. Water-to-air terminal units can handle both heating and cooling for each zone from hot or chilled water versus traditional hydronic terminal equipment which is heating only, radiant floor systems or radiators. In a forced air systems, air delivery temperatures should be as close as possible to the zone set-point to be defined as a low-exergy system [8]. Also thermal energy storage becomes easier to implement on a hydronic system versus a forced air system which can facilitate demand side management or improved utilization of on-site, solar photovoltaics, PVs.

Circulation pumps in hydronic HP systems have estimated pumping efficiencies of less than 30% based on feedback from a buffer tank manufacturer. In one study, pump efficiencies are reported to be approximately 10% [9]. Doubling pump efficiency has been estimated to improve the SPF by approximately 4–9% [9]. While hydronic pumps currently used have low efficiencies, they have lower energy draws than traditional forced air blowers [7]. When hydronic systems are connected to multiple zones, the required number of pumps increases and could amplify the collective negative impact of the low efficiency pumps. Experimental data published identified a pump control problem for one of the zone loops [10]. One study recommends further research focused on the development of packaged controls for zoned systems [6].

A study conducted on HVAC systems in low-load homes reported many installed systems are custom in nature and are installed by contractors who learn best practices through trial and error [11]. The authors recommend future work on the development of system sizing and installation guidance specifically for low-load HVAC technologies. HP manufacturer rated coefficients of performance, COPs, account for auxiliary equipment, such as fans and pumps, but do not include any duct or piping resistances present in a real installation [12]. As a consequence, actual system COPs are lower than their manufacturer ratings. One study reports an average reduction of COP across three monitored systems of 27% during low stage operation and a 13% drop during high stage operation [12]. Surprisingly, the same study reported higher COPs during high stage versus low stage operation when referencing actual ground-source heat pump (GSHP) usage. Typically, HP operation at part load will have higher efficiencies compared to full load.

Intermittent HP operation requires delivery of higher temperatures to reject enough heat during the on and off cycles. Thus, HP efficiency is reduced by requiring higher condensing pressures during intermittent operation. A study of variable speed technologies for HP compressor and water pumps attempted to address this set-back [9]. Drive energy was shown to be higher for variable speed pumps compared to intermittent pumps. Improved controls and pump efficiency would improve the overall system efficiency. Adjusting heat pump capacity with variable speed technology can reduce the number of on and off cycles.

Buffer tanks (BTs) help to avoid excessively short on-and-off cycle operation and provide heating during HP transients [10,13]. A buffer storage tank is integrated into the hydronic system to increase the thermal inertia of the system and reduce the annual number of operating cycles of the HP or boiler. The impact of the BT size on the HVAC system performance is investigated by varying tank sizes between 13–132 gallons (50 and 500 liters) [5]. Simulation results show number of annual operation cycles decrease as the BT volume increases. While larger tank sizes decrease cycling, they also increase the amount of heat loss and the associated investment cost of a larger tank. Low thermal mass systems like radiators have benefits when coupled to large tanks acting as thermal energy storage to improve temperature control and avoid excessive heat pump cycling [13]. A common approach to reduce the heating capacity of radiators during milder weather conditions is to lower the supply temperature according to the heating curve of the equipment to match the room heating load [5]. While BTs are needed for low-temperature radiators, large volume heating loops such as radiant floor systems can be used as the buffer volume and no longer requires a separate tank [13]. A GSHP coupled with a radiant floor provides the highest second law efficiencies when compared to boiler driven hydronic systems, while also being primarily electricity driven [8].

Several different supply and return water temperatures were investigated for typical hydronic terminal equipment. Two general categories are identified, low-temperature for underfloor or radiant heating and high-temperature for radiators. Supply temperatures of 86–104 °F (30–40 °C) [13] and 97–115 °F (36–46 °C) [10] were investigated for low-temperature applications with one reporting both supply and return temperatures of 95/82 °F (35/28 °C) [9]. For high-temperature applications, supply water at 113–131 °F (45–55 °C) [13] and under the Swedish standard system with supply and return temperatures of 131/113 °F (55/45 °C) [5,9]. Another study did not report the application but simulated and tested supply and return temperatures of 91/82 °F (33/28 °C), 95/86 °F (35/30 °C), and 104/95 °F (40/35 °C) [14].

Two studies, one on an AWHP and another on a GSHP used HFC refrigerant R407C [9,13], which was designed as a drop-in replacement for HCFC refrigerant R22 versus another study of 3 GSHPs systems using HFC refrigerant, R410A [12]. HPs with R410A have higher refrigeration capacities relative to R407C allowing smaller heat exchangers; although the thermodynamic properties of R410A restrict its use under high pressure ratios due to elevated discharge temperatures. Therefore, the compressor envelope inhibits high, load side temperatures of supply water or BT storage temperatures [15]. A GSHP using CO<sub>2</sub> was determined to have higher COPs when operating in combined space heating, SH, and DHW versus a HFC refrigerant GSHP having higher COPs in SH only [14]. A couple studies considered DHW production as part of the hydronic system [8,14]. The temperatures investigated were 140, 158, and 176 °F (60, 70, and 80 °C) with an average city main temperature of 44 °F (6.5 °C) [14]. Existing homes have DHW to SH ratios of 10–25% versus well-insulated homes or low energy homes having ratios around 25–45%. Higher DHW to SH ratios show equal or higher SPFs for CO<sub>2</sub> GSHPs when compared to the most efficient R410A GSHP

[14]. The impact of DHW production on the HVAC performance was not investigated here.

Three residential GSHP installations in U.S. cold climates were monitored and discovered a couple issues after installation. One system was found to have air trapped inside the ground loop and a second problem from air in the lines caused an air handler to freeze up [12]. Commissioning of hydronic equipment is important to obtain the maximum efficiencies present with these advanced HVAC systems. Additional data on field performance of hydronic systems are also identified as an area of future research needed [7].

To fit best within the existing building, a combined air and hydronic driven HVAC system was installed. The system is referred as a hybrid air-hydronic HVAC system. It combines elements of a traditional, ducted, forced air system supplying two zones with dampers and a hydronic system with wall mounted water-to-air coils in the second floor zones. The hybrid approach easily allowed zoning within the existing structure of the home. By upgrading the HVAC system to interface with multiple zones, complications can result from a mismatch between equipment rated capacities and the zone heating requirements. The advanced HVAC system has been run over two heating seasons and adjustments were made to the BT temperature settings to improve the heating energy effectiveness of the HVAC system. The equipment installed, the overall control strategy, and modifications applied are explained and their associated impacts are investigated.

## 2. ReNEW house project

A joint research project was started between a higher-education institution and an industry representative in the fall of 2013. The goals were to renovate an existing building over multiple phases, ultimately reaching net-zero energy, net-zero water, and net-zero waste-to-landfill. The reference timespan for each net-zero goal is one calendar year. In the first year of the project, no physical improvements were made to the home but a whole-home monitoring system was installed to establish the baseline energy consumption. Several aspects of the home were recorded: the entire electrical consumption down to each circuit, air temperature and relative humidity levels throughout living spaces, and water usage traits from supply side flow meters and temperature sensors as well as waste water temperatures. For the second year of the project, in-depth renovations occurred during the summer of 2014 to upgrade the house reaching net-zero energy. Building materials such as insulation levels or window types were replaced, sealing methods deployed to make the house air-tight by reducing natural infiltration, and highly efficient technologies introduced to minimize the energy consumption from heating and cooling. Additional measures were taken by installing two sets of solar, PV arrays for on-site electrical production. The house was grid tied and therefore did not use any on-site electrical storage. A comprehensive investigation and analysis was performed comparing the heating energy demand before and after the net-zero energy renovations [4]. Additionally the impact of the solar production on offsetting the home energy needs is also reported.

In the summer of 2015, new renovations were made to the interior of the home to upgrade the living spaces on the first floor. The original kitchen was updated and some walls were removed to open up the kitchen and living room. The main focus of the 2015 renovations was installing systems to support the net-zero water pillar of the project. A large scale rainwater collection and treatment system was designed and installed to reduce and hopefully eliminate the usage of city water in the home. Two underground storage tanks provided roughly 2800 gallons (10,600 liters) of rainwater storage and the treatment train applied two stages of UV treatment to disinfect rainwater to a potable level. With rainwater

being a finite supply, restricting its usage to mainly potable needs was desired. One approach reduced the potable water demand by installing a greywater treatment system collecting shower water to supply toilets with processed greywater for flushing.

The new HVAC system installed during the net-zero energy renovation was causing an undesirable operation of the GSHP by short cycling. Changes were applied to the controls of the hybrid air-hydronic system near the end of the first heating season and near the start of the second heating season. The effectiveness of the implemented changes was identified by calculating a heating system efficiency. The daily energy usage of the HP, kWh, is divided by the daily, heating degree day, HDD. The goal is to generate a factor indicating how efficiently the HVAC system is in satisfying the heating load of the home. The HDD is calculated by taking the difference between the outdoor temperature and an assumed, balance point temperature of 65 °F (18 °C), shown in Eq. (1). A weather station located at the West Lafayette, Indiana airport provided 30 min increments of the outdoor, dry-bulb air temperature in Fahrenheit.

$$HDD_{65} = 30 \text{ min} \cdot (65F - T_{\text{outdoor}}(t_{30})) \cdot \left( \frac{1 \text{ day}}{1440 \text{ min}} \right) \quad (1)$$

## 3. Hybrid air-hydronic heating and cooling system

Replacing the existing air distribution system in the home was important as it was poorly designed. Due to the age of the home and the methods employed at the time, an insufficient amount of heated air was being delivered to the second floor. The three air registers on the first floor were connected to three registers on the second floor within each bedroom. The damper on each first floor register had to be closed to allow conditioned air pass the first floor register to reach the second floor bedroom register. In order to heat the second floor bedrooms, dampers on the first floor registers had to be closed and heat would no longer be available to those first floor areas. A floor plan for each level of the house along with the floor area for each heating zone can be seen in Fig. 1.

The goal of redesigning the HVAC system within the existing structure was to minimize the amount of required physical changes to the home. With this approach the complexity of the renovation is minimized, resulting in cheaper installation costs. The selected HVAC type is a hybrid air-hydronic system. Five heating zones were identified. Conditioned air is supplied via water-to-air coils either directly in the zone with wall hung terminal units in each bedroom, or from a central air handling unit with a water coil using dampers in the ductwork for the basement or first floor zones. High efficiency, hydronic terminal equipment, such as in-floor, radiant loops, were not explored due to their retrofit challenges. The benefit of switching to a hydronic system allowed individually zoned bedrooms and prevented major modifications the home. The original ductwork connecting the bedrooms was disconnected and reused as conduit to hold piping delivering conditioned water to the bedroom zones. A complete layout of the HVAC system and images of the installed equipment can be seen in Fig. 2. The location of the original register for the bedroom can be seen on the floor below the bedroom space conditioner in the far left image. Recognize how the wall hung unit lines up with the floor register, indicating where the water lines run within the duct.

### 3.1. Ground-source heat pump (GSHP)

The HVAC contractor applied the ACCA Manual J method to estimate the design cooling and heating loads of the house and identify the required HVAC equipment capacity [16]. For primarily electrically driven HVAC systems, a GSHP provides higher efficiencies compared to an air-source heat pump (ASHP) due to elevated source temperatures below ground. The limited ground

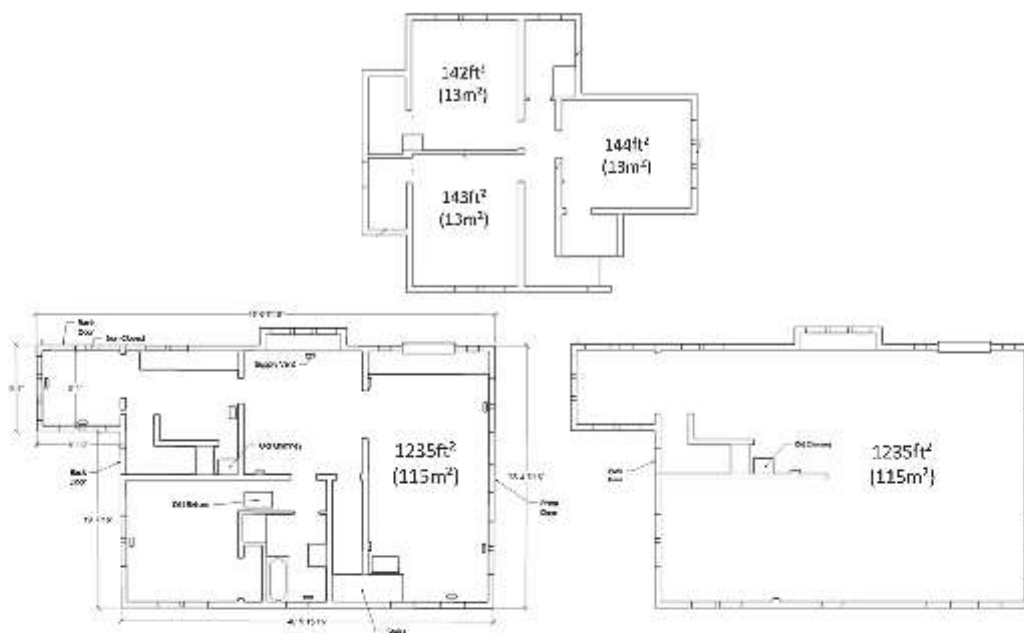


Fig. 1. ReNEW House Floor Plan – (Top) 2nd Floor, (Left) 1st Floor, (Right) Basement.

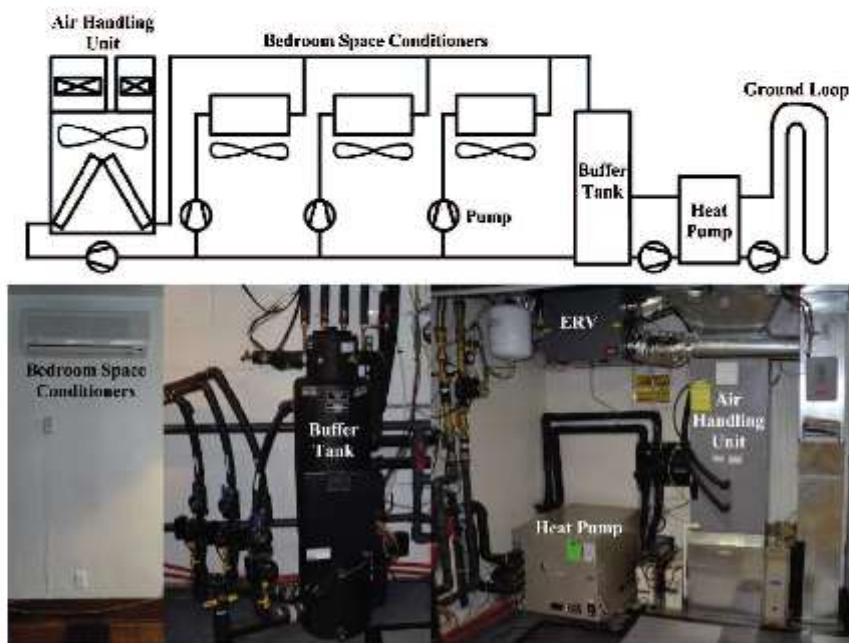


Fig. 2. Schematic and Images of House HVAC System Components.

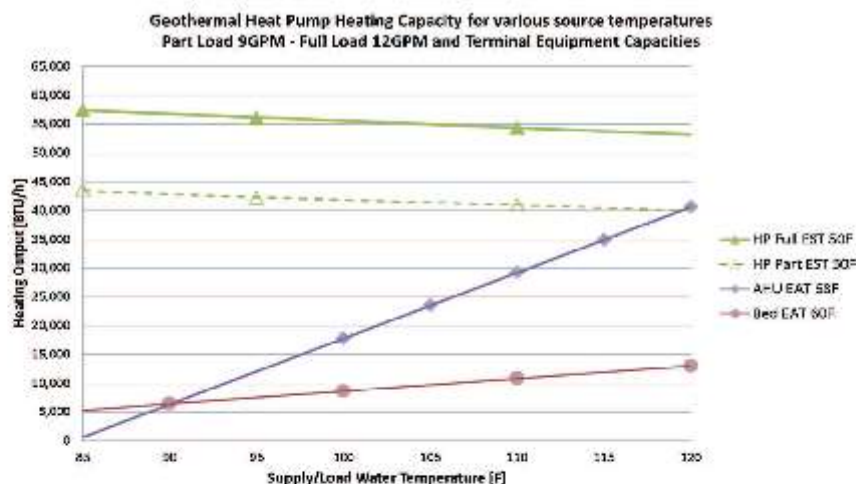


Fig. 3. HVAC Equipment Rated Capacities for Varying BT or Load Water Temperatures at a GSHP Entering Source Temperature, EST of 50°F (10°C), an AHU Entering Air Temperature, EAT, of 68°F (20°C) and a bedroom space conditioner EAT of 60°F (15.6°C).

area around the home required the installation of vertical ground loops. Three, 250 foot (76 m), vertical wells were drilled and U-pipes installed using glycol-water mixture as the working fluid. Specifically a hydronic GSHP was selected as it easily supports zoning. To improve GSHP efficiencies during off-design heating loads, a variable capacity GSHP is desired but is only offered by the manufacturer in select capacities. Therefore a higher capacity, 4-ton, two-stage, GSHP was selected instead of the lower, 3-ton option to avoid needing electrical auxiliary back-up. The GSHP heating rating at full-load is 44,100 BTU/h (12.9 kW) and at part-load is 35,700 BTU/h (10.46 kW). The respective rated COPs are 3.0 and 3.1. The GSHP charges a BT and controlled by the temperature settings of the BT. The layout described can be referenced in Fig. 2. Therefore, the GSHP operates between ground temperatures on the source side and the BT water temperature on the load side. The GSHP capacity rating is also a function of the BT temperature. Fig. 3 presents the GSHP capacity as function of the load or BT temperature. The GSHP selected uses an HFC refrigerant, R410A. Due to the limitations in the operating envelope discussed earlier, BT load temperatures in excess of 125°F (52°C) cannot be generated safely by the GSHP. This limitation presents a potential complication with the heating controls of the wall hung, water-to-air bedroom space conditioners. A predetermined and fixed threshold temperature of the water coil is required to be surpassed before the fan motor can activate. The GSHP also is equipped with a desuperheater to provide DHW up to 130°F (54°C).

### 3.2. Buffer tank (BT)

The manufacturer of the BT recommends approximately 6 gallons (23 liters) of storage per ton of HP capacity. With a GSHP rating of 4-tons, 24 gallons (91 liters) of storage was required. The closest storage size available by the manufacturer is 20 gallons (76 liters).

The BT uses four water pumps connected to three bedroom zones and one water coil in the air handling unit connected to two zones, the basement and first floor. A fifth pump on the BT connects the GSHP. When a zone calls for heat, the respective pump is energized and tempered water is delivered to the associated equipment. The temperature in the BT drops due to rejecting heat to the zone.

A built-in controller on the BT signals the GSHP to run at predetermined temperature level. As the zone continues its call for heat, the GSHP continuously rejects heat to the BT until a second temperature threshold is reached. If the zone becomes satisfied during GSHP operation, the BT automatically kicks off the GSHP even if the OFF (set point) threshold temperature is not surpassed. The approach is to prevent GSHP operation when no zone is calling for heat. The very next time there is a call for heat, and the BT temperature control was not satisfied from the last run, the GSHP will turn on with the zone call, rejecting heat to the BT while the zone is calling for heat. Once the BT reaches the programmed threshold temperature and a zone is still calling for heat, the GSHP will turn off while the BT continues to supply the zone. The BT controller supports two sets of ON-OFF threshold temperature settings for the two-stage capacity control of the GSHP. The first set controls part-load operation of the GSHP and the second set controls full-load capacity. The BT uses the same controls approach when in cooling mode although its cooling operation and performance was not investigated. The diagram in Fig. 4 indicates the threshold temperatures programmed on the BT and identifies dates when changes were to the temperature settings to improve the HVAC system performance. The BT requires a master thermostat be established to indicate if heating or cooling set-point temperatures are followed. The first floor thermostat acts as the master thermostat. The required feature limits the flexibility of the HVAC system during swing months between heating and cooling seasons. As the house reaches the end of the heating season around April and May, the first floor thermostat is switched from heating to cooling. Any zone call for heating from the bedrooms will result in chilled water being delivered to the zone and generating an uncomfortable zone. The homeowner needs to be educated with this type of system to ensure the switch between heating and cooling occurs when no heating loads are expected by any of the zones.

### 3.3. Bedroom space conditioner

Each bedroom has a wall hung, water-to-air unit to directly condition the space. The rated capacity is 9000 BTU/h (2.64 kW) but a table is provided in the installation manual with specific capacities

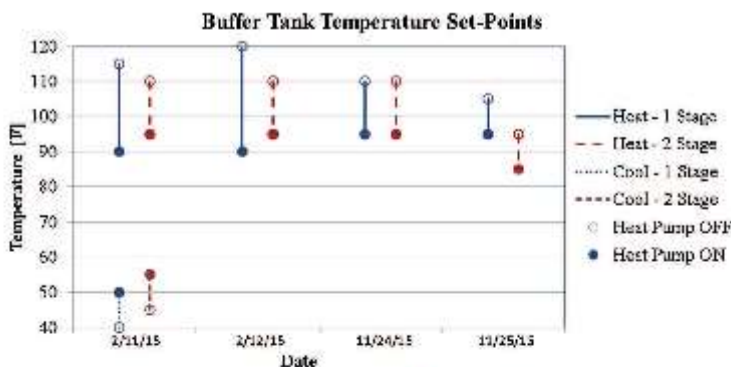


Fig. 4. Changes Made to the Temperature Set-Points of the Buffer Tank.

for various room temperatures, supply water temperatures, and supply water flow rates. See Fig. 3 for the rated capacity of the bedroom space conditioner as function of load or BT temperature. The fan can be run at three different speeds, high, medium, and low. On high, the fan air flow rate is rated at 270 CFM (7645 l/minute). A handheld controller for each unit sets the desired air temperature in the bedroom, the heating or cooling mode, and the fan speed. In heating mode, the unit activates a water pump at the BT when the air temperature is below the set-point. A temperature probe measures the water coil temperature until threshold is reached before activating the fan to prevent uncomfortable cold air blowing onto the occupants in the space while the coil heats up. From this temperature dependent control, too low of a temperature set-point on the BT can prevent the unit from operating properly. To eliminate this concern, the manufacturer recommends water temperatures above 95 °F (35 °C) – 105 °F (41 °C). With the current settings on the BT this situation has not been encountered.

#### 3.4. Air handling unit (AHU)

To heat and cool the basement and first floor zones, an air handling unit, AHU, with a water-to-air, A-coil delivers conditioned air through newly installed ductwork. Two dampers are located at the exit of the AHU and are controlled by individual, smart thermostats in each zone. One pump on the BT activates when either zone calls for heat since each zone utilizes the AHU. The AHU has a rated capacity of 36,000 BTU/h (10.5 kW). See Fig. 3 for the rated capacity of the AHU as function of load or BT temperature. The internal blower is driven by an ECM motor and operates at an air flow rate preset by jumpers on the ECM board. A slight range of flow rates is reported for each rating flow rate due to the different static pressure drops possible but is mainly controlled by the jumper settings. The ECM motor is able to adjust the fan speed in response to the measured torque to maintain a constant air flow rate. The benefit is the AHU can be connected to ductwork with different levels of static pressure drop and still maintain the designed air flow rate. The blower is configured to deliver roughly 1300 CFM (36,800 l/min) on high and roughly 1000 CFM (28,300 l/min) on low. While the AHU is able to provide roughly the same air flow rate with varying static pressures, the associated power draw of the blower will not be constant. The unit works harder with high static pressure drops. Between the first and second heating season, renovations on the first floor changed the in-floor air registers. Also a separate research project called the Biowall required a connection to the air return ductwork. The introduction of this system added another

return register to the ductwork installed during the net-zero renovation. Due to these modifications, the ductwork static pressure drop was altered between heating seasons and within the second heating season.

#### 3.5. Energy recovery ventilator (ERV)

As mentioned in Section 2, the net-zero energy renovation of the home greatly reduced the amount of outside air infiltration. To maintain proper indoor air quality, outside fresh air is introduced in a controlled manner into the home with a dedicated system. Usually, older homes do not require this secondary system as the original construction of the home is leaky due to the natural cracks and gaps in the building envelope. Naturally occurring infiltration through the building walls provide sufficient fresh air into the home. In new construction where the home is built to be airtight, different options are available to introduce fresh, outside air into the home. One simple, inefficient option is a damper connected between a vent on an outside wall to the return ductwork of the AHU. The damper can be fixed open in different positions where a fixed level of outside air is always drawn into the duct or a timer controls when the damper is open. While this option is cheap and effective, it increases the building heating and cooling loads. A more efficient option is to install a system where the outside air is preconditioned before entering the return duct. Two types of preconditioning are available, only sensible heat transfer or both sensible and latent heat transfer. The only sensible heat transfer systems are heat recovery ventilators (HRVs) and the system that do both sensible and latent heat transfer are energy recovery ventilators (ERVs). Both types follow the same flow paths but utilize different heat exchangers. As outside air is drawn into the system, inside air is drawn into a separate channel in the same system. The two air streams cross inside the system through a closed heat exchanger before leaving. For an ERV during the heating season, cold dry air is drawn into the system as well as warm inside air. As both air streams pass over the heat exchanger, heat and moisture are transferred between them. The cold, dry air is heated and slightly humidified by the warm, indoor air. The benefit of the outside air being preconditioned is the reduction of an increased heating load from the fresh air. Preconditioning is possible since the stagnant, indoor air needing to be exhausted is already at the desirable temperature and humidity. An ERV was selected for the house over a HRV to capture the full benefits possible for a recovery, ventilation system. An image of the installed ERV with the ductwork connections is shown in Fig. 2. The unit is rated at 150 CFM

**Table 1**  
Zone Determination for HVAC Equipment from Electrical Circuit Power Draw.

Electrical Circuit	Zone Description	Zone Number	Programmed Pwr. Range [W] [Low End – High End]		Snapshot Pwr. 11/15/2016
Bedroom Space Conditioner	1 unit	1	30	60	48
	2 units	2	60	90	85
	3 units	3	90	–	120
Buffer Tank	1 Bed	1	5	140	125
	AHU	2	140	230	160
	2 Bed	3	230	250	250
	AHU + 1 Bed	4	250	320	285
	3 Bed	5	320	380	375
	AHU + 2 Bed	6	380	475	410
	AHU + 3 Bed	7	475	–	535
Air Handling Unit	ERV	1	20	275	260
	Both Floors	2	275	310	287
	First Floor	3	310	350	335
	Basement	4	350	–	395

(4250 l/minute) and 49% total recovery efficiency. The operation is controlled by an adjustable ON duty cycle. The allowable range on the controller is 30% to 100% ON of every hour. The current setting is 30% ON or 20 min of every hour to minimize the impact from the energy consumption of the unit. Due to the house hosting various research projects throughout the different phases, the ERV was forced to 100% ON for short periods of time. When the ERV is on, the AHU must also be activated to distribute fresh air throughout the home. Both dampers on the AHU are opened when running the ERV but if a call for heat comes from either the basement or first floor, the damper for the non-heating zone closes. Therefore, the system prioritizes the heating call, sets the AHU dampers, and when the ERV turns on, the incoming fresh air is only directed to the heating zone.

#### 4. Heating zone identification

The electrical circuits of the HVAC system generate distinct power levels when operating in the various possible heating modes. By applying a filtering method to these circuits, different heating modes can be identified. Three electrical circuits are investigated; bedroom space conditioners, central AHU, and the hydronic BT.

To estimate expected power levels associated with different possible HVAC modes, the individual systems are manually operated and run in each mode to document the power level during operation. The snapshot power levels help generate a range of expected wattages for each operation mode. A zone determination number is created and set for each possible wattage range, corresponding to a specific case. An overview of all power ranges established for each HVAC electrical circuit is shown in Table 1.

##### 4.1. Bedroom space conditioner

Three distinct power levels are observed when one, two, or all three bedroom units are on at one time. Fig. 5 shows an example of the power level measured every minute by the bedroom space conditioner electrical circuit during a 24 h period. Within the same plot, the zone number is shown on the second y-axis to the right of the graph. Here, a filtering method identifies the number of bedroom units on by referencing the instantaneous power level of the circuit. On this particular day, the programmed ranges do a good job identifying the number of units powered on. A couple data points show a power draw but no zone number was assigned. Relaxing the lower end of the one unit range would eliminate this error but presents issues for other time periods.

When any one unit is on, there is some fluctuation in the circuit power draw when at a distinct power level. By referencing other circuits for the HVAC system, it can be determined that the bedroom

space conditioner uses a higher fan speed when heating is activated. Once the heating set-point for the specific bedroom is reached, the unit continues to draw power by running the fan at a lower speed.

##### 4.2. Air handling unit (AHU)

Four operating modes are possible for the AHU and correspond to four distinct levels in power draw; first floor only, basement only, both first floor and basement, and ERV modes. Fig. 6 provides an example 24-h period of the measured AHU and ERV electrical power draw every minute. Also, on the same plot is the zone number estimating the operating mode of the AHU. Some of the zone assignments appear to be incorrect for this example period. In two instances, the ERV is on and the AHU shows a similar power draw, within the first 100 min and around minute 1200. Most likely the AHU is in ERV mode while the zone number assigned is 3 at approximately the 100 min point and is 2 at the 1200 min point. During some AHU on-period, the power level is steady while the zone number constantly jumps between two distinct levels. In this case, the power level is on the edge between the two ranges established for each zone number. One explanation for such inconsistencies is the static pressure drop of the ductwork for both zones has altered throughout the two heating seasons. First floor renovations resulted air diffusers being replaced in the in-floor after the first season. An additional return register was installed during the second heating season to support a test stand for a research project at the house. An experimental air filter was installed halfway through the first heating season and removed before the second heating season. Throughout all these changes the static pressure of the ductwork is varied and the power required by the AHU blower increases or decreases to maintain the same air flow rate set by the ECM board. The snapshot values developed during the third heating season are not the best indicators of the AHU operating mode during both, the first and second heating seasons. Modifying the filtering algorithm to consider the modes of the other HVAC equipment could improve the accuracy of determining the AHU operating modes.

##### 4.3. Buffer tank (BT)

The number of different operating modes possible is higher for the BT. Being centrally located within the hybrid air-hydronic system four individual zone pumps result in seven possible operating modes, and hence seven different power levels. With water pumps being the main power draw, the individual power levels are easier to distinguish and are more consistent across the heating seasons. Three modes correspond to the bedroom space conditioners being the only pumps on; one, two or all three. A separate mode exists for

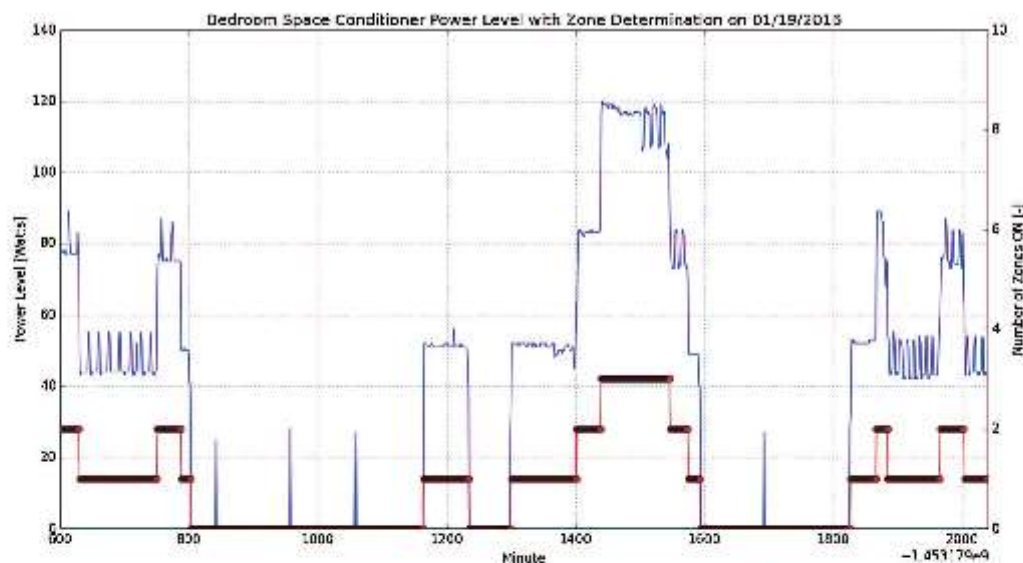


Fig. 5. 24 h Period Sample Operation of the Bedroom Space Conditioners Electrical Circuit (left axis) with Zone Determination (right axis).

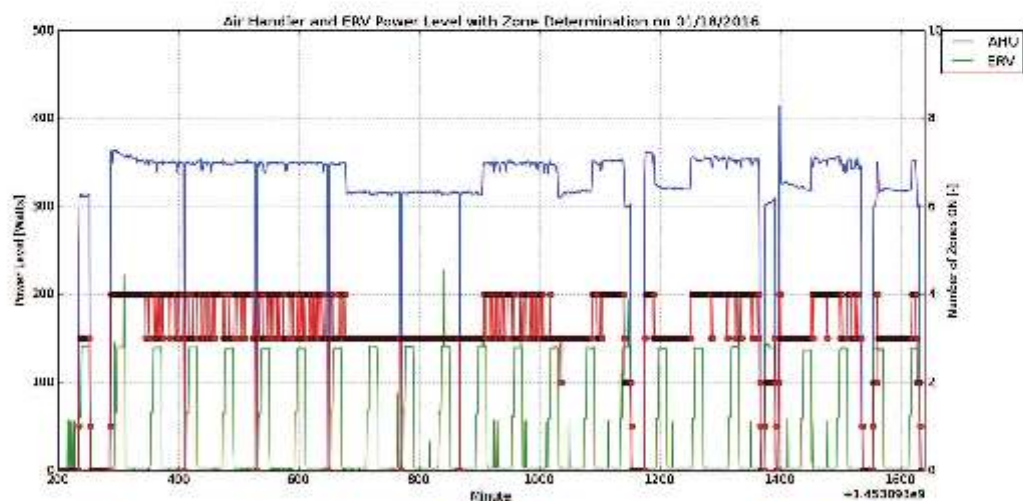


Fig. 6. 24 h Period Sample Operation of the Air Handling Unit and ERV Electrical Circuits (left axis) with Zone Determination (right axis).

only the AHU being on. The last three operating modes come from both the bedroom space conditioner and the AHU pumps being on with one, two, or all three bedroom units being on together with the AHU. Fig. 7 has a sample 24-h period of the power consumption for the BT electrical circuit measured every minute. On the same plot is the number of zones on determined by the power ranges established for each operating mode. Outside of any transition periods between operating modes, the zone number is consistent and matches the power draw trend. In the example shown during the

last 300 min, the fluctuations in zone number represent the actual operation of the BT. In this situation, the AHU is on while one and two bedroom space conditioners turn on and off.

## 5. Results

Referencing the dates associated with changes made to the BT controller, shown in Fig. 4, three time periods of interest are identified. Within these time periods, one day was selected for each

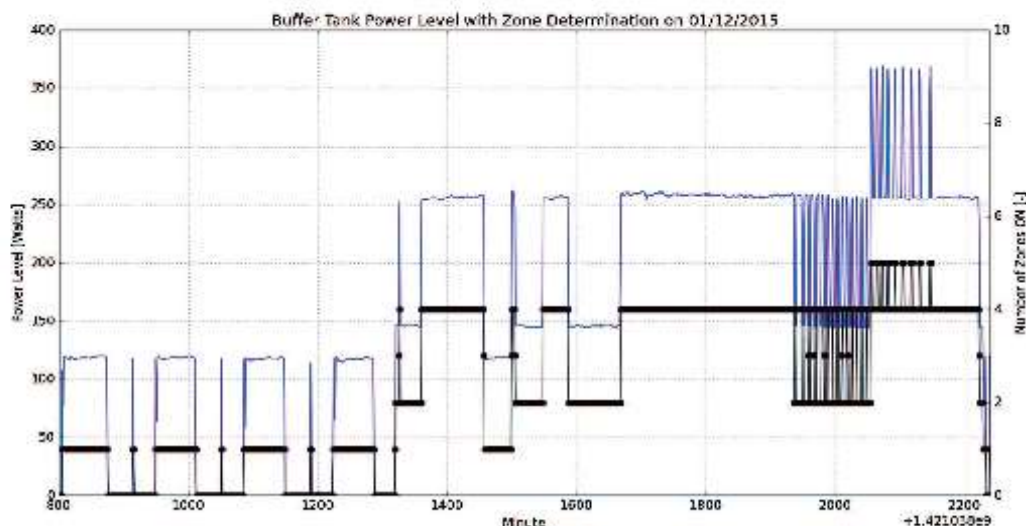


Fig. 7. 24 h Period Sample Operation of the Buffer Tank Electrical Circuit (left axis) with Zone Determination (right axis).

**Table 2**  
Electrical Summary of HVAC Equipment for 3-days of Interest.

Day	Outdoor Avg. [F]	HDD [F-Day]	HP/HDD [kWh/F-Day]	Heat Pump [kWh]	HP ON Cyc [-]	HP Tot. Time ON [min]	HP Avg. Pwr. ON [W]	Buffer Tank [kWh]	Bedroom Space Cond. [kWh]	AHU [kWh]	ERV [kWh]
11/18/2014	13.7	51.3	1.40	71.8	28	1057	3584	3.53	0.68	5.14	2.16
2/19/2015	11.2	53.8	1.34	72.0	26	1106	3533	2.90	0.18	7.22	1.19
1/19/2016	10.7	54.3	1.31	70.9	18	1120	3437	4.55	0.85	6.74	1.02

with all having similar weather conditions on the home. Table 2 provides a summary of the power consumption for the individual HVAC equipment during these selected dates.

As shown in Table 2, the selected dates have similar HDD. As changes were applied to the BT set-point temperatures, the number of HP on cycles decreases while the total on-time increases. The HP electrical energy is slightly unchanged between the first two dates, while a decrease is identified for the third date. The decrease occurs with a higher measured electrical energy demand from the BT and bedroom space conditioners.

A closer look is taken within each date of interest by plotting minute-by-minute electrical data for several circuits of the HVAC system over the entire day. Same plots are generated for each date. First, for each day listed in Table 2, the electrical power draw of the AHU, ERV, bedroom space conditioners, and BT, are shown plotted in Figs. 8, 10 and 12. The interactions between the operation of the zone, terminal equipment and their associated impact on the central BT are observed. For example, during a call for heat, the controller for a bedroom space conditioner cycles on and off a pump on the BT, causing an oscillation in its power level. Second, the electrical usage of the HP relative to the BT electrical usage for each day listed in Table 2 are shown in Figs. 9, 11 and 13.

The zone determination number for the BT is plotted over its electrical power consumption to indicate the level of heating demand on the BT. With the HP only connected to the BT, the conditions provided by the BT directly influence the HP efficiency and capacity. The impact on the HP electrical power draw can be recognized by this comparison. After looking at instanta-

neous interactions between HVAC equipment, the improvement to the BT controls are compared between the two heating seasons. Fig. 14 plots the HP daily energy consumed as a function of the daily HDD. The electrical energy demand by the HP indicated an improved consistency for given HDDs. The first heating season has many outliers around similar HDDs.

A second comparison between the two heating seasons is performed by plotting the daily, heating system effectiveness as a function of the daily HDD. The resulting graph can be seen in Fig. 15. One useful aspect of generating daily, heating system effectiveness as a function of HDD is the HP energy consumption can be estimated by multiplying with other HDDs. Similar to the previous plot, the first heating season produces many outliers.

A summary of the monthly totals of electrical consumption is presented in Table 3. The generated summary compares the electrical consumption associated with the HVAC equipment between the two heating seasons. The first heating season registered more extreme, colder weather relative to the second heating season. As expected the HP consumes more energy, while during the second heating season an improvement of the heating efficiency, 0.82 kWh/F-day versus 0.89 kWh/F-day is calculated.

## 6. Discussion and conclusion

Renovating an existing home with new, advanced HVAC technology can result in poor system performance if not properly executed and commissioned. A hybrid, hydronic-air system installed in a 1920 residential home provided the ability to easily support zoning within the existing building while interfacing

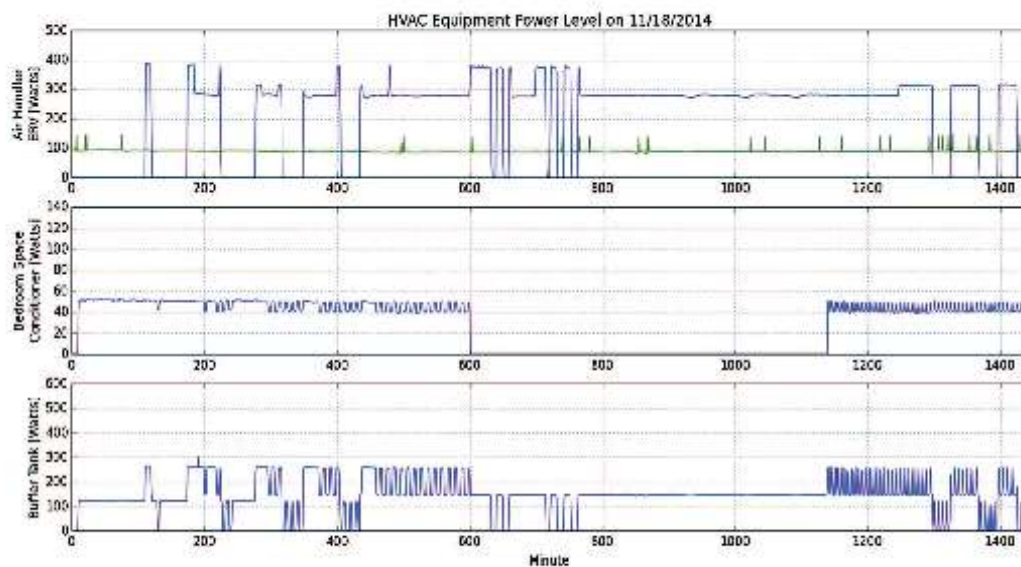


Fig. 8. Power Level of HVAC Equipment on November 18th, 2014.



Fig. 9. Power Level of Ground-Source Heat Pump and Buffer Tank with Zone Level on November 18th, 2014.

with a high efficiency, water-to-water, ground source heat pump (GSHP). By selecting water-to-air terminal units, the installed hybrid, hydronic-air system can handle both heating and cooling demands of the home without any concerns of dehumidification during cooling. Typical hydronic equipment often requires separate

systems for cooling due to concerns from dew point temperature causing condensation on hydronic terminal equipment in the zone.

The temperature set-points of the buffer tank (BT) directly impact the energy efficiency of the GSHP. For heating, the highest set-point temperature is limited by the safe operating envelope

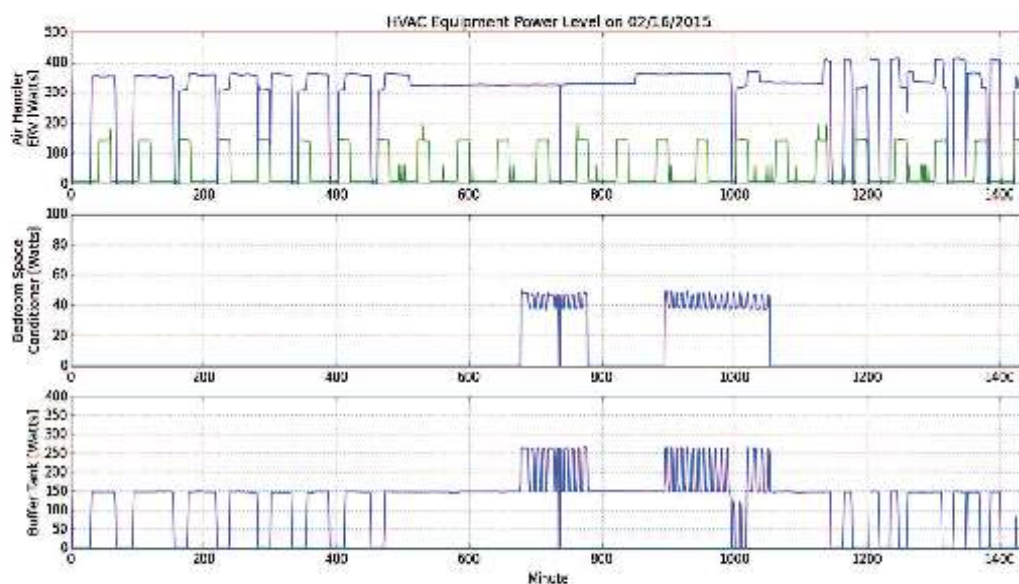


Fig. 10. Power Level of HVAC Equipment on February 16th, 2015.

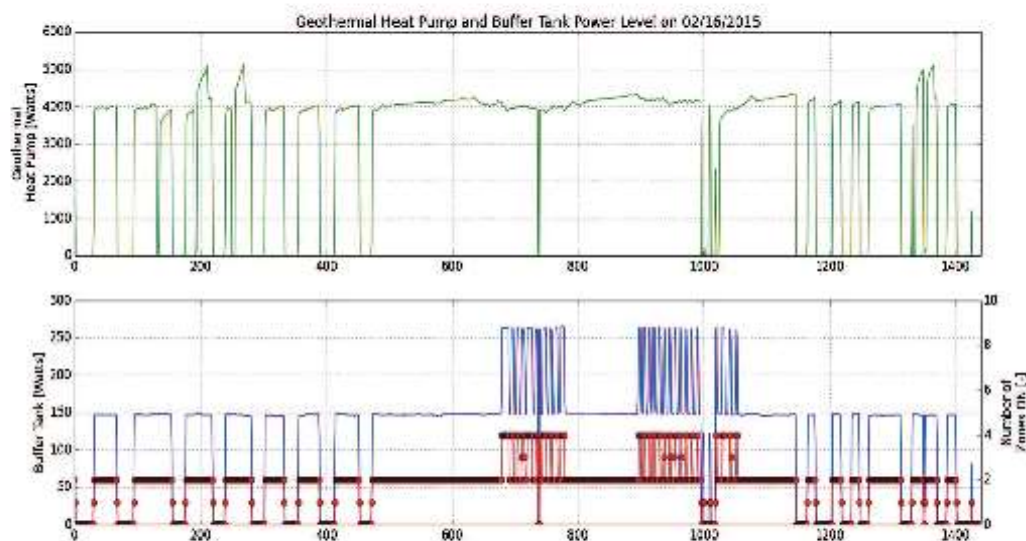


Fig. 11. Power Level of Ground-Source Heat Pump and Buffer Tank with Zone Level on February 16th, 2015.

of the HP compressor due to using HFC refrigerant R410A. Low load temperatures ensure the condensing pressure of the GSHP is within limits. The associated temperature levels are in stark contrast to high BT water temperatures when connected to a boiler. Also, the preset factory temperature set-points of the BT assume connected heating zones are in-floor radiant terminal units having a slow response on the temperature fluctuation of the BT. Therefore larger

temperature swings are enabled for the BT. In the actual installation, water-to-air terminal units are used instead and directly heat air, having a faster impact on the temperature fluctuations of the BT. To reduce the cycling of the GSHP, smaller temperature ranges were programmed into the BT controller. If the BT is allowed to operate over a large range, the quick response of water-to-air terminal equipment prevents the BT reaching the GSHP, off threshold

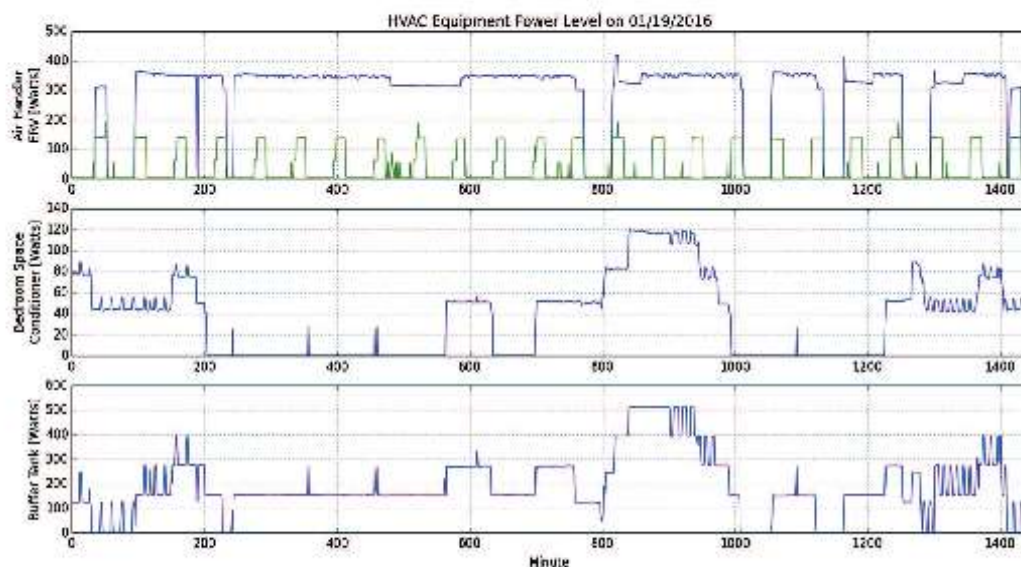


Fig. 12. Power Level of HVAC Equipment on January 19th, 2016.

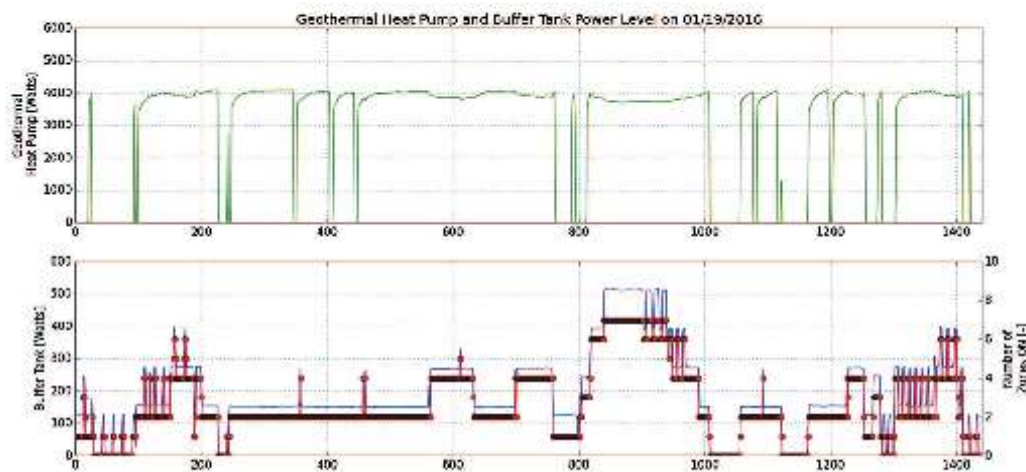


Fig. 13. Power Level of Ground-Source Heat Pump and Buffer Tank with Zone Level on January 19th, 2016.

temperature. The GSHP operation becomes coupled with the terminal equipment operation. Fig. 3 indicates the mismatching that can occur between the capacities of the GSHP and the terminal equipment for various BT temperatures.

From looking at the power consumption of the bedroom space conditioners, the electrical draw oscillates frequently when on. The fan runs continuously when activated for heating and changes speed when calling for heat by kicking on the associated water pump on the BT. This power cycling then directly impacts the on and off cycling of the GSHP. Relaxing the set-point temperatures and temperature span on the BT provides a reduction of the num-

ber of on cycles of the GSHP, the on-duration for a cycle, and the instantaneous electrical power draw. The improvements are verified throughout two heating seasons. Longer on cycles of the heat pump help reduce the amount of cyclical losses and equipment wear. Lower water temperatures result in reduced GSHP power draw due to the lower condensing temperatures and hence condensing pressures. Further reductions of the BT temperature need to be consulted with the required coil temperatures for the bedroom space conditioners. The built-in controller can prevent the unit from turning on if temperatures are reduced too much. One reason is suspected for this high, on temperature. The bedroom

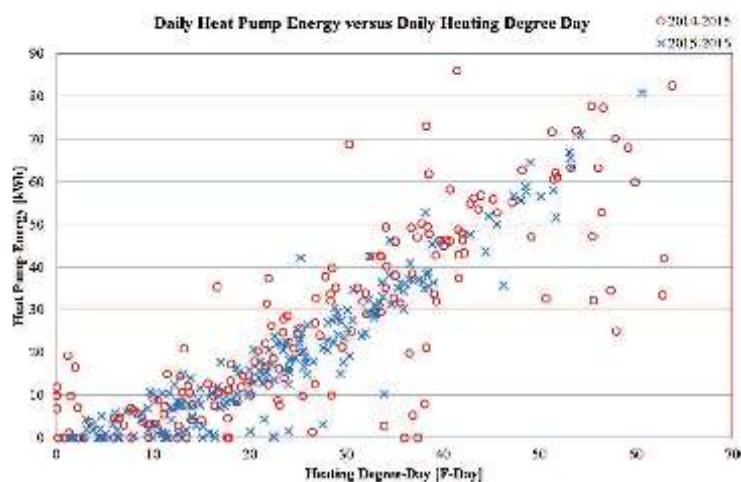


Fig. 14. Daily Heat Pump Energy for Both Heating Seasons as a Function of Heating Degree Day.

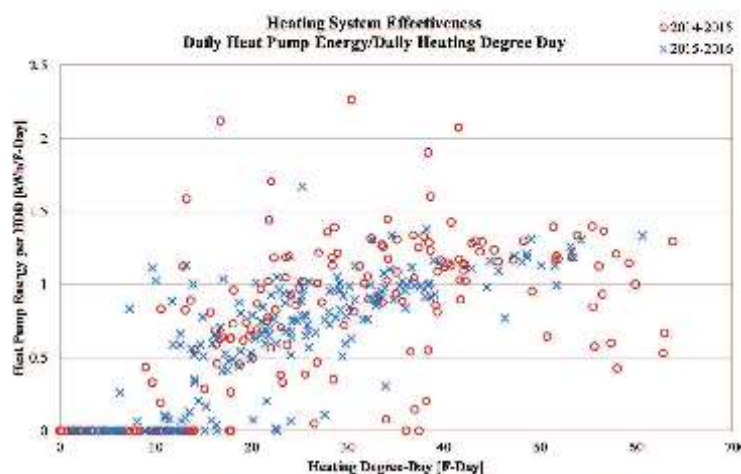


Fig. 15. Heating System Effectiveness as a Function of Heating Degree Day.

units are believed to be designed for supply temperatures traditionally seen by hydronic boilers and not lower temperatures seen in hydronic HP systems.

Throughout the entire two heating seasons, the full-load, heating operation of the HP is not observed from its electrical consumption. Additional improvements can be made to the current BT set-points to better utilize the GSHP full-load capacity. Larger overlap between the temperature ranges between part and full-load heating would reduce BT recovery time during start-up at low tank temperatures. During high heating demands on the BT, part-load of the GSHP might not have enough capacity to raise the BT temperature. If the heating water supply temperature to the zones is too low, the corresponding air supply temperatures will therefore be reduced. Thermal comfort by the occupants could be impacted due to improper controller settings. Enabling full-load heating at an

earlier point and requiring the GSHP operate until the same, final temperature of the part-load operation will recharge the BT quickly and provide improved supply air temperatures.

The BT manufacturer provided one suggestion that was not explored by the authors. The introduction of an outdoor reset temperature for the BT temperature controls could help reduce the excessive amount of cycling on the GSHP. The idea is during high heating loads from low outdoor temperatures, the BT could be configured to maintain a fixed temperature from an outdoor reset. The GSHP would run during these periods to keep the BT at the fixed temperature regardless if a zone was calling for heat or not, similar operation as a DHW storage tank. Then above the outdoor reset temperature, the BT controls would resort back to the method used initially, and allow the GSHP to shut-off after the BT is satisfied. While the amount of GSHP cycles could be reduced with this

**Table 3**  
Monthly Electrical Summary of all HVAC Equipment.

		HDD [F-Day]	HP/HDD [kWh/F-Day]	Heat Pump [kWh]	Buffer Tank	Bedroom	AHRU	ERV
2014	October	396.1	0.40	158.1	7.8	1.47	15.2	8.4
	November	896.2	1.03	923.9	43.4	10.5	81.2	58.2
	December	981.2	0.69	679.3	34.9	8.4	100.3	45.0
2015	January	1267.5	0.91	1159.7	64.9	14.0	112.8	21.5
	February	1260.0	1.18	1488.3	58.1	6.4	155.8	32.7
	March	876.9	0.92	804.5	32.0	5.5	138.5	54.0
	April	392.5	0.57	225.7	8.8	5.5	68.0	35.8
	<b>Total</b>	<b>6080.4</b>	<b>0.89</b>	<b>5439.5</b>	<b>250.0</b>	<b>65.1</b>	<b>671.8</b>	<b>256.5</b>
	October	341.6	0.35	121.0	8.6	5.3	25.7	12.0
	November	572.1	0.60	396.6	23.1	15.6	74.2	32.3
December	744.3	0.68	508.6	28.7	7.8	70.5	20.9	
2016	January	1176.3	1.09	1280.1	76.0	18.6	130.4	20.7
	February	954.5	1.01	963.7	50.7	20.1	114.4	31.3
	March	565.9	0.72	400.5	26.3	7.8	82.3	33.2
	April	442.5	0.54	240.0	13.2	11.3	72.4	32.5
	<b>Total</b>	<b>4997.3</b>	<b>0.82</b>	<b>3919.5</b>	<b>235.7</b>	<b>86.6</b>	<b>579.0</b>	<b>182.9</b>

approach, the GSHP annual heating output could be increased due to operating when no heating demand exists. Further exploration is needed on utilizing the full-load of the GSHP before considering the introduction of an outdoor reset controller.

The installation of an ERV is required to reduce the added heating and cooling loads associated with fresh-air requirements for a low-load, air-tight building. A secondary benefit of the hybrid HVAC system was the combination of ventilation provided by the ERV with hydronic terminal equipment for heating and cooling. By installing a combined hydronic-air system, the separate demands for fresh air ventilation and low-energy HVAC equipment can be nicely combined within the existing space of an older residential building.

Due to the connection of terminal equipment from three separate manufacturers, proper commissioning is required to verify the HVAC controls are operating as intended. Without advanced monitoring capabilities of the ReNEW House, these issues would not have been recognized and the homeowner or contractor would be at a loss as to the cause of higher than expected energy consumption. When this aspect is coupled with on-site electrical production from solar PV panels, a monthly utility bill would provide no insight into the poor performance of the HVAC system.

#### Acknowledgement

The authors thank Whirlpool Corporation for funding the research project.

#### References

- [1] D.O.E.U, The 2011 Building Energy Databook, US Department of Energy, Washington, DC, 2011.
- [2] California Energy Commission, Integrated Energy Policy Report Summary, 2007 [http://www.energy.ca.gov/2007\\_publications/IEP-100-2007-008/IEP-100-2007-008-CMF-ES.PDF](http://www.energy.ca.gov/2007_publications/IEP-100-2007-008/IEP-100-2007-008-CMF-ES.PDF).
- [3] D.O.E.U, Residential Energy Consumption Survey (RECS): Housing Characteristics 2009, Table HC2.1, EIA, Energy Information Administration, US Department of Energy, Washington, DC, DOE, 2009.
- [4] S.L. Caskey, E.J. Bowler, E.A. Groll, Analysis on a Net-Zero Energy Renovation of a 1920 Vintage Home. *Science and Technology for the Built Environment*, 22 7 (2016) 1060–1073.
- [5] K. Klein, K. Huchtemann, D. Müller, Numerical study on hybrid heat pump systems in existing buildings. *Energy Build.* 69 (2014) 193–201.
- [6] C. Backman, A. German, B. Dakin, D. Springer, Air-to-water Heat Pumps with Radiant Delivery in Low-load Homes. *National Renewable Energy Laboratory Technical Report*, 2013.
- [7] D. Springer, B. Dakin, C. Backman, A Feasibility Study: Ductless Hydronic Distribution Systems with Fan Coil Delivery. *National Renewable Energy Laboratory Technical Report*, 2012.
- [8] R. Zmeureanu, X.Y. Wu, Energy and exergy performance of residential heating systems with separate mechanical ventilation. *Energy* 32 (3) (2007) 187–195.
- [9] F. Karlsen, P. Fahlén, Capacity-controlled ground source heat pumps in hydronic heating systems. *Int. J. Refrig.* 30 (2) (2007) 221–229.
- [10] A. Afram, F. Janak-Sharif, Gray-box modeling and validation of residential HVAC system for control system design. *Appl. Energy* 137 (2015) 134–150.
- [11] S.A. Birnwn, B.A. Thornton, S.H. Widdler, Review of Residential Low-Load HVAC Systems. *Pacific Northwest National Laboratory Technical Report*, 2013.
- [12] S. Puitaganta, R.A. Aldrich, D. Owens, P. Mantha, Residential ground-source heat pumps: In-Field system performance and energy modeling. *Geotherm. Resour. Council Trans.* 34 (2010) 943–948.
- [13] A. Artecconi, N.J. Hewitt, F. Polonara, Domestic demand-side management (DSM): Role of heat pumps and thermal energy storage (TES) systems. *Appl. Therm. Eng.* 51 (1–2) (2013) 155–165.
- [14] J. Stene, Residential CO<sub>2</sub> heat pump system for combined space heating and hot water heating. *Int. J. Refrig.* 28 (8) (2005) 1259–1265.
- [15] E. Winandy, C. Handy, Refrigerant and scroll compressor options for best performance of various European heat pump configurations. *Proceedings of the 12th International Refrigeration and Air Conditioning Conference (2008)* <http://docs.lib.purdue.edu/cgi/viewcontent.cgi?article=1804&context=iracc>.
- [16] ACCA/ANSI, Manual J Residential Load Calculations, Eighth Edition (2011).